Copy No. 7

SID 65-1466

REQUIREMENTS STUDY FOR SYSTEM IMPLEMENTATION OF AN ATMOSPHERIC LASER PROPAGATION EXPERIMENT PROGRAM

(Volume II)

8 November 1965

NORTH AMERICAN AVIATION, INC.
SPACE and INFORMATION SYSTEMS DIVISION

FOREWORD

This document is the concluding report of Task III, System Implementation Study, of the Laser Space Communications System (LACE) Study. It was prepared by the Space and Information Systems Division of North American Aviation, Inc. This report is submitted in accordance with requirements of Contract NASw-977, Supplemental Agreement, dated 15 February 1965.

NORTH AMERICAN AVIATION, INC. SPACE and INFORMATION SYSTEMS DIVISION

TECHNICAL REPORT INDEX/ABSTRACT

ACCESSION NUMBER	DOCUMENT SECURITY CLASSIFICATION
10788-65	UNCLASSIFIED

TITLE OF DOCUMENT

REQUIREMENTS STUDY FOR SYSTEM IMPLEMENTATION OF AN ATMOSPHERIC LASER PROPAGATION EXPERIMENT PROGRAM - VOLUME II

LIBRARY USE ONLY

AUTHOR(S) H.E. HENRY, R.N. HATHAWAY, J.O. GARVEY, E.J. STEGELMANN, D.G. LUBNAU, R.J. MUNICK, STAFF

CODE	ORIGINATING AGENCY AND OTHER SOURCES	DOCUMENT NUMBER
	NAA-S&ID	SID 65-1466

PUBLICATION DATE	CONTRACT NUMBER
8 NOVEMBER 1965	NASw-977

DESCRIPTIVE TERMS

*LASER PROPAGATION, *LASER EXPERIMENTS, *ATMOSPHERIC OPTICAL EFFECTS

ABSTRACT

This document constitutes the conclusion of Task III, System Implementation Study, of the Laser Space Communications System (LACE) Study. As such, it is a continuation and expansion of earlier published work under this same contract.

The areas of study covered in the report include: (1) the definition and component performance analysis of, a system configuration for each of the measurement approaches described in the Task II report; (2) an evaluation of alternative measurement approaches by means of a system synthesis analysis; and (3) an analysis of experimental implementation requirements including availability and applicability of existing equipment and facilities with respect to sites, measurement platforms, and propagation links.

FORM 131-V REV 11-64
PUBLICATIONS USE ONLY

CONTENTS

Page

ILLUSTRATIONS

IMPLEMENTATION AND RELATED ANALYSES ILLUSTRATIONS

TABLES

INTRODUCTION AND CONCLUSIONS

INTRODUCTION

SCOPE

The overall objective of the Laser Space Communications System (LACE) Study is to provide a plan for the implementation of a comprehensive experimental program to determine atmospheric effects on laser propagation, with particular emphasis on effects related to optical space-ground communication. The present study effort is a continuation and expansion of earlier work under this contract and is divided into four tasks: Task I, Problem Definition; Task II, Experiment Specification; Task III, System Implementation Study; and Task IV, Program Specification. The results of all four tasks also will be summarized in a final summary report.

This volume contains the results of the System Implementation Study, Task III. The objectives of this task, as derived from the program task definition can be summarized as follows:

1. The definition, and assessment of the component performance, of a system configuration for each of the measurement approaches described in the Task II report (Reference 1).

2. The evaluation of alternative measurement approaches by means of a system synthesis analysis.

3. The performance of an analysis of experiment implementation requirements including the availability and applicability of existing equipment and facilities with respect to sites, measurement platforms and propagation links.

The relationship of these objectives to those of Task II should be noted. Where the earlier task was concerned with identifying and analyzing the sources of measurement errors associated with each of the experiments, the present report prescribes and analyzes the performance of specific measurement configurations for implementing these experiments, along with the broader implementation requirements enumerated in the third

objective stated above. On the other hand, this analysis is not intended to represent detailed system design; this must be carried out as part of the actual implementation phase of the experimental program.

SUMMARY OF CONTENTS

The organization of the report parallels the order of the objectives as stated above. The following section comprises a description and component performance analysis for each of the thirteen experiments described in the Task II report (Reference 1). (Note that the original numbering of the experiments has been retained, so that No. 18 follows No. 12. See Reference 1 for a discussion of the re-definition and partial elimination of Experiments 12-17.) The discussion of each experiment consists of a re-statement of the experiment objectives followed by an implementation section which includes a description of the experiment configuration, with a block diagram and list of required equipment, and the component performance analysis, which constitutes the major portion of the discussion. Experiments 4 and 11 also contain an evaluation of alternative measurement schemes. Experiment No. 6 consists of a description and discussion of an actual measurement which was successfully carried out recently at the Electro-Optical Laboratory of S&ID.

The third section of the report presents the system synthesis envisioned in the second of the stated objectives. In this section, the thirteen experiments are first organized into four groups representing recommended measurement programs suitable for implementation with stationary ground-to-ground links. The rationale for these groupings, described in detail in the text, is based on recognition of the need for a variety of experimental programs tailored to meet objectives ranging from the purely scientific to the investigation of potential techniques for engineering applications. The latter part of this section is devoted to an analysis and discussion of the feasibility of each of the experiments for use with up- and down-links involving satellite (in particular, synchronous satellite) terminals. The section concludes with a chart summarizing the results of the system synthesis for the two classes of links.

The last of the objectives is covered in the fourth and fifth sections on siting support considerations (including meteorology) and optical links, respectively. The fourth section discusses some of the key factors which must be considered in selecting suitable sites for carrying out the experiments, and also presents information on certain specific sites in the U.S. and abroad, together with a listing of available weather facilities and pertinent statistical weather data for the U.S. The fifth section offers relevant discussions on ground, airborne, balloon and satellite links, supported by several detailed appendixes.

The report concludes with a collection of the appendixes cited throughout the text. It is suggested that the first four of these, covering the subjects of lasers, laser transmitter optics, photo-detectors and recording materials, be examined before beginning a study of the experiment component analysis, since these appendixes are of a general nature and broadly applicable to many or all of the experiments. Because of the rapid rate of technological advance in these areas (particularly lasers) the information contained in these appendixes should be regarded as being representative of available components and techniques, rather than as a complete catalog of current state-of-the-art data. The remainder of the appendixes are more specialized, and are to be read in conjunction with their specific antecedents in the main body of the report. Appendix H, which describes an existing optical link should also be read in connection with the implementation discussions of the second, fourth and fifth sections.

In addition to making use of common appendixes, several of the discussions of measurement techniques which are applicable in some degree to more than one experiment are cross-referenced. Particularly in the later experiments, this procedure helps to minimize unnecessary repetition and reduce the length of the discussions.

CONCLUSIONS

In addition to the specific results obtained from the analyses of the several experiments, a number of general conclusions can be drawn from the results of this task study. These are enumerated below:

1. The experiments which have been proposed in this study can all be implemented for stationary ground-based links using available system components, and do not require the application of any unusual or exotic measurement techniques. However, it must be realized that these experiments, as a group, are rather sensitive to environmental factors, particularly weather and vibration, and they demand a standard of care and experimental skill comparable to that to be expected of any moderately sophisticated scientific investigation.

2. Well-instrumented, accessible sites, suitable for carrying out a measurement program of this type are available in a variety of locations. A relevant conclusion from earlier studies is that the first stages of the measurement program should be conducted over long, topologically uniform horizontal ground links. Such links are included among the available sites.

3. Aircraft and balloon platforms with the required instrumentation and logistic support are available for use in making vertical-link measurements during the later stages of the field-test program.

4. Before the final design for a satellite-link atmospheric-propagation measurement program is concluded, thorough field-testing with ground-based and airborne platforms is called for.

COMPONENT PERFORMANCE ANALYSIS

MEASUREMENT OF SPATIAL AND TEMPORAL LOGARITHMIC AMPLITUDE CORRELATION FUNCTION AND PHASE STRUCTURE FUNCTION—EXPERIMENT NO. 1

OBJECTIVE

To obtain the spatial and temporal statistics of amplitude and phase of coherent (laser) light after propagation through the atmosphere.

IMPLEMENTATION

Summary

An analysis of the components used to implement the experiment is presented, along with a discussion of some practical considerations involved in making the measurements. In particular, the aperture sizes and correlation distances at which the measurements should be made are indicated.

Component Performance

Introduction

This analysis centers on the effect each component has on the light as it progresses through the measurement system. A short listing of the components and the problems expected is appropriate (Figure 1.1, Table 1.1).

The first analysis gives an estimate of the size of the sampling aperture. This is important since a hole too large will introduce an average over the very quantities being measured. The maximum distance over which the correlation measurements are to be performed is also specified for a downlink (space-earth transmission). For other link configurations, the solution to the narrow beam problem should be used.

The second, third and fourth analyses deal with filters, lens systems, beam-splitters and mirrors which are needed to guide and combine the sampled light beams. Here the concern will be in finding how these components affect signal power by decreasing intensity and how the polarization of the incoming field is modified and the consequent of any modification.

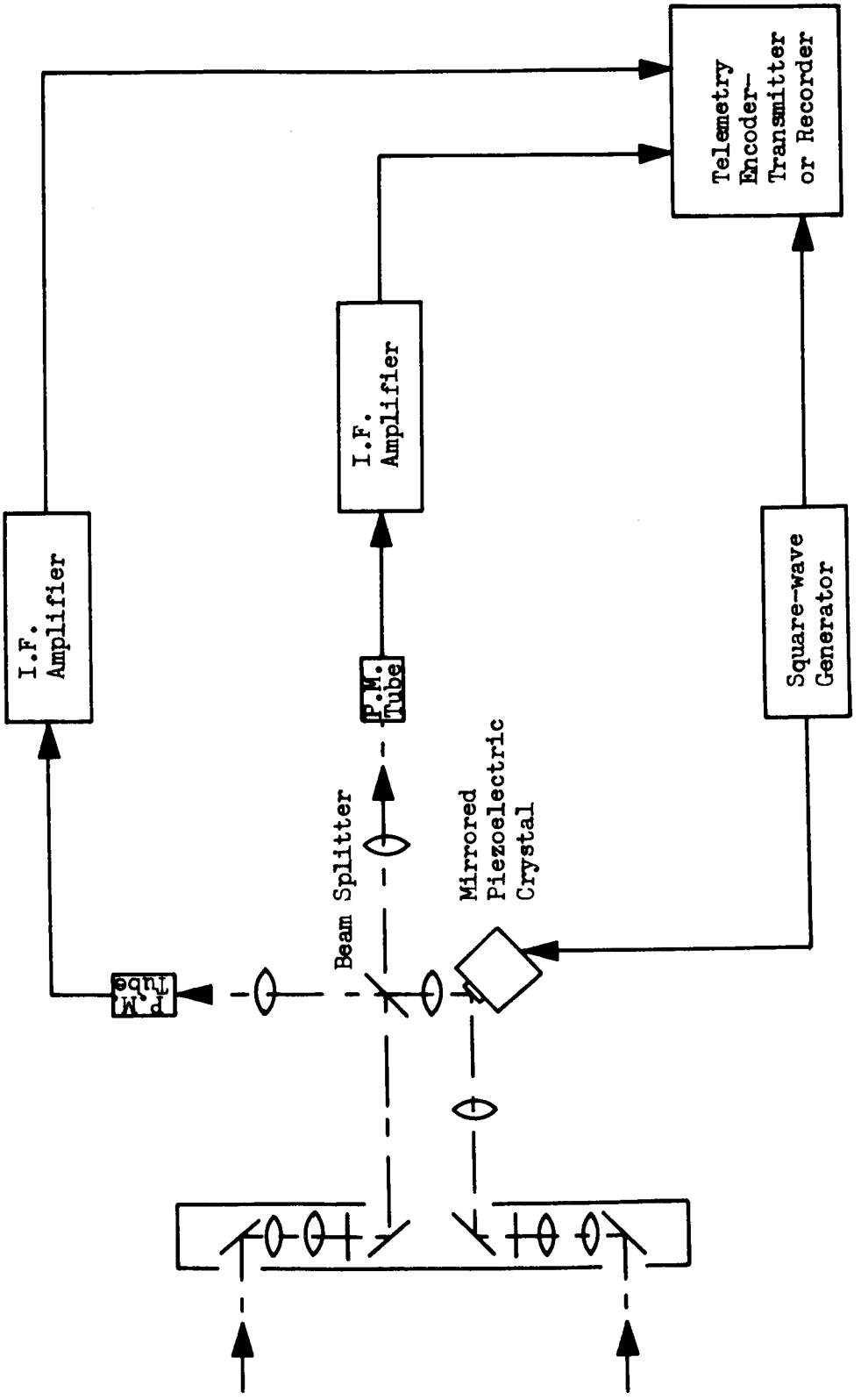

Figure 1.1. Configuration for Measurement of Spatial and Temporal Log Amplitude Correlation Function and Phase Structure Function

Table 1.1. Experiment No. 1 Equipment List

Quantity	Item
1	Extendable-aperture housing with two variable-diameter apertures
4	Aluminized mirrors
2	Pair diameter-correcting lens (achromatic)
4	Focusing lens (achromatic - two optional)
2	Photomultiplier tubes
2	I. F. amplifiers
1	50/50 beam splitter with a $(2n+1)\frac{\lambda}{4}$ phase shift
1	Calibration light source (tungsten lamp)
1	Square-wave generator
1	Face-mounted, mirrored piezoelectric crystal
1	Electronic switch
Supplementary Equipment	
	Telemetry
	Data recording and reduction

The fifth analysis is that of the piezoelectric crystal used to change the path length of light. Since results are highly dependent on obtaining the $\lambda/4$ path difference, the availability of precise path differences from such a

device must be judged. Also the maximum sampling rate (the rate at which the path length is changed) is dictated by the frequency response of the crystal. At high sampling rates, the path difference as a function of time cannot be made a true square wave.

The last analysis is that of the signal-to-noise ratio for the case of no turbulence.

The electronics needed for the measurement are straightforward and will not be analyzed in depth. Their operation will be examined in the discussion section.

Requirements on the laser source and optical detector are fairly obvious. The laser must be single-frequency and single-mode, preferably TEM_{00}, and have good coherence (both temporal and spatial). The detector should have high quantum efficiency at the laser frequency, low dark currents and a photocathode whose area has uniform sensitivity. A more thorough discussion of sources and detectors is given in Appendixes A and C.

Since the components and parameters examined here are common to many of the LACE experiments, the results of this analysis apply also to these other experiments. This fact should be kept in mind as the other experiments are encountered.

Aperture Size and Distance Between Apertures

In selecting the size of the sampling hole, two conflicting requirements must be considered: a large aperture is needed for adequate S/N ratio, while a small aperture is needed to reduce averaging of the effects which are being measured.

The averaging effects of the aperture occur in two ways. The first way is that of an amplitude average of the light over the photocathode. The second is the interaction of the wave front from one aperture with the wave front from the other aperture at the photodetector surface. The interference pattern of these wave fronts is averaged over the surface of the phototube and is essentially an average over the phase difference between the two waves at each point on the photosurface.

The selection of the sampling hole will be more critical for the phase measurements than for amplitude measurements so that the hole size should be chosen to keep this averaging effect at a minimum. An estimate of the aperture averaging effect in measuring the phase structure function can be had from the phase structure function itself. The theoretical expressions which have been so far evaluated for the phase structure function are for the

case of an infinite plane wave propagating either horizontally or vertically through the atmosphere. For the most important case, that of a finite beam, results have yet to be obtained, although the framework exists for such computations (Reference 2).

The calculation carried out here will be for the case of downward propagation. This serves as a model for calculations in the other cases. From Tech Memo 127, (Reference 3), the phase structure function for the case of vertical transmission is

$$D_{\phi\phi}(\rho) = \frac{1.43 \times 10^3}{\lambda_\mu^2} \frac{\Gamma(2/3,\ H/3200)}{\Gamma(2/3)} \rho^{5/3} \qquad (1.1)$$

for $0 < \rho < L_o$

where

λ_μ is the wavelength in microns (μ)

H is the receiver height above earth (m)

ρ is the spatial correlation variable (m)

L_o is the outer scale of turbulence (m)

$\Gamma(a,x)$ is the incomplete gamma function

The error introduced by one aperture in measuring the phase structure function will be approximately $D_{\phi\phi}(r_c)$ where r_c is the diameter of the aperture. The value of r_c to give the error $D_{\phi\phi}(r_c)$ in the phase structure function is found by solving Equation 1.1 for r_c. The result is

$$r_c = \left[\frac{\lambda_\mu^2}{1.43 \times 10^3} \frac{\Gamma(2/3)}{\Gamma(2/3,\ H/3200)} D_{\phi\phi}(r_c) \right]^{3/5} \qquad (1.2)$$

This relation is graphed in Figure 1.2 as a function of receiver altitude H for radiation at 6328 Å and for errors in the phase structure function of 1 radian and 10 radians ($D_{\phi\phi}(r_c) = 1, 10$). To complete the picture, the aperture error should be compared to the phase structure function $D_{\phi\phi}$ as

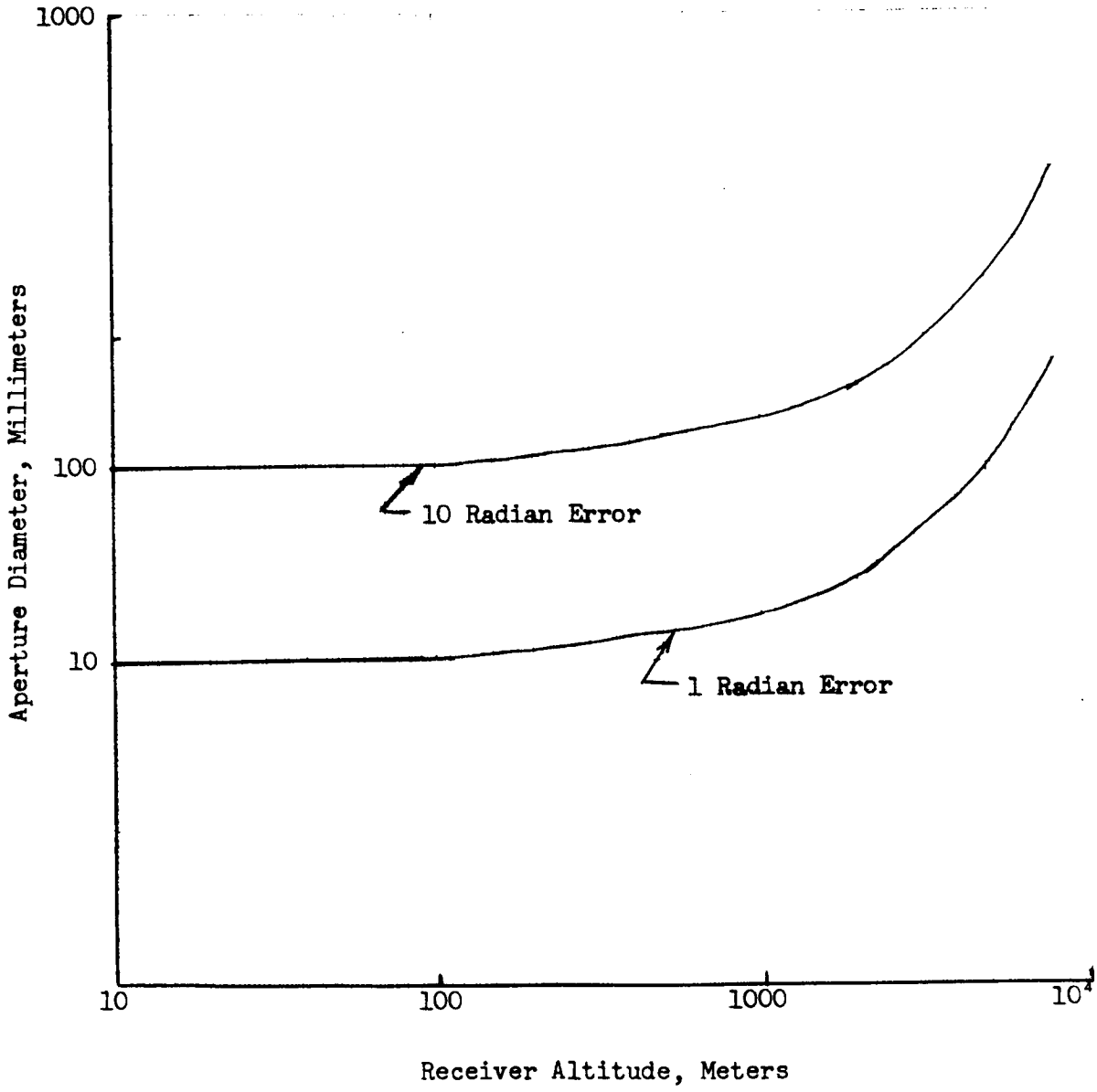

Figure 1.2. Error in Phase Structure Function Caused by Single, Finite Aperture

a function of ρ. A normalized relative error in $D_{\phi\phi}(\rho)$ due to the finite aperture can be written as (Reference 1)

$$\Delta_{\phi\phi} = \frac{2\, D_{\phi\phi}(r_c)}{D_{\phi\phi}(\rho)} \tag{1.3}$$

With the aid of Equation 1.1, this becomes

$$\Delta_{\phi\phi} = 2\left(\frac{r_c}{\rho}\right)^{5/3} \tag{1.4}$$

Obviously, the formula gives a good approximation to the actual relative error when $\rho >> r_c$ i.e., when the separation between apertures is much greater than the aperture size itself. It seems evident that the formula would hold for ρ as small as ten times r_c. Using this arbitrary condition as the point where Equation 1.4 no longer holds, a plot of $\Delta\phi\phi$ vs r_c/ρ is given in Figure 1.3. From the plots of Equations 1.2 and 1.4 the size of apertures allowed as a function of receiver height can easily be found.

As a practical matter for both analysis and experiment, the sampling hole should be so large that diffraction effects are not present, given the size constraints of the averaging effect.

Figure 1.4 gives the dimensions of a circular aperture in terms of (aperture diameter/wavelength) and (distance from the aperture/aperture diameter) for which the electromagnetic field can still be regarded as the near field; i.e., the region in which the propagating field has approximately the same form as the geometrical optics field (Reference 4). From this, the path length from the sampling aperture to any lens system can be determined so that the field is still the near field. This path length is a function of the maximum displacement for which the correlation functions are to be determined. For spatial correlation distances on the order of centimeters or less, the problem of aperture size is about the same. For while the near field zone begins closer to the aperture, the path lengths traversed by the light are also reduced.

The maximum separation between sampling apertures for which measurements would be taken will be equal to L_o, the outer scale of turbulence. Figure 1.5 is the graph of L_o vs altitude and is the same as Figure 1 in Tech Memo 91 (Reference 3).

Figures 1.4 and 1.5 are used to calculate whether or not the full correlation distance L_o can be measured while still keeping the field at the lens in the near field at any receiver height. A rough calculation shows that

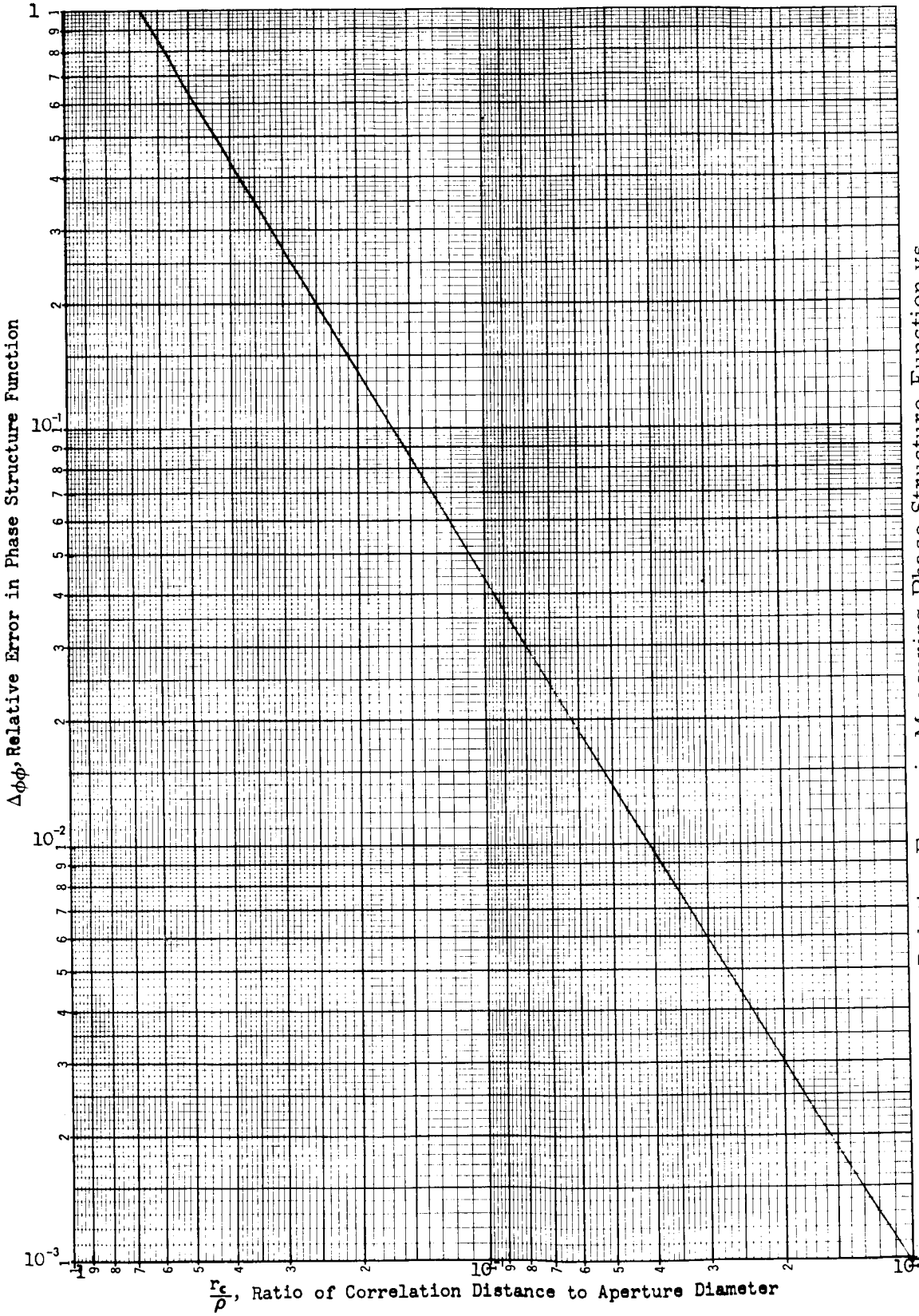

Figure 1.3. Relative Error in Measuring Phase Structure Function vs. Ratio of Correlation Distance to Aperture Diameter

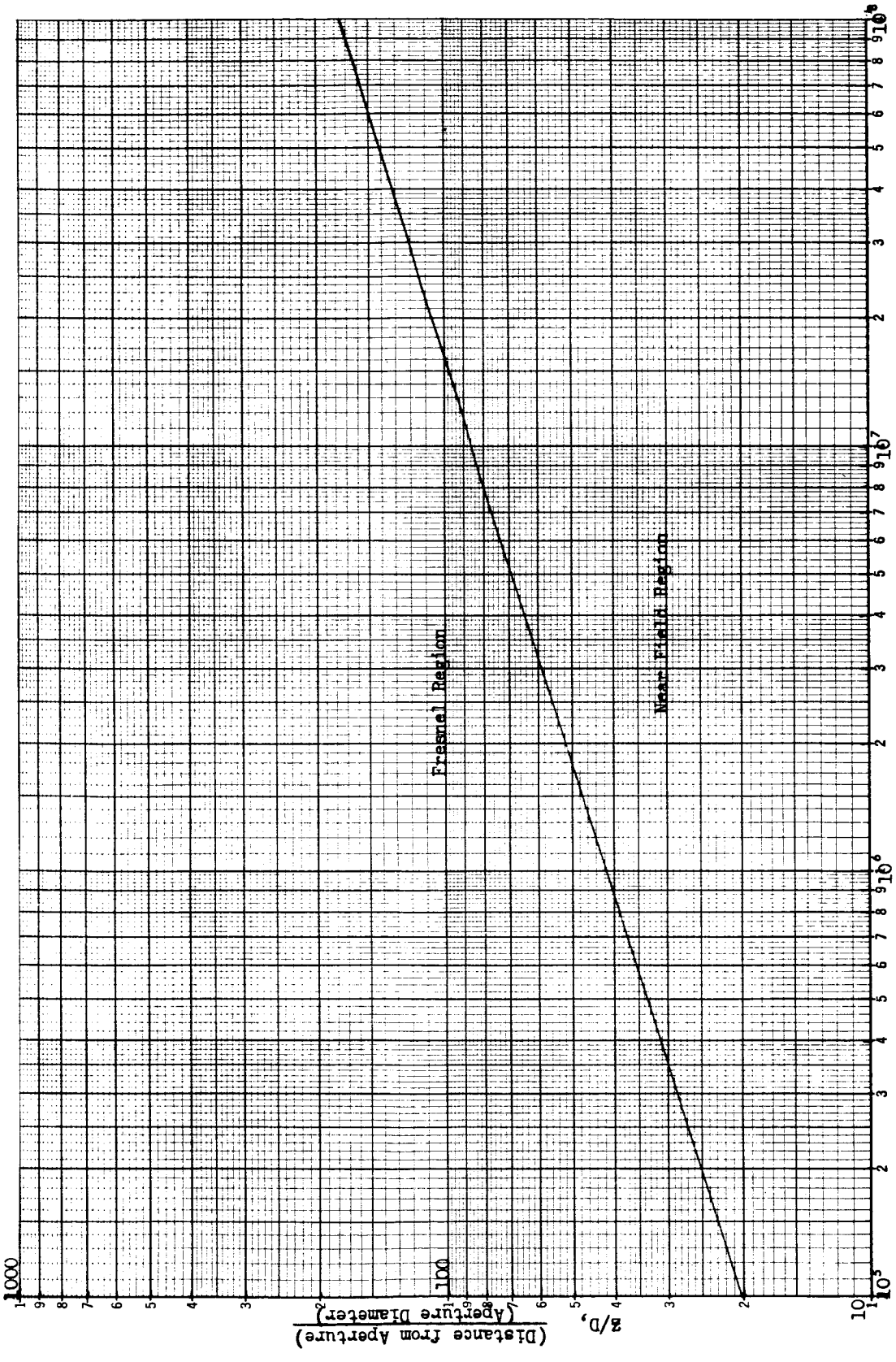

Figure 1.4. Boundary of Near Field Region

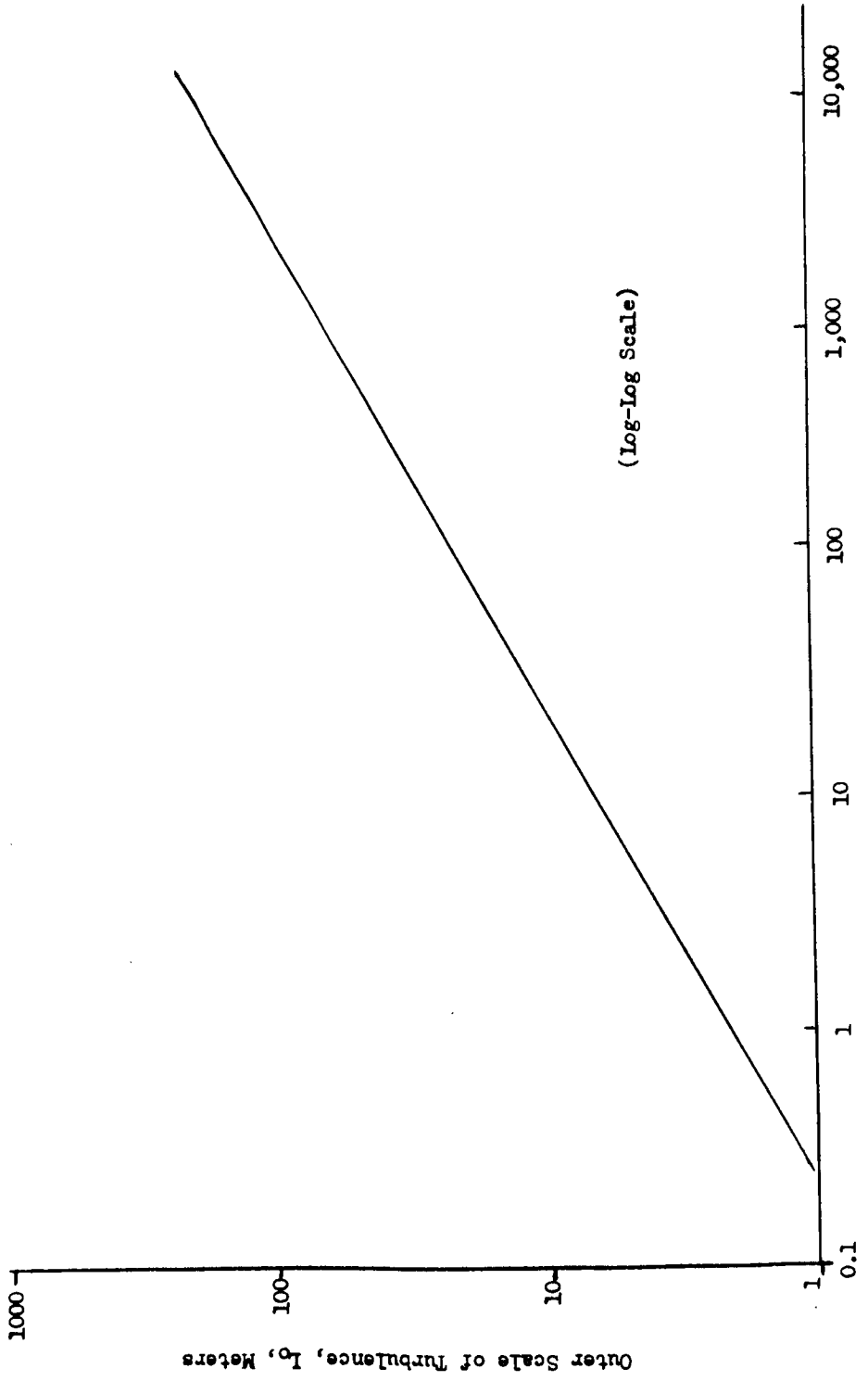

Figure 1.5. Outer Scale of Turbulence with Height

if points are sampled a distance L_o apart using the aperture sizes suggested, then the field at the lens will be in the Fresnel region and not the near field region. For samplings a little less than $L_o/2$ apart, however, the field at the lens will be very near to the near-field region, so it may be treated as the geometrical-optics field.

Mirror Analysis

The important points to cover in the analysis of the mirrors are the amplitude, phase and polarization effects of reflection.

Dielectric mirrors provide reflectivities higher than 0.99; however, this figure is highly dependent on incident angle below the critical angle. Metallic (gold, silver, aluminum) mirrors in the 1μ to 10μ region have reflectances of .98 to .99. While the exact reflectance does depend on the angle of incidence, the variation for angles 0° - 90° is not more than 10% of the reflectance at normal incidence for aluminum. For this reason, and because gold and silver are subject to several environmental problems, aluminum-surfaced reflectors are suggested for the experiments.

Figure 1.6 defines the variables used in discussing the polarization and phase shift phenomena of a metallic surface.

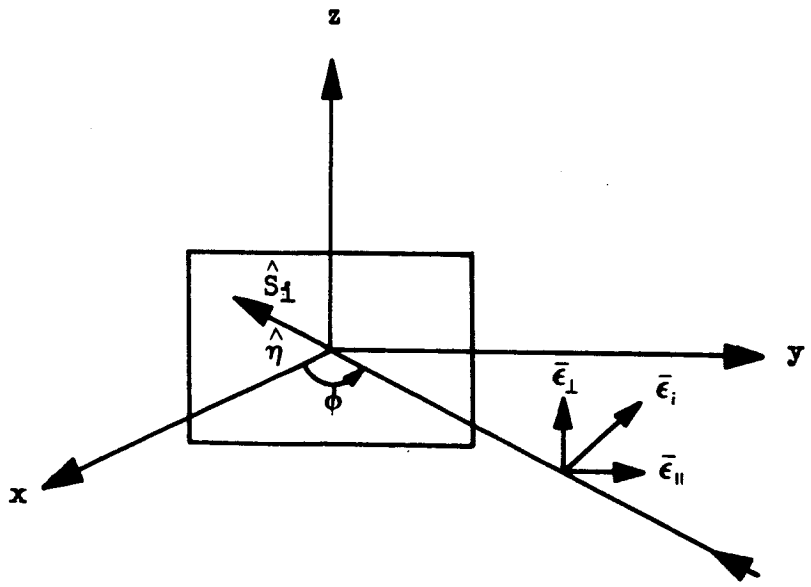

Figure 1.6. Coordinate System for Discussion of Reflection at a Metal Boundary

The x - y plane is termed the plane of incidence. An electric field $\bar{E}_i$ incident on the mirror can be decomposed into components $E_\perp$ and $E_{||}$ which are perpendicular to, and parallel to the plane of incidence, respectively. For simplicity, the normal to the E_i wave-front is also taken in the plane of incidence. This will be true if good boresight can be maintained.

If the incident, linearly polarized field is other than normal to the plane of incidence, the light will be reflected as elliptically polarized light. In relation to the incoming components of the field, the components of the reflected field can be written

$$E_{R_\perp} = \rho_\perp E_\perp \exp(j\theta_\perp)$$

$$E_{R_{||}} = \rho_{||} E_{||} \exp(j\theta_{||}) \qquad (1.5)$$

where $E_{R_{\perp,||}}$ refers to reflection perpendicular and parallel to the plane of incidence and $\rho_\perp$, $\theta_\perp$, and $\rho_{||}$, $\theta_{||}$ are reflection coefficients and phase angles in these directions. When the permeabilities of the two media are the same and the conductivity and frequency are high (Reference 5),

$$\rho_\perp^2 = \frac{\left(\sqrt{\frac{\sigma}{2}} - \sqrt{\omega \epsilon_2} \cos \phi_o\right)^2 + \frac{\sigma}{2}}{\left(\sqrt{\frac{\sigma}{2}} + \sqrt{\omega \epsilon_2} \cos \phi_o\right)^2 + \frac{\sigma}{2}}$$

$$\theta_\perp = \tan^{-1}\left\{\frac{\sqrt{\frac{\omega \epsilon_2 \sigma}{2}} \cos \phi_o}{\omega \epsilon_2 \cos^2 \phi_{oo} - \sigma}\right\}, \qquad (1.6)$$

where

σ is the optical conductivity

ω is the optical radian frequency

ϕ_o is the angle of incidence

μ is the permeability of both media (taken as equal)

ϵ_2 is the dielectric constant of the host dielectric;

and

$$\rho_{\parallel}^{2} = \rho_{\perp}^{2} \frac{\left(\sqrt{\frac{\sigma}{2}} - \sqrt{\omega \epsilon_2}\ \sin\phi_o\ \tan\phi_o\right)^2 + \frac{\sigma}{2}}{\left(\sqrt{\frac{\sigma}{2}} + \sqrt{\omega \epsilon_2}\ \sin\phi_o\ \tan\phi_o\right)^2 + \frac{\sigma}{2}} \qquad (1.7)$$

$$\theta_{\parallel} = \tan^{-1}\left\{ \frac{\sqrt{2\omega\epsilon_2\sigma}\left[\sigma - \omega\epsilon_2 \sin^2\phi_o\right]\ \cos\phi_o}{\omega^2\epsilon_2\mu\sigma - \omega\mu\sigma^2\cos^2\phi_o} \right\} .$$

Two effects may occur when light from the two sampling apertures is mixed in a photodetector, after several reflections from guiding mirrors. The first possibility is that the mirrors will impart to the $\perp$ and $\parallel$ components of the sampled field a phase difference for which the beat output is very low. An easy adjustment of path length by varying the mirror separation would compensate for this in fixed-receiver/transmitter experiments.

The second possibility arises when there is relative motion between the receiver and transmitter. Here, making the reasonable assumption that the fields at the sampling holes have the same polarization, $\theta_{\perp}$ and $\theta_{\parallel}$ for each channel will be time dependent through $\phi_o(t)$. Under conditions where the reflection histories of the sampled beams are the same (same angle of incidence, same incident polarization, same number of components) there will be no difference in the phases of the $\perp$ and $\parallel$ components that beat together in the photodetector. The time variation should not matter then in the measurement of the log amplitude and phase correlation functions. When the channels are not matched, however, there will exist a time-varying phase difference which will affect the measurements. To avoid this, it is essential that the channels be matched exactly.

Filters and Beam Splitters

There are two types of optical filters—absorption and interference. Since both are dielectric materials, reflected and transmitted field components will obey the law of refraction at the air-dielectric interface. For the electromagnetic boundary conditions to be satisfied, the phase of the reflected and transmitted fields will depend on the initial angle of incidence, among other things. Again, if the channels have similar filter arrangements, no influence on the measurements should be experienced in situations involving relative motion.

Pure dielectric filters will not change the polarization of the reflected or transmitted light from that of the incident light. Absorption filters have transmittance as high as .9, but with a restriction on the narrowness of the frequency band passed (nominal width of 20 Å).

Interference filters are composed of thin dielectric films of various refractive indexes which, in transmission line terminology, present a match at some frequencies and a mismatch at others. High transmittances ($>.99$) can be achieved, but the narrowness of the band passed is sacrificed. Interference filters are also used as beam splitters with the addition of thin metallic films to increase the reflected light. This, however, introduces the polarization problem and makes a brief analytical study impossible.

Beam splitting can also be accomplished using prisms which act to frustrate the total reflection which occurs in a single prism. Energy is then coupled from one prism to the other. The reflection and transmission properties of such a beam splitter depend on the incident polarization and the angle of incidence. Hence for a situation in which relative motion occurs between transmitter and receiver, one would expect some sort of phase modulation.

Current commercially available beam splitters are of the metallic-film type. The ability to match the 50-50 intensity split has a tolerance of about 3%. Concurrently, the ability to give a quarter-wave-length phase shift has an error of about 5%.

The Lens System

After each aperture, a pair of fixed lenses is placed to recollimate the beam. The lenses need be only slightly larger than the sampling apertures. In one channel, another pair of lenses is needed, the first to focus light on the mirrored surface of the piezoelectric crystal and the second to recollimate the reflected light.

Lenses may or may not be needed to focus the radiation onto the photomultiplier tube. A requirement on the alignment of the two channels is that the aperture images coincide on the photodetector; otherwise heterodyning does not occur. If the channel alignment is so poor that the images do not overlap when focusing lenses are used, it would be best to de-focus, or not use the lens at all. It might be supposed that since the instantaneous direction of the incoming wave-front at each aperture is changing, a lens will focus the pair of images on different portions of the photodetector. This would naturally influence the statistics. However, if the channels were initially aligned so the images overlapped, the measured statistics would be the same, since it makes no difference in photocathode current whether a focusing lens is present or not (Reference 6).

The main purpose of focusing the radiation on the photodetector is that at the focal point, the unperturbed phase front is plane. At an intermediate distance, the phase front is spherical, a fact which will tend to color the statistics of the phase and amplitude. This leads to the conclusion that if the optical channels are aligned well enough, lenses should be used to focus the radiation, but if alignment is poor, no lens at all should be used.

Piezoelectric Crystal

A convenient way of mounting a piezoelectric disk is to fix one end on a relatively massive component so that it has one free- and one fixed-boundary condition. In this case, the change in position of the mirror face in the direction of the applied field is given by

$$\Delta x = d_{33}\, \Delta V \frac{\tan\left(\frac{\omega}{4f_r}\right)}{\left(\frac{\omega}{4f_r}\right)} \qquad (1.8)$$

where

d_{33} is the piezoelectric strain constant (cm/volt) in the direction of the electric field and depends on the material.

ΔV is the peak change in the applied voltage (V)

ω is the applied radian frequency (rad/sec)

f_r is the resonant frequency of the first resonant mode (cps)

The above formula is derived for sine wave excitation. It is easy to see that if the path is to change in a square-wave manner by $(2n + 1)\ \lambda/4$ wavelengths, there must be many harmonics of the square-wave driving voltage below the frequency f_r. The piezoelectric strain constant d_{33} of the piezoelectric ceramic composed of lead, titanium and zirconate is 3.5×10^{-8} (cm/volt). To get a displacement of $\lambda/4$ for 6328×10^{-8} cm, the applied voltage would have to be around 319 volts peak-to-peak. Since this type of ceramic has one of the highest values of d_{33}, it appears that the drive voltage will have to be of this magnitude. (In attaining this drive voltage it must be remembered that the crystal is mounted at a 45° angle to the incoming beam.)

S/N Ratio

Because signal detection is accomplished by beating together two signals of the same frequency, the process described constitutes homodyne detection. The present analysis evaluates S/N ratio for the case of no atmospheric turbulence.

The outputs of the two phototubes are combined to give a signal power of

$$P_s = 4 \left(\frac{\eta q}{\hbar \omega}\right)^2 P_1 P_2 \tau_a \tau_o \cos^2\theta \qquad (1.9)$$

The power collected by the two apertures is designated P_1 and P_2; θ is the phase difference between signals and will be caused by any difference in the length of the optical channels (this distance can be adjusted to give $\cos^2\theta \approx 1$);

and

η is the photodetector quantum efficiency $\left[\frac{\text{amp}}{\text{watt}}\right]$

q is the electronic charge (coulombs)

$\hbar$ is $h/2\pi$; h, Plank's constant (erg-sec)

ω is the radian frequency of the laser light (rad/sec)

τ_a is the loss in signal power due to angular misalignment (see Appendix E)

τ_o is the loss in signal power due to the optical components

Noise power, including background but not current noise, is

$$P_N = \frac{\eta q^2 \Delta B}{\hbar \omega} (P_1 + P_2 + P_B) \qquad (1.10)$$

where

P_B is the background power

ΔB is the low-pass filter bandwidth of the circuitry following the photodetector (Note: When the detection is a heterodyne process, as in Experiment No. 2, the noise bandwidth becomes twice the low-pass filter bandwidth.)

The source of background noise of most concern in a well planned experiment (no bright celestial object in the field-of-view) will be atmospherically scattered light which is intercepted by the receiver when it is on earth, at low altitude, and in near-earth orbits. To find this, the spectral radiance of light scattered from the atmosphere must be known (Appendix F). With the background spectral radiance specified, the value of P_B would be

$$P_B = \bar{N}_\lambda \Delta\lambda A_r \Omega \prod_{i=1}^{n} \tau_i \qquad (1.11)$$

where

$\bar{N}_\lambda$ is the spectral radiance as measured at the aperture (watts/m^2-sterad)

$\Delta\lambda$ width of any optical filter (Å)

A_r effective area of receiver (m^2)

Ω field-of-view of receiver (sterad.)

$\prod_{i=1}^{n} \tau_i$ product of transmittance of optical components and atmosphere

Relating signal power to geometric and laser parameters for a one-way link is the expression

$$P_1 = P_2 = \frac{4 P_T A_r}{(\theta_T R)^2} \tau \qquad (1.12)$$

where

P_T is the transmitted power [watts]

A_r is the effective area of the receiver [m^2]

R is the range [m]

τ is the transmittance of the atmosphere

θ_T is the beamwidth of the transmitter [rad].

Wavelength-Dependent Adjustments

In this experiment, as in others, the wavelength of the incoming radiation will be varied as part of the experimental procedure. This will require adjustment or special selection of components. The parameters which will be wavelength-sensitive are aperture areas, lens focal lengths, photodetector quantum efficiency, filter characteristics and in Experiment No. 1, the path length modulation and phase shift through the beam splitter.

To adjust to any changes in wavelength, the electrically controlled apertures can be pre-programmed to the correct size and changed accordingly. To keep focal lengths constant for two different wavelengths only, the usual corrective action of choosing an achromatic doublet is proposed. This would provide partial compensation if more than two wavelengths were used. Photodetectors and filters could be chosen (since their spectral response is fairly wide) so that they could be used for several wavelengths.

The phase shift caused by the beam splitter and the path length modulation is quite critical. In order to use components selected for use at one wavelength at other wavelengths, the components would have to have an equivalent phase shift of $2\pi n$ radians ($n = 1, 2 \ldots$) at the new wavelengths to make the measurements and statistical calculations valid. If this cannot be accomplished, components designed to operate specifically at the other frequencies would have to be used.

Discussions of Components

In this section, the basic flow and processing of the signal is discussed from the viewpoint of practical implementation. The problems involved in choosing the optical components have been discussed in some detail in the Component Performance section. Here the emphasis is on the electronic and electro-optical components.

The device on which the success of the experiment most depends is the mirrored piezoelectric crystal. If this does not give the proper $\pi/2$ phase shift, errors will result in the computation of $D_{\phi\phi}$ and C_{LL} as discussed in Reference 1. Fortunately, because the values of the piezoelectric strain constant and the coefficient of thermal expansion are so low, the sensitivity of the $\lambda/4$ path length modulation to small changes in drive voltage and temperature is not great and under ordinary conditions, should not be a large contributor to the measurement error.

In the event that electric field strengths are too large, the displacement of the crystal will not be linearly dependent on the applied voltage. With large field strengths, the dissipation factor of the material will increase

also, heating the material more. Whether or not these field strengths will be reached depends on the material thickness and the maximum voltage to give the $\lambda/4$ displacement. The thickness will also determine the frequency of first resonance which determines the rate at which the path length may be changed. The matter of possible high field strengths needs to be examined more closely.

Results from an experimental modulator show a break frequency of about 3 Mc (Reference 7). To preserve the square-wave modulation of path length, the sampling rate (the pulse repetition frequency of the square wave) must be much greater than the reciprocal of the crystal's first resonant frequency, f_r. The rule of thumb is that if 10 Fourier components of the driving wave form are passed undistorted, the original wave will be reconstructed with little error. If this is the case, the PRF of the driving square wave can be around 300 Kc. Since in the case of measurements made under stationary conditions, the power spectrum of the sampled signal will only be around 10 Kc wide (baseband), a center frequency of 300 Kc for any signal-processing electronics is quite adequate. Thus, the choice of i.f. amplifiers in the equipment list.

To the basic equipment, a calibration light source of the type used in photometric measurements (such as a tungsten lamp) is added to monitor channel gain before, after and during the experiment. The retractable mirror directs the calibration light source. When the calibration procedure is under way, an electronic switch at the output of the PM tubes is needed to sample the signal at the same rate as the square wave driving the crystal, in this case 300 Kc. This translates the calibration signal to the frequency of the i.f. stage.

Telemetry and recording equipment is standard, and because of the signal spectrum, need not be very wide-band. The telemetry and encoding equipment, where needed, will undoubtedly be available in the vehicle for other purposes. There is a need to identify which coefficient C_n has been recorded or telemetered since the method of reducing the data does depend on knowing which coefficient C_n of the set $\{C_n\}$ is being processed, (Reference 1). This identification can be achieved by monitoring the position of the piezoelectric crystal through the square-wave drive voltage. Thus, three recording or telemetry channels will be needed.

PHASE STRUCTURE FUNCTION MEASUREMENT — EXPERIMENT NO. 2

OBJECTIVE

To measure directly the phase difference between two points on the wave front of a laser beam so that the phase structure function may be calculated. A secondary objective is to measure, depending on implementation, the log amplitude correlation function or the amplitude correlation function.

IMPLEMENTATION

Summary

The measurement of the log amplitude correlation function and phase structure function can be carried out electronically without the need for a data reduction step as in Experiment No. 1. This method uses automatic gain control and phase-locked loop circuitry along with several analog circuits to compute the desired statistics. The operation of the components needed are analyzed in some depth and possible practical problems in implementation are discussed.

System Configuration

The measurement of the phase structure function and amplitude correlation functions is carried out using the arrangement shown in Figures 2.1 and 2.2. The optical field is sampled at two points separated by a distance ρ. After one of the optical signals has been offset in frequency by the Debye-Sears modulator, the two beams are allowed to interfere on the surface of the photodetector. The electronics following the photodetector are at i. f. to ease problems of signal processing. Following the i. f. amplification stage is automatic gain control (a. g. c.) and phase locked-loop (p. l. l.) circuitry. The a. g. c. circuitry suppresses amplitude fluctuations which would affect the measurement of phase fluctuations. With some modification, it also provides statistical information about amplitude fluctuations. This information, depending on the gain control law used (described in detail later), can be either the correlation function of the log amplitude or of the amplitude alone. To calculate these quantities, the average power or intensity must be measured. To provide for this, a 50/50 beam splitter is incorporated in each optical channel. Each averaging channel has its own photodetector and averaging circuitry.

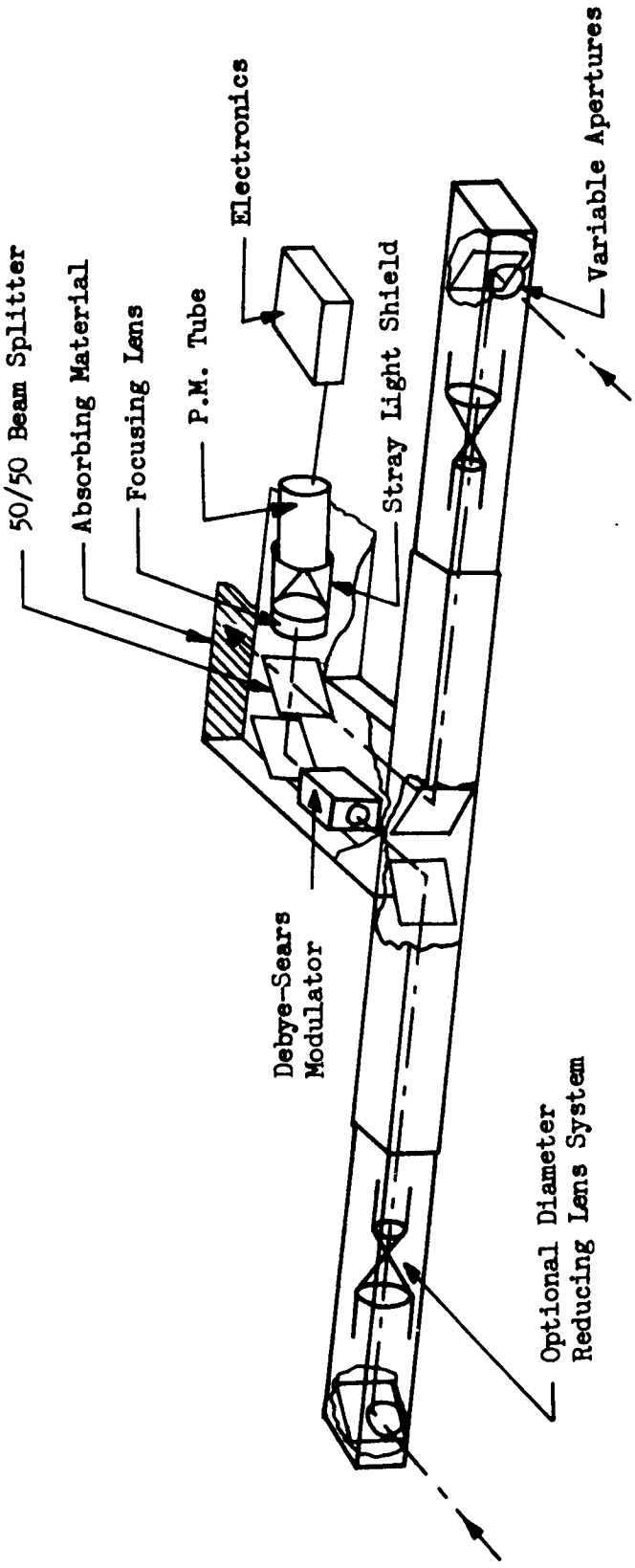

Figure 2.1. Configuration for Measurement of Phase Structure Function

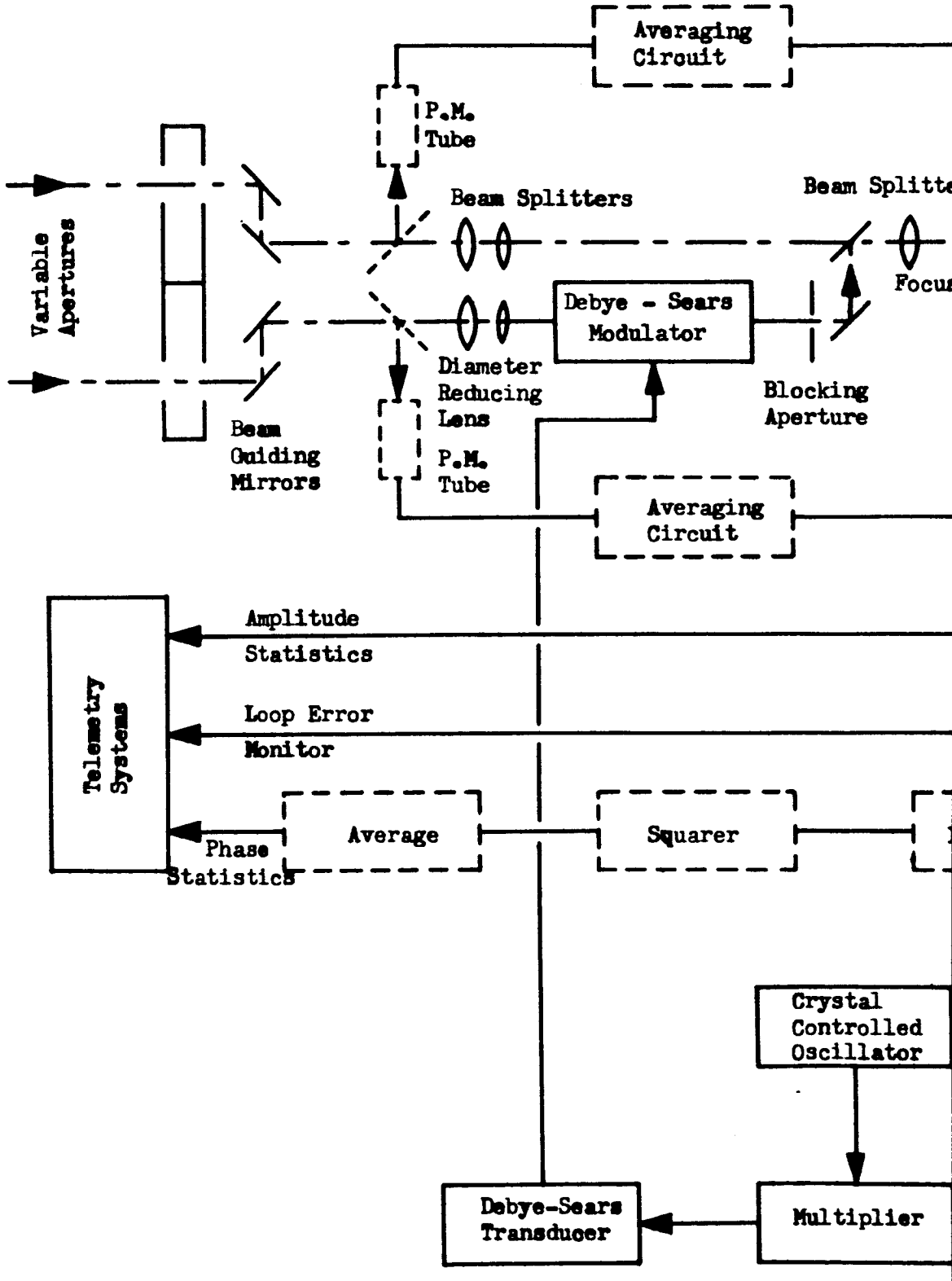
Averaging Circuit
P.M. Tube
Beam Splitters
Beam Splitte
Variable Apertures
Debye - Sears Modulator
Focus
Diameter Reducing Lens
Blocking Aperture
Beam Guiding Mirrors
P.M. Tube
Averaging Circuit
Amplitude Statistics
Telemetry Systems
Loop Error Monitor
Average
Squarer
Phase Statistics
Crystal Controlled Oscillator
Debye-Sears Transducer
Multiplier

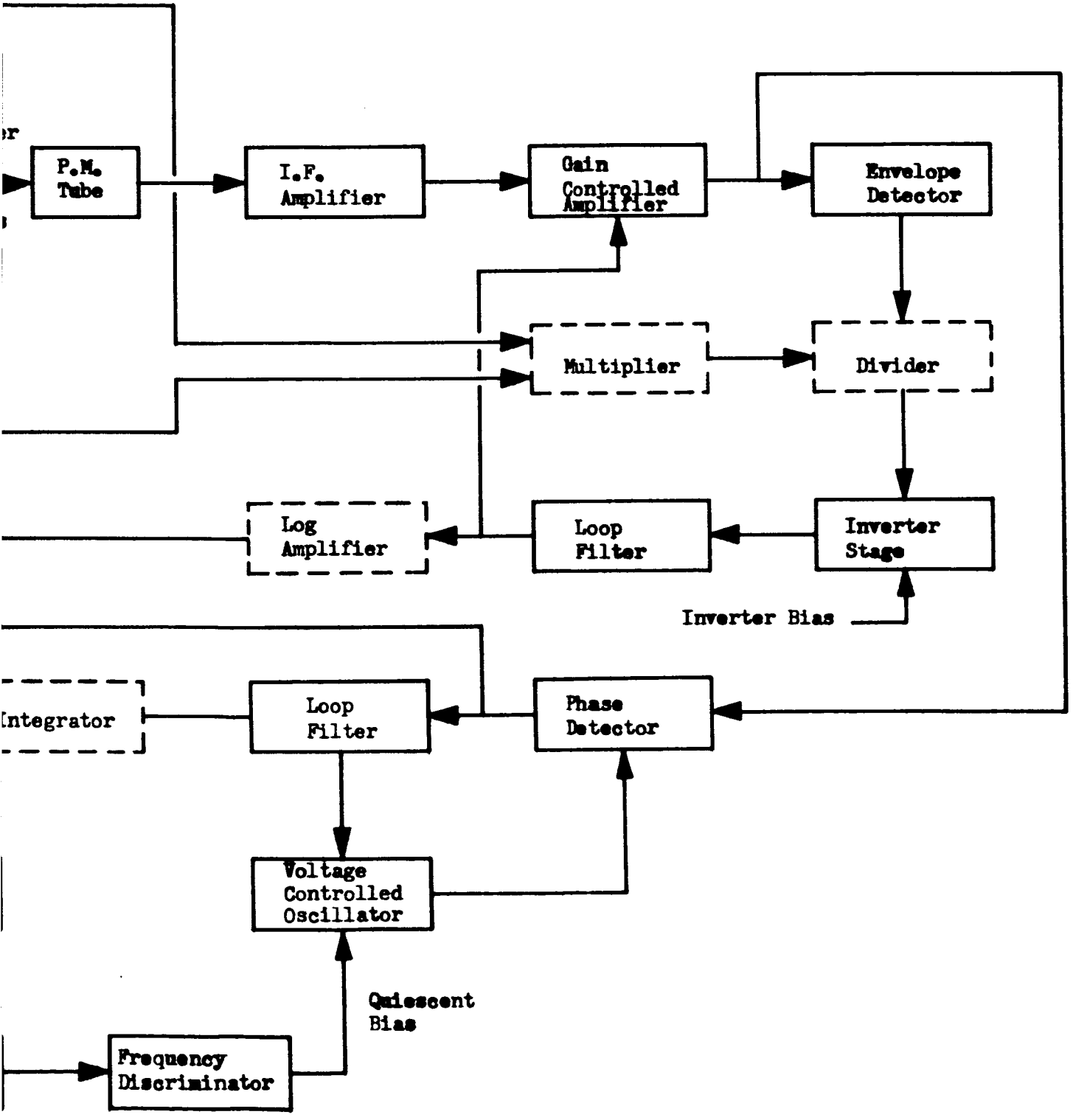

Figure 2.2. Schematic of Implementation for Experiment No. 2

Table 2.1. Experiment No. 2 Equipment List

Quantity	Item
2	Electrically controlled variable-diameter apertures
2	Pairs (optional) of beam-diameter-reduction-telescope type lens, achromatic corrected
5	Aluminized, high quality optical mirrors
1	Debye-Sears modulator, quartz medium
3	Half-aluminized, mirrored beam splitter (50/50), $(2n + 1)\ \lambda/4$ phase shift. (2 optional)
1	Blocking aperture
1	Achromatic lens of same diameter as largest beam diameter (after reduction)
3	Photomultipliers (2 optional)
1	I. F. amplifier (10 or 20 mc center frequency) and BW 1 mc.
1	A. G. C. circuit consisting of a controlled amplifier whose gain follows a logarithmic or linear law, an envelope detector, an inverter stage with inverter bias power supply, and a loop filter
1	Phase lock-loop consisting of a phase detector, loop filter and voltage-controlled oscillator.
1	Operation amplifier-integrator (optional)
3	Averaging circuits (optional)
1	Squaring circuit (optional)
1	Temperature-regulated, crystal controlled oscillator (5 or 10 mc)
1	Frequency multiplier stage
1	Frequency discriminator

Miscellaneous Equipment

The telemetry system will be present for all experiments as will be the tracking and transmitting systems. By itself, the experiment does not need other equipment.

After being multiplied together, the averages are introduced into the a. g. c. loop through an amplifier whose gain is inversely proportional to the product of the averages. The components needed for measuring the amplitude correlation functions are shown dotted in the figure.

The output of the phase-locked loop is processed to give the phase structure function for each correlation distance ρ. This can be done either at the time of the experiment or (if the data is recorded) at a later time.

Component Performance

Debye-Sears Modulator

The experimental arrangement of the modulator is shown in Figure 2.3. The Debye-Sears modulator (Reference 8) will give rise to modulated light components of all orders, i. e. the incident light frequency is modulated by the acoustic drive frequency ω_a to give frequency components

$$\omega_o + m\omega_a, \quad m = 0, \pm 1.$$

It will also shift the exit angle θ_m according to the applied acoustic frequency in relation to the incident angle θ_i. This relation for the 1st order modulation component (m = -1) is

$$\sin \theta_{-1} = \sin \theta_i - \frac{\lambda \omega_a}{2\pi v} \tag{2.1}$$

Here λ is the wavelength of light outside the modulator, and v is the acoustic velocity in the medium. Any random component present in the acoustic drive frequency will not only change the modulation frequency but will also cause the exit angle θ_{-1} to vary. If this effect is large enough, the angular alignment between the optical channels will be affected and amplitude variations will result.

Current commercially available oven-controlled quartz oscillators have rms frequency deviations of from 5×10^{-9} to 5×10^{-11} cps (at a frequency of 5×10^6 cps), depending on the sampling time. When the basic oscillator frequency is multiplied to give an i. f. of 30 or 60 mc. , the r.m.s. frequency deviation is increased in the same ratio.

Drift of the nominal frequency in these same instruments may average about 10^{-15} cps under normal operating conditions (25° C±5° C).

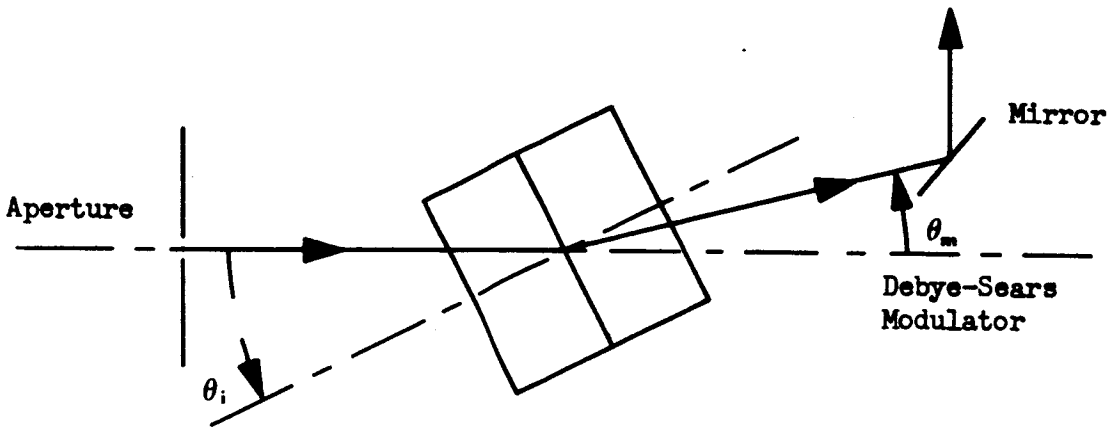

Figure 2.3. Debye - Sears Modulator

Using the small angle approximation, Equation 2.1 becomes

$$\theta_{-1} = \theta_i - \frac{\lambda \omega_a}{2\pi v}$$

The variance in θ_{-1} will be $\sigma_\theta = \frac{\lambda}{v} \sigma_f$ (m = -1). Using fused quartz for the acoustic medium, for which $v = 5.79 \times 10^3$ m/sec, a wavelength $\lambda = 1.15\mu$ and the frequency variance $\sigma_f = 5 \times 10^{-9}$ cps, the variance of θ becomes $\sigma_\theta \approx 10^{-18}$ rad, which is negligible.

The first order side band (m = -1), which is combined with the input from the other aperture, can be made to give its maximum output if the incident light satisfies the Bragg condition

$$\theta = \theta_\beta = \frac{\omega_a}{2\pi V} .$$

In one measurement made in a water medium (Reference 9), the power in the first order mode was experimentally determined to be around 90% of the incident power. Since the power distribution is independent of the refractive index, this value may also be expected to hold for quartz media.

There should be no great power loss in the modulation process. It should be noted that the phase and amplitude are functions of both time and space.

The basic stages comprising the a. g. c. circuit are a gain-controlled stage, a synchronous detector (with proper filtering, an ordinary full-wave rectifier could be used to extract the signal envelope), an inverter and a loop filter (Reference 10). The gain-controlled stage can be considered to attenuate the incoming signal so that the a. g. c. output is a constant amplitude signal. The law of attenuation followed by the gain-controlled stage is some function of the control voltage. The laws usually followed are either logarithmic or linear. Such a. g. c. loops can cover a fairly large dynamic range. Based on the mean signal power, the a. g. c. loop should easily be able to compensate for 30 db changes above and below this mean.

Analysis of the a. g. c. with a linear attenuation law leads to a non-linear problem. However, if the law followed is logarithmic, a linearization is possible and the analytical problems are eased. This is the approach taken here. The flow of the signal is pictured in Figure 2.4.

Automatic Gain Control and Phase-Locked Loop

In previous reports (References 1 and 11), the basic ideas behind the measurement of the phase structure function with a phase-locked loop were described. A fuller discussion is given here.

Selection of a phase-locked loop and a. g. c. circuitry instead of a simple discriminator and limiter circuit is based on the large dynamic ranges needed to adequately cover the amplitude and phase variations expected. This is especially true of the phase measurements and, except for the benefits of the a. g. c. in giving the statistics of amplitude fluctuations, it would be possible to use a limiter and filtering arrangement to keep the amplitude of the input signal to the phase-locked loop nearly constant.

The importance of a constant amplitude input to the phase-locked loop can be seen from the basic equation of the p. l. l. output (Reference 12):

$$\theta(t) = K \int_0^t \int_0^\tau h(\gamma - \tau)\, A(\gamma) \sin(\phi(\gamma) - \theta(\gamma))\, d\gamma\, d\tau \qquad (2.2)$$

Here $A(t) \sin \phi(t)$ is the input to the phase-locked loop and $\theta(t)$ is the output; $Kh(t)$ is the loop filter impulse response. Ideally, when $A(t)$ is constant, $\theta(t) \approx \phi(t)$, but with $A(t)$ fluctuating, errors will be introduced.

An analysis of the a. g. c. and p. l. l. circuitry follows.

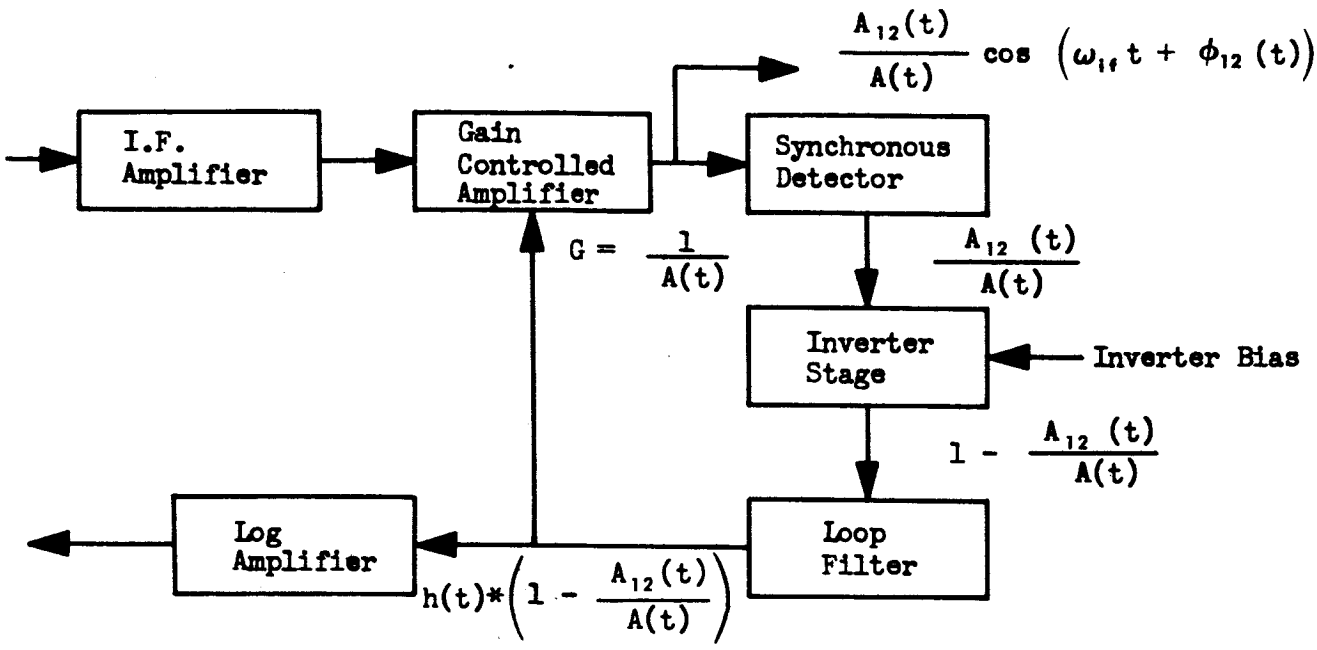

Figure 2.4. Schematic of A.G.C. Circuitry

A.G.C. Analysis. The signal out of the i.f. amplifier can be written as

$$A(\bar{x},t)\ A(\bar{x}+\bar{\rho},t)\ \cos(\omega_{if}t + \phi(\bar{x}+\bar{\rho},t) - \phi(\bar{x},t))$$

where $A(\bar{x},t)$ and $A(\bar{x}+\bar{\rho},t)$ are proportional to the amplitudes at the sampling apertures; likewise $\phi(\bar{x}+\bar{\rho},t)$ and $\phi(\bar{x},t)$ are the phase values at the apertures. For convenience, the following quantities are defined:

$$A(\bar{x}+\bar{\rho},t)\ A(\bar{x},t) \equiv A_{12}(t)$$

and

$$\phi(\bar{x}+\bar{\rho},t) - \phi(\bar{x},t) \equiv \phi_{12}(t)$$

The output of the gain-controlled stage is

$$\frac{A_{12}(t)}{A(t)} \cos\left(\omega_{if}t + \phi_{12}(t)\right)$$

Combining the functions of the synchronous detector, the inverter and the loop filter gives the input to the gain-controlled stage. The input to the gain-controlled stage is the function

$$E(t) = h(t) * \left(1 - \frac{A_{12}(t)}{A(t)}\right)$$

Here h(t) is the impulse response of the loop filter and * signifies the convolution operation. This signal is now modified according to the logarithmic law giving

$$A(t) = 10^{\left\{K_1 h(t) * \left(1 - \frac{A_{12}(t)}{A(t)}\right)\right\}} \qquad (2.3)$$

K_1 is the sensitivity of the gain-controlled stage in db/volt. The gain of the input stage is made the reciprocal of this quantity. As it is, A(t) is a highly non-linear quantity. If the loop's control is effective so that A(t) never varies more than 30 db from the value of $A_{12}(t)$, the approximation

$$1 - \frac{A_{12}(t)}{A(t)} \simeq 20 \log_{10} \frac{A_{12}(t)}{A(t)}$$

can be made so that

$$A(t) \simeq 10^{\left|20K_1 h(t) * \log_{10} A_{12}(t) \,/\, A(t)\right|} \qquad (2.4)$$

and the voltage gain of the control stage is

$$G = 10^{-\left|20\, K_1 h(t) * \log_{10} A_{12}(t) \,/\, A(t)\right|}$$

It is easily seen that this stage acts as an attenuator.

There are two areas of interest to investigate. The first is what statistics of amplitude fluctuation can be computed; the second is the variance of the input amplitude to the phase-locked loop.

If the signal A(t) is the input to a logarithmic amplifier, the resulting output will be (log to the base 10 is understood)

$$\text{Log } A(t) \simeq 20K_1 h(t) * \left(\log A_{12}(t) - \log A(t)\right) \tag{2.5}$$

The Wiener transform of the autocorrelation function of log A(t) gives the result

$$S_A(\omega) = \frac{(20\ K_1)^2\ H(\omega)\ H^*(\omega)\ S_{A_{12}}(\omega)}{1 + 40\ K_1\ \text{Re}\ \left|H(\omega)\right| + (20\ K_1)^2\ H(\omega)\ H^*(\omega)} \tag{2.6}$$

where

$S_A(\omega)$ is the Wiener spectrum of log A(t)

$S_{A_{12}}(\omega)$ is the Wiener spectrum of log $A_{12}(t)$

Re $\left|H(\omega)\right|$ is the real part of $H(\omega)$

$H(\omega)$, $H^*(\omega)$ are the system function of the loop filter and its complex conjugate, respectively. If $(20\ K_1)^2 \gg 1$ or $20\ K_1\ H(\omega)$, then $S_A(\omega) \simeq S_{A_{12}}(\omega)$. Then the correlation function $C_A(\tau) \simeq C_{A_{12}}(\tau)$ so that the loop output does indeed mirror the statistics of log $A_{12}(t)$.

The statistical quantities which can be calculated are obviously

$$\left\langle \left(\log A(t)\right)^2 \right\rangle_T \text{ and } \left\langle \log A(t) \right\rangle_T$$

where the brackets $\langle\ \rangle_T$ indicate a time average. From the previous paragraph, these statistics are related to those of log $A_{12}(t)$.

A problem now arises in interpreting the experimental statistics. The theory of light propagating in a turbulent medium is based on ensemble averages, while the measured quantities are averaged in time. Theoretical and experimental results can only be compared in a meaningful way if the process under investigation is ergodic. This is an assumption which is made in the following discussion.

The statistics of $\log A_{12}(t)$ are examined next. Based on ensemble averages (denoted by $\langle\ \rangle_E$),

$$\left\langle \left(\log A_{12}(t)\right)^2 \right\rangle_E = \left\langle \left(\log A(\bar{x},t) + \log A(\bar{x}+\bar{\rho},t)\right) \right\rangle_E$$

$$= \left\langle \left(\log A(\bar{x},t)\right)^2 \right\rangle_E + \left\langle \left(\log A(\bar{x}+\bar{\rho},t)\right)^2 \right\rangle_E$$

$$+ 2\left\langle \log A(\bar{x},t) \log (\bar{x}+\bar{\rho},t) \right\rangle_E$$

To establish a relation between this average and that developed in theory would be a difficult task. Suppose, however, that the averages

$$\left\langle A(\bar{x},t) \right\rangle_T \text{ and } \left\langle A(\bar{x}+\bar{\rho},t) \right\rangle_T$$

(assumed equal to the ensemble averages) are known by averaging a fraction of the power at each aperture. Then the signal amplitude before the a. g. c. can be modified to give

$$\frac{A(\bar{x},t)\ A(\bar{x}+\bar{\rho},t)}{\left\langle A(\bar{x},t) \right\rangle_T \left\langle A(\bar{x}+\bar{\rho},t) \right\rangle_T}$$

Taking the logarithm of this, squaring and time averaging gives a function

$$C_{A_{12}}(\bar{\rho},t) = \left\langle \left(\log \left[\frac{A_{12}(t)}{\langle A(x,t)\rangle \ \langle A(x+\rho,t)\rangle} \right] \right)^2 \right\rangle$$

$$= \left\langle \left(\log \left[\frac{A(\bar{x}, t)}{\langle A(x, t) \rangle} \right] \right)^2 \right\rangle_T + \left\langle \left(\log \left[\frac{A(\bar{x}+\bar{\rho}, t)}{\langle A(x+\rho, t) \rangle_T} \right] \right) \right\rangle_T$$

$$+ 2 \left\langle \log \left[\frac{A(\bar{x}, t)}{\langle A(\bar{x}, t) \rangle} \right] \log \left[\frac{A(\bar{x}+\bar{\rho}, t)}{\langle A(\bar{x}+\bar{\rho}, t) \rangle} \right] \right\rangle_T \tag{2.7}$$

Employing the ergodic assumption and the assumptions of spatial homogeneity and time stationarity allows Equation 2.7 to be written

$$C_{A_{12}}(\rho, 0) = 2 \left[C_{LL}(0,0) + C_{LL}(\rho, 0) \right] \tag{2.8}$$

with $C_{LL}(\rho, 0)$ being the log amplitude correlation function to the base 10. In terms of the measured quantity $C_{A12}(\rho, 0)$, $C_{LL}(\rho, 0)$ can be written

$$C_{LL}(\rho, 0) = \frac{1}{2} C_{A_{12}}(\rho, 0) - \frac{1}{4} C_{A_{12}}(0,0) \tag{2.9}$$

Thus, with a little more in the way of signal processing, the output of the a. g. c. can be used to give the log amplutide correlation function.

The variance of the signal amplitude at the p. l. l. input is next examined. For this analysis the amplitude is taken as $A_{12}(t)/A(t)$. Here $A(t)$ has been modified to include the averages $\langle A(\bar{x}, t) \rangle$ and $\langle A(\bar{x}, + \bar{\rho}, t) \rangle$. Making the valid assumption that $\langle A_{12}(t)/A(t) \rangle_T \simeq 1$, the variance in the input amplitude (denoted by σ_m^2) will be

$$\sigma_m^2 = \left\langle \left(1 - \frac{A_{12}(t)}{A(t)} \right)^2 \right\rangle_T$$

As long as the a. g. c. loop keeps $\frac{A_{12}(t)}{A(t)} \simeq 1$ so the approximation

$$1 - \frac{A_{12}(t)}{A(t)} \simeq 20 \log \frac{A_{12}(t)}{A(t)}$$

can be used, the variance of the amplitude can be written as

$$\sigma_m^2 \simeq \left\langle \left(20 \log \frac{A_{12}(t)}{A(t)} \right)^2 \right\rangle_T$$

With knowledge of the Wiener spectrum of $A_{12}(t)$, $S_{A_{12}}(\omega)$, and $A(t)$, $S_A(\omega)$ or the autocorrelation function of $20 \log \left[A_{12}(t)/A(t) \right]$, the variance σ_m^2 can be calculated.

From Equation 2.5 it is easily seen that

$$S_M(\omega) = \frac{S_A(\omega)}{K_1^2 H(\omega) H^*(\omega)} \quad , \tag{2.10}$$

where $S_m(\omega)$ is the Wiener spectrum of $20 \log \frac{A_{12}(t)}{A(t)}$. The variance in amplitude is related to $S_m(\omega)$ by

$$\sigma_m^2 = \frac{1}{2\pi} \int_{-\infty}^{\infty} S_m(\omega)\, d\omega$$

Using Equations 2.6 and 2.10, the variance becomes

$$\sigma_m^2 = \left(\frac{200}{\pi} \right) \int_{-\infty}^{\infty} \frac{S_{A_{12}}(\omega)\, d\omega}{1 + 40 K_1 \mathrm{Re}\, H(\omega) + (20 K_1)^2 H(\omega) H^*(\omega)} \tag{2.11}$$

If the a.g.c. is designed so that $\sigma_m \ll 1$, the amplitude fluctuations of the signal into the p.l.l. should cause no problems.

The analysis in the case of a "linear" gain control law (gain inversely proportional to the output of the loop filter) is non-linear and no simple results can be had. However, the statistics which could be calculated would be $\langle A_{12}(t) \rangle$, the amplitude correlation function.

Phase-Locked Loop Analysis. The analysis of the p. l. l. proceeds using Figure 2.5 and the indicated input-output relations. It is assumed that the a. g. c. circuit adequately suppresses amplitude fluctuations and holds the input amplitude at unity.

The measure of error introduced by the loop is given by

$$\phi_\epsilon^2 = \left\langle \phi_{12}^2(t) - \psi^2(t) \right\rangle_T , \qquad (2.12)$$

which is the error in computing the phase structure function $D_{\phi\phi}(\bar{\rho}, 0)$ using $\psi(t)$, the phase output from the p. l. l., rather than the phase input $\phi_{12}(t)$ from which $D_{\phi\phi}(\bar{\rho}, 0)$ should be calculated.

The approach used to evaluate the loop error is that of finding the Wiener spectrum for $\phi_{12}(t)$ and $\psi(t)$ and then evaluating $\left\langle \phi_{12}^2(t) \right\rangle_T$ and $\left\langle \psi^2(t) \right\rangle$ by the well known relation $\sigma_x^2 = R_x(0) = \frac{1}{2\pi}\int_{-\infty}^{\infty} S_x(\omega)\, d\omega$.

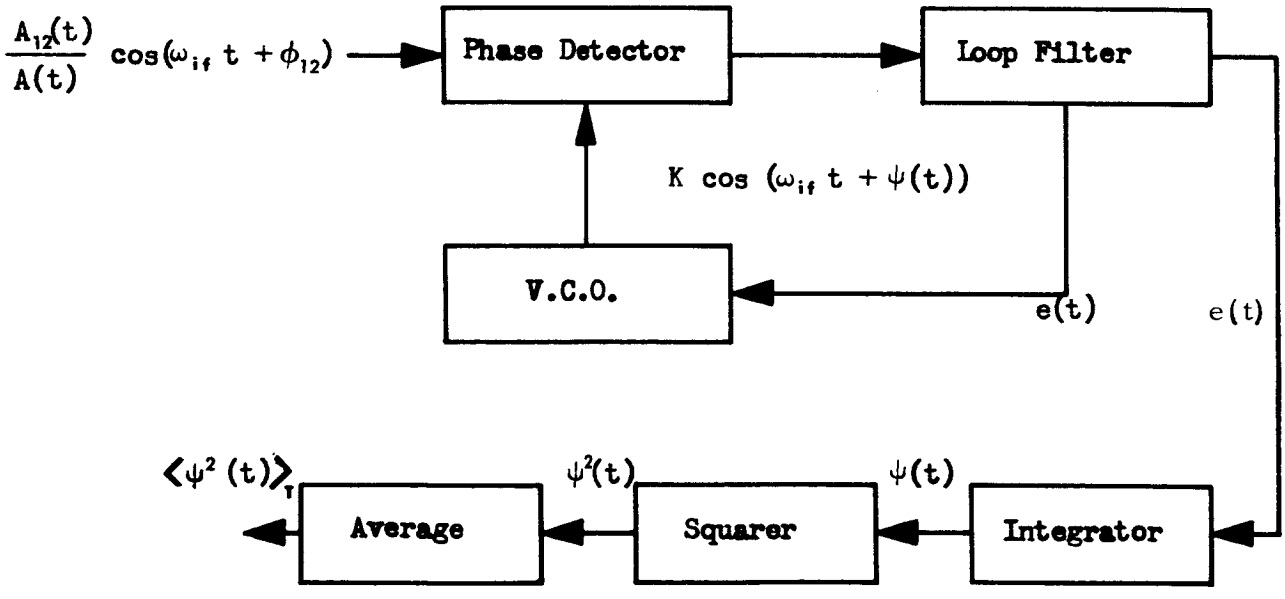

Figure 2.5. Schematic of Phase-Locked Loop Circuitry

Before the quantities given in Equation 2.12 are actually present, the output must be integrated and squared. After these operations, averaging gives the phase structure function. For the analysis, these operations are taken as ideal. As far as the error is concerned, it makes no difference if these operations are done along with the experiment later.

Equation 2.12 may be rewritten as

$$\phi_\epsilon^2(\bar{\rho}) = D_{\phi\phi}(\bar{\rho}, 0) - D_{\psi\psi}(\bar{\rho}, 0)$$

when time and ensemble averages are taken equal. Because of this equivalence, $D_{\phi\phi}(\bar{\rho}, 0)$ and $D_{\psi\psi}(\bar{\rho}, 0)$ are the autocorrelation functions of $\phi_{12}(t)$ and $\psi(t)$ when the correlation variable takes the value $\tau = 0$. Then

$$\phi_\epsilon^2 = \left[C_{\phi_{12}}(\tau) - C_\psi(\tau)\right]_{\tau=0} \qquad (2.13)$$

The problem of finding the Wiener spectrum of $\phi_{12}(t)$ and $\psi(t)$ is approached next. Actually $S\phi_1(\omega)$, the spectrum of $\phi_{12}(t)$ is assumed known and the real problem is to solve for $S\psi(\omega)$. To compute this, the spectrum of $C\psi(\tau)$ must be found; this can be done using the phase-locked loop equations.

The output of the p.l.l. can be written

$$\psi(t) = K\int_0^t h(t - \lambda) \sin\left(\phi_{12}(\lambda) - \psi(\lambda)\right) d\lambda$$

Because of the a.g.c., the signal amplitude is taken as unity. K is the loop gain. Assuming that the loop can keep $(\phi_{12}(\lambda) - \psi(\lambda)) \leq \pm \pi/2$, and using the piecewise-linear approximation, $\sin x \simeq 2/\pi x$, the spectrum of $\psi(t)$ is (Appendix G)

$$S\psi(\omega) = \frac{\frac{2K}{\pi\omega}}{\left(\frac{2K}{\pi\omega}\right)^2 - 1}\left[\frac{4K^2\left|H^2(\omega)\right| + 4K\omega\pi\,\mathrm{Im}\left\{H(\omega)\right\} - (\omega\pi)^2}{4K^2\left|H^2(\omega)\right| + (\omega\pi)^2}\right] S_{\phi_{12}}(\omega) \qquad (2.14)$$

Finally, the error in the phase structure function as it depends on the loop filter and the input Wiener spectrum of $\phi_{12}(t)$ can be written

$$\phi\epsilon = \frac{1}{2\pi}\int_{-\infty}^{\infty}\left[S_{\phi_{12}}(\omega) - S\psi(\omega)\right] d\omega$$

or using Equation 2.14,

$$\phi_\epsilon = \frac{1}{2\pi}\int_{-\infty}^{\infty} S_{\phi_{12}}(\omega)\left\{1 - \frac{(2K)^2\left[4K^2\left|H^2(\omega)\right| + 4k\pi\omega\,\mathrm{Im}\left\{H(\omega)\right\} - (\omega\pi)^2\right]}{\left[(2K)^2 - (\pi\omega)^2\right]\left[4K^2\left|H^2(\omega)\right| + (\pi\omega)^2\right]}\right\} d\omega \qquad (2.15)$$

The derivation considers the signal $\phi_{12}(t)$ existing for the interval $(-\infty, \infty)$. For finite time intervals of observation $[-T, T]$, the proper spectrum to use is that of the truncated function

$$\left[u(t+T) - u(t-T)\right]\phi_{12}(t), \qquad \text{where } u(t)$$

is the unit step function. Here $[-T, T]$ must be interpreted as the time interval during which the condition $\phi_{12}(t) - \psi(t) \leq \pm\frac{\pi}{2}$ is met and not the time the signal is actually present. It should be emphasized that the spectra $S\phi_{12}(\omega)$ and $S_A(\omega)$ are derived from the time, not spatial variations in phase and amplitude.

These spectra are not available from the present experiment but must be obtained from Experiment No. 1. A theoretical estimate of their form can be found using the theory of frozen in turbulence as done in Reference 3. Experimental evaluation of the spectra can be had from the data of Experiment No. 1. Preliminary data from this experiment would thus be of great use in designing the equipment for the present experiment.

Discussion

Aside from the acoustical modulator, the optics portion of the measurement system acts merely to guide the light field sampled by the aperture. As such, angular and centerline alignment of the two guiding optical systems is critical, with angular alignment the overriding cause of a decreased signal-to-noise ratio, as discussed in Appendix E and Experiment No. 1. The expression for the S/N ratio in Experiment No. 2 is the same as that derived in Equations 1.9 and 1.10 of Experiment No. 1.

Choice of the size of the sampling aperture as dictated by the error $D_{\phi\phi}(r_c)$ (discussed in Experiment No. 1) pertains directly to the choice of the aperture size used in the present experiment.

The components unique to the present experiment are the electronic circuitry and the Debye-Sears modulator. These will be looked into more fully.

The selection of the Debye-Sears modulating frequency is based on four requirements: the practical matters of (1) being able to build an i.f. amplifier whose bandpass is large enough to accommodate the spectrum of the random signal, (2) having photodetectors with acceptable frequency response, (3) having the unwanted diffraction modes (or orders) separated in angle from the usable mode so that they may be easily blocked out, and (4) being able to drive the modulating medium at the selected i.f. frequency.

In connection with these requirements, the following facts are known. Preliminary measurements and calculations on amplitude and phase fluctuation spectra show that the spectrum of amplitude fluctuations is negligible above 1 Kc. and the spectrum of phase fluctuations negligible above 10 Kc. These values hold for stationary experimental conditions. In some cases where a relative velocity exists between the transmitter and measurement equipment, as will be the case for earth-satellite links, the spectrum may be widened by as much as a factor of 10 (Reference 13). Neither the i.f. amplifier nor any other wide-band component used in either the a.g.c. or the p.l.l. should be of concern, since 10% bandwidths are easily obtained when center frequencies of 10 mc. or above are used. An i.f. amplifier of center frequency 10-20 mc. with a 1 mc. bandwidth will be quite adequate. Should this bandwidth allow too much noise power through, the bandwidth could be made smaller based on preliminary data from Experiment No. 1 or the present experiment. The medium producing the diffraction modes can be driven at megacycle frequencies if quartz is used as the medium.

Photodetectors (photomultipliers) presently available have usable bandwidths up to 100 mc. so should not be a limiting component as far as frequency response is concerned.

The angular separation between successive orders exiting from the modulator is

$$\gamma = \frac{c}{v}\frac{f_2}{f_1} \qquad (2.16)$$

where

c is the speed of light (vacuum), m/sec.

v is the acoustic velocity of the medium, m/sec.

f_1 is the light frequency, cps

f_2 is the acoustical frequency, cps.

It may be necessary to use a lens pair before the modulator to decrease the diameter of the incoming beam so that the unwanted diffraction modes can be blocked out. For if the angle γ is such that the modes still overlap a good distance away from the modulator, because of the finite incident beam, measurement errors are sure to occur. By stepping down the diameter of the beam, the overlap could be controlled. (Note: for Experiment No. 2, a lens system may also have to be used after the aperture to keep the beam collimated when the apertures are displaced by distances greater than $L_o/2$ as discussed in Experiment No. 1.)

To prevent phase modulation caused by a changing polarization, the channels should have the same reflection characteristics, i.e. the same number and type of elements. In any practical arrangement where the total number of elements would be kept to a minimum, there would be an extra reflection in one channel. If problems seem to exist with the measurements, this effect could be investigated in greater depth.

The physical layout of the optical and electronics section is shown in Figure 2.2. The lens in front of the photomultiplier is used to focus the incident beams to give a plane-wave phase front at the surface of the photodetector.

So that the light present in the higher order diffraction modes does not scatter into photodetector stops, light-absorbant material must be placed after the modulator and beam splitters. A light shield may be added to the photodetector also. To compensate for the power lost by the beam which passes through the modulator, the beam splitter could be made in other than a 50-50 ratio. This would insure that the average amplitudes of the sampled field were equal at the photodetector.

In previous work (Reference 1), sources of errors in the measurement of the phase structure function were pointed out. Since this section deals with the p.l.l., only the errors in the measurement caused by the p.l.l. will be examined. This error was called loop error in Reference 1.

A point to note, not mentioned before, is that as long as the total time difference between the fields incident on the phototube is much less than the coherence time of the laser, the measurements will not have an error due to laser frequency instability. This condition holds for the measurement links to be proposed.

The electronics section consists of the i.f. amplifier following the photodetector and an a.g.c. circuit which incorporates a logarithmic (or linear) gain-controlled amplifier (or attenuator) in the loop. The phase-locked loop has a voltage controlled oscillator (v.c.o.), whose free-running or quiescent frequency is controlled by the crystal-controlled oscillator which drives the Debye-Sears modulator. This eliminates the problem of having to adjust the center frequency of the v.c.o., which may be drifting, to ω_{if} when the signal is first being acquired for tracking. This does not totally eliminate the acquisition problem. There still will be a period when the v.c.o. is changing its frequency to reduce the phase error $\Lambda(t) = \phi_{12}(t) - \psi(t)$. However, in a loop which is designed so that the ratio of input frequency excursion $\Delta\omega$(rad/sec) to the product of the loop signal amplitude (loop gain × input amplitude) and loop filter cut-off frequency ω_c (rad/sec) is much less than 1/2, locking will eventually occur (Reference 14). In making use of the measurements, one would like to exclude the data taken when the loop was not locked, since there will be a very large error $\Lambda(t)$. To insure good data, the voltage equivalent to $\Lambda(t)$ at the output of the phase detector should be monitored. If this voltage is always less than the voltage equivalent to a $\pm\pi/2$ radian error, the loop is locked. Data taken when the $\pm\pi/2$ radian error has been met should be excluded. To insure even better results, data runs taken during the time $\Lambda(t)$ was greater than ± 1 [rad] should be discarded.

As mentioned before, the results of Experiment No. 1 could provide a basis for the design of the p.l.l. and a.g.c. circuitry.

The biggest problem in implementing the a.g.c. loop is the design of the gain control circuit. An easy way of controlling the gain of a stage, whether a tube or solid-state element is to control the voltage used to bias the element. Undoubtedly the gain variations of the device with bias voltage follow neither the linear nor the power law exactly. However, portions of the gain-vs.-bias voltage curve of the gain-control circuit can be made to approximate the linear or power-of-tens law by using several stages which tend to fit the law or characteristic wanted.

Figure 2.2 is a functional block diagram of the optics and electronics section. The dotted portion indicates the equipment to be added when the log amplitude correlation function is desired instead of the amplitude correlation function. Also shown dotted are the stages needed for the on-site computation

of statistics. If the choice is to record the raw data, the a.g.c. and p.l.l. outputs are fed directly to the telemetry or recording stage. While incidental to this experiment, it should be noted that the spectrum of phase or frequency fluctuations caused by atmospheric turbulence can be computed from recorded values of the output of the p.l.l.

AMPLITUDE CORRELATION MEASUREMENT - EXPERIMENT NO. 3

OBJECTIVE

To obtain the log amplitude correlation function for a laser beam after transmission through the atmosphere, from irradiance measurements made at two points within the received beam.

IMPLEMENTATION

Summary

Computation of the statistics of amplitude or power fluctuations can be done either at the time of the experiment or, by means of recorded data, at a later time. The implementations of these two approaches to the measurement of the log amplitude correlation function of the received laser beam are discussed. Particular attention is directed to the need for component linearity, the probable values of the component-induced errors, and the circuitry for the on-site data reduction.

System Configuration

The Task II report (Reference 1) described three alternative systems for measuring the log amplitude correlation function. Of these, only the systems designated a. and c. are considered here, since the third (b.) is effectively a variation of System c. Figures 3.1 and 3.2 show block diagrams of these two systems, together with a list of the experimental equipment required for each.

System a.

The first system simply transforms the irradiance fluctuations to voltage or current fluctuations through the use of phototubes and amplifiers. These signals are recorded for later analysis. While this method is both simple and flexible, it can only be justified if a more extensive investigation of the statistics of power or amplitude fluctuations is made. Of particular usefulness would be the spectrum, probability density and correlation functions of both the amplitude and log amplitude functions.

To correct for the inevitable drift of the photomultiplier tubes, a calibration circuit comprising a lamp and two retractable mirrors can be

Table 3.1. Experiment No. 3 Equipment List

Qty	Item	Qty	Item
	Direct Computation of Log Amplitude Correlation Function		Recording of Irradiance Functions
2	Photomultiplier tubes	4	Aluminized mirrors
2	Bandpass amplifiers	2	Photomultiplier tubes
2	Averaging operational amplifiers	2	Achromatic objectives
4	Electronic switches	2	D. C. amplifiers
2	Logarithmic amplifiers	1	Extendable aperture housing with variable-diameter apertures
2	Logarithmic amplifiers (D. C., gain-controlled)	2	10 Å filters
4	Aluminized mirrors	2	Electronic switches
2	Achromatic objective lenses	1	Calibration lamp
1	Extendable-aperture housing with variable-diameter apertures	2	Retractable mirrors
2	Differential amplifiers		Supplementary Equipment
4	Low-pass filters		
1	Multiplier (quarter-square type)	1	Two-track tape recorder
1	Averaging operational amplifier (baseband)	1	Telemetry system
2	10 Å filters		

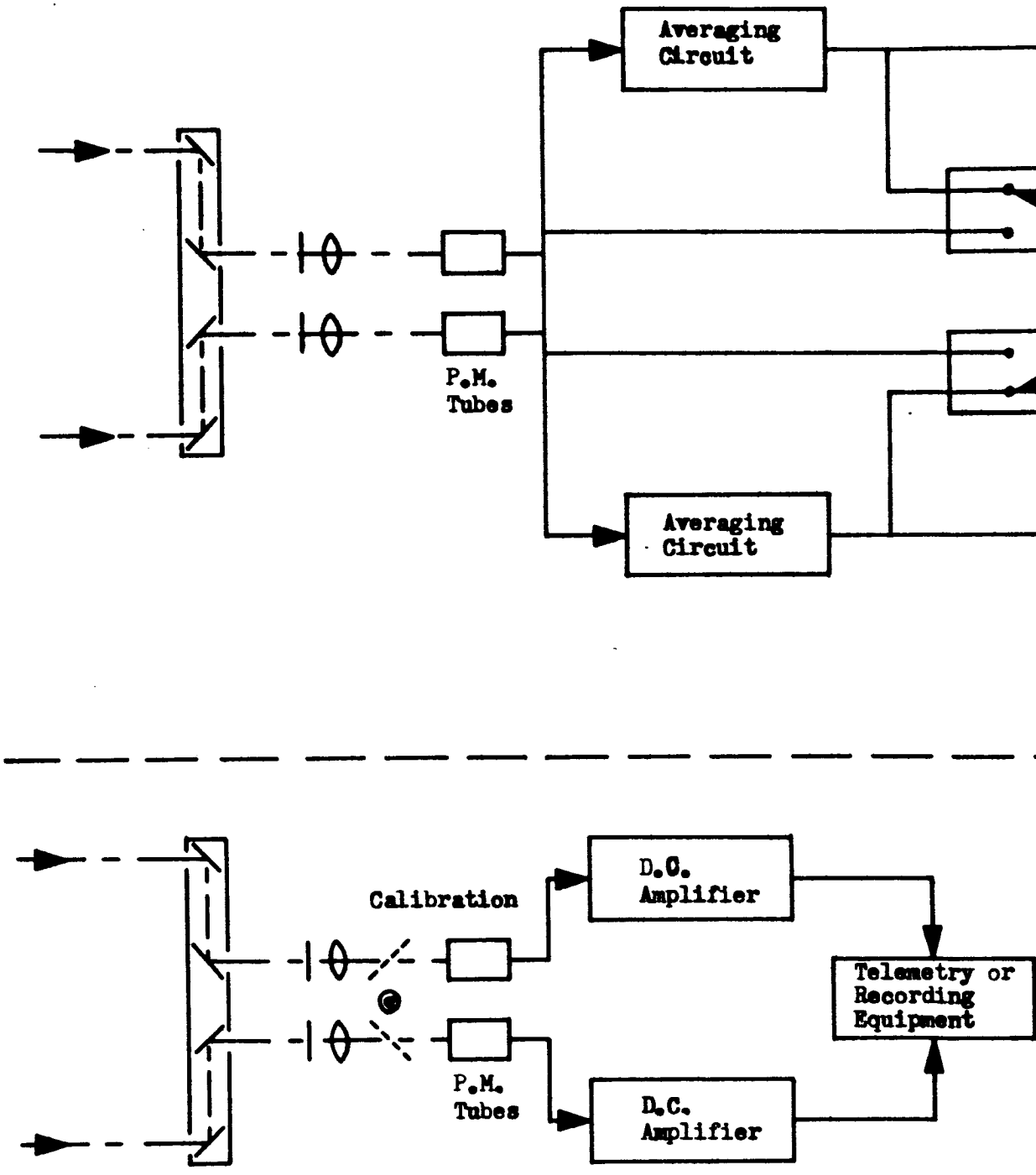

Figure 3.1. Configuration for Logarithmic Amplitude Correlation Measur
(Recorded Data)

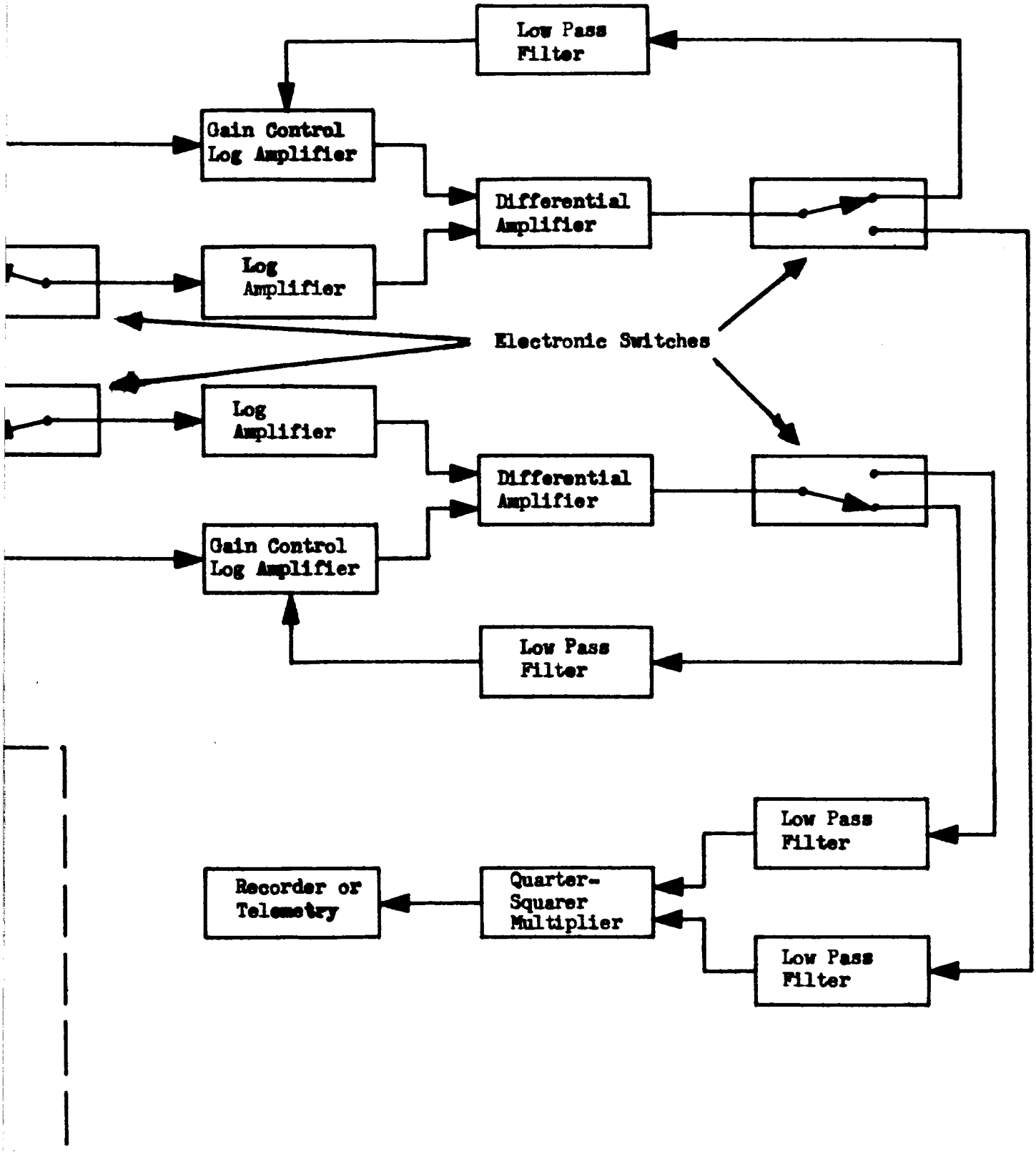

ement

Figure 3.2. Configuration for Direct Computation of Logarithmic Amplitude Correlation Function

used. Calibration should be done before, after, and during each experimental run to detect any change in photomultiplier operation and adjust statistical computations accordingly.

Implementation of this system is easily achieved by using two signal processing channels, each consisting of a photomultiplier tube and one or two stages of d. c. amplification.

System c.

Since this system does real-time computation of the log amplitude correlation function, it is more complicated than System a. The logarithm of the average $\langle A^2 (\bar{x}, t) \rangle$ is computed as well as the logarithm of the instantaneous quantity $A^2 (\bar{x}, t)$ (the values actually computed are proportional to amplitude squared or power). To insure that the logarithmic computations are equivalent, the input of one amplifier is switched alternately from the average value $\langle A_1^2 (\bar{x}, t) \rangle_T$ to the instantaneous value $A^2 (\bar{x}, t)$. The gain of the other amplifier is controlled by the difference between the value of log $\langle A^2 (\bar{x}, t) \rangle$ as computed by one amplifier and that computed by the gain-controlled amplifier. When the difference is zero, the condition $\log \langle A^2 (\bar{x}, t) / A^2 (\bar{x}, t) \rangle = 0$ is assured. The gain-controlled logarithmic amplifier operates at baseband, and while the other log amplifier has an input filter centered at the sampling frequency, its output is also at baseband, as are the differential amplifiers.

At the output of the differential amplifiers are electronic switches which are synchronized with the sampling switch that feeds the log amplifier. In one position, the switch feeds the gain-control circuit, while in the other it feeds the quarter-squarer multiplier (Reference 15) from which the log amplitude correlation function

$$C_{LL} (\bar{\rho}, 0) = \frac{1}{4} \left\langle \log \left[\frac{A^2 (\bar{x}, t)}{\langle A^2 (\bar{x}, t) \rangle} \right] \log \left[\frac{A^2 (\bar{x} + \bar{\rho}, t)}{\langle A^2 (\bar{x} + \bar{\rho}, t \rangle} \right] \right\rangle$$

is computed.

The operation of quarter-squaring multiplication is best done at baseband, so low-pass filters are placed ahead of this circuitry. After being computed, the correlation function is either recorded or telemetered. Data is recorded for each value of $\bar{\rho}$.

Component Analysis

The important qualities which the signal processing components must have in this experiment are good linearity, large dynamic range, high gain stability and (for System a.) good matching of channel gain characteristics. These are obviously important since any saturation or nonlinearity will bias the statistics of the amplitude fluctuations.

Dynamic Range

First the dynamic range and operating point required for a complete channel will be determined. The signal power P_s at the output of the photomultiplier tube in the absence of turbulence, referred to a unit resistance is

$$P_s = \left(\frac{4 \eta q P_L \prod_{i=1}^{n} \tau_i A_r}{\pi (R \theta_T)^2 \hbar\omega} \right)^2 \qquad \left[\text{watts}\right] \qquad (3.1)$$

where

η is the quantum efficiency of the detector photosurface

P_L is the laser output power

$\prod_{i=1}^{n} \tau_i$ is the product of the atmospherical-optical component transmittance

A_r is the effective area of the receiver aperture (circular)

q is the electronic charge in coulombs

$\hbar\omega$ is Planck's constant $h/2\pi$ times the radian frequency ω of the laser radiation

R is the range to the detector

θ_T is the transmitter beamwidth to the half-power points of the transmitter pattern

The signal-to-noise ratio, including background but not dark current is, at the photomultiplier output

$$\frac{S}{N} = \frac{\eta P_s^2}{2 \hbar\omega \Delta B_o (P_s + P_B)} \qquad (3.2)$$

where

P_s = average received signal power

P_B = average received background power

ΔB_o = bandwidth of the filter following the photomultiplier.

A check on the maximum power density at the photosurface should also be included. For a system with no focusing lens (no diffraction), the maximum irradiance H_{max} at the photoelectric surface is

$$H_{max} = \frac{4 P_L \prod_{i=1}^{n} \tau_i}{\pi (R\ \theta_T)^2} \quad \left[\frac{\text{watts}}{m^2}\right]$$

In case a lens is used in the system, an approximate expression for the maximum irradiance at the focal plane is increased by the factor $4/\pi^2 \times A_r^2/(1.22 f\lambda)$, where A_r is the effective aperture area, f is the lens focal length, and λ is the wavelength of the incident light.

Equation 3.1 can be used to establish the mean power level of the processed signal at which the various components must operate. To find the dynamic range which the components must have, the probability density function of the amplitude or power fluctuations must be known; it then becomes possible to compute the percentage of the data which is affected by the nonlinearity or saturation of the component when the input is greater than its usable (dynamic) range. For instance, the current from the phototube is related to the incident power by $i = \eta q P_s/\hbar\omega$. If i_1 and i_2 are the

current levels at which this linear relation fails to hold, then the percentage of data which is biased by not having a greater usable dynamic range is $1 - F(i_1 \leq i < i_2)$ where $F(i_1 \leq i \leq i_2)$ is the cumulative distribution function

$$F(i_1 \leq i \leq i_2) = \int_{i_1}^{i_2} p(x)\, dx, \quad p(x) \text{ being the probability density function.}$$

From previous investigations (Reference 16), there is reason to believe that the normalized intensity fluctuations of light received through a turbulent atmosphere have a log-normal distribution. Since intensity is related to power through the intrinsic impedance of the propagation medium, the received power will have the same distribution. Mathematically, if the quantity x has a log-normal distribution, then it has the cumulative distribution function

$$p(\log x) = \frac{1}{\sqrt{2\pi}\,\sigma} \int_{-\infty}^{\log x} \exp\left\{ - \frac{(y - \bar{y})^2}{2\sigma^2} \right\} dy$$

where $\bar{y}$ is the mean value of y and σ is the standard deviation. Thus, the percentage of unbiased data in terms of the normalized received power P_1/P_o is

$$1 - F\left(\frac{1}{2} \log \frac{P_1}{P_o} \leq \frac{1}{2} \log \frac{P}{P_o} \leq \log \frac{P_2}{P_o} \right) = 1 - \frac{1}{\sqrt{2\pi}\,\sigma} \int_{1/2 \log \frac{P_1}{P_o}}^{1/2 \log \frac{P_2}{P_o}} \exp\left\{ - \frac{(y - \bar{y})^2}{2\sigma^2} \right\} dy$$

which in terms of the tabulated error function

$$\text{Erf}(a) = \frac{1}{\sqrt{2\pi}} \int_{-\infty}^{a} \exp\left\{-\frac{\gamma^2}{2}\right\} d\gamma$$

is

$$1 + \text{Erf}\left\{\frac{1}{2\sigma}\left(\log\frac{P_1}{P_o} - \overline{\log\frac{P}{P_o}}\right)\right\} - \text{Erf}\left\{\frac{1}{2\sigma}\left(\log\frac{P_2}{P_o} - \overline{\log\frac{P}{P_o}}\right)\right\} \quad (3.5)$$

where σ^2 is the variance of $\log (P/P_o)$ and $\overline{\log (P/P_o)}$ is the mean of $\log P_1/P_o$.

These last quantities can be derived from theory (Reference 16) to permit approximate determination of the necessary component dynamic range. Experimentally, the problem is that σ^2 and $\overline{\log (P_1/P_o)}$ must themselves be measured before the needed dynamic range can be specified. The best that can be done is to choose components of large dynamic range and look at the resulting statistics. During the measurement, the dynamic range of the components can be purposely limited in a known manner (e. g. clipped at a certain level) in incremental levels, and the output statistics examined to see if the limiting process changes the statistics. If the statistics do not change up to a certain point, the range of the measuring equipment can be considered adequate.

As an example of the dynamic range possible with photomultipliers, consider the RCA type 931A (an S-4 surface) (Reference 17). This PM has very good linearity over an 80 db range, and can be safely used at light levels (irradiance) up to approximately 5×10^{-5} $[\text{watts/cm}^2]$. Pre-experiment investigations should be performed on this, as on all equipment in order to check out the dynamic range.

The dynamic range of available logarithmic amplifiers is around 80 db and the dynamic range of the multiplier circuit can be expected to be about 60 db. The latter will be the limiting factor for the dynamic range of the entire measurement system.

Component Errors

The components following the photomultiplier in both systems are highly stable, low level d. c. amplifiers operating at microvolt input levels.

Amplifiers currently available have amplitude responses which vary less than .01% over a frequency range of 0 to 10 Kc, together with a gain stability of .01%. In system b., the pulse repetition frequency of the electronic switches will determine the center frequency of the input to the log amplifiers. The frequency response required of the circuits used for processing the amplitude fluctuation signal has been discussed in Experiment No. 1, (Measurement of Spatial and Temporal Logarithmic Amplitude Correlation Function and Phase Structure Function).

The deviation from linear log amplification is normally ±1 db, but with special attention to construction, this may be reduced to ±0.15 db. The multiplication process is carried out by means of a fairly conventional analog technique using differential amplifiers and a special squaring circuit, the so-called quarter-squarer circuit. The errors here depend on the channel balance, but an accuracy of 1 to 2 percent can be expected. The low-pass filter in the gain-control circuit performs the averaging of $A^2(\bar{x}, t)$ prior to the computation of log $\langle A^2(\bar{x}, t)\rangle$ by the two log amplifiers. It should therefore have a time constant τ which is very much greater than the reciprocal of the fluctuations' cut-off frequency.

STATIONARITY TEST - EXPERIMENT NO. 4

OBJECTIVE

To test the stationarity of the log amplitude correlation function $C_{LL}(\vec{\rho})$ for a laser beam after transmission through the atmosphere, and to measure the spatial wandering of the beam. A secondary objective is to check the isotropy of $C_{LL}(\vec{\rho})$.

IMPLEMENTATION

Summary

After establishing system design criteria for laser beamwidth, detector exposure time and atmospheric transmittance, the analysis considers two basic classes of prospective detectors—film and electronic image tubes—and evaluates them in terms of their applicability for this experiment. It is concluded that either a suitably chosen film or a slow scan vidicon show the most promise, the latter being favored because of its real-time readout capability.

System Configuration

As seen from the diagram of Figure 4.1, the configuration of this system is particularly simple. A Fresnel lens intercepts the incoming laser beam which is imaged by means of a field lens on either a stationary film or a slow scan vidicon (or image orthicon), depending on the detector chosen. The detector integrates the image for a time which is less than the period of the maximum expected frequency of the intensity fluctuations within the laser beam. In this way, a series of "pictures" of the "instantaneous" intensity distribution can be obtained.

Component Performance

Design Considerations

The theory underlying this experiment assumes plane-wave propagation, a condition which is not fulfilled when the beam is narrow. For this reason, the beam should be widened by using wide-aperture optics at the laser transmitter. Since this experiment should be evaluated in conjunction with the results of Experiments 1 and 3, it is also advisable to make all of these measurements over the same optical link and, to the extent possible, under

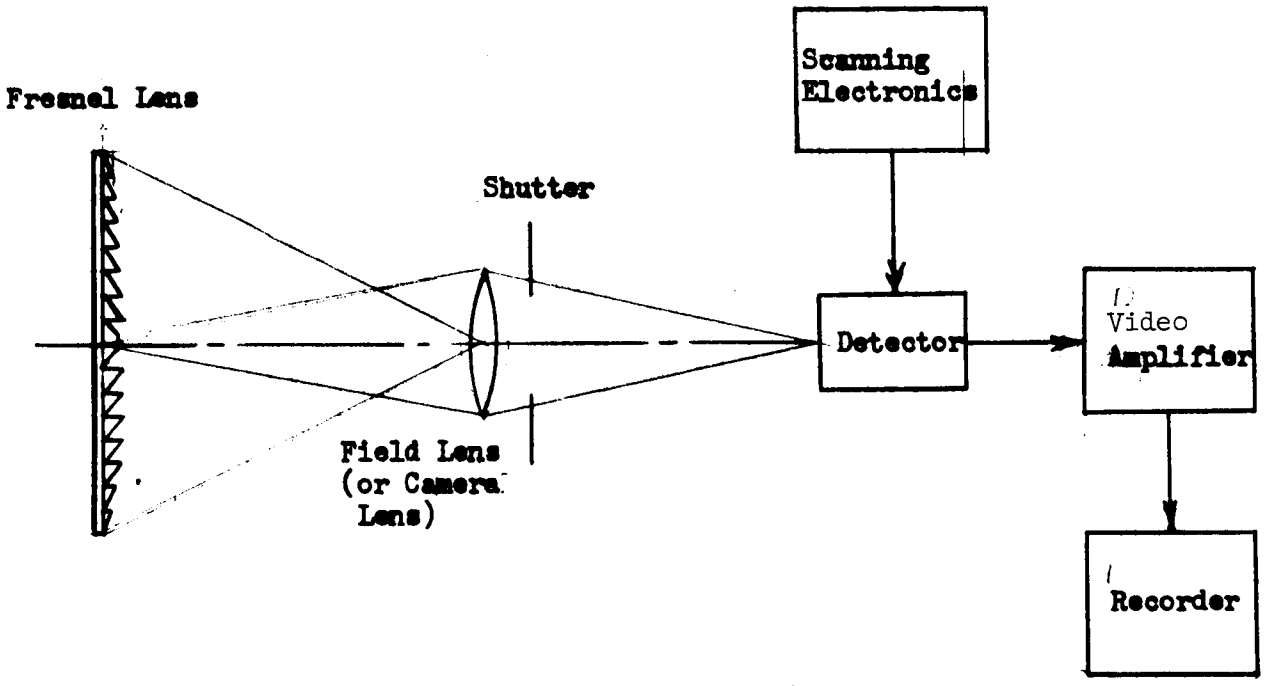

Figure 4.1. Configuration for Stationarity Test

Table 4.1. Experiment No. 4 Equipment List

Quantity	Item
1	He-Ne Gas Laser
1	Laser Power Supply
1	Fresnel Lens (e.g., Bolsey R&D Lens No. 1720)
1	Field Lens ($f/_2$, 1" dia.)
1	Film, Film Holder and Shutter
1	Slow Scan Vidicon
1	Video Amplifier (not required if recorder has low pass preamp.)
1	10 Å Optical Filter (6328 Å Bandpass)
2	Collimating Lenses
1	Transmitting Reflector
1	Magnetic Tape Recorder, 7 channel (6 channel FM carrier recording, 1 channel direct analog) Ampex FR-100A

the same meteorological conditions. In view of the previous statement, this implies that these experiments should also be made with the same trans-

mitter aperture in order to eliminate this variable from the comparison. (For additional comments on the effects of changing the transmitter aperture, see the discussion of Experiment No. 6 - Power Fluctuation Measurement.)

Of particular importance for this experiment is a meaningful definition of the term "instantaneous," since one objective of the measurement is to obtain a series of "instantaneous pictures" of the intensity distribution across the laser beam, from which ensemble averages can be formed for the purpose of determining the log amplitude correlation function for the beam. To establish a quantitative definition of this concept, upon which the choice and design of a detector can be based, the following criterion is invoked. Experimental evidence to date (Reference 18) indicates that the intensity fluctuations involved in the measurement are limited to frequencies of a few hundred cps or less. By designing the detector to measure frequencies up to 1000 cps, the resulting pictures will be "instantaneous" in the sense that the highest frequency components present in the fluctuations will be detected. In terms of detector sensitivity, this means that the experiment should be designed for an exposure time of 1/1000 = 1 millisecond; this is the value that will be used in the following discussion.

Finally, in order to establish a basis for the sensitivity calculations, the size of the receiver aperture must be assumed, and the power loss due to atmospheric attenuation must be known. The largest Fresnel lenses which are easily available at present run to the order of 20 inches in diameter, and this will be taken as the design figure. The degree of atmospheric attenuation depends on both the condition of the atmosphere and the range to the receiver. A transmittance (power received/power transmitted) of 0.15, corresponding roughly to a range of 10 miles, provides a realistic design estimate.

The two basic types of detectors which have possible application in this experiment, namely film and electronic image tubes, will now be discussed.

Silver Halide Film

A typical film for this application has a sensitivity of about 10^{-6} joules/cm^2 for a wavelength $\lambda = 6328$ Å. (A description of film specifications is contained in the discussion of Experiment Nos. 9 and 10.)

Assuming that the receiver optics reduces the cross section of the beam down to an effective film diameter of 3/4 inch, and neglecting absorption in the optical system, the irradiance of the light received by the 20 inch collector is increased in the ratio $k = (20/0.75)^2 = 711$ at the film. If the laser beam just fills the collector (which should be possible at ranges less than about 10 miles), then the minimum detectable received (signal) power P_s, is specified for an exposure time τ by the condition:

$$P_s \cdot \tau = 10^{-6} \left[\frac{\text{joules}}{\text{cm}^2}\right] \cdot A_f ,$$

where A_f is the illuminated film area, in cm^2. In this case, $\tau = 10^{-3}$ sec, $A_f \approx \tau (3/8 \times 2.5)^2 = 4.4\ cm^2$, so

$$P_s = \frac{10^{-6} A_f}{\tau}$$

$$= \frac{(10^{-6})(4.4)}{10^{-3}}$$

$$P_s = 4.4 \times 10^{-3} \left[\text{watts}\right]$$

Assuming an atmospheric transmittance of 0.15, the minimum laser transmitted power P_t is then $P_t = P_s/0.15 = 29$ milliwatts, a requirement which can be met by any of several commercially available CW lasers. (See Appendix A .)

Resolution for films of the type being considered is of the order of 100 lines/mm, although films having considerably higher resolution are available. That such resolution is adequate for this experiment is seen by multiplying the resolution distance, 10^{-2} mm by the linear beam reduction factor $20/0.75 = 26.7$. Thus $(10^{-2})(26.7) = 0.27$ mm is the separation between two points on the incoming wavefront which can just be resolved by the film, according to this criterion. Clearly this represents much better resolution than is required for the correlation measurement.

Recording materials other than conventional silver halide film have been developed, but their suitability for application to the LACE experiments has not been investigated for this report. Brief discussions of three such recording techniques are contained in Appendix D .

Image Tubes

Slow Scan Vidicon and Image Orthicon. The 30-frames-per-second scanning mode employed by standard image tubes makes them unsuitable for use in recording the instantaneous intensity pattern of a laser beam, a task which requires that the entire image be allowed to integrate on the photosurface for the specified exposure time (10^{-3} sec) before being read out by the scanning beam. For this purpose, special slow scan image tubes are available. One such is the General Electro-dynamics Model 7290 slow scan vidicon.

In common with other image tubes, sensitivity data for this special vidicon is given in photometric units, referred to a standard tungsten lamp source at a temperature of 2870°K. A straightforward calculation yields the conversion factor 1 foot-candle = 5×10^{-5} watts/cm^2 for a 6328 Å laser source. Thus the given sensitivity (minimum detectable luminous energy) of 10^{-2} ft-candle-sec, or 10 foot candles for 10^{-3} seconds, converts to 5×10^{-4} watts/cm^2, integrated over this exposure time. This represents the minimum image irradiance at the face of the vidicon which, when integrated for a millisecond, will yield a TV picture (or video tape record) of acceptable quality. Assuming a raster area of about 1 cm^2 (a typical raster has the dimensions 1/2" by 3/8"), the minimum required power at the receiver is 5×10^{-4} watts. Allowing for 15% transmittance as before, the minimum laser power P_t becomes, for this case $P_t = 5 \times 10^{-4}/0.15 = 3.3$ milliwatts, a very modest requirement. At distances shorter than 10 miles the atmospheric transmission is, of course, reduced, and the power required becomes even smaller. A higher irradiance, if needed for any reason, could be achieved by reducing the area of the image at the vidicon by either changing the field lens or reducing the width of the beam at the receiver (by adjusting the transmitter optics).

The resolution of an image tube is a function of the incident illuminance and also deteriorates with time (thus limiting the scan-delay time). However, a resolution of 800 lines is typical for the slow scan vidicon described above with a 1 millisecond scan delay. Assuming a 20 inch collector, this corresponds to a resolution of 40 lines per inch or about 1.6 lines per millimeter in the incident beam. Thus the resolution distance in the beam is less than 1 mm, which is entirely adequate for the correlation measurements.

The image orthicon has a higher sensitivity than the vidicon, although the resolution at low light levels is substantially reduced. For example, the Westinghouse Model WL-22722 high sensitivity image orthicon (which is also capable of slow scan) has a sensitivity of 3×10^{-7} foot-candles for a 1/30th second frame time, with a resolution, at this illuminance, of 200 lines, increasing to around 600 lines at higher light levels.

Standard Vidicon and Image Orthicon. Although, as explained above, these devices are not well suited to the stationarity measurement, they can nevertheless be used if the power fluctuations occurring in the beam during a frame time (e.g., 1/30 sec) can be accepted as an error in the measurement. Errors of this type may in fact be inconsequential in comparison to other experimental inaccuracies, but only an actual test measurement will reveal the magnitude of this effect. In other respects, the conclusions pertaining to the sensitivity and resolution of the slow scan image tubes are applicable here as well.

An important difference between these two image tubes is the greater complexity, and hence higher cost of the image orthicon. For this reason, the vidicon is to be preferred unless the higher sensitivity of the orthicon is clearly needed.

Evaluation of Alternative Measurement Systems

The salient factors governing the choice of a detector for the stationarity measurement will be summarized here.

When comparing the various detectors proposed for this experiment, it is important to keep in mind the interdependence of sensitivity and image resolution as criteria of performance. As one example, the resolution of an image tube is a function of the light level, so that while an image orthicon is capable of detecting a substantially weaker optical signal than is a vidicon, its ability to resolve the image at that level of illuminance may be reduced by a factor of 3 or 4 in comparison to the vidicon at its minimum operating level.

Equally important, the lower absolute sensitivity of the silver halide films compared to that of the image tubes is more than offset by their superior resolution, which enables the illuminance at the film to be increased many hundred-fold (over 700 x in this case) by reducing the size of the optical image and without losing any significant data in the process.

Thus, from the standpoint of sensitivity and resolution, there is little to choose between film and image tubes. On the other hand, film has the unique property that the density of the exposed emulsion (which can be measured with a micro-densitometer) increases logarithmically with the illuminance (or irradiance) of the exposing light (for a given source), a characteristic which could be used to advantage in measuring the log amplitude correlation function.

Another factor weighing in favor of film is the absence of noise generated in the readout process. Readout of the image tubes is accomplished by means of a scanning electron beam which introduces noise into the data and also requires an information bandwidth that increases in size with increasing scan speed. In a vidicon, however, this noise level is much lower than that of the noise generated in the load resistor and video pre-amp, so a high-gain amplifier can be employed to produce useful, high quality video signals even at very long frame times. In practice, the signal-to-noise ratio is less a function of the vidicon than of its associated electronics.

From the standpoint of complexity, film offers the simplest means of recording the beam intensity pattern, an advantage, however, which is of no avail if real-time data processing is required. Among the image tubes discussed here, the vidicon is to be preferred over the image orthicon because of its lesser complexity and consequent lower cost, except in the unusual circumstance where the laser signal is so weak that the greater sensitivity of the orthicon is required. In either case, one of the special slow scan models of these image tubes should be chosen in order to obtain the best experimental data.

In spite of these considerations, the choice of a detector for the experiment may ultimately be dictated by the exigencies of budgetary or other program constraints, coupled with "in-house" availability of particular components and capabilities. For example, the existence of a well-equipped photographic laboratory at or near the experiment site would constitute a legitimate bias in favor of the film technique, while even a standard commercial vidicon, if available with the required electronics, should be utilized at least for exploratory measurements.

SPECTRAL SPREADING MEASUREMENT - EXPERIMENT NO. 5

OBJECTIVE

To measure the frequency spreading of laser light transmitted through the atmosphere, resulting from fluctuations in the refractive index of the air along the transmission path.

IMPLEMENTATION

Summary

The system described measures the spectral spreading of the laser light by splitting the transmitted beam, shifting the frequency of one portion, and measuring the fluctuations in this difference frequency after the two beams have traversed different paths through the atmosphere. The performance of the major system components is discussed, and the origins of the frequency fluctuations (spectral spreading) and their effect on system performance are examined in some detail.

System Configuration

The measurement of the spectral spreading is accomplished by the arrangement shown in Figures 5.1, 5.2 and 5.3. The object of this arrangement is to provide two optical signals of slightly differing frequency, which are made to traverse (to the extent possible) separate paths along which the refractive index fluctuations are statistically independent of each other (Figure 5.1). The two signals are obtained by power-splitting the output beam of a He-Ne gas laser into two beams. (Figure 5.2). One of the beams is then passed through a Debye-Sears acoustically driven, single-sideband-suppressed carrier modulator, and the other is left unaltered. The modulator output frequency is offset from the entering frequency by an amount corresponding to integral multiples of the modulating acoustic frequency ω_a. If the beam is made to enter the modulator entrance aperture at the proper angle of incidence, then nearly all of the incoming signal can be transferred to a frequency separated by ω_a from the entering frequency.

After traversing independent paths, the two optical signals are brought together at the surface of a photomultiplier tube which photomixes them (Figure 5.3). The output of the PM contains a dc term plus a time varying portion centered about the difference frequency, which in this case is ω_a. The signal is then passed through an IF amplifier centered at ω_a, which is

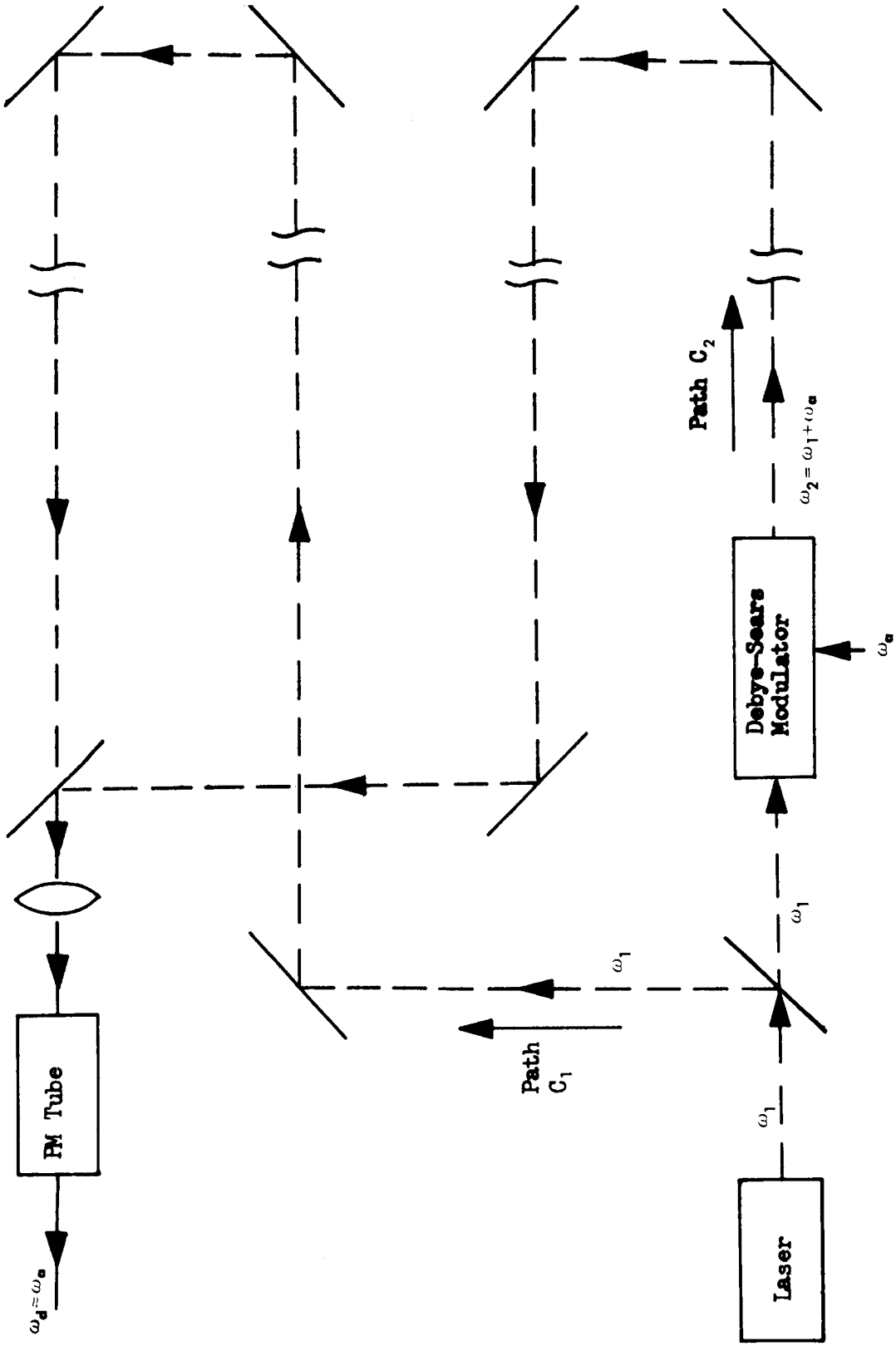

Figure 5.1. Experimental Path Configuration for Spectral Spreading

Table 5.1. Experiment No. 5 Equipment List

Quantity	Item
1	Optical filter
1	Field stop
1	PM tube
1	PM tube power supply
1	IF amplifier - limiter - discriminator combination
1	Spectrum analyzer
1	Oscillograph camera for spectrum analyzer
1	4 track magnetic recorder
1	He-Ne Gas Laser with good single mode output + modulator optics
1	Gas Laser power supply
1	Acoustic frequency modulator (Debye-Sears)
1	Acoustic modulator driver and oscillator
1	Optical beam (power) splitter
6	Plane mirrors
1	Half-silvered mirror
1	Collecting lens
1	Field lens

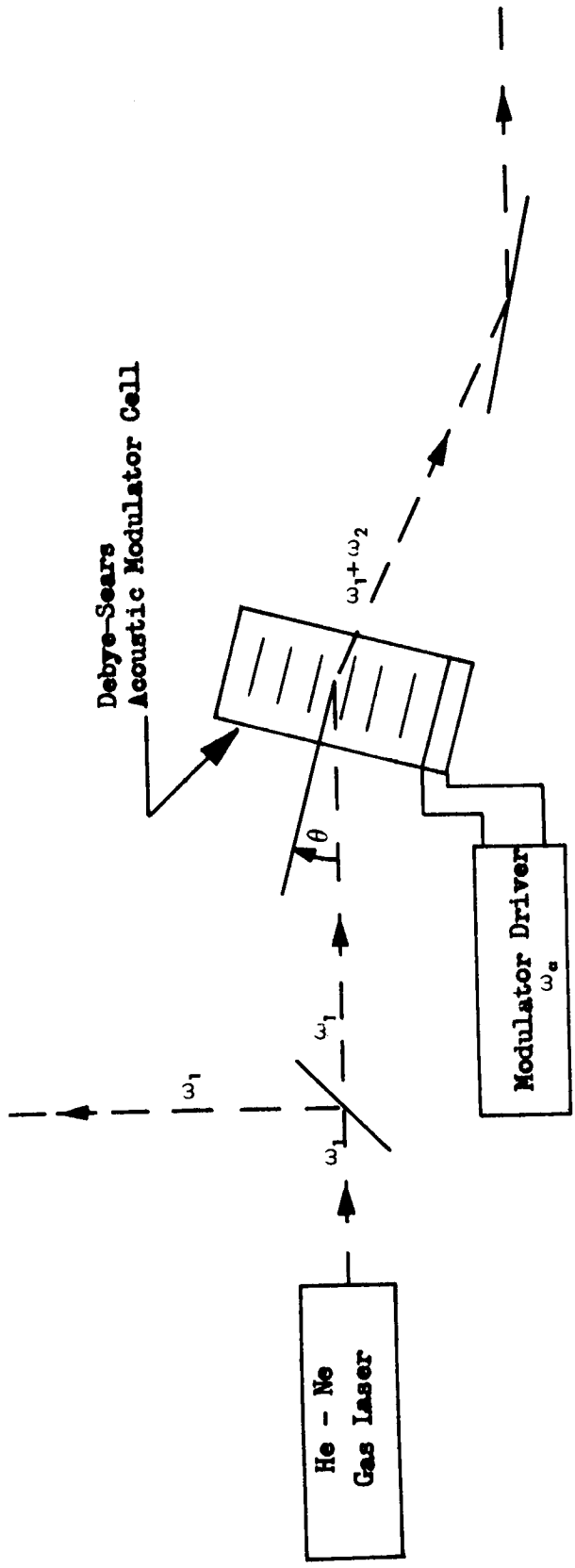

Figure 5.2. Transmitter Arrangement for Spectral Spread Measurement

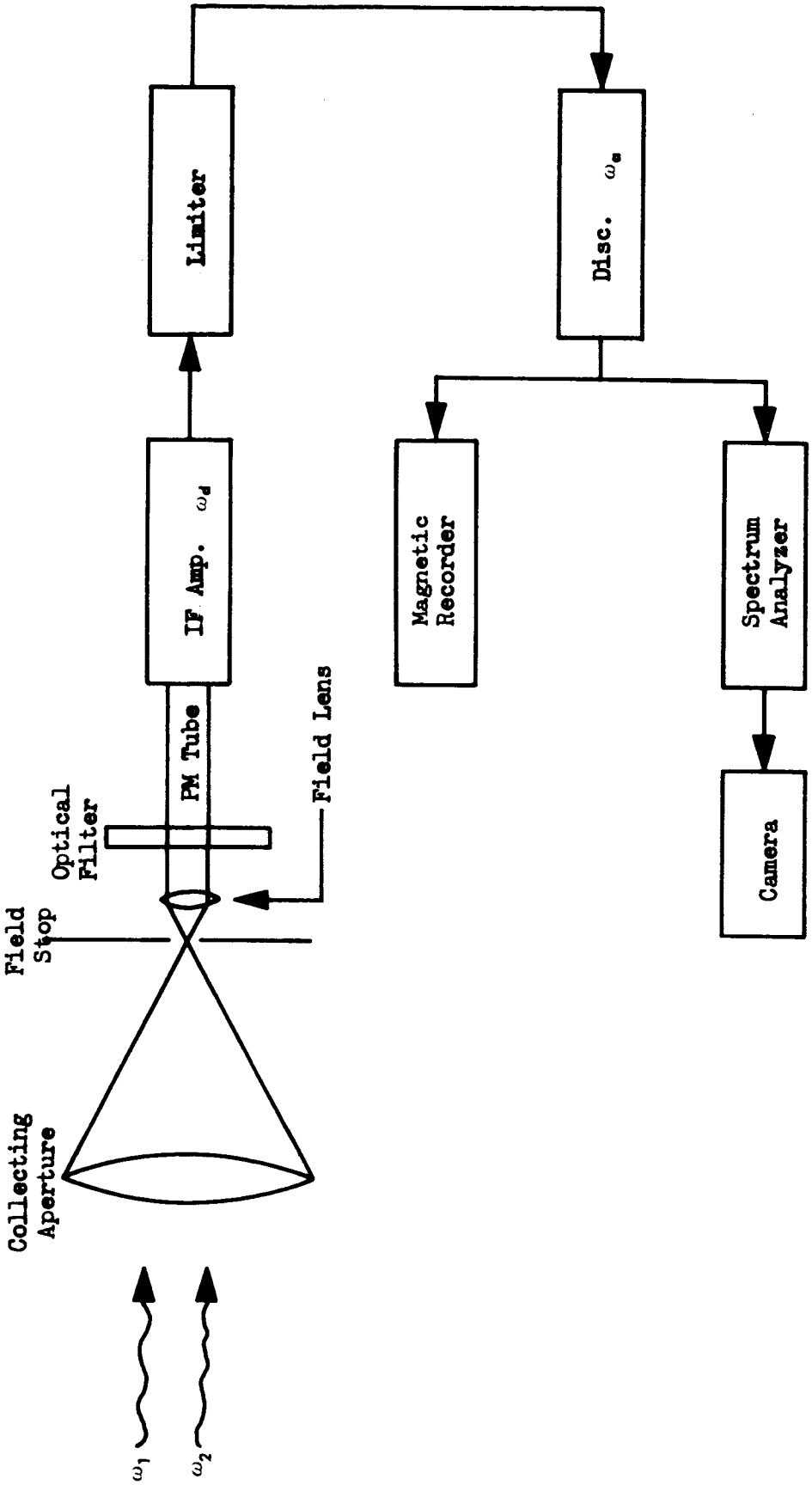

Figure 5.3. Receiver Configuration for Spectral Spread Measurement

followed by a limiter. The output of the limiter is then demodulated using a conventional FM discriminator tuned to a center frequency of ω_a. The output voltage signal from the discriminator is thus proportional to the fluctuation in the instantaneous frequency difference between the two received optical signals. It is the spectrum of the discriminator output which is of principal concern in this experiment.

Two alternative methods of analyzing the data are evident. The first is to record the discriminator output directly and analyze its spectrum at a later time. The other alternative would be to analyze the spectrum in real time, and perhaps by optical presentation of the spectrum on a scope, record on film the spectrum of the analyzed signal. These methods will be discussed further in the following description of the receiver.

Component Performance

Transmitter

From Figure 5.2, it can be seen that the major components at the transmitting end are the He-Ne gas laser and Debye-Sears acoustic modulator. This particular laser is recommended for this experiment since it is the only available optical source having sufficient short term frequency stability to permit measurement of the frequency fluctuations induced by the propagation path. From the several output wavelengths available with this laser, the 6328 Å line should be chosen since it is not only the line of maximum output power, but is also closest to the maximum quantum efficiency of the detector. As with the other proposed experiments, a reasonable degree of stability in the laser output intensity is required, so a well-regulated, low-ripple laser power supply should be selected.

The acoustic modulator is driven at a frequency ω_a and transfers most of the output energy to an optical frequency of $\omega_2 = \omega_1 + \omega_a$. That efficient frequency translation is possible has been experimentally verified (Reference 9), with transfer efficiencies of 90 percent being achieved at angles of incidence θ, equal to the Bragg angle, $\theta_B = \frac{\lambda}{2\Lambda}$ where λ is the optical wavelength and Λ is the wavelength of the acoustic waves in the liquid medium inside the cell. In theory, the other condition which must be satisfied to ensure efficient frequency translation is that $\alpha k_o z = \pi$, where α is the amplitude of the sinusoidal oscillation of the liquid's index of refraction about the average value, k_o is the magnitude of the optical wave vector in the unperturbed liquid medium, and z is the acoustic cell dimension in the direction of the optical wave propagation. The experimental model used an acoustic driving frequency of ω_a = 15 Mc. This frequency corresponds to the IF center frequency at the receiving end. From the demonstration of 15 Mc modulating capability, there appears to be no great obstacle to modulating at some lower HF frequency which, because of the availability of suitable FM receiving equipment, might be preferred.

The other box in Figure 5.2 represents the oscillators and driving amplifier. The oscillator should be crystal controlled (and if possible, the crystal should be placed in an oven such that a short term (1 sec) frequency stability of 1 part in 10^7 is possible) to ensure that the short term frequency stability is good enough to avoid the introduction of a significant bias error in the frequency measurement at the receiving end. If synchronization via cable is provided between the modulator driver and the discriminator in the receiver, the above requirements for frequency stability can be relaxed considerably since then frequency drifts do not create a problem unless the drifting is so fast that it occurs over periods of the order of several microseconds.

Receiver

At the receiving end, shown in Figure 5.3, the first item is the collector lens. The requirements on the size of this lens will to a large extent be dictated by how much signal energy must be collected to provide a reasonable signal-to-noise ratio in the measured and recorded signal. From another standpoint, certain practical limits exist on maximum collector size due to the limited lateral spatial coherence (lateral spatial correlation ~ 1) of an optical signal transmitted over atmospheric paths. This value is on the order of $\sqrt{\lambda R}$ where λ is the optical wavelength and R the range over which the initially plane wave-front signal has traversed the atmosphere. Using λ = 6328 Å and R = 1 kilometer, the spatial correlation distance is roughly one inch. It would appear then that at ranges between 1 and 10 kilometers, aperture sizes much larger than 5 or 6 inches in diameter do not give much in the way of increased post-detection (IF) signal-to-noise power ratio. The quality of the lens or reflector should be such that the lens does not significently alter or add to the existing wavefront distortion.

The next item is the field stop, which limits the receiver field-of-view and reduces the amount of collected background noise power (see Experiment No. 12). The optical bandpass filter which lies immediately to the right of the field lens also serves to exclude unwanted background. The next item is the PM tube which for 6328 Å laser light should use the S-20 surface (See Appendix C). Some thought should be given to a possible distance limitation on C_1 and C_2 (Figure 5.1) since not only is single mode ouput significantly less than the rated total laser output, but in addition, the transmitted "reference" or transmitted "local oscillator" signal configuration represents a somewhat inefficient technique for transmitting information (in this case atmospheric propagation noise) from a signal-to-noise standpoint. Losses incurred with a straightforward video detection signal carrier scheme are on the order of 10-15 db, depending on the post-detection filtering scheme employed. The combination of IF amplifier, limiter and discriminator can best be chosen as a single "black box" specified by a transfer function which gives volts/frequency. The limiter is included to enhance the output signal-to-noise ratio from the discriminator for input (or IF) signal-to-noise ratios

greater than unity, (Reference 19). The overall combination of amplifier-limiter-discriminator can also conveniently be specified to maintain the desired linearity requirements over the expected range of frequency fluctuations.

The last two boxes in Figure 5.3 are concerned with recording the detected and measured information. The upper box represents the more important of the two since the function of the bottom box can be duplicated at a later time from a record of the discriminator output. For recording frequencies down to dc, the magnetic recorder should be an FM carrier recording type such as is available from Ampex (Catalog Model FR-100A). The lower recording method, if used for real time visual inspection in addition to providing the permanent film record, should prove useful in making quick assessments of the validity of the measurements.

Returning to Figure 5.1, it is evident that many plane mirrors must be used. Their sizes and shapes will depend on the exact dimensional layout of paths C_1 and C_2.

Frequency Fluctuations

Fluctuations in the instantaneous difference frequency result principally from three factors. First, it is obvious that any fluctuation in the acoustic modulator driving frequency will introduce fluctuations in the difference frequency. Another cause is the non-synchronous optical path length fluctuations seen by the two signals. The third factor is the short-term frequency drift of the laser, which will introduce uncontrollable fluctuations when the optical path lengths for the two signals differ by roughly the coherence length of the laser single-mode output. Some consideration of laser mode separation for multimode laser output may be pertinent here and should be investigated more thoroughly (Reference 20). The following discussion briefly describes the interrelationships among the three factors contributing to the difference frequency fluctuations. The discussion is intentionally simplified through the assumed validity of the geometrical optics approximation, in order to avoid unnecessary complexity.

Let e_1 and e_2 represent the electric field intensities of the two optical signals at the surface of the photomultiplier tube. It is further assumed that e_1 and e_2 are combined on the photocathode of a PM tube in such a manner that in the plane perpendicular to the direction of propagation (the x-y plane) e_1 and e_2 are independent of x and y. In terms of the laser output radian frequency ω_1, with $\omega_2 = \omega_1 + \omega_a$, e_1 and e_2 are given by

$$e_1 = A_1 \cos \left\{ \omega_1(t)t - \frac{\omega_1(t)\, S_1(t)}{c} + \phi_1 \right\} \qquad (5.1)$$

$$e_2 = A_2 \cos \left\{ \omega_2(t)t - \frac{\omega_2(t)\, S_2(t)}{c} + \phi_1 \right\} \qquad (5.2)$$

where

$$S_1(t) = \int_{C_1} n_1 (s_1, t - \frac{s_1}{c})\, ds_1$$

= optical path length which the signal e_1 arriving at the receiver at time t has traversed in going from transmitter (laser) to receiver (photomultiplier tube) along the path C_1. The integration along the path starts at the receiver and extends backwards to the transmitter.

$n_1 (s_1, t - \frac{s_1}{c})$ = index of refraction at the point along the path identified by the variable s_1 at the time $t - \frac{s_1}{c}$.

$$S_2(t) = \int_{C_2} n_2(s_2, t - \frac{s_2}{c})\, ds_2$$

= optical path length which the signal e_2 arriving at the receiver at time t has traversed in going from transmitter (laser) to receiver (photomultiplier tube) along the path C_2. The integration along the path starts at the receiver and extends backwards to the transmitter.

$n_2(s_2, t - \frac{s_2}{c})$ = index of refraction at the point along the path identified by the variable s_2 at the time $t - \frac{s_2}{c}$.

ϕ_1, ϕ_2 = phase angles of the transmitted signals corresponding to e_1 and e_2, respectively, at time t = 0.

If the lengths of the paths, C_1 and C_2 are short enough that the propagation times to traverse the paths are short relative to the length of time in which

the index of refraction at a point along the path can change appreciably, then $S_1(t)$ and $S_2(t)$ can be expressed with reasonable accuracy as

$$S_1(t) = \int_{c_1} n_1 (s_1, t)\, ds_1 \tag{5.3}$$

$$S_2(t) = \int_{c_2} n_2 (s_2, t)\, ds_2 \tag{5.4}$$

The mixing process which the signals e_1 and e_2 undergo in the photomultiplier tube will be characterized by summing, squaring and low-pass filtering. The first two steps are described by the expression

$$(e_1+e_2)^2 = \left\{ A_1 \cos \left[\omega_1 t - \frac{\omega_1 S_1}{c} + \phi_1 \right] + A_2 \cos \left[\omega_2 t - \frac{\omega_2 S_2}{c} + \phi_2 \right] \right\}^2$$

$$= A_1^2 \cos^2 \left[\omega_1 t - \frac{\omega_1 S_1}{c} + \phi_1 \right] + A_2^2 \cos^2 \left[\frac{\omega_2 S_2}{c} + \phi_2 \right]$$

$$+ 2 A_1 A_2 \cos \left[\omega_1 t - \frac{\omega_1 S_1}{c} + \phi_1 \right] \cos \left[\omega_2 t - \frac{\omega_2 S_2}{c} + \phi_2 \right].$$

Using the trigonometric identity $\cos A \cos B = 1/2 \cos (A+B) + 1/2 \cos (A + B)$ and low-pass filtering, the signal voltage output v_s from the PM tube will be proportional to

$$v_s \propto A_1 A_2 \cos \left[\omega_1 t - \frac{\omega_1 S_1}{c} + \phi_1 - \omega_2 t + \frac{\omega_2 S_2}{c} - \phi_2 \right]$$

Recalling that $\omega_2 = \omega_1 + \omega_a$, and letting $\Delta S(t) = S_2(t) - S_1(t)$ and $\Delta\phi = \phi_2 - \phi_1$, v_s can be written

$$v_s = k A_1 A_2 \cos \left[\omega_a t - \frac{\omega_1 \Delta S}{c} - \frac{\omega_a S_2}{c} + \Delta\phi \right] \tag{5.5}$$

where k is the constant of proportionality. Assuming that A_1 and A_2 are constant, the instantaneous radian frequency of v_s is given by

$$\omega_d = \omega_a + t\frac{d\omega_a}{dt} - \frac{\omega_1}{c}\frac{d(\Delta S)}{dt} - \frac{\Delta S}{c}\frac{d\omega_1}{dt} - \frac{\omega_a}{c}\frac{dS_2}{dt} - \frac{S_2}{c}\frac{d\omega_a}{dt}$$

$$= \omega_a + (t - \frac{S_2}{c})\frac{d\omega_a}{dt} - \frac{(\omega_1 + \omega_a)}{c}\frac{dS_2}{dt} - \frac{\Delta S}{c}\frac{d\omega_1}{dt} - \frac{\omega_1}{c}\frac{dS_1}{dt}.$$

By considering the relative magnitudes of each of these terms, some simplification in the expression can be made. The first term, ω_a is the Debye-Sears acoustic modulation frequency; the second term represents the drift in this modulation frequency occurring during the propagation time along path C_2 and is negligible; $\frac{(\omega_1 + \omega_a)}{c}\frac{dS_2}{dt}$ is approximately equal to $\frac{\omega_1}{c}\frac{dS_2}{dt}$ since $\omega_a \ll \omega_1$. Hence, ω_d is approximately $\omega_d \simeq \omega_a - \frac{\omega_1}{c}\frac{d}{dt}(\Delta S) - \frac{\Delta S}{c}\frac{d\omega_1}{dt}$.

In this simplified expression, the term $\frac{1}{c}\frac{d}{dt}(\Delta S)$ can now be identified as the frequency fluctuation induced by the propagation along the paths C_1 and C_2, and the term $\frac{\Delta S}{c}\frac{d\omega_1}{dt}$ as the effective frequency fluctuation seen by the receiver, due to the frequency drift of the laser output. Since $\Delta S(t) = S_2(t) - S_1(t)$, this latter contribution to the frequency fluctuation can be removed as a contributing factor to the measurement by ensuring that the optical paths of C_1 and C_2 (S_1 and S_2, respectively) are nearly equal. If for example, $\Delta S \leq 300$ meters, then $\frac{\Delta S}{c} \sim 10^{-6}$ sec. If a He-Ne laser is used in the experiment, frequency drift rates, $\frac{1}{2}\frac{d\omega_1}{dt}$, on the order of 10 cps/sec can be expected (Reference 20).

The frequency fluctuation in $f_d = \omega_d/2\pi$ due to laser drift will thus amount to roughly 10^{-5} cycles/sec, which in this experiment must be considered negligible. Under such conditions then, the frequency deviation about ω_a is proportional to

$$\Delta\omega = \omega_d - \omega_a \simeq \frac{\omega_1}{c}\frac{d}{dt}(\Delta S)$$

where

$$\Delta S = S_2(t) - S_1(t).$$

From Equations 5.2 and 5.3, it can be seen that if C_1 and C_2 are identical paths, then $S_1(t) = S_2(t)$ so that $\Delta S(t) = 0$ = constant and hence, $\frac{d}{dt}(\Delta S) = 0$.

Obviously then, the measured frequency deviation represents only those path length fluctuations which occur on those portions of path C_1 and C_2 which are not common to both. The path representations given in Figure 5.1 were designed to provide reasonable independence of path length fluctuations. To further reduce the analytical complexity in the interpretation of collected data, some consideration must also be given to minimizing the length of path which is traversed twice by the same signal. This condition exists immediately in front of most types of mirrors and in general is unavoidable. The best that can be done is to arrange the path configuration such that this effect is minimized.

POWER FLUCTUATION MEASUREMENT - EXPERIMENT NO. 6

Note: The discussion of this experiment is based on an actual power fluctuation measurement which was carried out recently (June '65) over a five-mile optical link by the Electro-Optical Laboratory of S&ID, as part of a current program for experimentally evaluating the statistical character of atmospherically induced intensity fluctuations of a laser beam. Since this measurement was successful in terms of both instrumentation and theoretical results, it merits special (but not exclusive) consideration as a means of implementing the present LACE experiment. For this reason a description of the experiment is presented below in place of a formal component performance analysis.

OBJECTIVE

To measure the light power and fluctuations in light power from a laser after transmission through the atmosphere, as a function of the aperture of the receiver.

IMPLEMENTATION

System Configuration

The measurement was carried out using the optical link described in Appendix H of this report. The experimental technique used was the following (see Figures 6.1 and 6.2). Light from a 6328Å gas laser is transmitted over the five-mile link to a large (approximately 1 meter) paraboloidal receiver which focuses the collected light through an adjustable field stop (set at approximately 2 mm for the experiment), after which it is recollimated, passed through 50Å optical filter, and detected by an RCA 7265 photomultiplier with an S-20 photosurface. The photomultiplier circuit, diagrammed in Figure 6.3 has a response from dc to about 2 megacycles. Before entering the field stop, the light passes through a larger iris (item 1 of Figure 6.2) which is separated from the field stop (item 2). This iris acts as an aperture stop and can be used to vary the effective diameter of the system, as shown in Figure 6.4.

Data collection for the power fluctuation measurements is performed using the arrangement shown in Figure 6.1. The point detector assembly, which provides a small-aperture reference measurement, consists of a 3.5 mm diameter flat collector mirror oriented at 45 degrees to the incoming

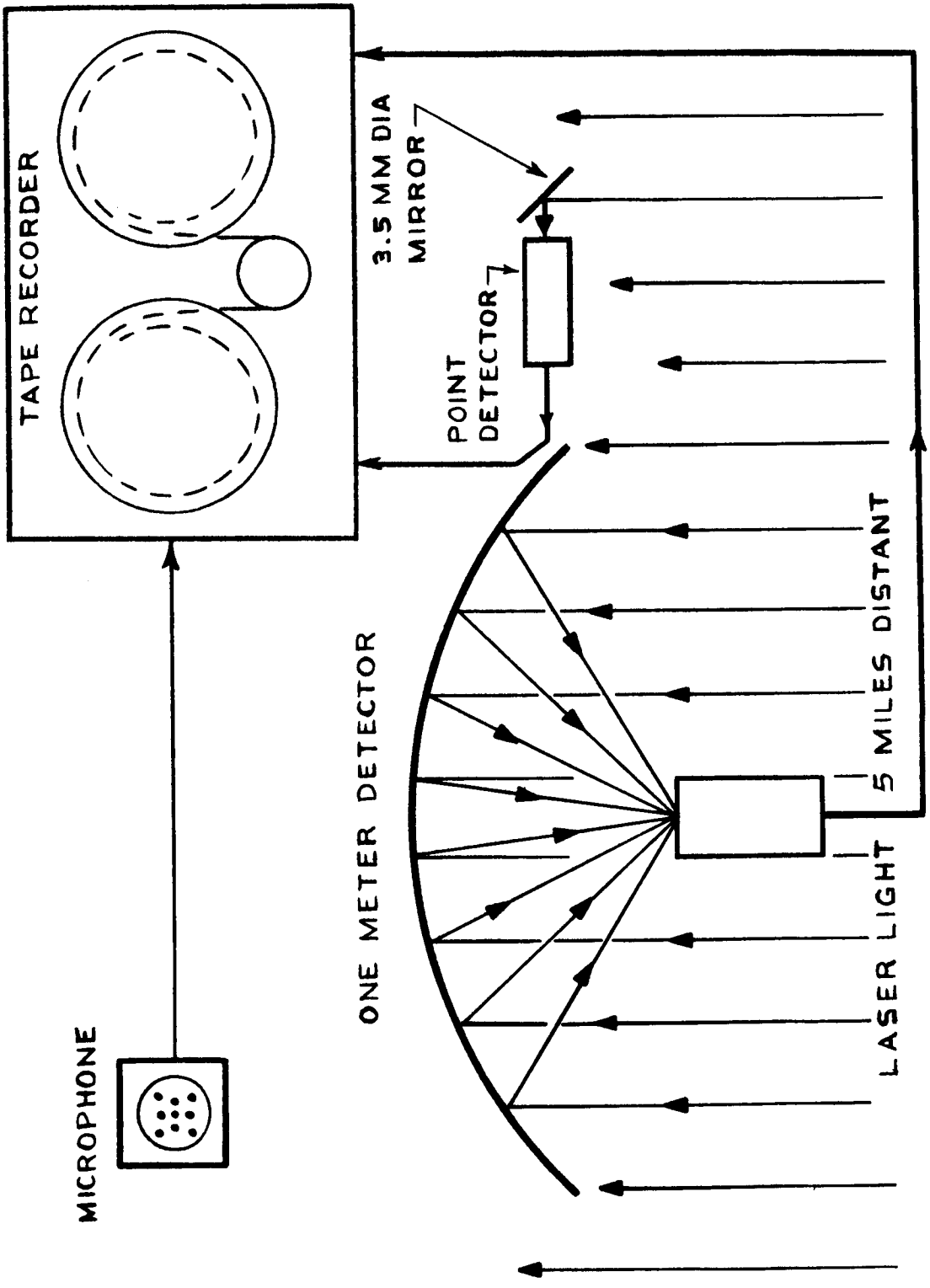

Figure 6.1, Data Collection Technique - Power Fluctuation Measurement

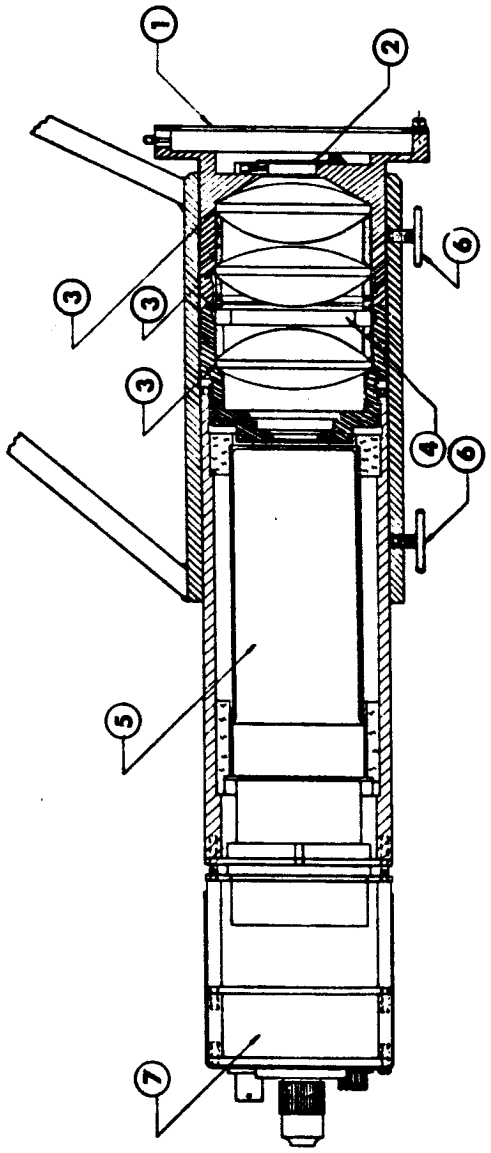

1. APERTURE STOP IRIS
2. FIELD STOP IRIS
3. COLLIMATING LENSES
4. 50 Å BAND PASS FILTER, CENTERED AT 6328 Å, BLOCK TO 8000 Å
5. RCA 7275, 14-STAGE PHOTOMULTIPLIER
6. LOCK SCREWS
7. PREAMP LINE DRIVER ELECTRONICS

Figure 6.2. Mechanical Schematic of Detector Package for One-Meter Receiver

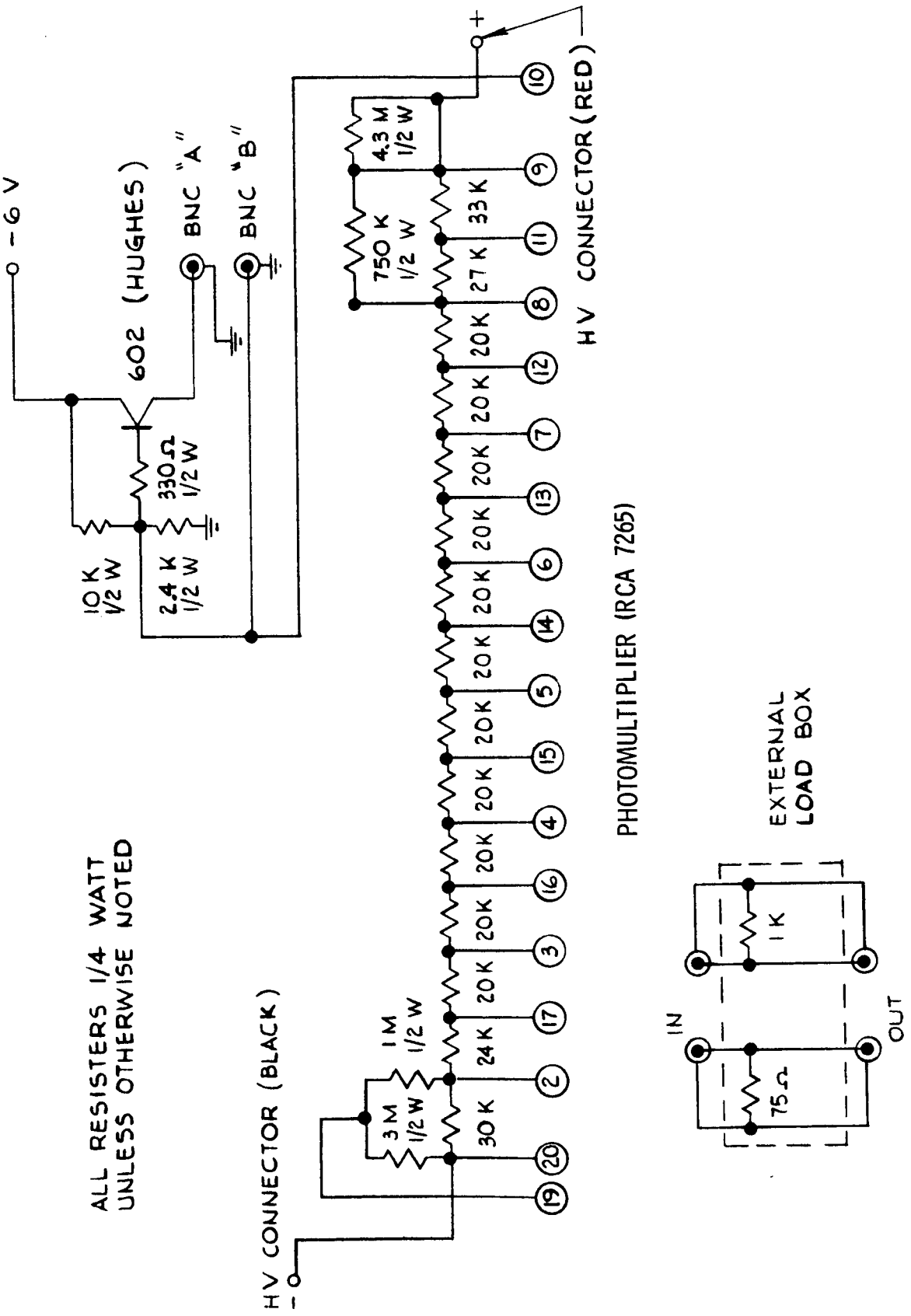

Figure 6.3. Photomultiplier Circuit for One-Meter Receiver

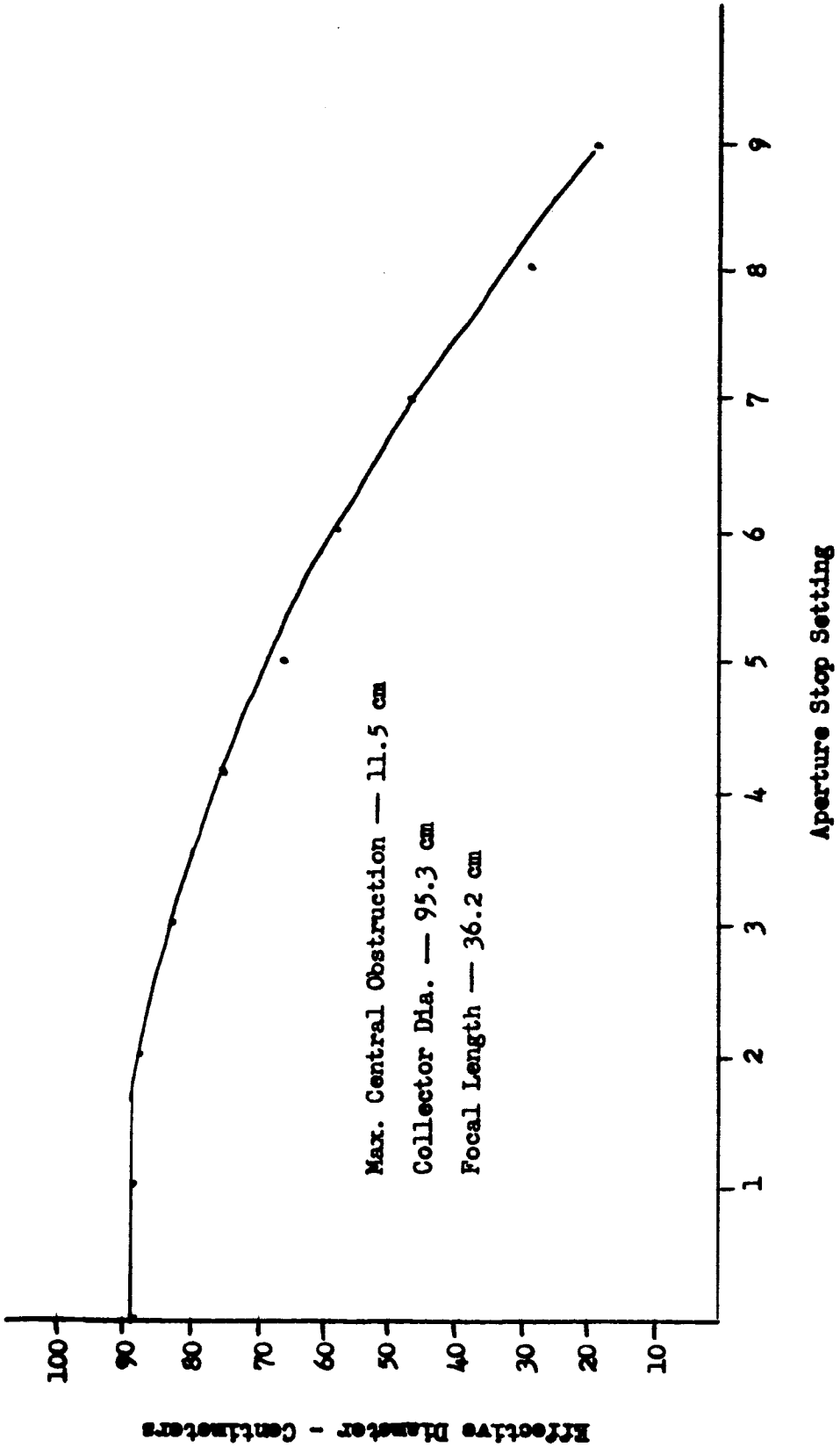

Figure 6.4. One-Meter Receiver Calibration - Experimental

beam followed by a focusing lens with a focal length of 170 mm, a 1 mm diameter field stop, a 50Å optical filter, and an S-11 RCA 6342-A photomultiplier having the circuit configuration shown in Figure 6.5. The outputs of the large receiver and the point detector are recorded on two FM channels of the data recorder at a rate of 60 inches per second, and a direct record channel is used for voice to record the aperture stop settings and wind speed. For each aperture stop setting, approximately one minute of data should be recorded.

Discussion of the Measurement

Alignment of the transmitter and receiver to establish the optical link can be accomplished by the following procedure. First, the laser is pointed at the receiver, using a telescope mounted to the laser pointing head, which has previously been boresighted with the laser beam. In this way, the operator at the transmitter site can position the laser beam to within a few meters of the receiver station. Fine alignment of the beam is accomplished by radio communication between the two stations.

Once the laser beam has been properly aimed at the receiver, the receiver can be easily aligned by moving it around until the focal spot is seen on a piece of white paper held in front of the field stop. For fine adjustments, the paper is removed and the receiver adjusted until the light passes through the stop. The receiver is then locked in place. This method proved to be more direct than using a spotting scope mounted on the receiver. The focal spot was quite bright; in fact, for data collection, a No. 2 neutral density filter was required to prevent saturation of the photomultiplier. To facilitate alignment, the large receiver was attached to a mount supplied with counter-weights and fixed to a heavy tripod with "AZ-EL" adjustments.

In performing the measurements, it is desirable to keep the angular stability of the laser transmitter to within ±15 arc seconds during the time required to make one measurement (approximately 15 minutes). This pointing stability is necessary because the forward scatter caused by haze greatly reduces the intensity of the beam near the edge. This results in unbalance and reduction in the receiver output signals; also, during the data reduction the performance of the computers suffers from the low signals. The short-term pointing stability (less than the integration time constant) used in the data reduction must be less than ±5 arc seconds. As a result of the change in intensity across the beam, short-term instability (jitter caused by wind buffeting) will produce false correlation signals.

Data Reduction and Experimental Results

With the data collected from the power fluctuation experiment runs, two measurements were made. One was the fractional power fluctuation

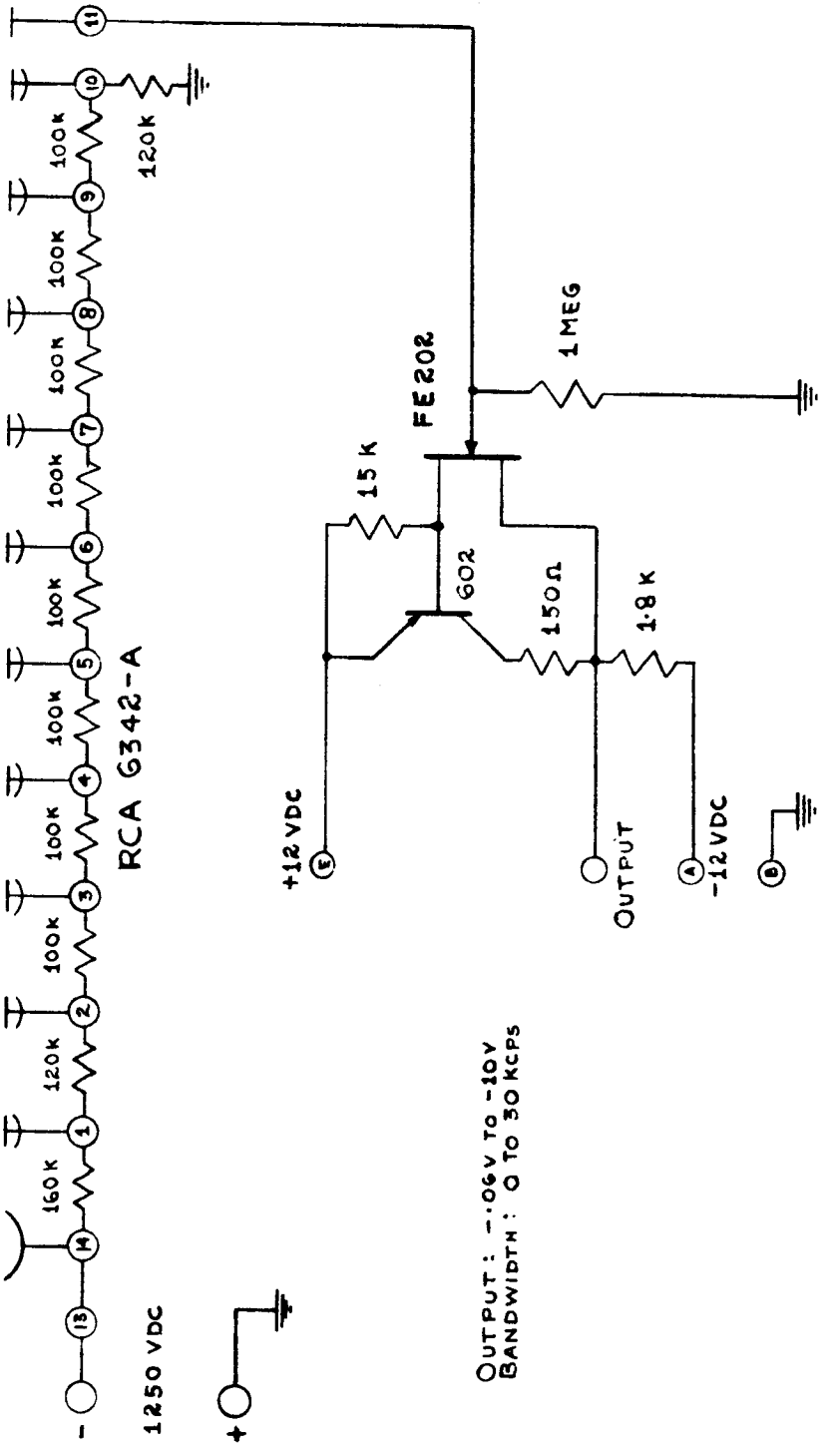

Figure 6.5. Photomultiplier Circuit for Transmitter Measurements

experiment as a function of collector diameter, and the other was the log intensity variance, also as a function of collector diameter. The analog computer program for the fractional power fluctuation measurement is shown in Figure 6.6, and that for the log-intensity variance is shown in Figure 6.7. The results of the fractional power fluctuation measurements are shown in Figure 6.8.

The experimental results disagree with the predictions of infinite plane wave theory. This theory predicts that the product of the fractional power fluctuation with the diameter of the receiver should remain a constant for diameters greater than the correlation distance ($C_{LL}(r) = 0$ when r is approximately 7 cm according to predictions). The experimental results, however, show that the fractional power fluctuation is approximately constant over the range of effective diameters from 90 to 20 cm. This measurement suggests that the diameter of a collimated beam transmitter operating in the atmosphere is also an important consideration in controlling the character of the intensity fluctuations. The results of the measurement of log intensity variance as a function of collector diameter are shown in Figure 6.9. This measurement, also according to theory, should decrease with diameter, but the experimental results show that the log intensity variance, like the fractional power fluctuations, remains approximately constant over the full range of effective collector sizes. The same conclusions may be drawn from this measurement as from the fractional power fluctuations.

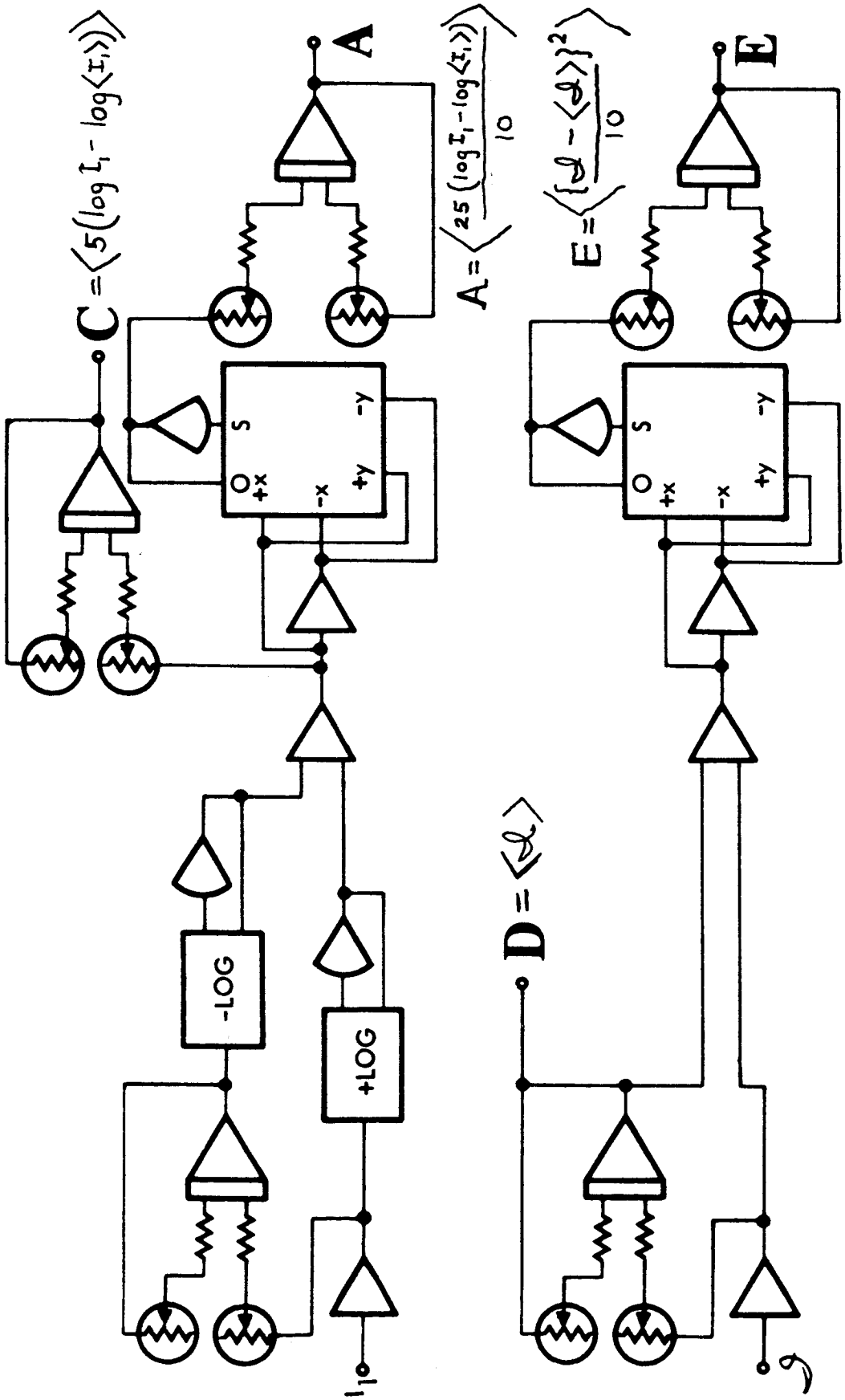

Figure 6.6. Analog Computer Program for Fractional Power Fluctuation Measurement

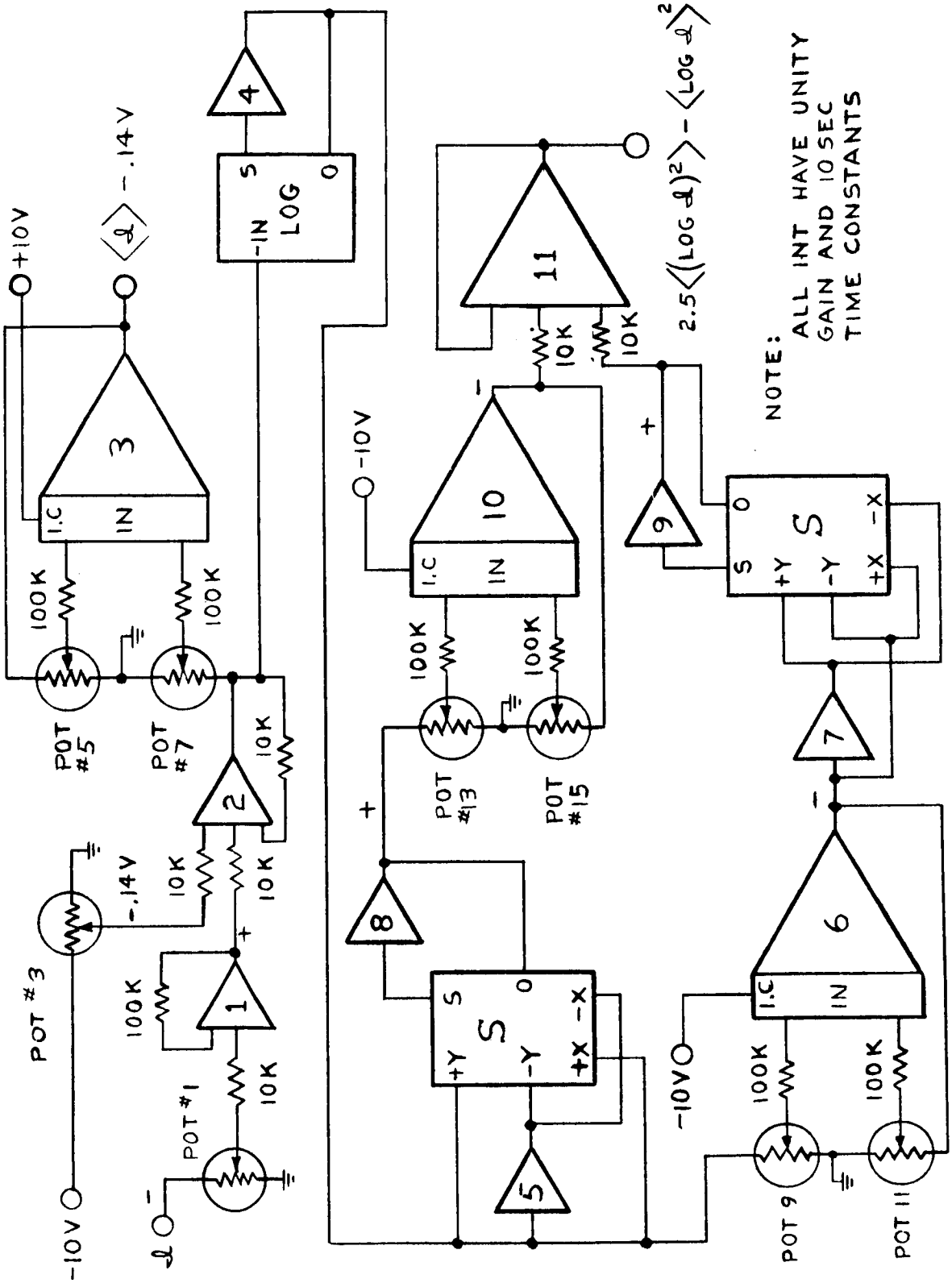

Figure 6.7. Analog Computer Program for Log Intensity Variance Measurement

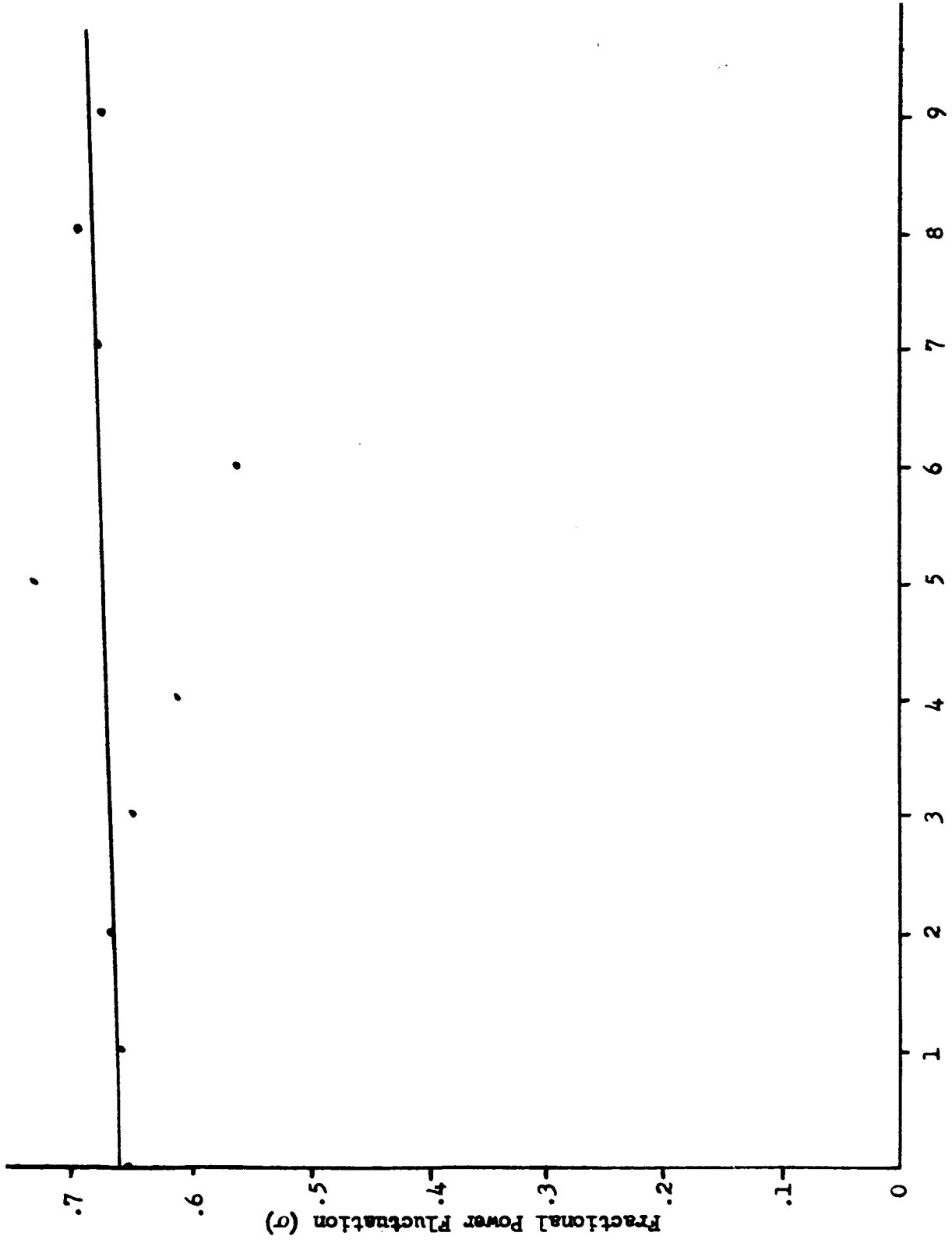

Figure 6.8. Fractional Power Fluctuation as a Function of Effective Collector Diameter

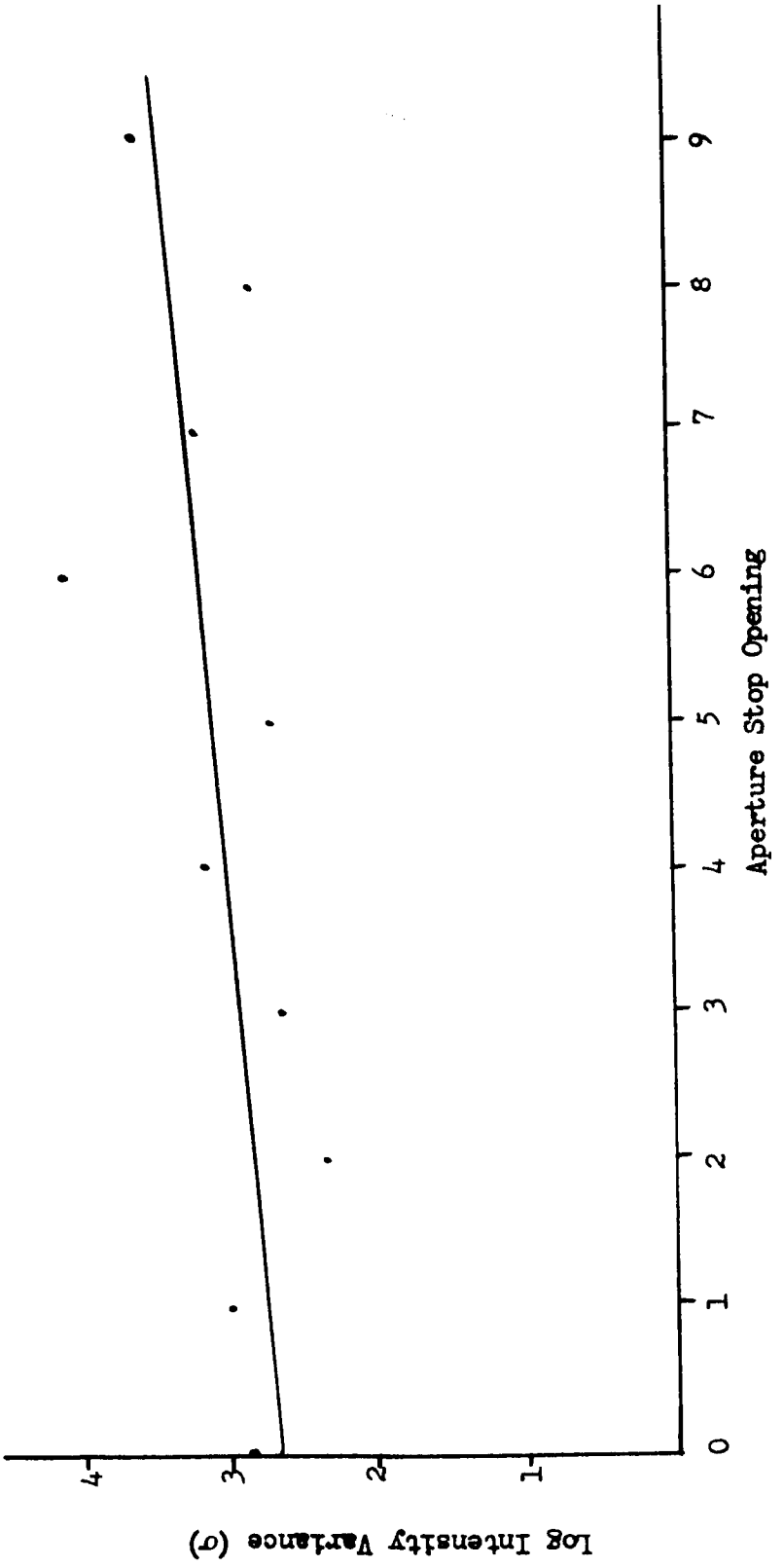

Figure 6.9. Log Intensity Variance as a Function of Effective Collector Diameter

HETERODYNE EQUIVALENT MEASUREMENT SYSTEM AND ANGULAR FLUCTUATION MEASUREMENT - EXPERIMENTS 7 AND 8

OBJECTIVES

Experiment No. 7

To measure the average irradiance at the center of the focused image of a received laser beam as a function of the diameter of the collecting aperture. The measurement gives, indirectly, the heterodyne efficiency of the collecting aperture.

Experiment No. 8

To determine the probability distribution and frequency spectrum of the angular image fluctuations of the focused laser beam after transmission through the atmosphere.

IMPLEMENTATION

Summary

Some of the practical problems which must be solved in implementing Experiments 7 and 8 are discussed. An outline is given of the analysis which must be performed in order to include the aberrations of the optical system in the measurement of the heterodyne efficiency.

System Configuration

The functional schematic for Experiments 7 and 8 is shown in Figure 7-1. Common to both experiments are the collecting optics with variable apertures. To examine the full range of heterodyne efficiency vs. aperture size, two types of collecting systems are needed. The large reflective optical system is required since refractive optical components are difficult to fabricate. On the other hand, the reflective system, because of aperture blocking, cannot be used for small-aperture measurements. A need thus exists for both systems.

The experiments can be performed together simply by including a beam-splitter in the arrangement. Part of the focused light is directed onto a pinhole placed in front of a photomultiplier.

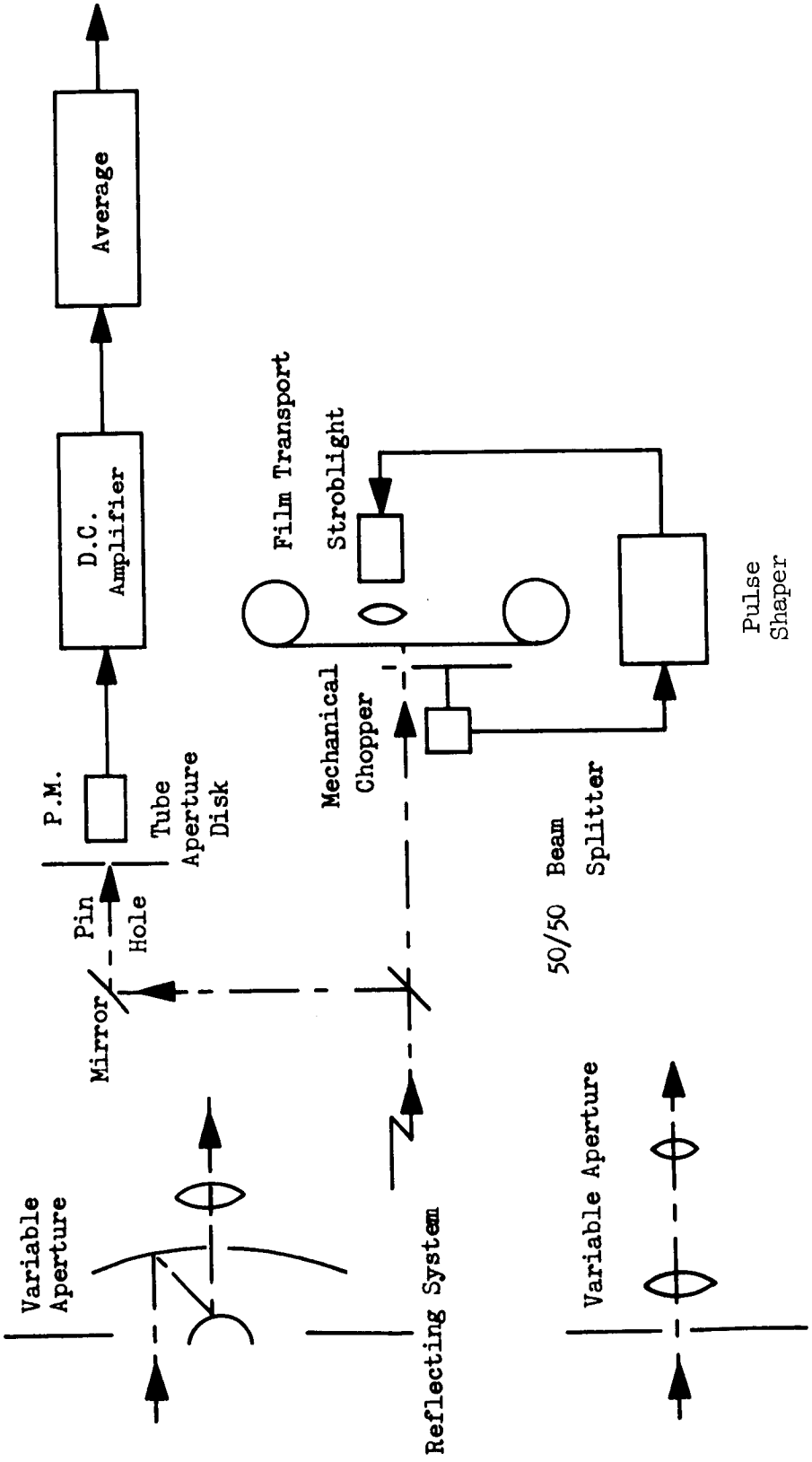

Figure 7.1. Configuration for Heterodyne Equivalent and Angular Fluctuation Measurements

Table 7.1. Experiment Nos. 7 and 8 Equipment Lists

Quantity	Item
	Experiment No. 7
1	Cassegrain telescope system, adjustable aperture, 1 meter maximum diameter, additional magnifying lens
1	Refraction optics telescope composed of objective and magnifying lens, adjustable aperture, 1 meter maximum diameter
1	50/50 Beam Splitter (used in conjunction with Experiment 8)
1	Aluminized mirror
1	Rotatable disk with pinhole size apertures
1	PM tube
1	Stabilized D. C. amplifier
1	Averaging operational amplifier
	Experiment No. 8
1	Mechanical chopper, with equally spaced radial slots
1	Continuous-transport motion picture camera
	Data Reduction Equipment
1	Projector for illuminating developed film
1	Moveable slotted aperture with position readout
1	PM tube
1	D. C. amplifier
1	Output pen recorder

To minimize error in the measurement of the irradiance at the center of the diffraction pattern at the PM, as explained in Reference 1 , the pinhole diameter must be smaller than 10 percent of the center diffraction spot. In order to maintain this condition as the aperture size is changed, a circular disc having pinholes of various sizes around its circumference is provided. The signal from the photodetector is amplified and averaged to give the measurement of equivalent heterodyne efficiency.

For measurement of angular image fluctuation, the second focused beam is chopped mechanically, using a rotating disc with radial slots placed around its perimeter. In order to get positional information about the image, it is necessary to know the precise time at which the center of the chopper slot was lined up with the center of the film (i. e. the center as defined by the image in the absence of atomospheric turbulence). This is accomplished by exposing the edge of the film with a pulsed light source (strobe light) triggered by a signal from an encoder on the motor driving the chopper disc. To trigger the light source, the signal from the encoder will probably have to be modified so a pulse shaping circuit is included. The film is continuously transported through the focal point. As pointed out in Reference 1 , the chopper speed and film speed must have a definite relation to insure small errors.

The problem of reducing the recorded images to the form of the required data—namely the spectrum of the image fluctuation and the probability distribution of the image displacement—has been adequately covered in Reference 1 . Since this equipment will have to be built especially for the reduction of the data, a separate equipment complement list is provided.

Component Performance

The quality of the results expected from Experiments 7 and 8 is intimately dependent on the optical system used. In Experiment No. 7, the Strehl definition gives the heterodyne efficiency without error only when all optics are aberration-free. In Experiment No. 8, unsymmetrical aberrations will influence the statistics of the angular fluctuation by seeming to give a preferred direction to the image fluctuation. Determining the nature and magnitude of the aberrations present in the optical system is a standard procedure (Reference 8), but the inclusion of aberrations in the calculation of the Strehl definition when atmospheric turbulence is also present is a complicated process.

The way of attacking this problem as it relates to Experiment No. 7, involves the modulation transfer functions of both the optical system and the turbulent atmosphere. In this case, however, the modulation function of the

optics is not simply that of a diffraction-limited system (i. e. the function $K_o(\omega)$ of Reference 11) but that of the system with aberrations. In this case the Strehl definition $\mathcal{D}$ becomes

$$\mathcal{D} = \frac{\int \tau_o(\vec{\omega})\, \tau_a(\vec{\omega})\, d\vec{\omega}}{\int K_o(\vec{\omega})\, d\vec{\omega}}$$

Here $\tau_o(\vec{\omega})$ is the modulation function of the optical system with aberrations, $\tau_a(\vec{\omega})$ is the modulation transfer function of the atmosphere, $\vec{\omega}$ is a radius vector in the aperture plane, and $d\vec{\omega}$ is a differential area in the aperture plane. The integral is taken over the area of the aperture. The characterization of $\tau_o(\vec{\omega})$ will be difficult but there are methods of attack (Reference 8).

In the Task II report, (Reference 11), the modulation transfer function of the atmosphere was expressed as $\exp\left\{-\frac{D_{\phi\phi}(\rho)}{2}\right\}$, a function of the phase structure function. This was derived, as was the expression for heterodyne efficiency, under the assumption that amplitude fluctuations were negligible. Experimental results will be affected by amplitude fluctuations, but as shown in Reference 2, the modulation transfer function in this case is simply

$$\exp\left\{-\frac{1}{2}\left(D_{LL}(\rho) + D_{\phi\phi}(\rho)\right)\right\},$$

where $D_{LL}(\rho)$ is the structure function of the log amplitude.

The conclusion is that the Strehl definition still gives a measure of heterodyne efficiency when amplitude fluctuations are taken into account.

The need for two optical systems (one of small, the other of large aperture) on all links over which the experiments are conducted may not exist if heterodyne efficiency saturates at small diameters. An idea of the maximum aperture sizes needed in the down-link measurement case can be obtained from Figure 7.2. A factor of 2 is included, ensuring that the saturation level is reached.

For earth-based measurements, the aperture sizes at which saturation occurs will be on the order of centimeters. Without the results of a finite-beam analysis, no theoretical estimates can be made to guide the selection of aperture size. In the up-link case, the aperture size required to give

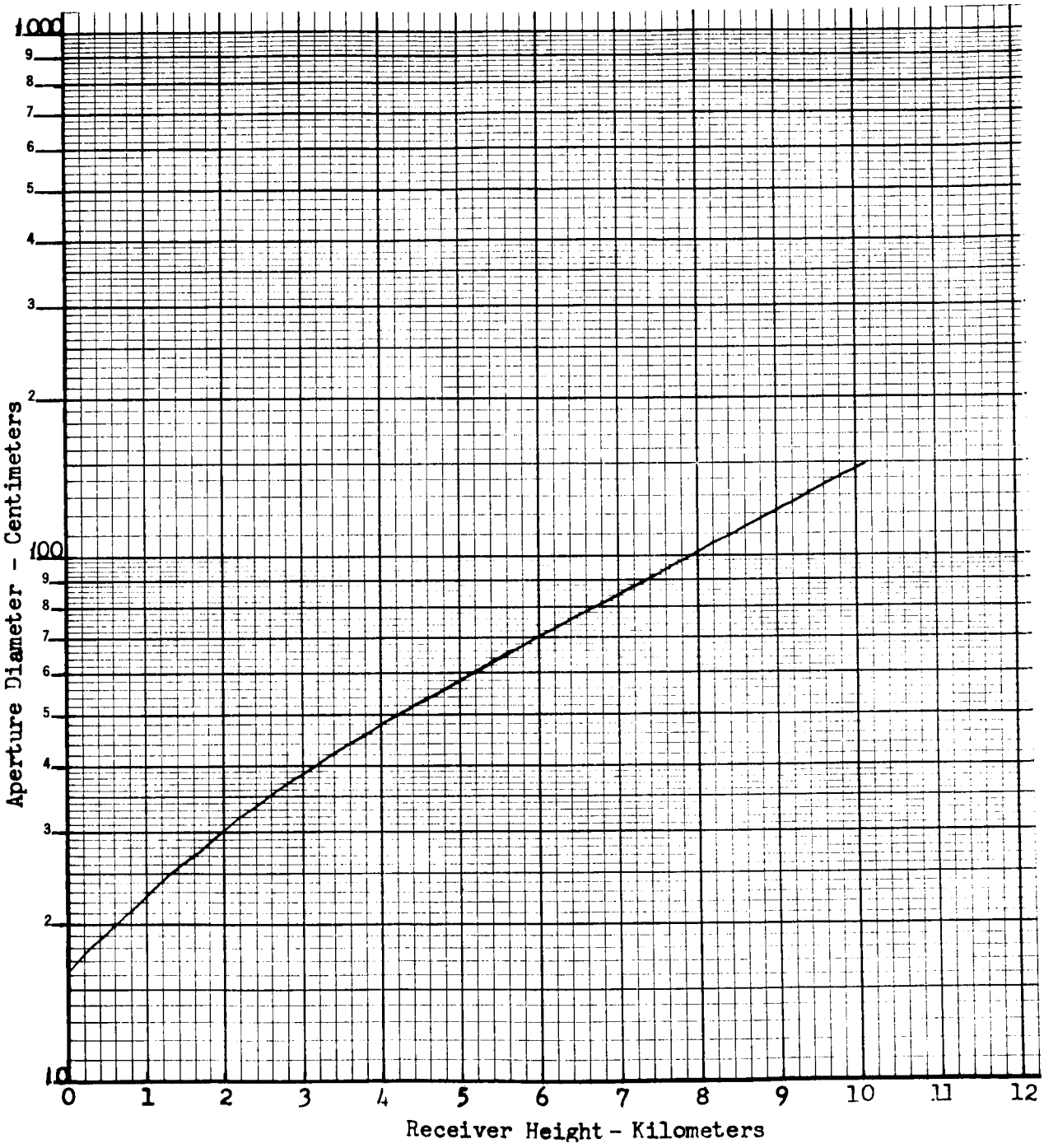

Figure 7.2. Aperture Diameter vs. Altitude to Give Saturation of Heterodyne Efficiency During Daytime (λ = 6328 Å)

saturation will increase with increasing height because of the "smoothing" of the phase front.

The large system is of the reflecting type with the secondary mirror partially blocking the primary. (Special off-axis systems do exist in which the primary mirror is cut from an off-axis section of reflector and hence is not blocked by the secondary, but these are costly to make.) This blocking affects the heterodyne equivalent method in the following way. When the aperture is blocked, the Strehl definition becomes proportional to

$$\mathcal{D}_B \propto \frac{\int_d^D K_o(\rho) \exp\left\{-\frac{D_{\phi\phi}(\rho)}{2}\right\} d\rho}{D^2 - d^2}$$

where D is the diameter of the primary and d is the diameter of the secondary blocking the primary. The ratio of the blocked to unblocked heterodyne efficiency then becomes

$$\frac{\mathcal{D}_B}{\mathcal{D}} = \frac{D^2}{D^2 - d^2} \frac{\int_o^D \rho K_o(\rho) \exp\left\{-\frac{D_{\phi\phi}(\rho)}{2}\right\} d\rho - \int_o^d \rho K_o(\rho) \exp\left\{-\frac{D_{\phi\phi}(\rho)}{2}\right\} d\rho}{\int_o^D \rho K_o(\rho) \exp\left\{-\frac{D_{\phi\phi}(\rho)}{2}\right\} d\rho}$$

This equation can be used to estimate the allowable values of D and d corresponding to a prescribed accuracy in the measurement of the heterodyne efficiency.

The values of the primary and secondary aperture diameters are also dependent on the physical arrangement of the system and the focal lengths obtainable, and should thus be calculated when the design of the system is finalized.

The basic design of the optical system and the selection of the pinhole size required for carrying out the measurement has been adequately described in Task II, Volumes 1 and 2, (References 1 and 11). The design is for a system with no aperture blocking. When aperture blocking is present, new calculations must be carried out. They will closely parallel those done previously.

Since the experiment will be performed for various aperture sizes, there will be a need to adjust the pinhole size accordingly. First it is necessary to insure that the pinhole diameter is always less than about 10 percent of the central diffraction spot, whose irradiance it measures. This is necessary if the measurement is to accurately yield the true irradiance at the center of the pattern.

The signal-to-noise ratio must be as large as possible, consistent with the first requirement. This simply means that the pinhole diameter should be exactly 10% of the "Airy disk" diameter, whatever the aperture size. If this requirement is met, calculation of the signal-to-noise ratio is quite simple. Since the pinhole intercepts approximately 10% of the power collected by the aperture (neglecting the small fraction of the power which falls outside the central disc) it is only necessary to calculate the signal and background power passing through the aperture and multiply these by the factor 0. 1. The correct S/N equation to use is that of Experiment No. 3, Equations 3. 1 and 3. 2.

In Experiment No. 8, the "Airy disk" is recorded directly on film. The same optics is used so that questions of irradiance at the film surface, size of the film and exposure time can be answered. For a discussion of film characteristics, the section in Experiments 9 and 10 on photographic recording should be read.

Most of the requirements concerning the drive speed of the film and chopper speed have been given in Reference 1 . For images of tenths of a millimeter in size and for the rate of angular fluctuation expected, the minimum speed will be on the order of 10 $\left[\frac{cm}{sec}\right]$. The rate at which the image must be chopped is approximately 2000 per second. The angular rate of the chopper disc can be made much lower than this by putting many slots around its perimeter.

The reduction of the photographic data to find the probability distribution and spectrum of angular image displacement has also been discussed previously in Reference 1 .

SPREAD FUNCTION AND BEAM SPREADING MEASUREMENTS - EXPERIMENTS NO. 9 AND 10

OBJECTIVES

Experiment No. 9

To measure the spreading of the intensity pattern of a laser beam transmitted through the atmosphere, as a function of the distance and the size of the transmitter aperture.

Experiment No. 10

To measure the spread of a laser beam, its total power and power distribution at a distance, as a function of the transmitter aperture.

IMPLEMENTATION

Summary

These two experiments are considered together because of their closely related objectives. A measurement technique is described for each—film recording for Experiment No. 9 and the use of a photomultiplier for sampling the beam in Experiment No. 10—following which a discussion of film characteristics is presented, with references to other parts of this report for related discussions.

System Configuration

Experiment No. 9

Figure 9.1 is a block diagram of the experimental arrangement. The laser beam is collimated and passed through a variable aperture which is smaller than the beam itself. This condition insures that the beam diameter does not become the effective transmitting aperture, whose diameter must be accurately known. In order to avoid saturating the film, it may be necessary to attenuate the laser output with a suitable filter. A standard light source is needed to calibrate each exposure of the film. This standard source has calibrated gray levels which correspond to known levels of irradiance at the surface of the film. The film must be exposed for a long enough time to average out the localized temporal fluctuations of the image intensity.

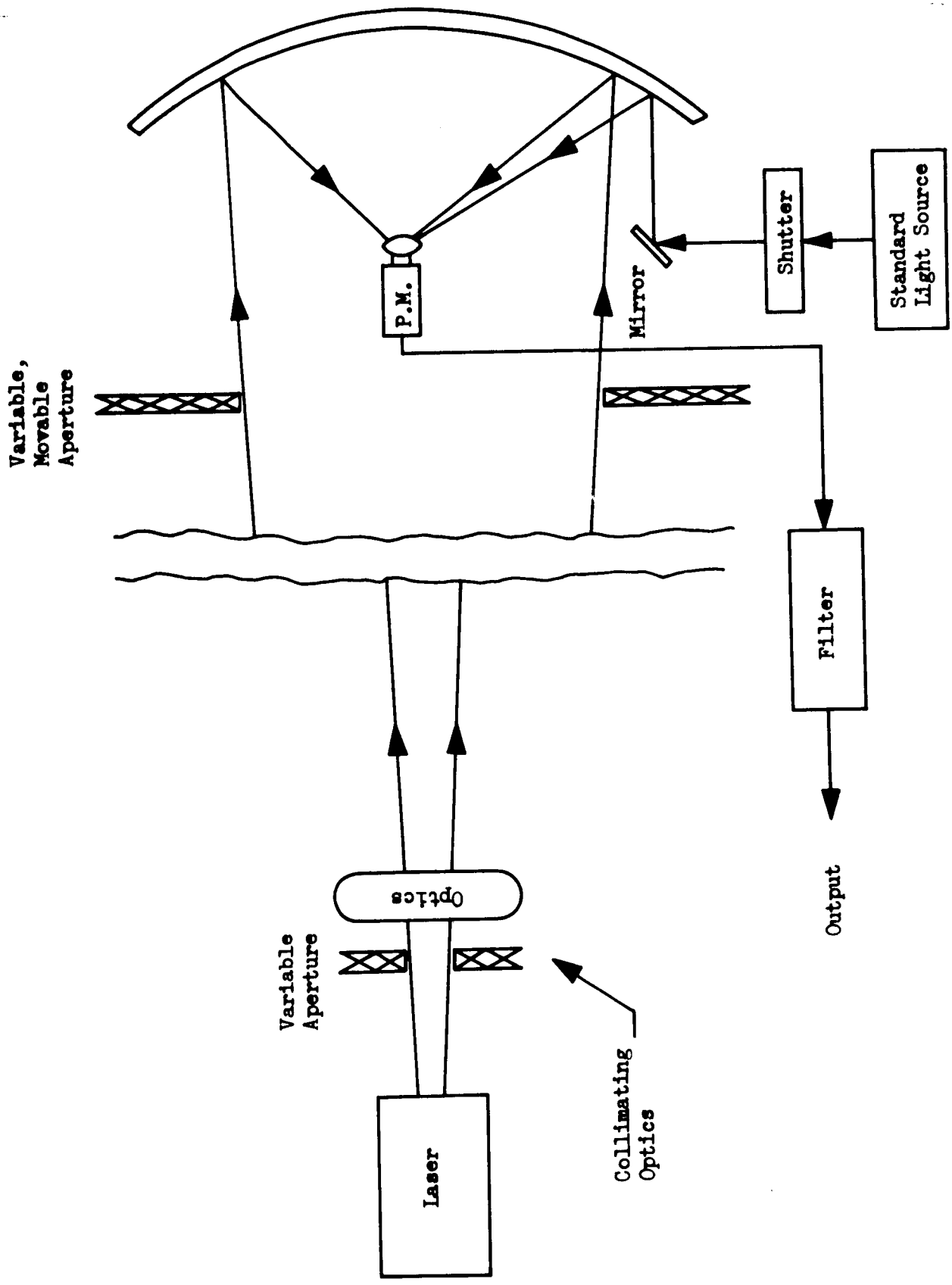

Figure 9.1. Configuration for Measurement of Spread Function

Table 9.1. Experiments Nos. 9 and 10 Equipment List

Quantity	Item
1	Collimating lens
2	Half-silvered mirrors
1	Optical bench
1	Photomultiplier tube
1	Photo tube output amplifier - filter
1	Real-time voltage Recorder (e.g., strip-chart recorder)
2	Standard light sources
1	Shutter (10 closures/sec or less)
1	Optical attenuator
2	Focusing lens systems
1	Small plane mirror
	Miscellaneous and Supplementary Equipment
	He-Ne Gas Laser
	Variable Apertures (stops)
	Dimensionally stable film (e.g., Kodak 2496 RAR)
	Film Advance Mechanism
	Film developing lab

Experiment No. 10

The transmitter arrangement is the same as that of Experiment 9. The receiver and recording system for this experiment are indicated in the diagram of Figure 9.2. When the beam is small enough (at intermediate distances), a large, variable aperture receiver can be used to measure the power for a series of apertures up to and including the total beam power at full aperture. The power is measured with a PM tube whose output current, averaged by a low-pass filter, is recorded for each aperture setting.

At large beamwidths (far distances) the power distribution (irradiance) within the beam is sampled along two perpendicular lines passing as nearly as possible through the center of the beam, using the photomultiplier tube either without optics or, if the power levels are too low, augmented by a lens which is small in comparison to the beamwidth. Periodically, the output of the low-pass filter must be calibrated with a standard light source.

Component Performance

There are at least two alternative techniques for recording the image of the laser beam at the receiver - film and photoelectric conversion. Film recording is convenient if data processing is to be employed after the data gathering is accomplished. On the other hand, if it is desired to reduce the data to numerical values in real time, photoelectric conversion is required. Either technique can be made to accommodate a wide range of intensity variations (several orders of magnitude). A discussion of the photographic process follows in this section. An analysis of photoelectric conversion is contained in Appendix C . For a comparative evaluation of these alternative techniques, the discussion of Experiment No. 4 (Stationarity Test) should also be reviewed at this point.

Photographic Recording

The most common format for specifying film data is the "characteristic curve," examples of which are shown in Figure 9.3. D is the unit of opacity; it is the logarithm of the inverse of the transmittance T. Thus, D = 0 means the processed emulsion is clear (T = 1) and D = 3 means that T = 1/1000 = .001 or only 0.1 percent of the incident light is transmitted through the emulsion. The $\log_{10}E$ scale refers to the amount of energy incident upon the emulsion during exposure. The value of zero for $\log_{10}E$ means that the incident luminous energy was one meter-candle-second.

In theory, the density of the exposure is dependent only upon the total energy received, regardless of how intense the radiation or how long the exposure. This is known as the property of reciprocity. Unfortunately reciprocity does not hold for emulsions in practice. Consequently, reciprocity

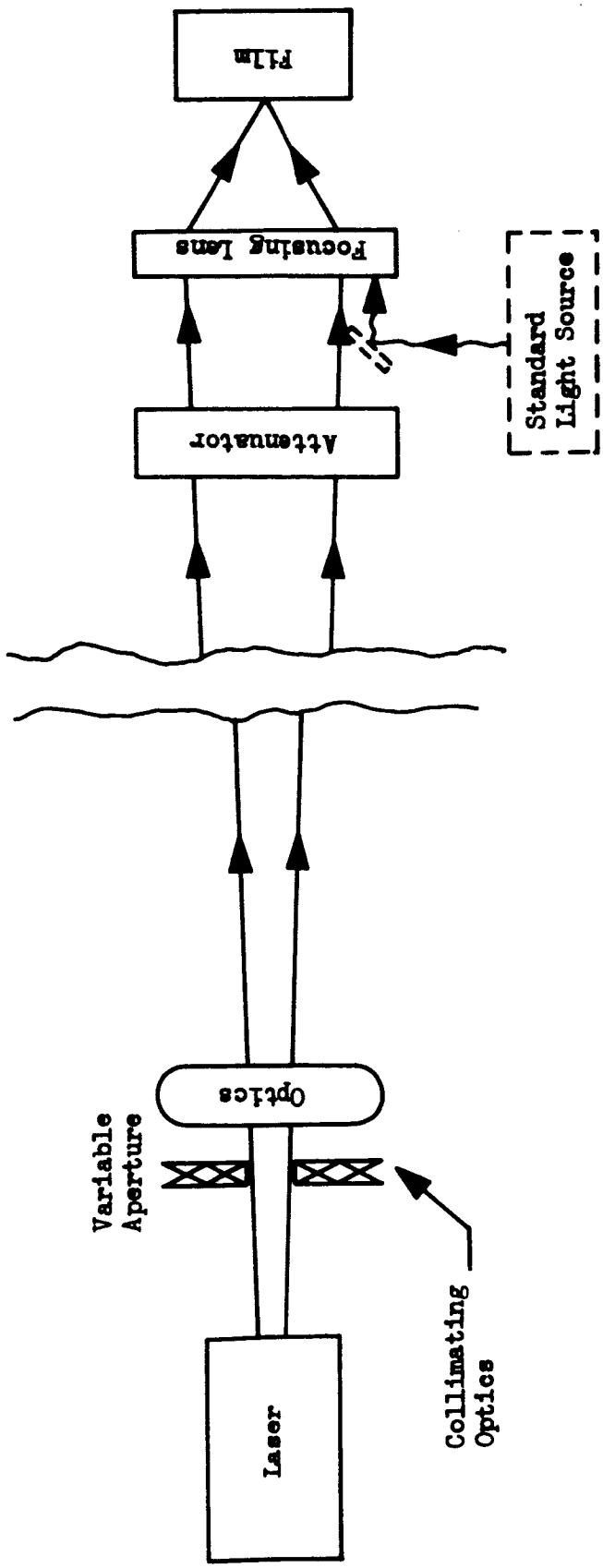

Figure 9.2. Configuration for Measurement of Beam Spreading

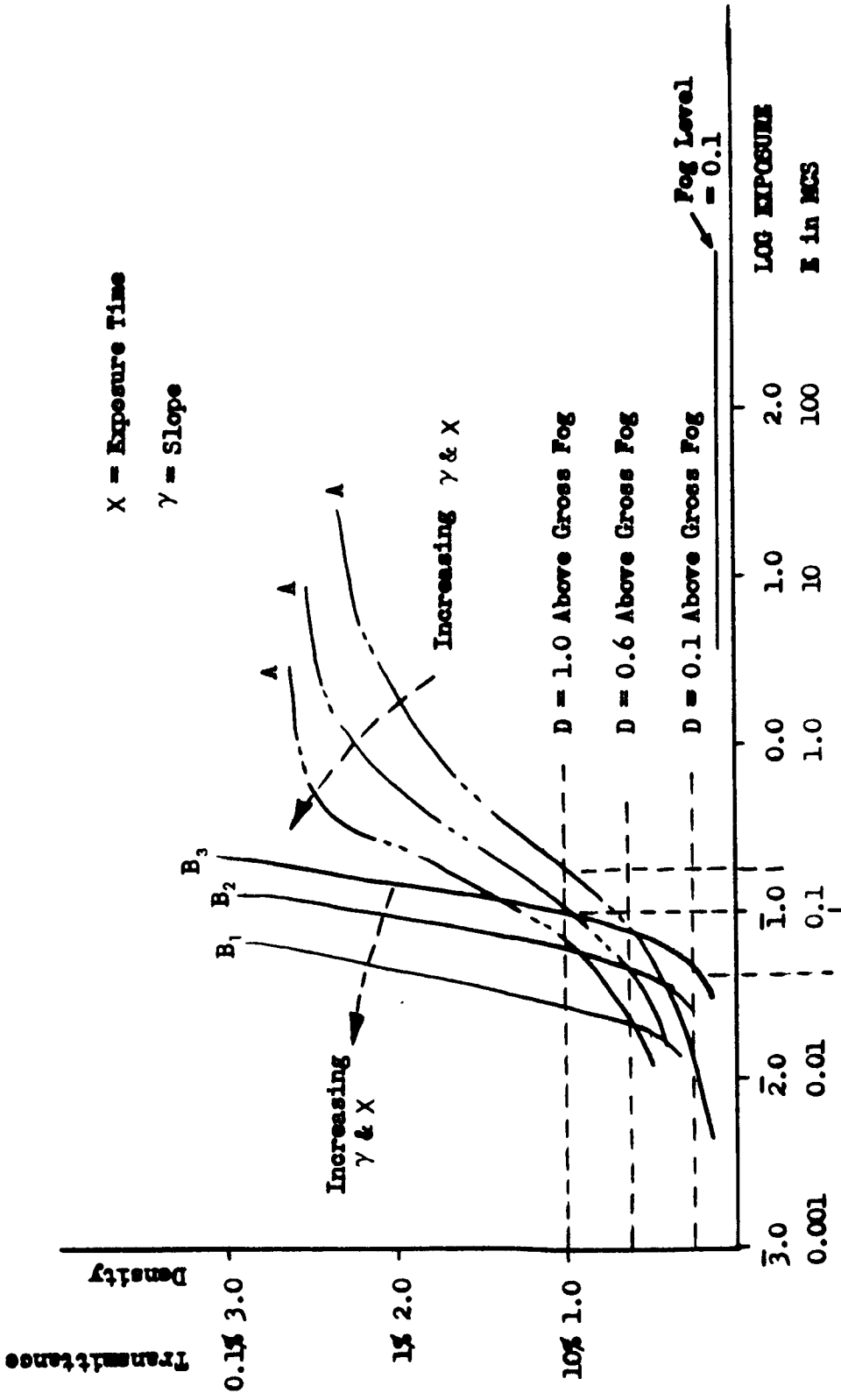

Figure 9.3. Characteristic Curves of Two Photographic Materials for Determining Speed Values

curves are specified for each film type (see Figure 9.4). Each curve corresponds to a particular exposure time X as labeled. Note that as exposure time increases, so does the tendency for the emulsion to darken with a given incident light flux. The quantity γ is the slope of the linear portion of the curve. Hence, the approximate relationship

$$\frac{\log E_o - \log E_1}{\log \frac{1}{T_o} - \log \frac{1}{T_1}} = \gamma$$

or

$$\frac{E_o}{E_1} = \left(\frac{T_1}{T_o}\right)^{\gamma} \qquad (9.1)$$

must hold for the emulsion in this linear range.

The gross fog level is the opacity in the developed emulsion which occurs without any exposure to light; it is due to the chemical processing and the inherent base density. Film speed and sensitivity are thus usually specified for a certain value of D above gross fog.

The differences in characteristics between film types A and B of Figure 9.3 are due to the different photographic materials used in the emulsion. Type B is typically used for photographic line copying whereas type A is used where continuous tones are desired. Experiment No. 9 would employ the Type A material.

Film speed is an inadequate specification of emulsions in general. Any film speed specification corresponds to one point in the three-dimensional space of E, D, and X. Points in this space are common to both material types A and B. Hence, either γ or one additional film speed point must also be specified to obtain an emulsion suitable for a particular measurement.

Figures 9.5, 9.6, and 9.7 illustrate the characteristic curves for an emulsion type that appears suitable for this experiment. Note that the emulsion is sensitive throughout the visible range, making it useful with HeNe or ruby lasers. The base has good dimensional stability. Other bases such as glass are also available.

It is difficult to maintain a high degree of repeatability from the development of one emulsion to the next. That is, the same incident flux and

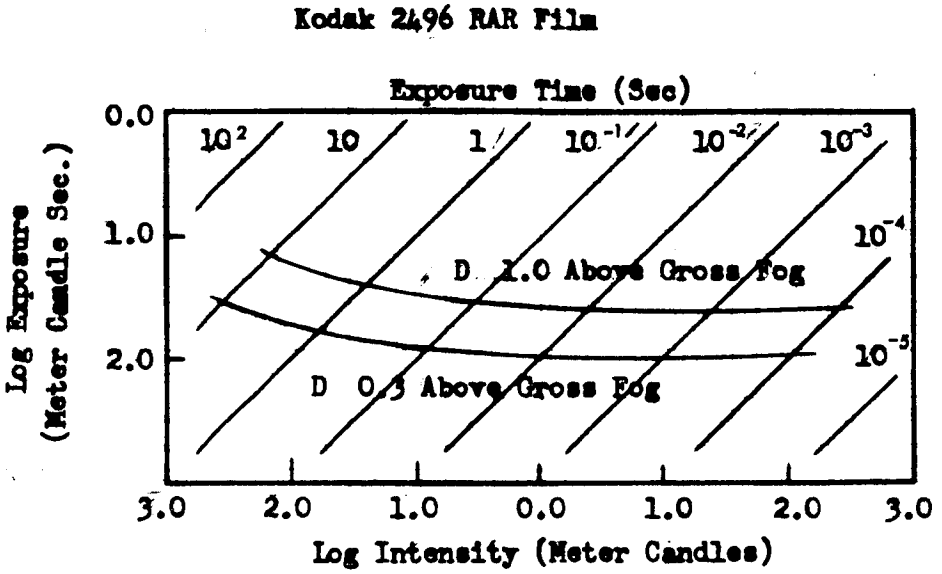

Figure 9.4. Reciprocity Characteristics of Film

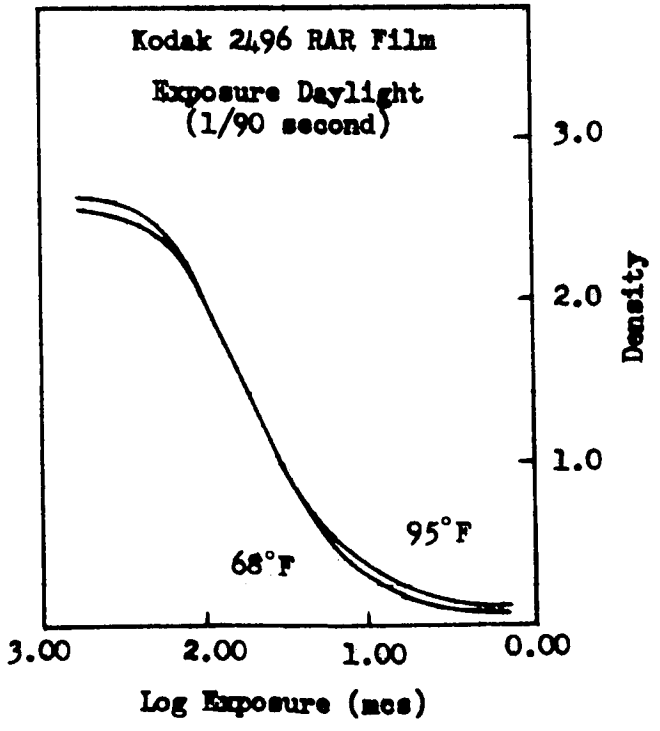

Figure 9.5. Characteristic Curves of Film

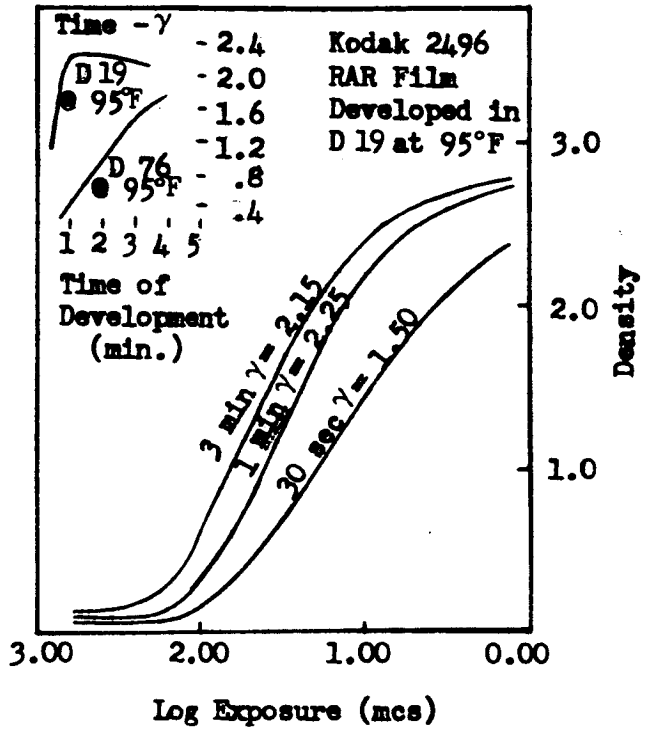

Figure 9.6. Characteristic Curves of Film

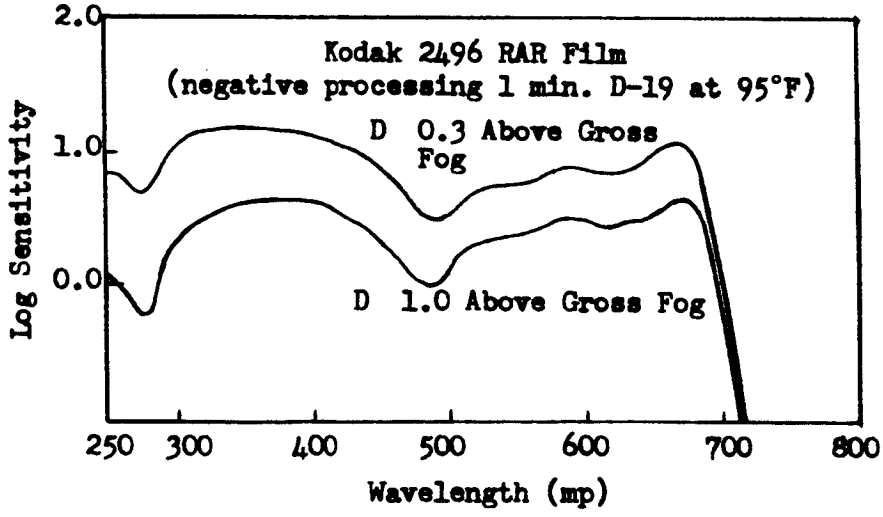

Figure 9.7. Spectral Sensitivity Curves

same exposure time will not necessarily produce the same transmittance on the same emulsion except in the sense of a long-term average. A number of factors affect the density of a developed emulsion, among which are:

1. Evenness and speed of flow of the developer fluid
2. The amount of fresh developer in contact with the emulsion
3. The characteristics of the lens systems and the position of the beam in the system
4. The speed and resolution of the film
5. The dimensional stability of the film base

As a result of the large number of factors to be controlled, it appears most practical to employ a means of calibrating developed emulsion transmittance to a common scale. This must be accomplished by a standard light scale which exposes the film at the proper wavelength and in the immediate vicinity of the image being recorded.

POLARIZATION FLUCTUATION MEASUREMENT - EXPERIMENT NO. 11

OBJECTIVE

To detect and measure any changes in the state of polarization of a laser beam which may result from transmission through a turbulent atmosphere.

IMPLEMENTATION

Summary

For this measurement, one primary and two alternative implementations are presented, the latter being described here for the first time in the LACE study. Following the description of each method and a performance analysis of the major components, a comparison and relative evaluation of the three approaches is given.

Primary System (Figure 11. 1)

This is the system which was described previously in Task II, Volume 2 of this report (Reference 1).

System Configuration

The distinguishing features of this system are a stationary Wollaston prism and two separate PM tubes and recorders. After passing through a narrow-band optical filter, the incoming plane-polarized laser beam is divided by the Wollaston prism into two orthogonally polarized components which travel over separate paths to two photomultiplier tubes. The outputs of the PM's and the difference between them is recorded. Any non-zero value of this difference indicates a difference in the signal strength (irradiance) of the two polarized components, provided that the gain of the two PM's has been equalized and the prism is accurately oriented at 45 degrees to the plane of polarization of the incoming beam. The polarization plane should be determined prior to the measurement by rotating the prism until the orientations for maximum and minimum transmission are established (the minimum should be zero for completely plane-polarized light).

Component Performance

The performance of this system was discussed in the Error Analysis of the Task II report (Reference 1). Appendix C of the present volume also contains relevant information on the operation of the PM tubes.

Alternative Systems (Figures 11.2 and 11.3)

These two systems have not been discussed previously. They are based on a common operating principle, discussed below, and differ from each other only in the method by which the polarization sub-carrier is generated.

System Configuration

System A. Figure 11.2 illustrates the basic system configuration, which is similar to the polarization shift detector shown in Figure 11 of Reference 11 . There are two important differences in the design, however. These are, (1) the method by which the frequency and phase reference is derived, and (2) the method by which the incident polarization angle is detected (note the hard limiters A and B, the flip-flop, and the integrator).

The operation of the measurement setup is as follows. Polarized light, transmitted from a laser over a turbulent atmospheric path, is incident upon the receiving lens system which collects and collimates the beam. The diameter of the received beam relative to the collector and collimator aperture is variable. The collimated beam then passes through a rotating polarizer which is driven by an electric motor through a suitable transmission system.

The rotating polarizer attenuates a portion of the received beam with a sinusoidal modulation, the period of which is one-half the rotation period. The amount of incident light transmitted through the rotating polarizer at a given instant is proportional to the square of the cosine of the angle x between the axis of the polarizer and the instantaneous polarization vector of the incident beam. Temporal variations in the orientation of the incident polarization plane are thus linearly proportional to temporal variations in x. Since the photomultiplier functions as a square law detector which doubles the frequency of the sub-carrier, the magnitude of the phase fluctuations at the output of the photomultiplier is equal to 2x.

A band-pass amplifier at the photomultiplier output extracts only the sub-carrier and adjacent phase-jitter sidebands. This signal is then hard-limited to extract only zero-crossing (i. e. phase) information. The output of limiter A drives the set input of the flip-flop. The operation of the flip-flop is discussed later.

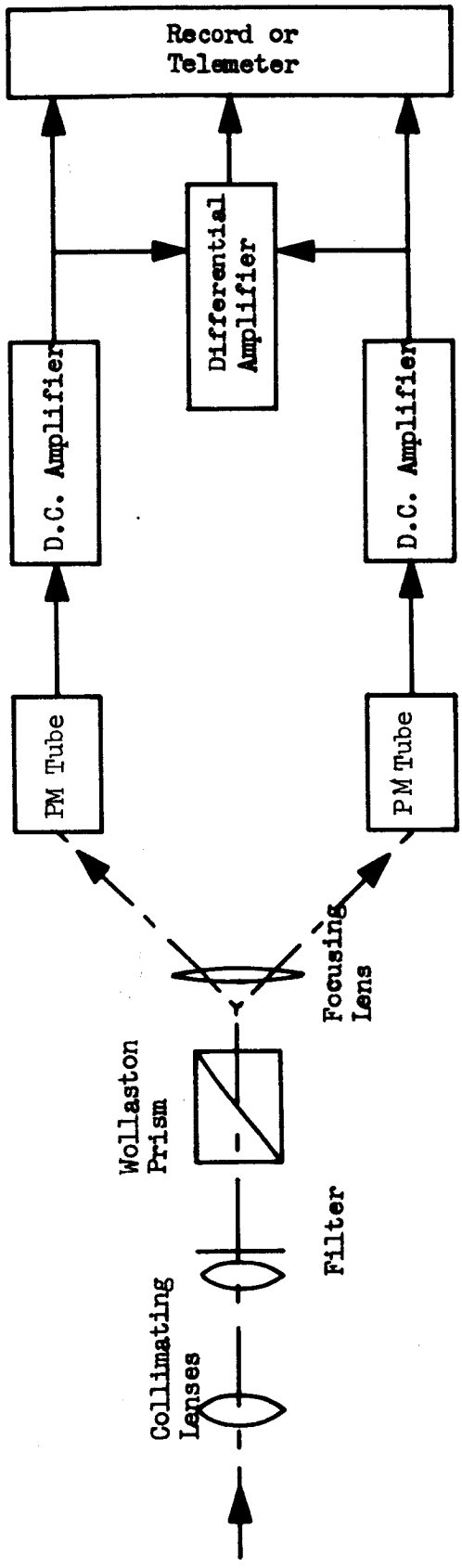

Figure 11.1. Primary System Configuration for Polarization Fluctuation Measurement

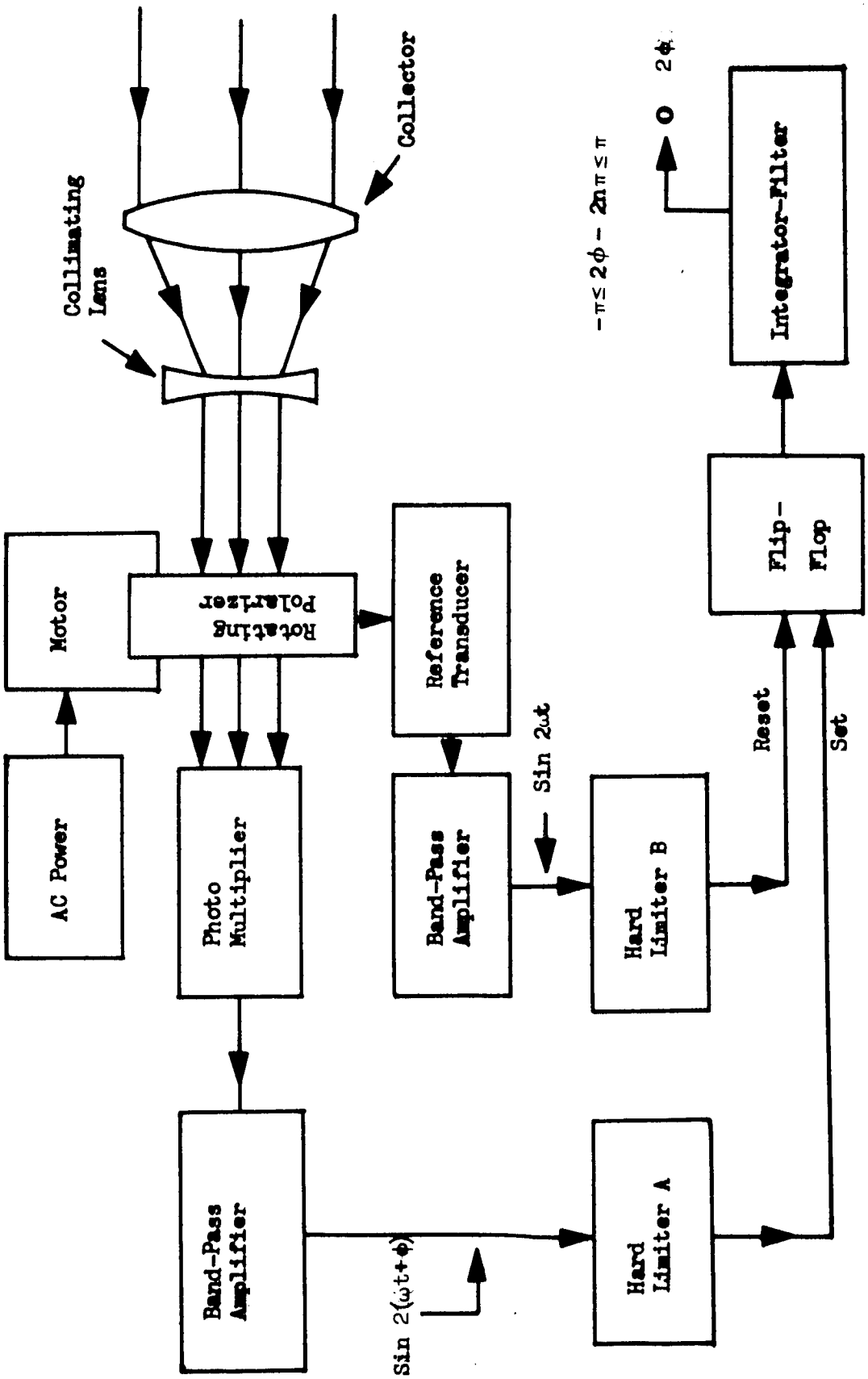

Figure 11.2. Configuration for "System A" Alternative Polarization Fluctuation Implementation

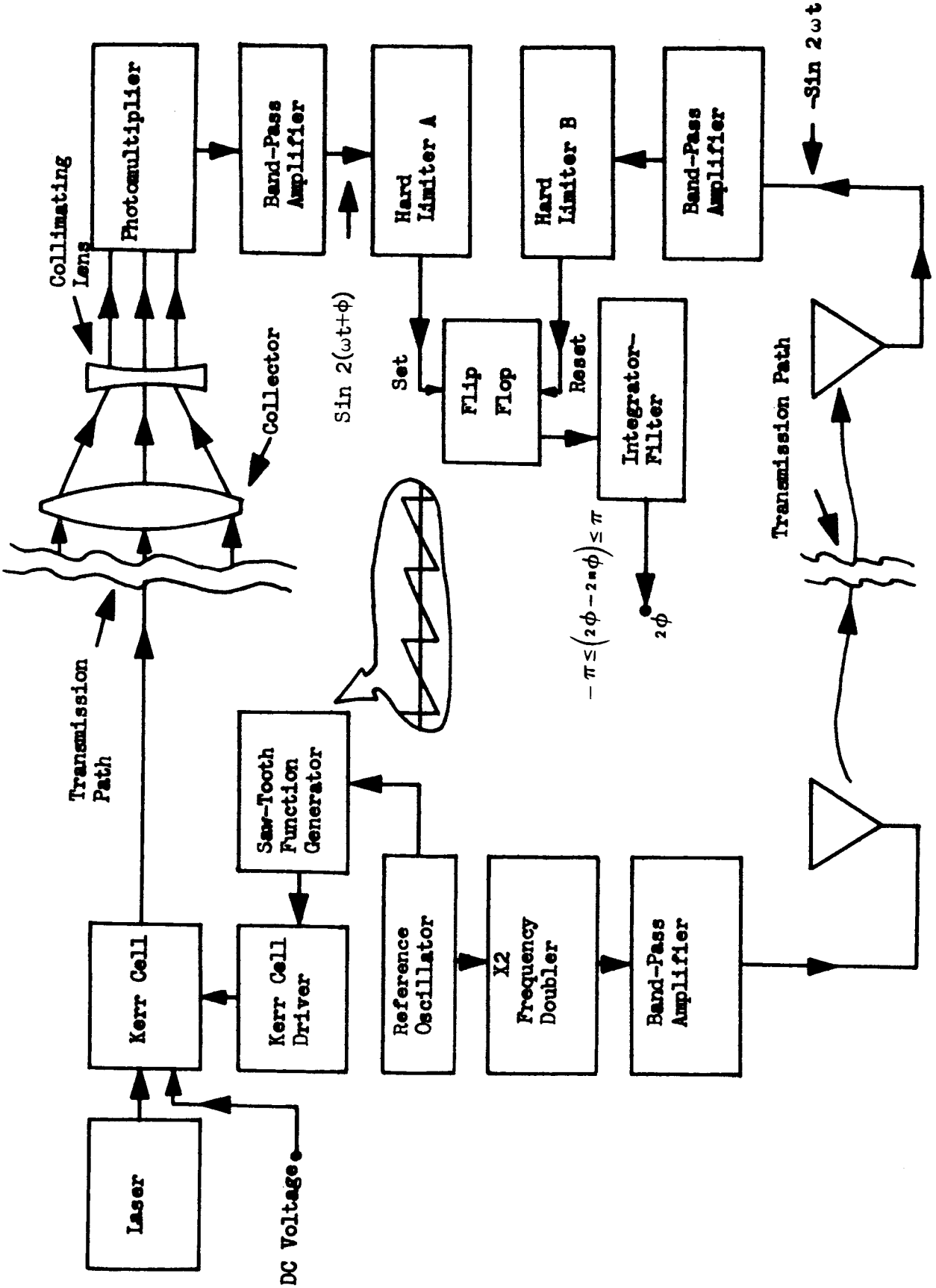

Figure 11.3. Configuration for "System B" Alternative Polarization Fluctuation Implementation

Table 11.1. Experiment No. 11 Equipment Lists
(Primary and Alternate Systems)

Qty	Item
	Primary System
1	Quarter wave plate (at transmitter)
2	Collimating Optics (2 lenses)
1	Focusing lens
1	Wollaston Prism
2	P.M. tubes
2	D.C. Amplifiers
1	Differential Amplifiers
	Supplementary Equipment
	Recording or telemetry system
	Alternate System A
1	Balanced AC Motor - low flutter and wow
1	Rotating polarizer with transducers energizer (e.g., small mirrors, magnets, mounted on periphery)
1	Reference transducer (magnetic, optical)
1	Multiplier phototube
1	Collector lens
1	Collimator lens
2	Band-pass amplifiers
2	Hard limiters (integrated into band-pass amplifiers)
1	Flip-flop (matched to limiter output voltages)

Qty	Item
	Alternate System A (Cont)
1	Integrator - filter output circuit
1	Real-time voltage recorder
1	He-Ne laser with collimating optics
	Alternate System B
1	He-Ne laser with collimating optics
1	Kerr cell
1	Kerr cell driver amplifier
1	Saw-tooth function generator circuit
1	RF Frequency Synthesizer
1	2X frequency multiplier
3	Band-pass amplifiers
2	RF antennas (or one RF cable)
2	Hard limiters (integrated into two band-pass amplifiers)
1	Flip-flop (matched to limiters)
1	Integrator filter
1	Real-time recorder
1	Multiplier photo tube
1	Collector lens
1	Collimator lens

Since there is generally a time varying error between the a. c. motor drive voltage and the angular displacement of a synchronous motor, a reference transducer operates from the rotating polarizer rather than from the a. c. supply (or even the motor armature). The error comes primarily from backlash and friction in the transmission. The magnitude of the backlash is generally less than 30 minutes of arc (Reference 21), and the spectral content of the jitter is not known. Because of the fact that polarization jitter due to turbulence may be of the same magnitude as that due to backlash, it is necessary to cancel this electromechanical slippage as much as possible. Deriving the reference frequency and phase from the rotating polarizer tends to cancel phase variations between the reference wave and the photomultiplier output except those due to variations in the polarization of the incident beam.

A second band-pass amplifier is used in the output of the reference transducer to remove harmonics which may be introduced by non-linearities between the angle transducer output and the cosine of twice the polarizer rotation angle. These harmonics appear at multiples of the sub-carrier frequency and hence do not affect the spectrum of the measured polarization jitter. The one exception to this occurs if the polarizer rotation frequency is not high enough to allow for measurement of the entire turbulence jitter spectrum. A method to compensate for this limitation is discussed in a subsequent section. The hard limiter is used to shape the reference wave to suitably drive the reset input of the flip-flop.

System B. Figure 11. 3 is a functional diagram of an alternative electro-optic technique. Note particularly that a Kerr cell polarizer modulates the laser beam before transmission through the turbulent medium, and that the sub-carrier reference phase and frequency is supplied to the receiver by a separate communications channel. (A retrodirective mirror could be used to avoid the necessity of transmitting the reference. However, the effects of atmospheric fluctuations would not then be the same, due to the different path length for this case.) Otherwise, the experimental setup is nearly identical to that of System A (Figure 11. 2).

Component Performance

It is common practice in optimizing communication systems to take full advantage of known distinguishing characteristics of system noise. In these two measurement schemes, this is done by generating a sub-carrier for polarization fluctuations. The sub-carrier places the polarization fluctuation spectrum at a frequency that is well beyond the 1/f noise inherent in photomultiplier tubes.

The concept of a polarization sub-carrier is basically not much different from the conventional notion of a frequency sub-carrier. In fact, any information which can be sent via a frequency sub-carrier can in

principle be sent via a polarization angle. In the present experiment, this sub-carrier is introduced by modulating or rotating the plane of the transmitted or received beam at a known rate. Moreover, the use of a sub-carrier enables the quadrature detection (required to determine polarization plane angle) to be accomplished after photodetection. The phase of the sub-carrier wave at the photodetector output contains the polarization fluctuation data. The output of each phase comparator consists of a known function of polarization angle, the function arguments differing by $\pi/2$ radians. Since this function is usually trigonometric (sine or cosine) special schemes must be employed to convert the quadrature functions to polarization angle. One such conversion scheme used for both alternative systems is discussed below.

Digital Phase Detector. The operation of the digital (flip-flop) phase detector is best described with the aid of a diagram such as that of Figure 11.4. The flip-flop changes to a positive state when the wave from either limiter goes to the positive state. The flip-flop goes to the null state when the other limiter goes to the positive state. The flip-flop output, therefore, is as illustrated in the figure. Note that for negative phase errors the output of the integrator must be a minimum and for positive phase errors the output must be a maximum. Phase error refers to the shift of the wave from A relative to that from B. It should be clear from observing the areas under the flip-flop output pulses in Figure 11.4 that the integrator output must be linear with phase error.

It should not be assumed that limiting must be so hard that the filtering provided by the bandpass amplifier is negated. Limiting need be only hard enough to establish a reasonable probability that the signal will rise above the decision level of the flip-flop circuit, even during amplitude fluctuations of the carrier wave.

Many commercial flip-flops have built-in limiters. This is done principly to protect the transistors from high voltage transients. If such is the case with the flip-flops used for the measurement, it may only be necessary to adjust the amplifier gain to the hardness of limiting desired.

The electro-optical technique (System B) requires a Kerr cell modulator with an associated function generator and driving amplifier. These will now be discussed.

Kerr Cell. A dc voltage is supplied to the Kerr cell in order to permit fine adjustments to compensate for delays in transmitting the reference frequency and phase signal. This establishes the proper dc level for the function generator, and thereby adjusts the median angular shift of the polarization plane through the Kerr cell.

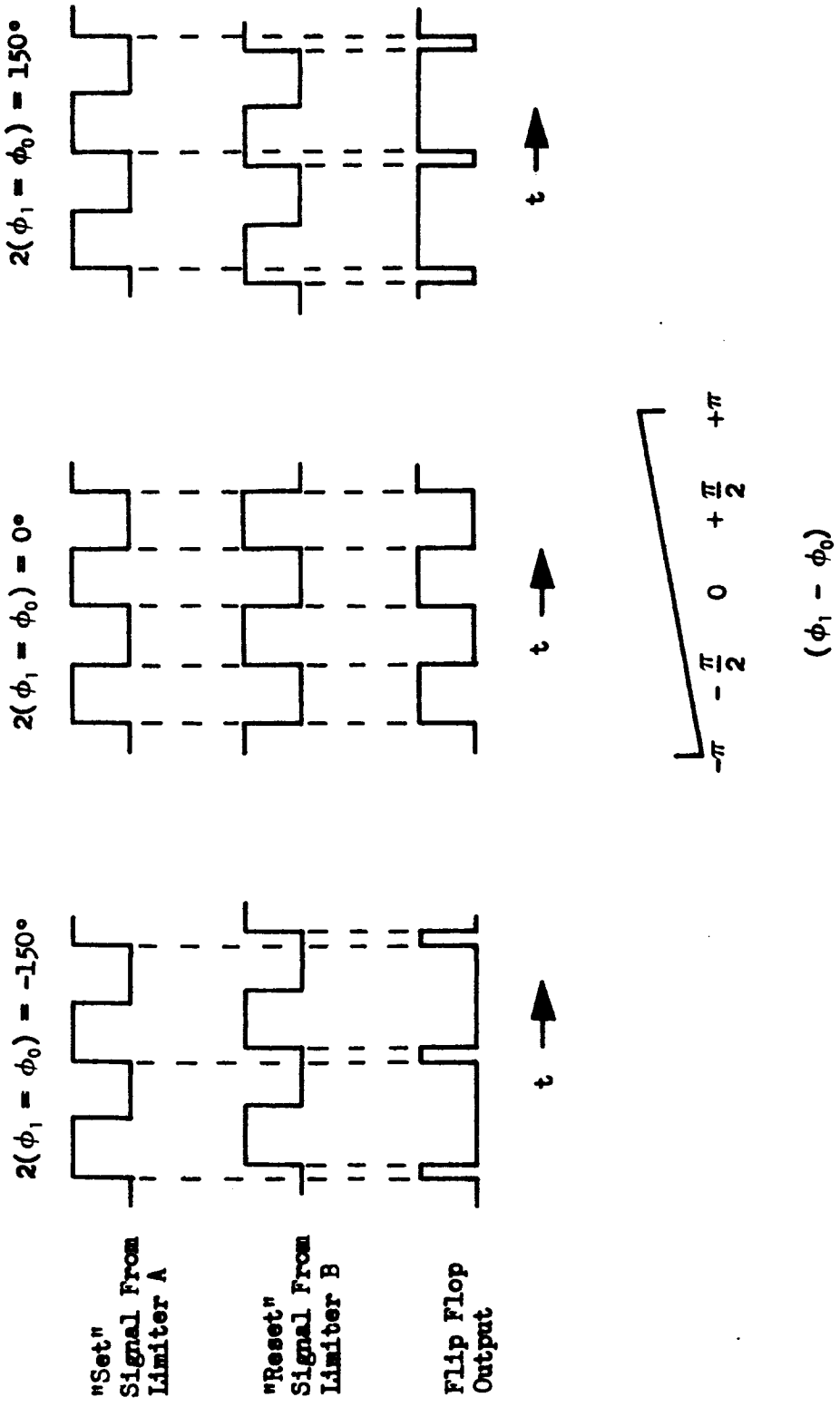

Figure 11.4. Digital Phase Detector Operation

The Kerr-cell driver is a band-pass amplifier with a step-up transformer on the output. The step-up transformer produces the high voltage that is necessary to drive the Kerr cell to provide a retard and advance of $\lambda/2$ in the quadrature polarization plane. It requires a high voltage to get this much path length shift. Kerr cells can be built (at a cost of about $500) which would require approximately plus or minus 2KV to achieve this performance. The frequency limit for this type of sub-carrier modulation would probably be due to circuitry external to the Kerr cell, for Kerr cells have response times of a very few nanoseconds.

Function Generator, Frequency Doubler and Bandpass Amplifier. The sawtooth function generator creates a periodic sequence of ramps as indicated in Figure 11.3. These linear ramps cause the polarization angle to increase through 2π radians before the polarization plane returns to its original orientation. The return is almost instantaneous compared to the time for the ramp to rise to a maximum value. Polarization rotation rates of a few hundred thousand rpm should not be difficult to achieve, at least insofar as bandwidth limitations are concerned. The use of functions other than linear ramps may be feasible, but this subject has not been thoroughly considered. The sawtooth generator itself is relatively simple. One version might consist of an integrate-and-dump filter with a constant input voltage.

The frequency doubler and bandpass amplifier provide the reference phase and frequency signal for transmission to the receiver. The receiver functions as in Figure 11.2, except that the rotating polarizer is no longer in front of the photomultiplier tube.

Transmission of the Sub-carrier Through the Turbulent Medium. In principle, it does not matter whether the polarization modulation sub-carrier is introduced prior to transmission through the turbulence or afterwards. According to theory, small, time varying changes in the refractive index should cause polarized light to be scattered from the beam regardless of whether polarization modulation already exists on the beam. The turbulence thus adds to the polarization fluctuations already present and the sub-carrier should contain additional polarization sidebands after reception at the photodetector surface. Therefore, the alternate measurement technique proposed here should provide a valid method for measuring polarization fluctuations.

The reason for not introducing the sub-carrier at the receiver as in System A (Figure 11.2) is that to do so would require an excessively large Kerr cell aperture. In view of the high driving voltages required for a window about 1 mm wide (as would be the case in Figure 11.2) introducing the sub-carrier electro-optically at the receiver would be impractical.

Evaluation of Alternative Measurement Systems

From the standpoint of both information gained and ease of implementation, the electromechanical system (Alternative A) is the least satisfactory of the three measurement techniques described. The most serious disadvantage of this method is the limitation on the available information bandwidth imposed by mechanical restrictions on the rotating polarizer. Such restrictions are a consequence of the need to keep the rotational stresses on the polarizer within safe limits. The mechanical tolerances for the rotating shaft which carries the polarizer must also be good enough to insure against rupture or serious distortion caused by vibration and torques at the designed rotation frequency.

To achieve a reasonable measurement bandwidth of 1000 cps, for example, the sub-carrier and its harmonics must be separated by at least twice this frequency, which requires a rotation frequency of 1000 revolutions per second to produce a sub-carrier at 2000 cps with harmonics at 4000 cps, 6000 cps, etc. But 1000 rps is 60,000 rpm, a very high rotation rate for a relatively fragile optical piece which was not designed with mechanical balance and stress in mind. Practical measurement bandwidths using the electromechanical method would therefore be limited to a probable range of 10-100 cps.

The use of a tourmaline crystal emulsion on a hardier base would permit somewhat higher bandwidths, but at the expense of considerable accuracy in the resolution of the polarization plane.

A better solution is to avoid these mechanical troubles entirely by making use of the electro-optical technique (System B). Although this system is more complex than the electromechanical version, requiring an auxiliary function generator and Kerr cell driver circuits, its advantage over the latter becomes decisive for high bandwidth use where the special machining techniques required for the rotating polarizer assembly become both difficult and expensive.

However, in comparison to the primary system, both of these alternative methods suffer from three major defects. First, while the primary system provides a continuous measurement of the polarization shift (it measures 2x when the angle is small; more accurately, sin 2x), and therefore also of its rate of change, the alternate methods only measure the polarization shift at intervals equal to half the period of the rotating prism, or equivalently, of the modulation frequency of the Kerr cell. Hence, the rate of change of the polarization plane (which is of considerable interest in this experiment) can only be determined to an accuracy which is proportional to these frequencies.

A second deficiency of the alternative systems is the fact that they are not capable of making measurements on circularly polarized light which, as noted in the Task II report (Reference 1), should also be employed to provide a complete test of the effects of a turbulent atmosphere on laser light. The primary system, on the other hand, is equally applicable to linearly, circularly, or elliptically polarized light. Similarly, the primary system measures the unpolarized component of the light, while the alternative systems do not.

Finally, the alternative systems presented here are burdened with the substantial disadvantage of complexity, with the attendant difficulties of experimental operation. By contrast, the primary system, using a single, stationary polarizing prism and avoiding the need for maintaining and transmitting a reference phase, is gratifyingly simple. For all of these reasons, the primary system is recommended as a first choice for implementing this experiment.

ATMOSPHERIC BACKSCATTER, TRANSMITTANCE, AND SKY RADIANCE - EXPERIMENT NO. 12

OBJECTIVE

To measure atmospheric backscatter, transmittance, and sky radiance.

IMPLEMENTATION

Summary

Consideration of the functions and parameters of the receiver optical system indicates that a large aperture telescope of long focal length, together with a photomultiplier is adequate to serve as the receiver for this experiment.

System Configuration

The equipment required for this experiment is listed and discussed in Table 12.1, and the elements of the receiver are indicated in the schematic diagram of Figure 12.1. The optical axis lies along the line $F_1F_2F_2'$. Light enters from the left and exits to the right onto the photocathode of a photomultiplier. The optical system is divided into two separate components, the objective and the eyepiece, of which the principal planes P and P' and the focal points F and F' are distinguished by subscripts 1 and 2 respectively. All focal lengths are positive in the sense of the usual convention, and the first and second focal lengths are equal. Thus, for the objective, the focal length f_1, the distance of P_1 from F_1 or of P_1' from F_1', is equal to f_1'. For the eyepiece, the focal length f_2 equals f_2' and is the distance of P_2 from F_2 or of P_2' from F_2'. The combined system is technically telescopic; that is, F_2 and F_1' coincide. Consequently, rays that enter parallel emerge parallel.

It is assumed that the entrance pupil is determined either by the rim of the objective lens or mirror or by a front aperture stop. The diameter of the entrance pupil is D_{en}. It is also reasonable to assume that the exit pupil of diameter D_{ex} is determined by the image of the front aperture stop or objective rim which is formed by the part of the system that follows it.

The field stop, located at a distance α behind F_1' and having a circular opening of diameter D_f, is indicated by the line S_f. The dashed line S_f' represents the image of S_f by the part of the system which precedes it. The angular field-of-view θ_r is the angle which S_f' subtends at the center of the entrance pupil.

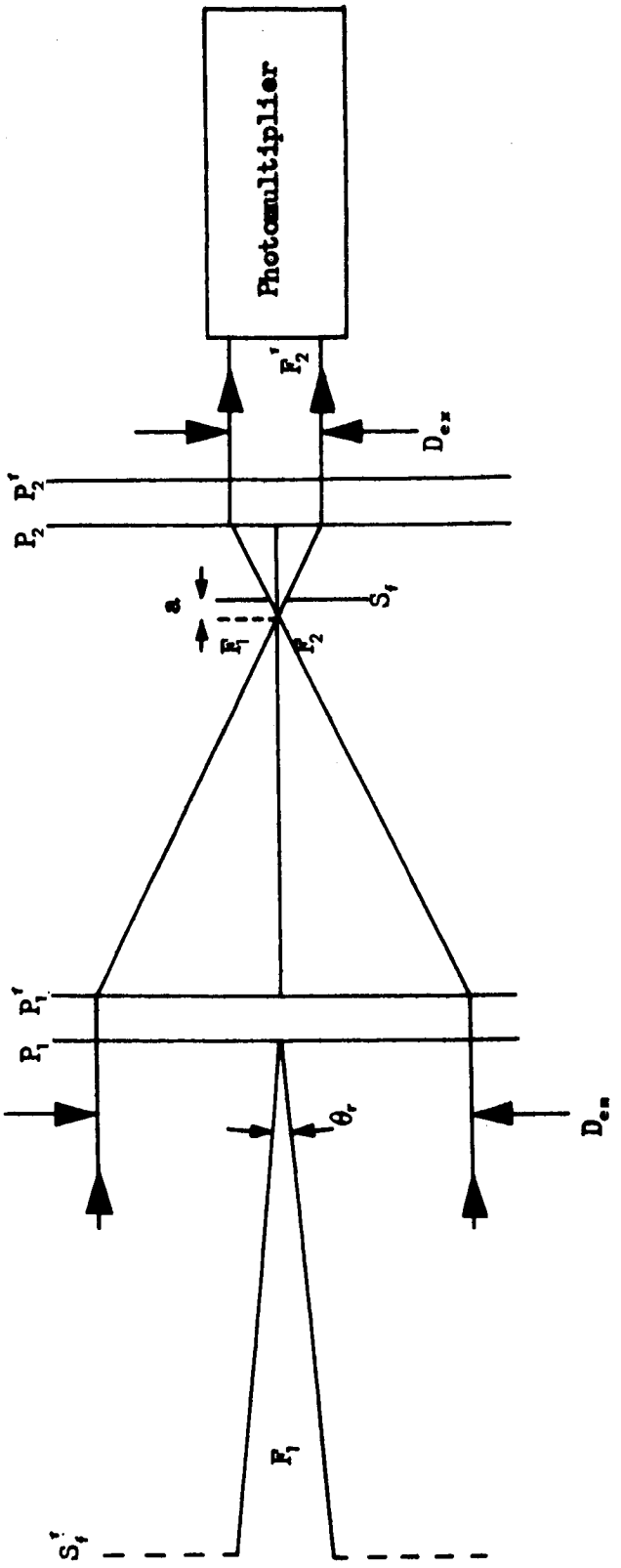

Figure 12.1. Configuration for Receiver Arrangement for Backscatter, Transmittance and Sky Radiance Measurements

Table 12.1. Experiment No. 12 Equipment List

Quantity	Item
1	Laser (giant-pulse ruby)
1	Transmitting telescope
1	Photomultiplier (RCA 7265 or equiv.)
1	Receiving telescope with field stop
1	Parallel mount for telescope
1	Power monitors
1	Beam splitters
1	Oscilloscope
1	Oscilloscope camera
Variable	Optical filters and attenuators

Component Analysis

The principal functions of the optical system are to increase the amount of backscattered light collected beyond the capability of the unaided receiver, and to keep out unwanted light by limiting the field-of-view. Each of these functions will now be discussed.

Collector Area

The collecting area A_r of the receiver, sometimes referred to as the effective aperture area, is given by

$$A_r = \pi \epsilon / 4 \, D_{en}^2 \qquad (12.1)$$

where ϵ is equal to or less than unity, depending upon the presence of opaque obstacles, such as a secondary mirror, along the axis. Not all of the light collected over the area A_r within the field-of-view θ_r is transmitted because some is scattered or absorbed by the optical components. The fraction transmitted is the transmittance τ_{op} of the system. It decreases as the number of components increases.

Optical Gain

The diameter of the photocathode is D_p, and the area is A_p. This area is only a small fraction of the area over which the backscattered irradiance falls.

The gain G in backscattered power achieved by using the objective system is given by

$$G = \tau_{op} A_r / A, \qquad (12.2)$$

where A_r is given by Equation 12.1. Hence, the gain may be increased by increasing the size of the receiver aperture. However, the focal length is usually some five or ten times the diameter of the lens or mirror, so that large components have long focal lengths.

Although the eyepiece could be eliminated so that the photomultiplier looks directly at the rays diverging from F_1', the focusing of the rays into an almost parallel beam offers two advantages. It spreads the light over the photocathode surface so that inhomogeneities of response are averaged out, and it relaxes the requirement for critical placement of the photomultiplier, since the beam is almost parallel.

The exit pupil diameter D_{ex} must be less than or equal to D_p, but the diameter of the eyepiece must be greater than or equal to D_{ex}. Preferably, the focal length f_2 should be short for compactness. The pupil diameters are connected through the relation

$$\frac{D_{en}}{D_{ex}} = \frac{f_1}{f_2}. \tag{12.3}$$

Accordingly, the telescope collects the light over a large area and focuses it to an area roughly $(f_2/f_1)^2$ times smaller.

Field of View

The half-angle $\theta_r/2$ of the field-of-view is given by the relation

$$\tan(\theta_r/2) = \frac{D_f}{f_1+\alpha}. \tag{12.4}$$

To keep the field stop S_f from reducing the exit pupil, it must be located at a distance α equal to or slightly less than

$$\alpha = f_1 D_f / D_{en}. \tag{12.5}$$

Since D_f is small and D_{en} is large, α is much less than f_1 and may be neglected in Equation 12.4. Therefore, for small values of θ_r, Equation 12.4 reduces to the form

$$\theta_r = 2D_f/f_1 \tag{12.6}$$

This relationship indicates that small D_f and large f_1 are needed to produce a small field-of-view. This is shown graphically in Figures 12.2, in which D_f is plotted as a function of f_1 for different values of the parameter θ_r.

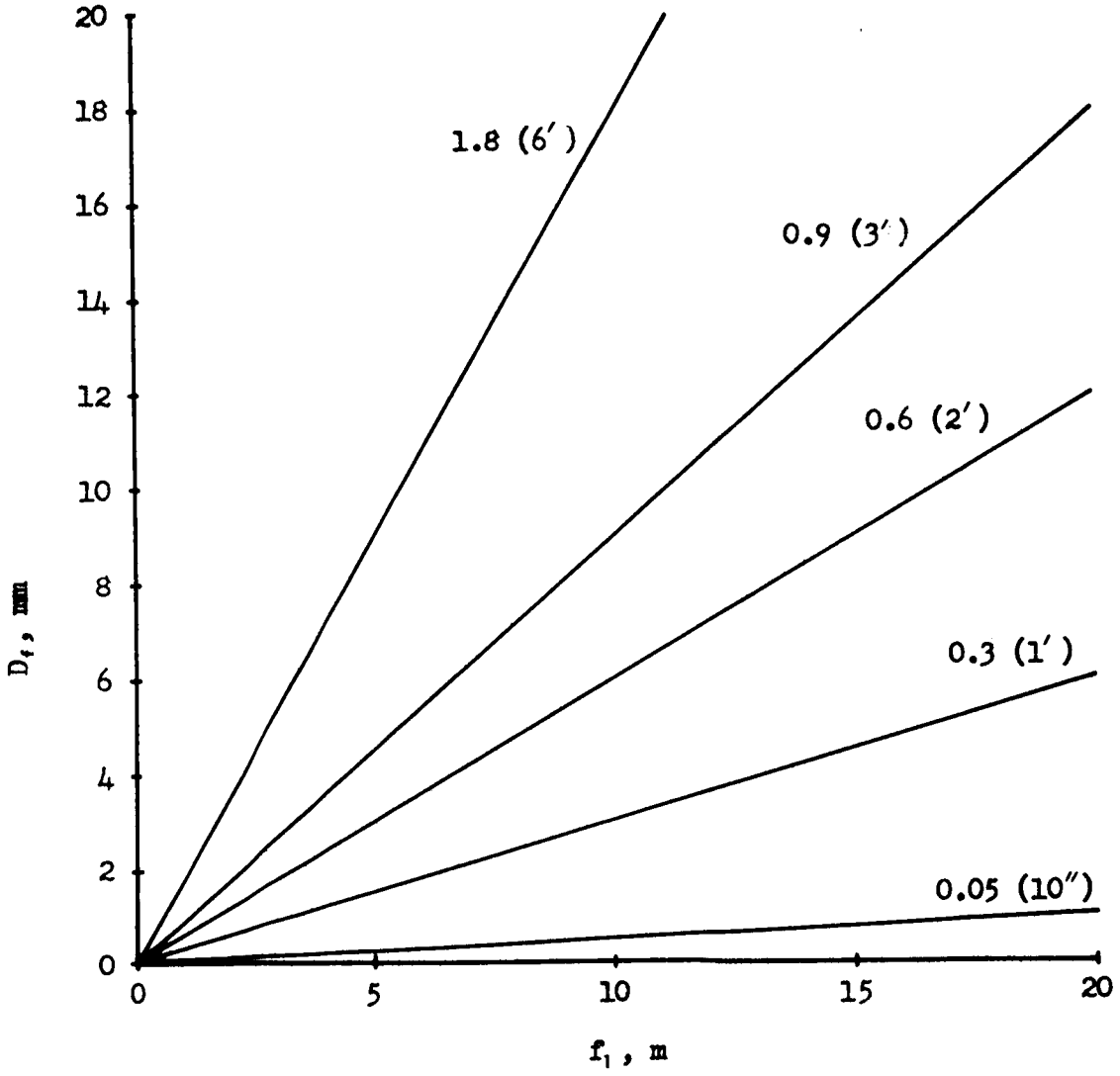

Figure 12.2. Stop Diameter, D_f, vs. Focal Length, f_1, for Different Fields of View (milliradians)

COMMUNICATION LINK ERROR RATE - EXPERIMENT NO. 18

OBJECTIVE

To measure the effect of a turbulent atmosphere on the information transfer capability of an optical communication system.

IMPLEMENTATION

Summary

An instrument configuration is described which measures bit error rates induced by:

1. The turbulent medium
2. Noise in the detectors and amplifiers
3. Vibration and miscellaneous biases

When laser power, path length, aperture size, geometric configuration, filtering, attenuation and gain are all controllable factors items 2 and 3 may be made negligible in comparison to item 1, so that only the errors induced by the transmission medium are measured in the experiment. The system makes use of a Kerr cell modulator, a photomultiplier detector, and integrated digital logic circuitry to simplify construction and obviate the need for storage tapes, magnetic drums and other electromechanical devices. The entire measurement configuration is compatible with variable "information" bit rates of up to 1 Mc without severe degradation of the modulation index and other system parameters. This capability is tested by transmitting a signal which contains frequency components distributed over the entire information baseband.

System Configuration

Figure 18.1 contains a detailed block diagram of the equipment configuration suggested for this experiment together with a list of the required equipment. In general terms, the output of a message generator modulates a laser beam which, after passing through a region of turbulent air to a reflector target (corner reflector or plane mirror) is returned to the receiver,

Table 18. 1. Experiment No. 18 Equipment List

Quantity	Item
1	He-Ne laser
1	Kerr Cell Modulator
1	Polarization Analyzer (Polarizer)
1	Kerr cell Driver Amplifier
1	Half-silvered mirror
1	Collimating lens (transmit)
1	Collector lens (receiver)
1	Corner reflector
1	Quarter-wave plate (for 6328 Å)
1	Bi-refringent prism
1	Three-sided mirror (beam splitter)
2	Multiplier photo-tubes
1	Difference-voltage amplifier
1	Sum-voltage amplifier
2	SPDT switches
1	SP Multiple Throw Turret Switch
2	Squaring Circuits (voltage-amplitude limiter)
1	0 - 1 Mc Tunable frequency synthesizor
1	0 - 1 Mc Video amplifier
1	Digital counter
1	Low-pass filter
	The following components may consist of integration circuit elements:
2	Modulo-two adders
3	Inverters (may be integrated into logic circuits)
1	"And" Gate
-	Flip-flops (Quantity will depend upon band spreading desired for message)

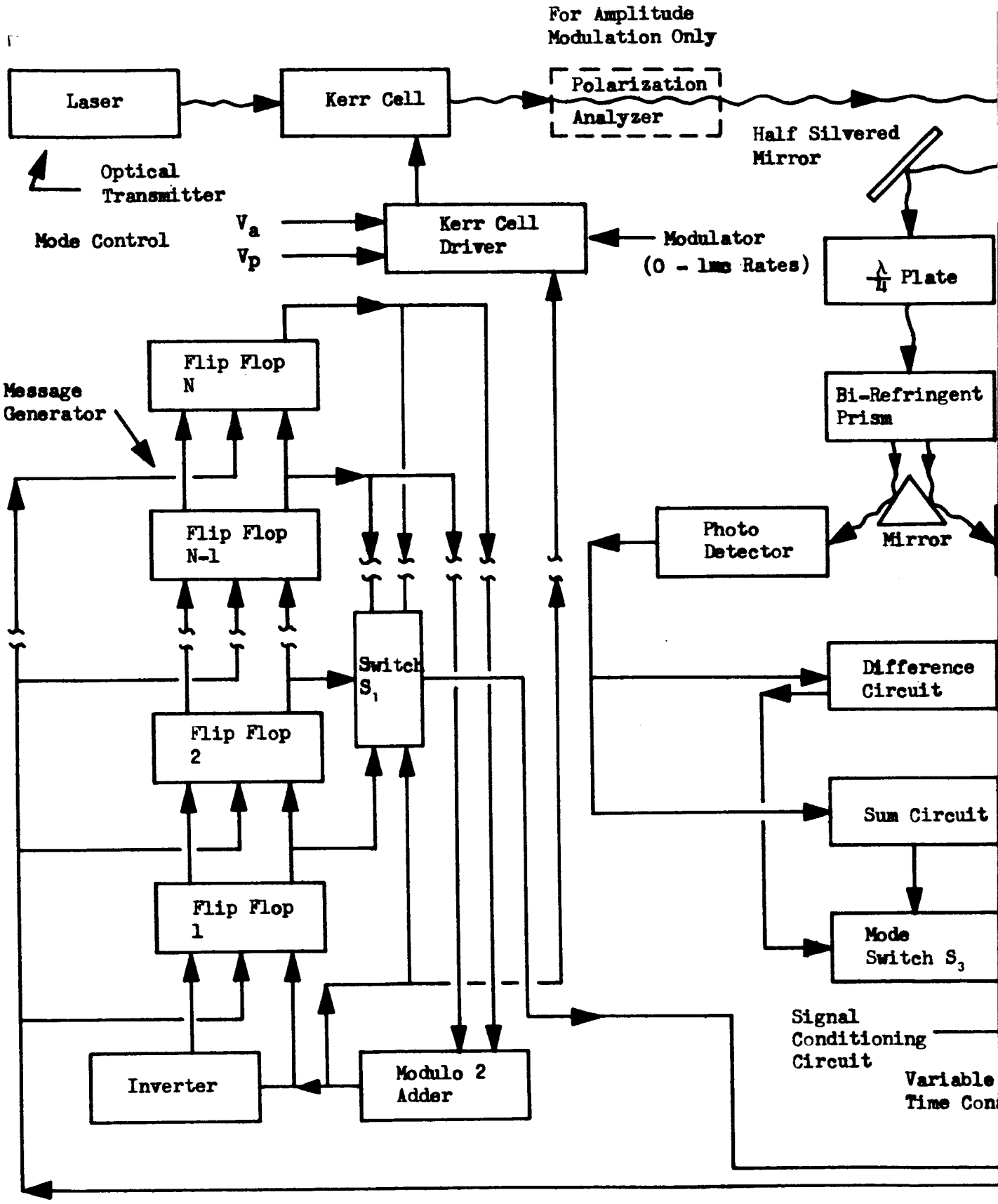
For Amplitude Modulation Only
Laser
Kerr Cell
Polarization Analyzer
Half Silvered Mirror
Optical Transmitter
Mode Control
V_a
V_p
Kerr Cell Driver
Modulator (0 - 1mc Rates)
$\frac{\lambda}{4}$ Plate
Flip Flop N
Message Generator
Bi-Refringent Prism
Flip Flop N-1
Photo Detector
Mirror
Switch S_1
Difference Circuit
Flip Flop 2
Sum Circuit
Flip Flop 1
Mode Switch S_3
Signal Conditioning Circuit
Variable Time Con
Inverter
Modulo 2 Adder

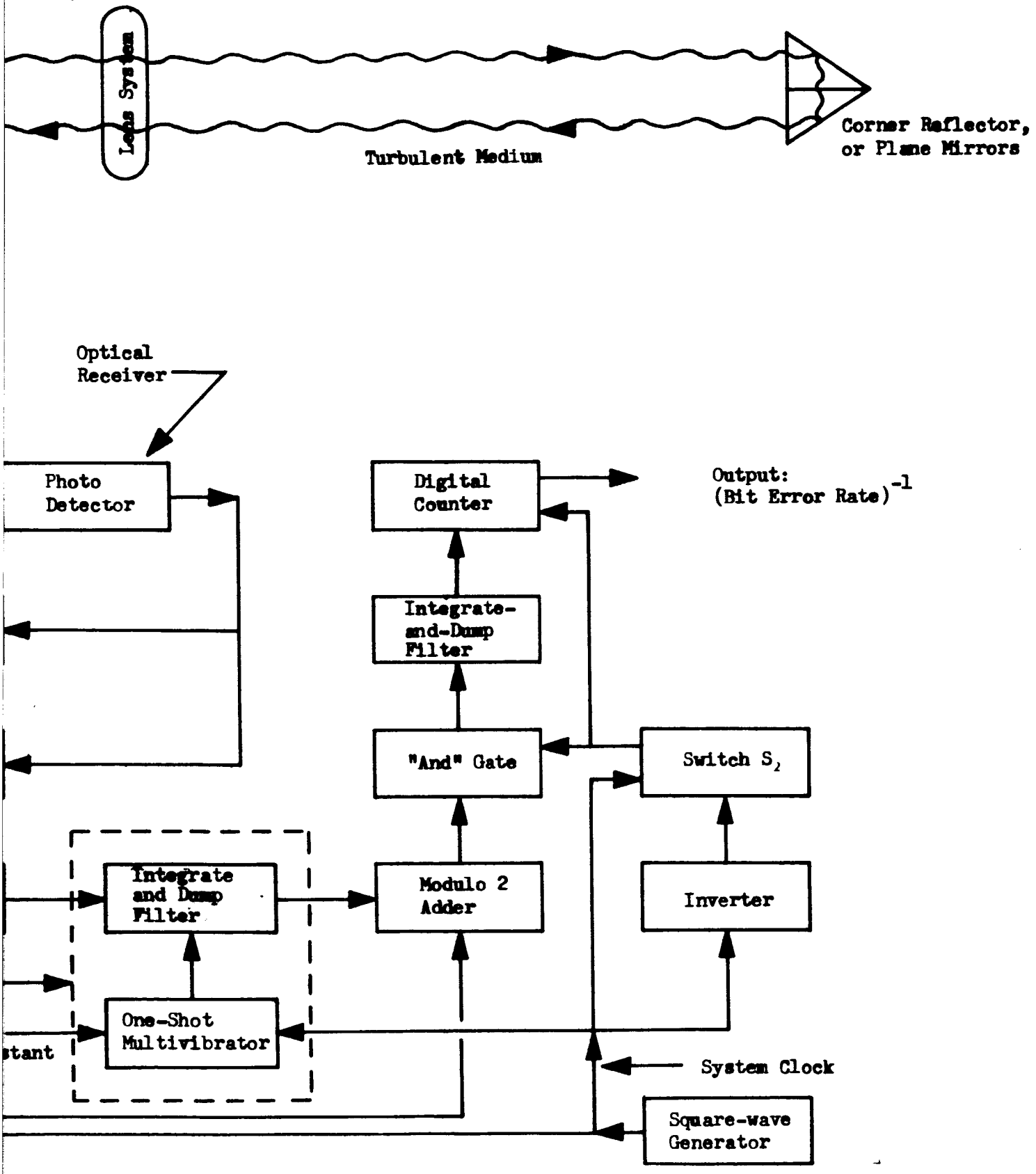

Figure 18.1. Configuration for Measuring Communication Error Rate

where the corrupted signal is detected and compared with a delayed replica of the transmitted signal. This reference signal is delayed by an amount equal to the round-trip transit time of the transmitted signal, thereby permitting direct real-time measurement of the bit error rate produced by the turbulent atmosphere.

Component Performance

Message Generator

The message generator consists of a pseudo-noise shift register. Each element of the register is a flip-flop with complementary inputs and outputs. The initial states of the flip-flops are generally pre-set to ensure code regeneration. The modulo-two adder is fed by the outputs of two flip-flops. Code length and bit sequence depend upon the choice of the two flip-flop outputs for modulo-two addition. The maximum code length is 2^N-1 where N is the length of the register. The register shifts one bit position with each clock pulse and a new random bit is entered from the modulo-two adder output into one end of the register, the bit at the opposite end of the register being discarded. The bit rate is thus the clock frequency. The outputs of subsequent flip-flops each contain an identical code, which is delayed by exactly one bit interval relative to the preceding output code. A zero-to-N bit delay is thus built into the message generation technique. The switch S_1 selects the required amount of delay in increments of one bit position. Finer delay adjustments will be discussed later.

Modulator

Compared to other currently available techniques, the Kerr cell analyzer combination shows the greatest potential for both polarization modulation and amplitude modulation of the laser beam. The principal advantages of this method are:

1. The Kerr cell can produce a relative shift between two orthogonal polarization components of up to half a wavelength ($\lambda/2$), and this can be done at modulation frequencies approaching one megacycle, providing the cell driver is capable of delivering the necessary power with such reactive loading.

2. Theoretical considerations indicate that the cell driver power requirements may be reduced by such measures as reducing the dimensions of the cell, applying a large dc bias voltage, and providing a heat sink for the polarizing medium.

3. Modulation of the Kerr cell should not produce (a) additive noise (as does modulation of the laser anode current) and (b) beam segmenting (as do interference modulators, because of alignment problems).

To achieve right- or left-hand circular polarization, the driving voltage advances or retards the phase of one polarization component by a quarter of a wavelength. For amplitude modulation, one component is advanced (or retarded) by a half-wavelength and the polarization analyzer (not present for polarization modulation) allows only one polarization component to be transmitted. Thus, for example, zero rotation of the polarization plane may correspond to maximum transmitted intensity and a 90° polarization rotation may correspond to minimum transmitted intensity. To change one component by $\lambda/2$ the median driving voltage may be altered, or the median driving voltage may be left unchanged and a $\lambda/4$ plate introduced between the laser and the Kerr cell.

Optical Path

The transmission path is comprised of the transmitter and receiver optics, a retro-reflector, and the turbulent medium. If a corner reflector is used, the transmitted beam will be returned directly back on itself. If the receiver is not co-axial with the transmitter, a half-silvered mirror may have to be placed in front of the transmitter in order to divert the return beam to the photodetectors.

One typical corner reflector is a 2-1/2 inch device made by Perkin-Elmer, priced at about $350. Its useful angular field of view is about 30°. It also increases the initial beamspread by an additional divergence of about two seconds of arc.

The use of a corner reflector has important consequences which must be considered. Backscattered light is received with the return beam and contributes to the turbulence error rate measurement. The experimenter must decide whether or not he wants this effect included. In addition, return of the beam over the same optical path will tend to cancel some of the angular fluctuations induced by the turbulent medium. Again, the experimenter must decide whether he wants this cancellation of angular jitter to occur, and how much control he wishes to exercise over this effect. An alternative is of course to use two or three plane mirrors orthogonal to one another and at 45° with respect to the incident beam. With this technique, the difference between the outgoing and returning paths can be controlled. In any case, after the limits of beam wander have been determined, the collector aperture must be chosen large enough so that it always contains the received beam.

Detector

The detector configuration, like that of the modulator, is readily adaptable to both the amplitude mode and the polarization mode of operation. The polarization of the incoming beam is resolved into two orthogonal planes through the action of the $\lambda/4$ plate. If, for example, when the polarization is right-circular, the plane is vertical after passage through the $\lambda/4$ plate, then when the polarization is left-circular, the $\lambda/4$ plate resolves it into the horizontal plane. The birefringent prism spatially separates these two polarization planes and the wedge-shaped mirror (see Figure 18.1) produces an angular separation which is convenient for placement of the photodetectors. For polarization modulation, mode switch S_3 selects the difference between the photodetector outputs and for amplitude modulation, S_3 selects the sum.

The photomultiplier tube appears to be the best available detector for this application for the following reasons:

1. PM's have low internal noise levels at room temperatures, which can be further reduced by cooling, if required. (See Appendix C.)

2. Frequency response at baseband is limited primarily by transit time effects and can be designed to be generally superior to that for the solid-state devices.

3. Solid-state devices usually require that the beam be focused on a very small cross-sectional area. Compromises have been achieved in some cases by sandwiching the active material between electrode lamina. Photomultipliers, on the other hand, have collecting surfaces which are comparatively large and hence, obviate the need for precision focusing.

4. Photo-TWT's are essentially the same as photomultipliers except that a traveling-wave tube is activated by the electron stream. To get a response near zero cycles per second at baseband, special mixing procedures at radio frequencies are required.

When using photomultipliers, care must be taken to avoid damage to the photoemissive surface resulting from high light levels. Recent experimental data obtained at S&ID indicates that 50 microwatts per square centimeter will cause damage. This problem would normally be important only for short optical paths and can be controlled by attenuating the beam and/or spreading it with the receiving optics.

Signal Conditioning Circuit

The squaring circuit at the output of the optical receiver section should contain synchronous integrate-and-dump circuitry in order to most efficiently detect the signal before comparison with the reference wave. The integrate-and-dump filter stores signal energy over one bit period, and stores a binary state in a register. The integrate-and-dump filter contains an integrator which is discharged after sampling by the signal from the one-shot multivibrator. The one-shot multivibrator delays the clock pulse over a period (a fraction of a bit period) determined by the time constant chosen. The sampling register makes a decision as to whether the signal is in a plus (+) or zero (0) state and holds this binary state for one information bit period. The output of the integrate-and-dump filter then consists of a stream of shaped and delayed pulses which resembles the transmitted wave.

System Clock

Since the error comparator utilizes two signals which originate from the same generator, a high degree of stability in the system clock is not necessary. The simplest device is an astable multivibrator. For such a circuit, the clock frequency may be controlled by varying the time constant in the external RC circuitry. An easier method (shown in Figure 18.1) is to employ a commercially available wave generator. Many of these have the square wave output required for this experiment as a standard selectable function.

Error Counting Circuit

Figure 18.2 illustrates graphically the principle of the error detection scheme. (a) and (b) represent the transmitted and received signals, respectively. After the received and detected wave is shaped in the signal conditioning circuit (c), it passes into the modulo-two adder, where it is compared with the delayed signal replica (d). The output of the modulo-two adder (e) is in the "true" state when the two waves being compared are unlike and the output is "false" otherwise. This process is called "exclusive-or" addition.

The example chosen for the figures is an extreme one in at least two respects. The error rate shown is roughly 10^{-1}, indicating considerable degradation in the received wave. Secondly, the fraction-of-a-bit delay originating in the transmission path and the detection process is the extreme case of exactly half a bit. The position of switch S_2, however, compensates for this error introduced by the fractional bit delay in such a way that the digital counter output is correct. Recognition of an incorrect setting of S_2 is straightforward: (1) an error rate of 1.0 is always incorrect, (2) an error rate distinctly less than 5×10^{-1} is usually correct, and (3) an error rate of exactly 5×10^{-1} signifies that no signal is present at the detector input,

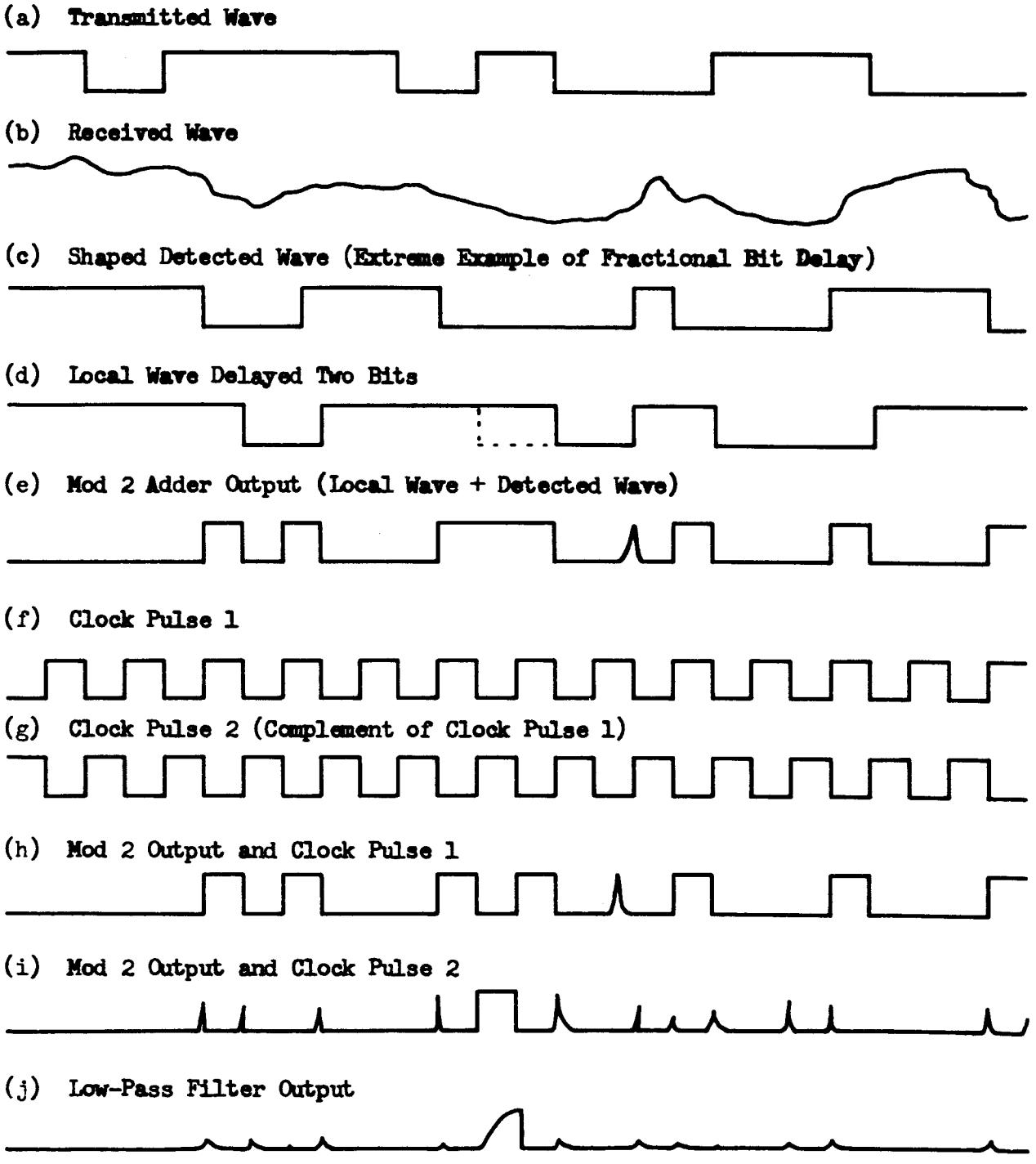

Figure 18.2. Example Illustrating Function at Error Comparison Network

that the proper output tap of the pseudo-noise generator is not being used, or that some malfunction is preventing the two waves from being processed in the manner shown in (e) through (j) of Figure 18.2. (An exception to item (2) is a malfunction preventing the operating of the mod 2 adder. In this case, and others like it, the error rate drops to exactly zero.)

Item (h) of Figure 18.2 is the output of the "and" gate when the clock pulse (not its complement) is used as one input and the modulo-two output is the other "and" gate input. In the "and" operation, both input states must be "true" to make the output state "true." In the example shown, the sequence at (h) contains all the error pulses due to the unwanted fractional bit delay.

The sequence at (i), however, contains only the actual error introduced by the turbulent medium, together with small, spike-like waveforms which integrate to an insignificant value over one bit interval. A low-pass filter is therefore used to remove these spikes from the "and" gate output, leaving only the bit error to be presented to the digital counter. Some commercially available digital counters have sampling circuits of this type already built in.

The bit-error-rate counting circuit described above gives essentially the same error rate as that present under the same noise conditions at the output of an integrate-and-dump binary detector.

SYSTEM SYNTHESIS

Having defined the experimental means by which various atmospheric effects on laser transmission can be investigated, the next logical task is to synthesize the 13 separate experiments into a number of rational groupings on the basis of specific program objectives and constraints. These objectives may range from the purely scientific to the investigation of potential techniques for engineering applications.

The experiment groups prescribed in this section are designed to accommodate this broad spectrum of goals and to provide a basis for establishing an implementation approach. In regard to the latter objective, the groupings involve some value judgements which take into account such factors as similarity of objectives, potential applications, limitations and constraints, and ease of implementation.

Since the experiments are identified only by number, a listing of all the experiments by number and title has been prepared in the form of a fold-out chart (Table 3) at the end of this section, providing a ready-reference to assist the reader in following the discussion. The inside page of the fold-out contains summaries (Tables 2 and 3) of the experimental groupings for the two general classes of optical links considered here: stationary ground-to-ground links, and vertical links involving satellite terminals. It is suggested that the three tables be examined at this point to provide a frame of reference for the following discussion.

STATIONARY GROUND-TO-GROUND LINKS

GROUP I

This group, which may be regarded as a basic application-oriented program, comprises Experiments 3, 6, 9, 10, 12 and 18, with Experiment No. 11 also included on an optional basis (signified by brackets [ ] in Table 1) contingent on a specific interest in polarization effects. Experiments 12 and 18 are also somewhat special in that they are not fundamental, from a theoretical viewpoint, but rather serve to provide background data necessary for system design.

The common denominator of Experiments 3, 6, 9, and 10, which gives them particular relevance for applications, is their concern with the distribution and fluctuation of power in the received beam. They also belong in the first group because, as a class, power measurements are the easiest to implement and carry out successfully. A number of measurements of this type have been made (References 47 - 50), although for the most part, they have been in the nature of exploratory or pilot tests, rather than comprehensive investigations of all the experimental parameters. Measurements of this type involve no exotic data recording or data processing techinques and they can be carried out in a straightforward manner with standard components and techniques.

These conclusions also apply to Nos. 12 and 18 and, provided the "Primary" receiver system is used, to No. 11 as well.

GROUP II

A minimum theory-oriented program is defined by adding to the Group I experiments either or both of the phase structure measurements, Experiments 1 or 2. The option is offered here because Experiment No. 1 alone is equivalent in potential information content to the combination of Experiments 2 and 3, but suffers the disadvantage of being more difficult to implement.

The first two experiments are assigned to Group II because not only is the phase structure function of paramount theoretical importance, but also because, in comparison to the "photon-counting" experiments of Group I, these heterodyne measurements require more effort to ensure good results

and are hence less attractive for application-oriented investigations. In addition, the data-processing requirements for Experiment No. 1 are greater than for the other experiments.

As in Group I, the inclusion of Experiment No. 11 is predicated on the desire for information on polarization effects. The other experiments (Nos. 3, 6, 9, 10, 12, and 18) - except Nos. 12 and 18, to which previous comments apply - have scientific as well as practical value and hence are included to round out Group II.

GROUP IIA

This group is defined as a sub-classification of Group II because, while it broadens the scope of the phase-related measurements, by the addition of Experiments 7 and 8, it still excludes those experiments which appear to offer the lowest "investment potential", and is therefore in this sense, still a kind of minimum program. The reason for not placing these two experiments in Group II is that, from a theoretical viewpoint, they do not have the fundamental importance of the $D\phi\,\phi$ measurements. Although Experiments 7 and 8 are concerned with phase effects, they are not heterodyne measurements. The only adjustment in Experiment No. 7 which requires more than ordinary care is the centering of the pinhole with respect to the focal spot. Experiment No. 8 likewise demands some experimental skill, but again the requirements are not as stringent as in the phase structure function measurements.

GROUP III

With the addition of Experiments 4 and 5, Group III constitutes the maximum program, including all 13 of the proposed experiments. The reasons for putting these measurements in the last group differ in the two cases. Experiment No. 5 has scientific interest, but, as shown in the Task II report (Reference 1), considerable care must be exercised in making the measurement in order to achieve successful results. On the other hand, No. 4 has little value to offer except as a scientific curiosity.

VERTICAL LINKS

It remains now to determine the applicability of the individual experiments to up- and down-links utilizing satellite or airborne terminals, and to re-evaluate, in this context, the groupings previously established for stationary ground links. In this discussion, primary attention will be devoted to satellite-ground (s-g) and ground-satellite (g-s) links, particularly those involving synchronous satellites (ss), which have often been suggested for spaceborne optical experiments.

GENERAL CONSIDERATIONS

Before re-examining the separate experiments, however, mention should be made of three problems, applicable to all the experiments, which are associated with the extension of ground links to vertical links. The first and perhaps most obvious of these is the problem of tracking, which becomes particularly acute for experiments which make use of heterodyne detection, as do Nos. 1, 2, and 5. In fact, a careful study of the permissible tracking errors for such measurements, in the light of current and projected tracking and vehicle stability capabilities, leads to the conclusion that these experiments cannot be successfully carried out with aircraft or non-synchronous satellite platforms, on either the up-link or down-link. In principle, the use of a synchronous satellite in a "stationary" orbit should overcome this problem, but at the higher altitude of such orbits the second and third problems referred to above come into play.

The second problem arises from the fact that at synchronous satellite altitude, the correlation distances in the laser beam are quite large. What this means in experimental terms is that at this altitude, the linear separation between the sampling apertures used in the correlation measurements must be on the order of several, or even tens of meters before any sensible difference in the measured quantities can be expected. Since any worthwhile correlation measurement must measure more than this minimum change (i.e. so that $C_{LL}(\rho)/C_{LL}(0)$ departs significantly from unity, or $D_{\phi\phi}(\rho)$ from zero), it is clear that such experiments should not be planned for a g-ss link.

The third factor which must be reckoned with in all the experiments (except No. 12) when long vertical links are considered, is the great reduction in the available power levels (irradiance) at the receiver due to spreading of the beam and atmospheric attenuation. For example, the

assumption of a 1 watt cw laser with a beamspread of 10^{-5} rad yields an irradiance at synchronous altitude (about 4×10^4 km) on the order of 10^{-10} watts/cm, which is marginal for these experiments, considering that apertures of satellite-borne receivers are limited. Since present limitations on laser power will presumably be overcome in due course as suitable lasers of higher output are developed, this factor will not be stressed further, but it must not be overlooked in assessing the feasibility of g-ss or ss-g experiments, in particular.

EXPERIMENT EVALUATION

The feasibility of each of the 13 LACE experiments will now be examined in the light of their individual characteristics as well as the general considerations just discussed. The experiments are taken up sequentially.

No. 1. This, being a heterodyne measurement, is one of the most difficult to perform. It is sensitive to environmental vibration such as would be encountered in tracking situations. Tracking requirements are also excessively high, thus excluding it from both up- and down-links involving either satellite or (especially) airborne terminals.

No. 2. Being also a heterodyne measurement, this must also be excluded from all vertical links.

No. 3. Since this is not a phase measurement, it can be performed over all vertical links, although on a g-ss link it will probably degenerate essentially into a simple power measurement because of the large correlation lengths involved.

No. 4. This experiment becomes meaningless whenever relative motion between the terminals is involved because in such cases the laser path through the atmosphere is continuously changing. It is thus eliminated from all vertical links except g-ss or ss-g.

No. 5. As a heterodyne measurement, and because it is also in Group III, this experiment should not be considered for vertical links.

No. 6. This experiment is feasible for satellite links, although because of the large correlation distance at synchronous altitude, it becomes identical to Experiment No. 3 for g-ss links.

No. 7. This is ruled out on two counts. First, the need for precise alignment imposes excessive demands on the stability of the receiver platform and the tracking capability of both receiver and transmitter.

Secondly, the measurement would have little value at synchronous altitude because of the large correlation distance, unless extremely large apertures could be employed.

No. 8. Because the angular fluctuations are so small in the case of a g-ss measurement (since the secondary source at the top of the atmosphere is so small) and because of the careful alignment and complex equipment which would be required in a satellite-carried receiver, as well as for tracking reasons, this experiment cannot be performed on an up-link. For the down-link, the measurement is possible but no new data is anticipated from ss-g links which closely simulate the conditions of stellar observations, and with other satellite orbits, tracking becomes a problem.

Nos. 9 and 10. The comments under Experiment No. 3 apply.

No. 11. This can and should be done on both the up-link and down-link, provided polarization effects have been detected previously over g-g links. A problem to be considered is the rotational rate of the satellite about the line-of-sight. So far as is known, polarization fluctuations will be small, so that the rate, or more importantly, the random error in keeping a constant rate will have to be small.

No. 12. Can be easily done, but has value only on the up-link, because of the backscatter measurement.

No. 18. Should be done on both up- and down-links.

The conclusions of the System Synthesis section are summarized in Tables 1 and 2.

Table 1. Experiment Groupings for Stationary Ground-to-Ground Links

Group	Rationale	Experiment by Number
I	Basic Application-Oriented	3, 6, 9, 10, 12, 18, [11]*
II	Basic Theory-Oriented	Group I + 1 and/or 2
IIa	Augmented Theory-Oriented	Group II + (2), 7, 8
III	Complete	Group IIa + 5, 4

*Optional - see text

Table 2. Experiments Suitable for Satellite-Link Measurement

Experiment No.	Remarks
3	Up- and down-links; becomes equivalent to No. 6 for g-ss*
4	g-ss,* ss-g* only
6	Up- and down-links; little value for ss-g*
9, 10	Up- and down-links
[11] **	Up- and down-links, contingent on detection of polarization effect over g-g* links
12	Up-link only
18	Up- and down-links

Note.

(1) All the listed experiments can be done over a-g and g-a links

(2) No. 2 marginally possible for a-g link

*g-ss = ground-to-synchronous satellite
ss-g = synchronous satellite-to-ground
g-g = ground-to-ground

**Optional - see text

Table 3. List of Experiments

Experiment No.	Title
1	Measurement of Spatial and Temporal Logarithmic Amplitude Correlation Function and Phase Structure Function
2	Phase Structure Function Measurement
3	Amplitude Correlation Measurement
4	Stationarity Test
5	Spectral Spreading Measurement
6	Power Fluctuation Measurement
7	Heterodyne Equivalent Measurement System
8	Angular Fluctuation Measurement
9, 10	Spread Function and Beam Spreading Measurement
11	Polarization Fluctuation Measurement
12	Atmospheric Backscatter, Transmittance and Sky Radiance
18	Communication Link Error Rate

SITING

TEST SITE ANALYSIS

The study of potential sites for implementation of the LACE program has been performed, on a limited basis, in order to examine some of the critical factors and provide some general guidelines on availability and supporting requirements. Some of the main factors that have had a bearing on the analysis are as follows: theoretical and operational criteria, location and availability of existing facilities and key research personnel, and meteorological conditions. These factors were considered in terms of their bearing on the development of a logical program approach.

It should be emphasized that no attempt has been made in this analysis to delineate all aspects of siting, for the effort required would have been substantial, and detailed data on particular sites can be obtained from specific handbooks and range manuals. It is further recognized that the actual implementation phase of the program must necessarily include a detailed survey of the site or sites selected.

GENERAL SUPPORT CONSIDERATIONS

The links anticipated for a complete measurement program range from simple ground-to-ground through ground-to-satellite paths. It has been found, during this analysis, that a minimum program to validate some of the propagation theory (as related to system performance) developed to date would require a long, uniform, horizontal ground path like a dry lake bed. Following this minimal testing, the links should be lengthened and expanded in scope to include near-vertical mountain-to-valley paths and ground-to-aircraft/balloon paths. Since good experimental design provides for a range of values for the test variables, it would be desirable to include experimentation at different climatological and orographic regions to establish the effect of this variation.

There are a number of well-instrumented government and private facilities located in a variety of different climatological regions around the country, which would satisfy the siting requirements of both an early pilot (or minimal) program and an extended experimental program. Figure 1 shows the locations of some of the most promising sites, and also indicates the general locale of some of the experimenters who are active in the study

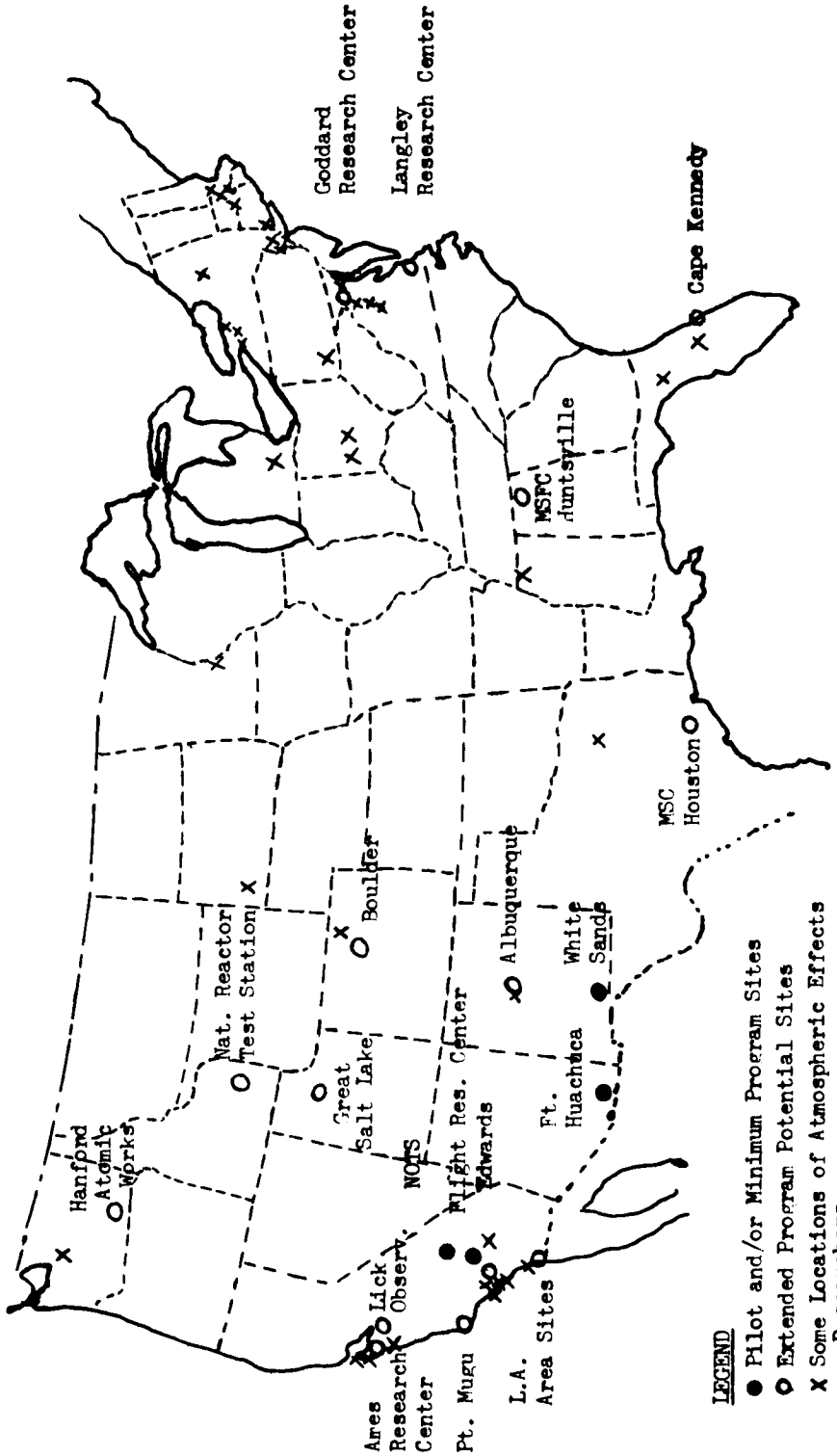

Figure 1. Examples of Potential LACE Implementation Sites

of laser propagation effects. In addition to the sites shown, most of the larger universities have researchers who have been active in related work such as particle diffusion, atmospheric optics, and applied meteorology and have equipment and field sites that would be applicable to an extensive measurement program.

All of the major locations and sites which have been examined (Figure 1) appear to be readily accessible and to have the logistic capability for supporting a test program of the proportions of LACE. This is particularly true of the missile range sites, which are capable of providing the complete range of support from target acquisition and tracking, data processing and reduction, communications, and meteorological instrumentation to such secondary, but essential support functions as repair shops, calibration shops, aircraft flight facilities and of course housing and associated personnel facilities.

Tables 4 and 5 give an indication of the meteorological and tracking equipment support available at most of the primary sites under consideration. Appendix I gives a description of some of the meteorological equipment considered essential to the measurement program. In addition to the specific equipment shown, some of the sites are capable of satisfying the requirement for meteorological towers (approximately 60 to 200 feet) for use in determining the verticle profile of the atmosphere along the path.

CLIMATOLOGICAL DATA

Cloudiness

Of all the meteorological phenomena which affect laser propagation for deep space optical communication, the degree of cloud cover in the vicinity of the atmospheric propagation path is probably the most restrictive in the sense that it governs the "go-no go" decision for each laser transmission. It is therefore important to examine the frequency of cloudiness when planning sites for laser links. Percent cloudiness can also generally be used as an indicator (though not a precise one) of the probability of inclement weather from precipitation. Figures 2 and 3 give the mean sky cover on a monthly and annual basis for the continental United States. It can be seen that the stations recommended for pilot testing generally have less than 40% sky coverage, while the extended program potential sites generally have in excess of 50% coverage.

Reporting Stations

The Office of Climatology of the Weather Bureau is a part of the Department of Commerce and is located in Suitland, Maryland. This office

is divided into three division-level segments: The Laboratory of Climatology; Field and User Services Division; and the National Weather Records Center (NWRC) located at Ashville, North Carolina.

The networks of observing stations which yield weather information useful for climatological purposes comprise (in 1964) more than 12,000 localities in the United States and the Caribbean. Since continuity in climatic records is very important, stations of four networks are maintained with a minimum of change. These four networks are: (1) the network of Principal Climatological Stations, called the 24-hour climatic network, (2) the network consisting of the foregoing plus the Ordinary Climatological Stations, called the "a" network, (3) the Upper Air Network, and (4) the Climatological Bench-Mark network of long-record temperature-and-precipitation stations. These climatically representative stations were chosen for continuity value and prospective permanence.

The 24-hour Climatic Network of 178 First Order Weather Bureau and Federal Aviation Agency stations (Figure 4), with few exceptions, record each hour a complete surface weather observation. This includes wet- and dry-bulb temperatures, dewpoint, relative humidity, sky cover, cloud types with height and direction of movement, wind direction and speed, atmospheric pressure and tendency, ceiling, visibility, and present weather.

The "a" Network consists of about 5,000 temperature and precipitation stations manned chiefly by cooperative volunteer observers. The Upper Air Network (Figure 5) consists of 70 Weather Bureau rawinsonde stations. Observations at these stations are made to altitudes of at least 100,000 ft. The Climatological Bench-Mark Network (Figure 6) has as its primary purpose the collection of data in local environments with minimal anticipated man-made changes, so that they are suitable for monitoring climatic changes. The stations are located for the most part on property owned by the Federal or State governments or public institutions (e.g., in National Parks, at Experiment Stations, or on University campuses) where supervision of the observing program, uniform instrument exposure, completeness and accuracy of record, and freedom from molestation are fairly well assured. It is planned to add recording equipment for observations other than precipitation and temperature (e.g., wind, solar radiation, soil moisture, soil temperature, lightning stroke count, and eventually, also electric potential, atmospheric pollution and radioactivity).

Routine Publications

The observational records from the meteorological observing points flow directly into the NWRC. Here they are placed on punched cards, prepared into various summaries, and finally become a part of the centralized

weather records library. The following is a list of publications that service the greatest number of routine purposes:

1. The Weekly Weather and Crop Bulletin, National Summary carries information of particular interest to agriculture.

2. The Local Climatological Data publication is prepared monthly for nearly 325 cities in the United States and outlying stations, and includes daily climatological information and summaries for the month.

3. For stations issuing the "Local Climatological Data", an annual issue, Local Climatological Data with Comparative Data, contains a brief description of the general climate of the locality and a station history.

4. Hourly Precipitation Data is published monthly with an issue for each state or combination of states (Maryland-Delaware, New England) except Hawaii.

5. Climatological Data is issued for each State (or group of States). It presents surface observations from all regular networks.

6. Climatological Data, National Summary contains pressure, temperature, precipitation, and wind data for selected U.S. stations.

7. Monthly Climatic Data for the World contains monthly mean values of surface temperature, pressure, relative humidity, and precipitation; and of upper air temperature, dew point and wind direction and speed for many locations throughout the world.

8. Storm Data presents monthly, by States the place, time, character, and estimated damage of all reported severe storms or unusual weather phenomena.

9. Synoptic Series, Daily Weather Maps, Northern Hemisphere consists of Part I and Part II. Part I is a publication which presents the Northern Hemisphere daily synoptic maps on a monthly basis. Each volume of the series consists of Northern Hemisphere maps for one month, with one sea level map and one upper air constant pressure surface map (500 millibars) for each day. Part II, Northern Hemisphere Data Tabulations, is made available in microfilm and contain daily synoptic surface and upper air reports.

Special Service Programs

A number of special climatological studies have been prepared by the Weather Bureau (as well as the military services) on subjects ranging from extreme environments for equipment design to the "Probability of Fallout Debris Deposition for Civil Defense Applications." Recently, the NWRC prepared for the George C. Marshall Space Flight Center statistical relationships of surface wind, winds aloft and total opaque cloud cover at Cape Kennedy (Reference 22). An example of the statistical correlations prepared in this report is illustrated in Table 6.

Table 4. Summary of Weather Instrumentation Locations

Instrumentation	Cape Kennedy	Valkaria	Grand Bahama	Fleuthera	San Salvador	Grand Turl	Antigua	Ascension	Pt. Mugu	Pt. Arguello	San Nicolas Is.	Enewetok	Kwajalein	Wake Is.	NOTS, China Lake	Edwards AFB	Ft. Huachuca	White Sands
Rawinsonde System	x								x	x	x	x	x	x	x	x	x	x
Wiresonde Set	x	x	x	x					x									
AN/GMQ-13A Cloud Height Set	x								x	x	x							
AN/GMQ-2 Ceilometer	x								x									
ML-121 Ceiling Light Projector	x		x	x	x	x	x	x	x									
AN/GMQ-11 Wind Measuring Set	x	x	x	x	x	x		x										
AN/GMQ-1A Wind Set			x	x	x	x	x	x										
AN/UMQ-5 Wind Set									x	x	x	x	x		x			
Theodolite	x		x	x	x	x	x	x	x	x	x	x	x	x	x	x	x	x
AN/GMQ-14 Auto. Weather Station									x	x	x				x			
Psychrometer	x	x	x	x	x	x	x	x	x	x	x	x	x	x	x	x	x	x
Hygrothermograph	x						x	x	x	x	x	x	x	x	x	x	x	x
Mercurial Barometer	x		x	x	x	x	x	x	x	x	x	x	x	x	x	x	x	x
Aneroid Barometer	x	x	x		x	x	x	x	x	x	x	x	x	x	x	x	x	x
Barograph	x	x	x	x	x	x	x	x	x	x	x	x	x	x	x	x	x	x
Arcas Met. Rocket Capability	x							x	x						x	x	x	x
Loki II Met. Rocket Capability	x								x						x	x	x	x
AN/GMQ-10 Transmissometer									x		x							
AN/AMQ-8 Aerograph Set									x						x			
AN/ASH-14 Microwave Refractometer									x									
Remote Recording Sites															x	x	x	x
Tethered (or Free Lift) Balloons Capability															x	x	x	x

Table 5. Summary of Some Applicable Electronic Tracking Facilities

Instrumentation	Cape Kennedy	Wallops Is.	Bermuda	Morris Town, N.J.	San Salvador	Bahamas	Antigua	Ascension	Pt. Mugu	Pt. Arguello	San Nicolas Is.	Hawaii	Kwajalein	Johnston Is.	NOTS, China Lake	Ft. Huachuca	White Sands	AEC Tonopah Is.
AN/FPS-16	x	x	x		x	x		x	x	x	x	x				x	x	
AN/FPS-16 (MN3)																	x	
AN/MPS-19										x								
SCR-584									x	x	x							
AN/MPS-25	x								x					x		x		x
M-33									x	x			x		x			
TRQ 18	x						x											
FPQ 6	x	x					x											
MPS-26															x			
FPQ 4				x														

UNITED STATES
DEPARTMENT OF COMMERCE
WEATHER BUREAU

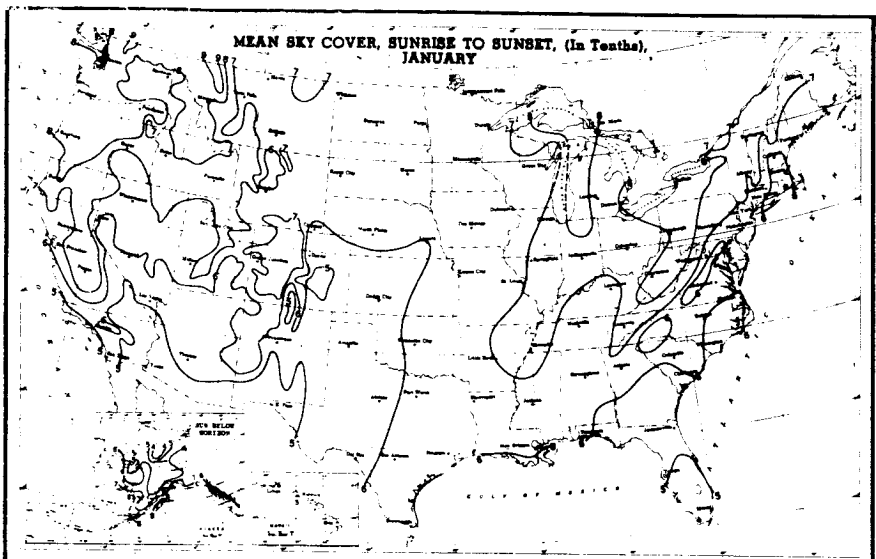

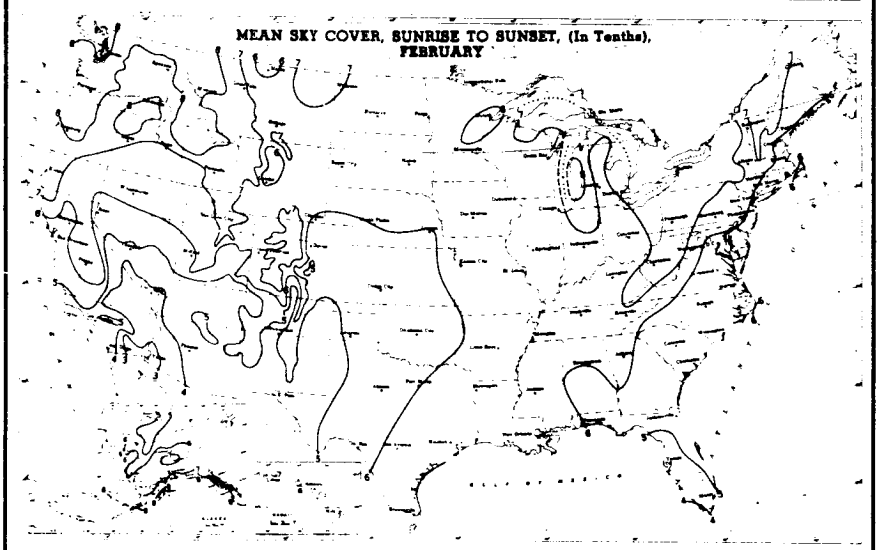

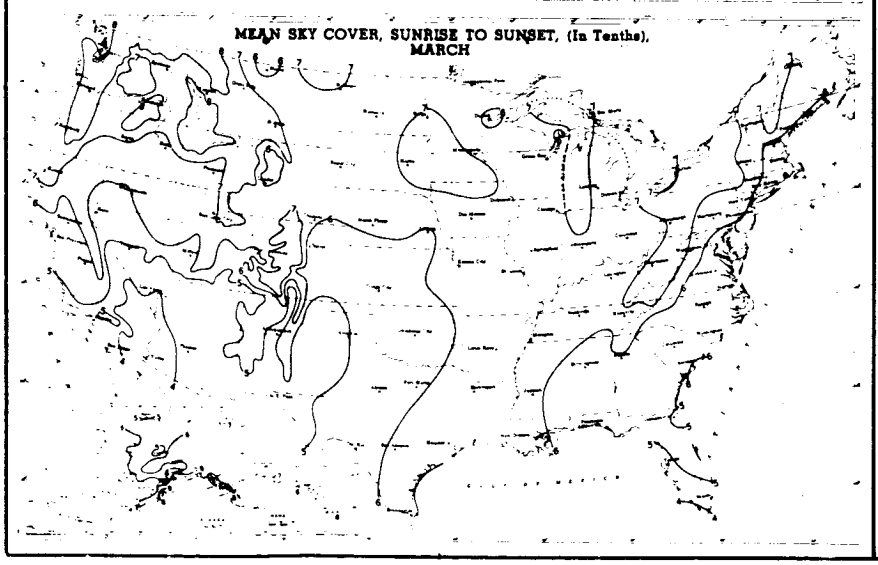

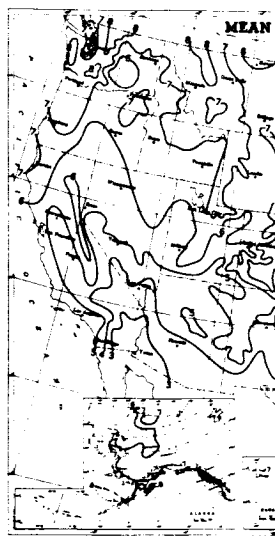

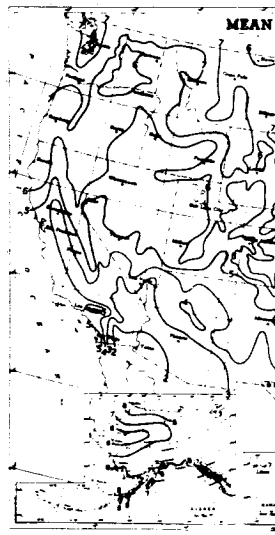

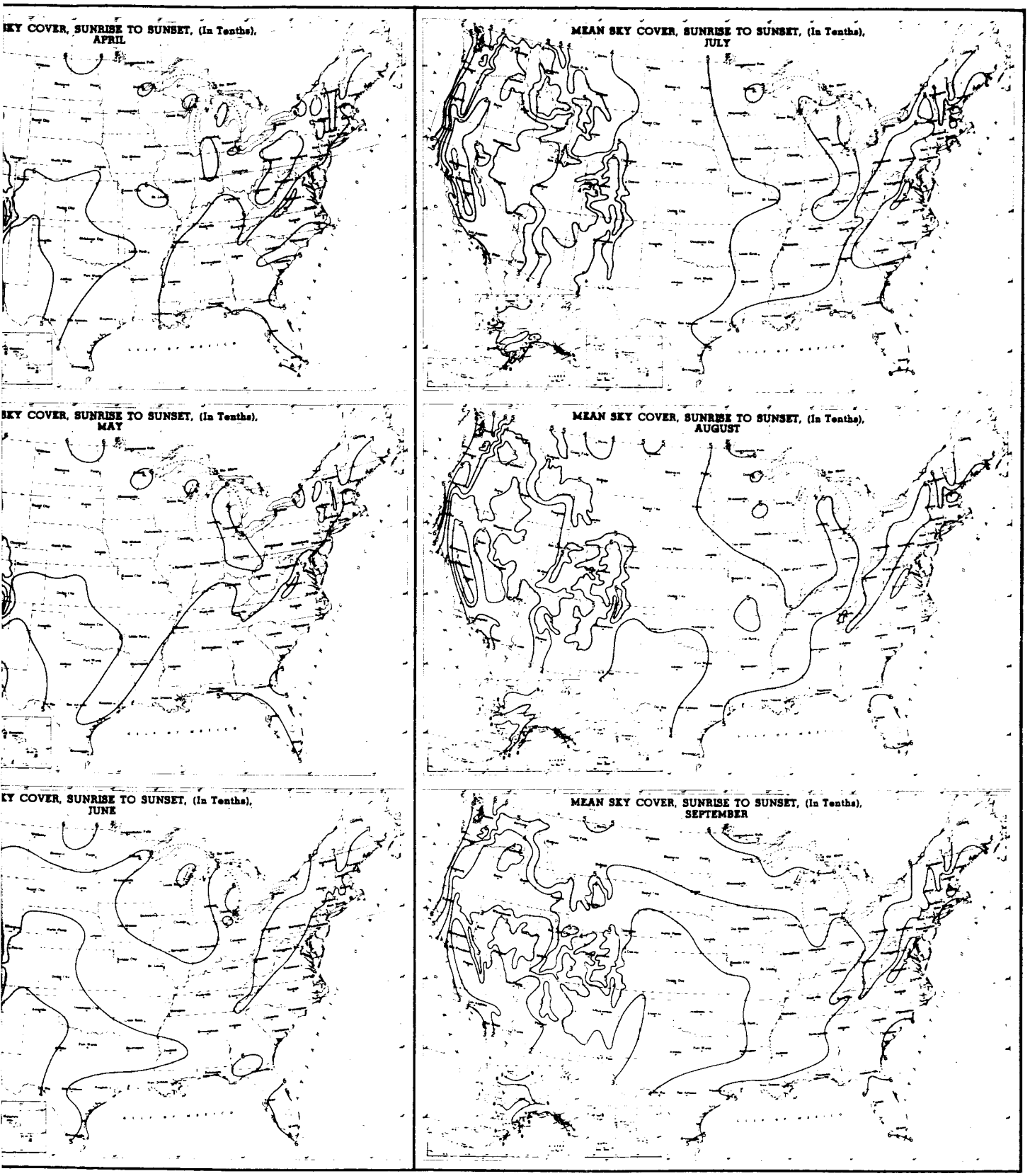

Figure 2. Mean Sky Cover, Sunrise to Sunset, Monthly and Annual

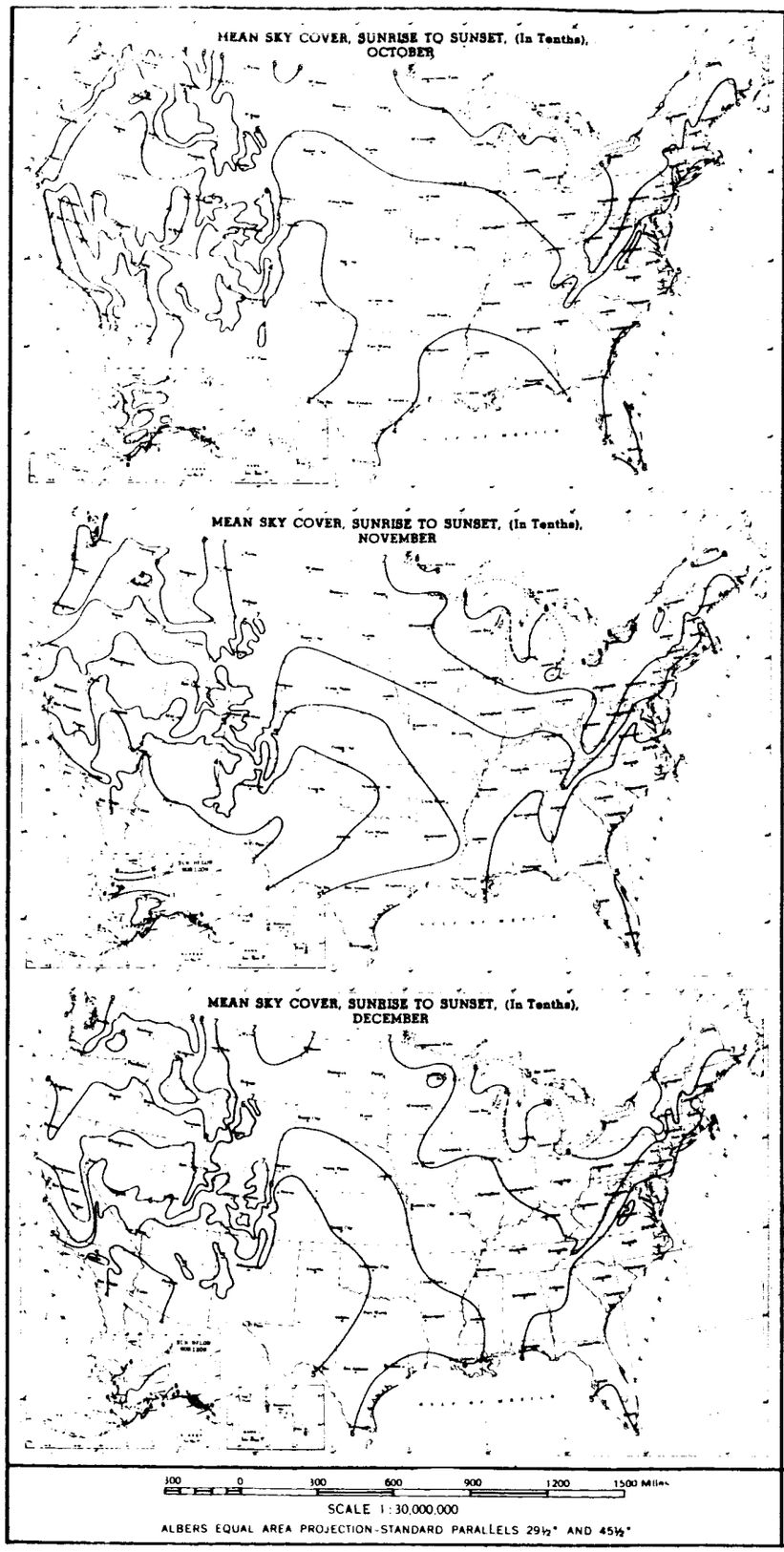
MEAN SKY COVER, SUNRISE TO SUNSET, (In Tenths),
OCTOBER
MEAN SKY COVER, SUNRISE TO SUNSET, (In Tenths),
NOVEMBER
MEAN SKY COVER, SUNRISE TO SUNSET, (In Tenths),
DECEMBER
300 0 300 600 900 1200 1500 Miles
SCALE 1:30,000,000
ALBERS EQUAL AREA PROJECTION-STANDARD PARALLELS 29½° AND 45½°

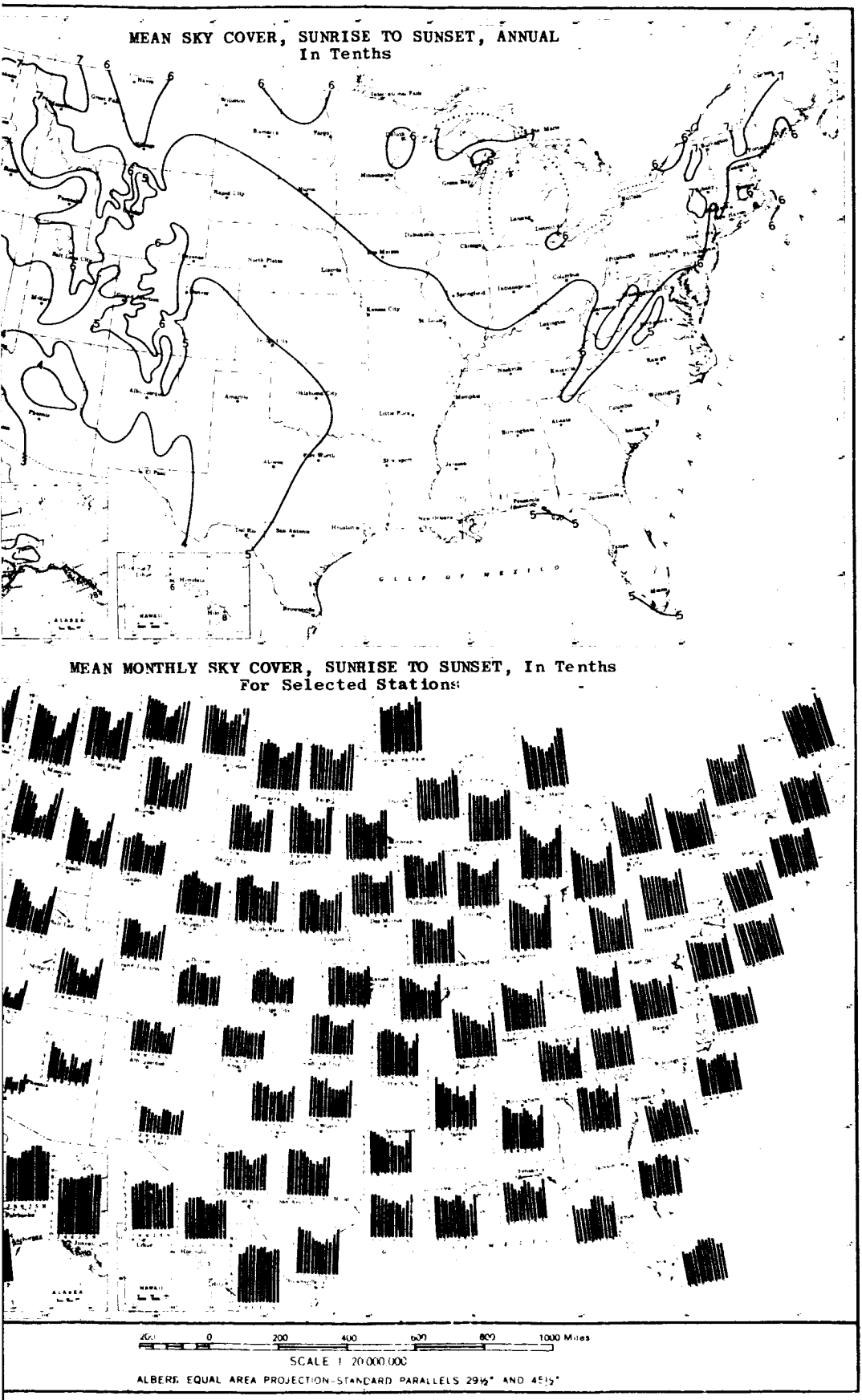

Figure 3. Mean Sky Cover, Sunrise to Sunset, Monthly and Annual - Continued

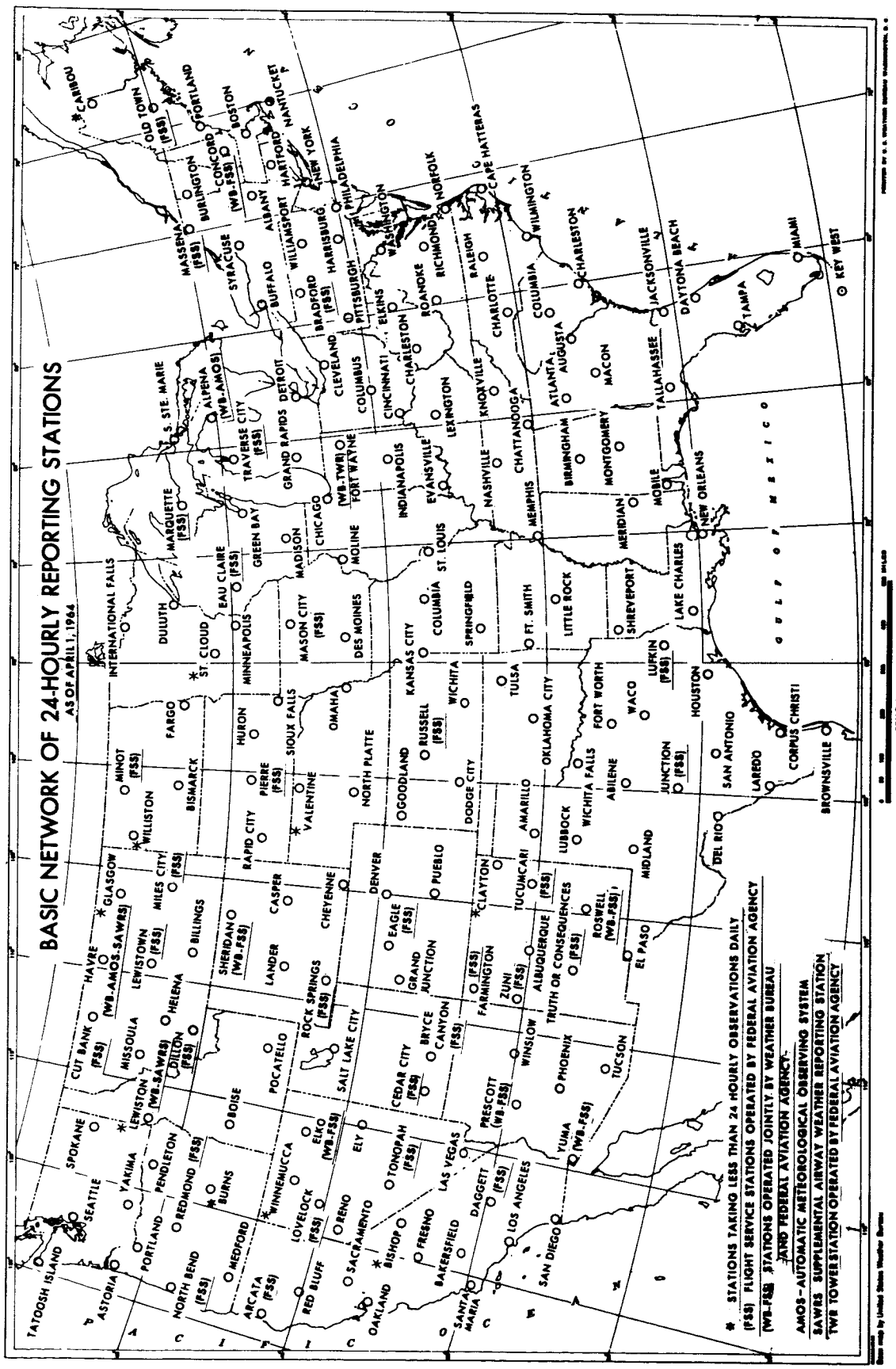

Figure 4. Basic Network of 24-Hourly Reporting Stations

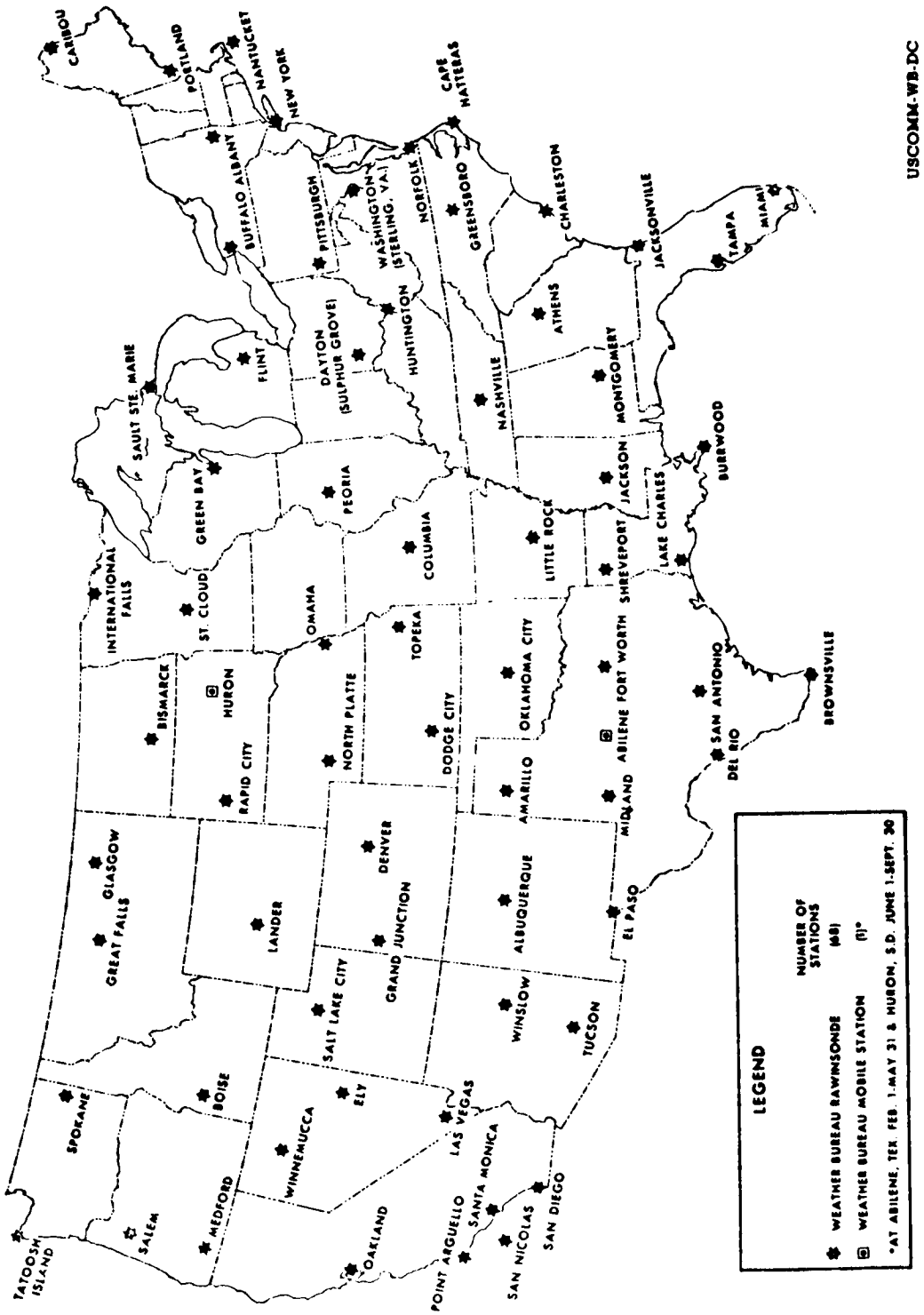

Figure 5. Rawinsonde Reporting Network as of July 1, 1964

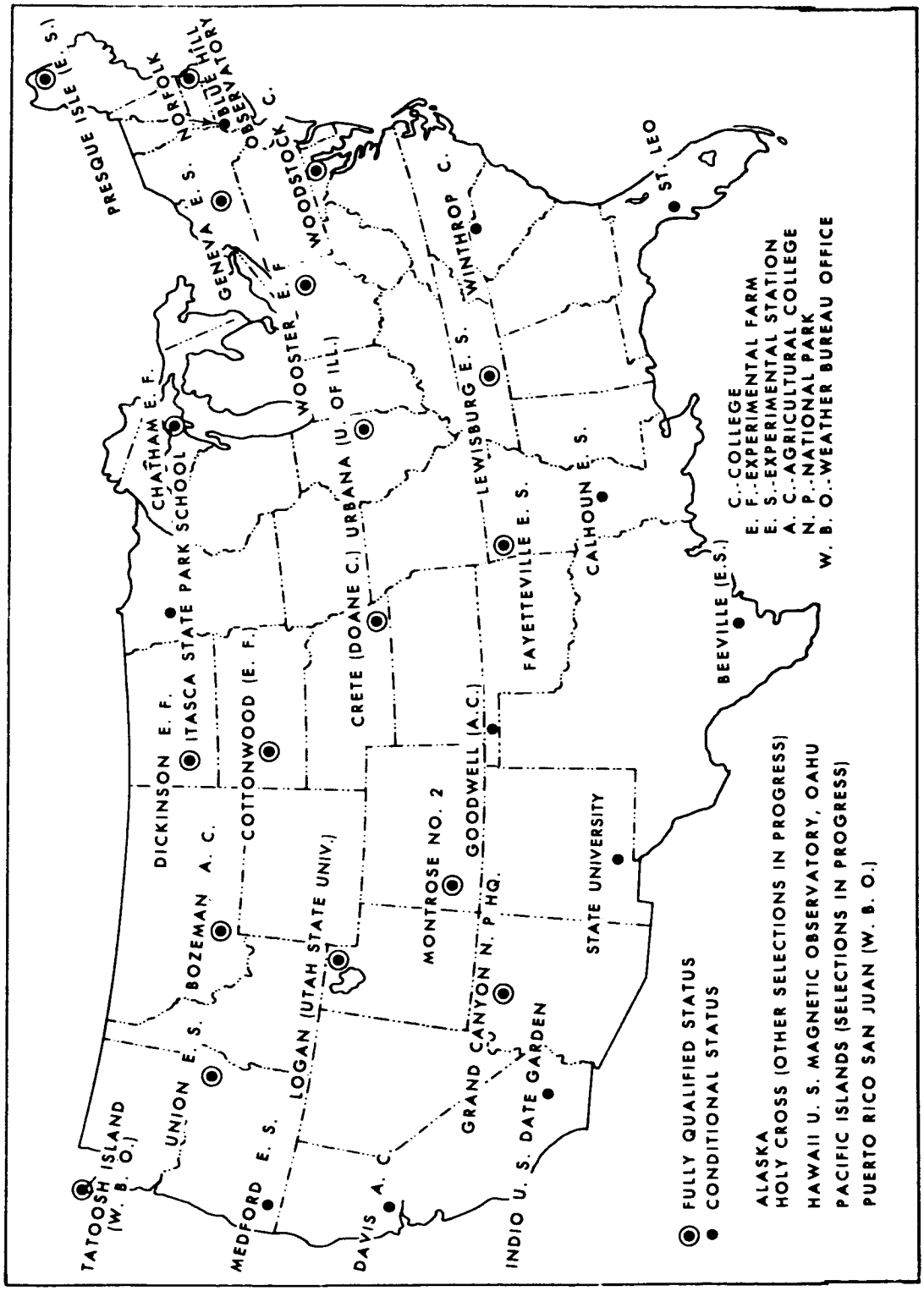

Figure 6. Climatological Bench Mark Station Network

Table 6. Interparameter Statistical Analysis of Surface Winds, Clouds and Winds Aloft at Cape Kennedy

GO: (S_1 = Surface Wind $\leq$ 6 mps. (C_1 = Cloud Cover $\leq$ 3/10 (U_1 = Upper Wind $\leq$ 60 mps.

NO GO: (S_2 = Surface Wind > 6 mps. (C_2 = Cloud Cover > 3/10 (U_2 = Upper Wind > 60 mps.

PERCENTAGE OCCURRENCE

	Mo. / Hr.	Jan. 07	Jan. 19	Feb. 07	Feb. 19	Mar. 07	Mar. 19	Apr. 07	Apr. 19	May 07	May 19	June 07	June 19	July 07	July 19	Aug. 07	Aug. 19	Sept. 07	Sept. 19	Oct. 07	Oct. 19	Nov. 07	Nov. 19	Dec. 07	Dec. 19
GO	$S_1U_1C_1$	23.3	26.4	16.8	23.9	16.2	25.4	24.6	30.9	31.2	27.9	26.2	21.3	47.6	28.9	44.5	23.3	32.7	28.1	36.4	37.3	34.0	40.1	25.8	33.1
NO GO	$S_1U_2C_1$	7.6	8.3	8.4	7.7	6.3	13.2	3.3	4.1	.6	.6									.6	1.9		1.4	4.4	10.1
NO GO	$S_1U_1C_2$	36.6	34.7	33.5	29.2	34.7	28.7	40.5	38.0	57.6	59.9	69.0	70.0	50.5	64.9	55.5	69.9	59.2	60.6	47.4	44.5	52.4	43.6	51.0	43.2
NO GO	$S_2U_1C_1$	1.8	4.9	5.6	3.5	1.2	2.5	4.7	4.2	2.5	3.0		2.0	1.3	1.2			.7	1.3	1.2	3.1	1.4	2.0	5.1	
NO GO	$S_2U_2C_1$	3.0	2.5	4.2	5.6	3.1	4.3		.7															1.3	
NO GO	$S_2U_1C_2$	9.4	5.1	14.0	14.7	12.0	6.3	9.4	8.7	7.5	8.0	4.8	6.7	.6	5.0		6.8	7.4	10.0	13.2	13.2	10.8	12.9	6.8	6.9
NO GO	$S_1U_2C_2$	13.9	14.4	10.5	13.3	20.8	15.3	11.4	8.7		.6									1.2		.7		5.6	4.9
NO GO	$S_2U_2C_2$	4.4	3.7	7.0	2.1	5.7	4.3	6.1	4.7	.6												.7			1.8

ALL OBSERVATIONS COMBINED

	Mo.	Jan.	Feb.	Mar.	Apr.	May	June	July	Aug.	Sept.	Oct.	Nov.	Dec.
GO	$S_1U_1C_1$	25.0	20.4	19.8	27.8	29.6	23.2	37.9	33.8	30.4	36.8	37.1	29.3
NO GO	$S_1U_2C_1$	8.0	8.1	9.8	3.7	.6					1.3	.7	7.3
NO GO	$S_1U_1C_2$	35.2	31.1	32.5	39.0	58.6	70.0	58.0	62.8	59.9	45.9	47.8	47.0
NO GO	$S_2U_1C_1$	3.4	4.6	1.9	4.5	2.8	1.0	1.3		1.0	2.2	1.7	2.6
NO GO	$S_2U_2C_1$	2.8	4.9	3.7	.4								.7
NO GO	$S_2U_1C_2$	7.3	14.4	9.2	9.1	7.8	5.8	2.8	3.4	8.7	13.2	11.9	6.9
NO GO	$S_1U_2C_2$	14.2	11.9	18.1	10.1	.3					.6	.4	5.3
NO GO	$S_2U_2C_2$	4.1	4.3	5.0	5.4	.3						.4	.9

SID 65-1466

NORTH AMERICAN AVIATION, INC.
SPACE and INFORMATION SYSTEMS DIVISION

PROPAGATION LINKS

PROPAGATION LINKS AND PLATFORMS

On the basis of the experiment accuracy analysis (Reference 1) and additional theoretical analysis related to Task I, it is strongly recommended that initial testing be conducted over well-instrumented horizontal (followed by mountain-terminus) ground paths. Not until the experimental configurations utilized during this test phase have been thoroughly evaluated is it practical to discuss detailed requirements for non-ground-based links.

GROUND LINKS

The ground links for the first LACE tests should be over a horizontal, uniform surface having fairly homogeneous properties. The path should be such that the turbulence properties (statistics) along the propagation path do not change. It appears that a dry lake bed would best satisfy these requirements. Following these initial tests it would be desirable to extend the length of the link and also change it to near vertical by placing the receiver or transmitter (possibly alternately) on a mountain observation site. Some of the sites that have been considered for this phase, and for later extended testing, were discussed earlier in the site analysis section.

The specific laser propagation experimental set-ups for the ground link phase is presented with the discussion on each experiment. It is recognized that each set-up will require detailed design and development prior to field implementation. Additionally, the proposed experimental design and specification of a total program approach will be presented in Task IV of this contract.

Some of the specific types of supporting equipment and usage have also been considered as a part of this analysis. (Additional discussion on tracking equipment and meteorological equipment has been covered under General Support Considerations and in Appendix I.) The equipment presented here is believed to be typical of that required to support a small field test operation on the order of that specified for the pilot-test phase. The supporting equipment has been divided into the categories of test equipment, tracking equipment, data recording, data analysis, and general purpose. A representative listing of this equipment is presented in Table 7. This equipment presented has been based to a large extent on requirements developed, after

Table 7. Supporting Equipment for Laser Experimental Ground Site

Test Equipment Requirements - for such things as calibration of recorders and amplifiers, optical and positional alignment and calibration of system electronics.	Tracking Capabilities - to provide open-loop and closed-loop tracking.	Data Recording - required to either obtain or route signals to appropriate recording devices.	Ground Purpose Equipment
Oscilloscopes (Tektronix Rm 585A), cameras and mounts	Paper Tape Reader	Strip-chart recorders (8 channel)	Weather Sensors (Described elsewhere in report)
Counter & DVM	Paper Tape Drive Logic	Magnetic Tape Recorder (14 channel wide band)	Intercom System or Radio equiped vehicles (to allow remote alignment of external equipment which is monitored inside the facility)
Test Oscillator	Paper Tape Spooler	Magnetic Tape Amplifiers	Equipment Racks (for mounting equipment listed)
Pulse Generator	Time Code Generator	Logarithmic Amplifier	Shelters (to protect tracking pedestals from wind and weather)
Noise Generator	Receiver Pedestal	D. C. Amplifiers (4 Gen. Purpose)	Short Range Walkie-Talkie (for optical tests and alignment at short ranges)
5,000 V. Power Supply	Pedestal Angle Readouts	Patch Panel & Cabling	Power Generator (to power the listed equipment)
Precision Rotary Table	Servo Electronics for Receiver Pedestal	Data Analysis - used to analyze collected data.	Regulated Power Transformers (to regulate generator voltage output)
Test Light Source	Servo Electronics for Transmitter Pedestal	Spectrum Analyzer	Optical Benches and Mounts
Theodolite & Tripod	Resolvers	Amplitude Distribution Analyzer	
	WWV Receiver	Wave Analyzer	
	Loran-C Receiver Precision Time Delay	True RMS Meter	
	Bases (2)	Analog Computer	
	Optical Receiver		
	400 cps Converter		

considerable analysis, for the North American S&ID "Laser Application Research" (LAR) facility, which is ideally suited for the LACE application. A more detailed discussion of the LAR facility is presented in Appendix J.

AIRBORNE LINKS

It is expected that early results from the pilot tests will indicate the desirability of conducting additional tests on moving and fixed platforms (i. e. aircraft and balloons) over a wide range of altitudes, elevation angles, and experimental equipment configurations. This type of testing should be the natural forerunner of space testing and should, in fact provide much of the same type of data to be obtained from space tests, but at a lesser cost.

It is felt, however, that the scope of this type of testing cannot be firmly defined at this time, because realistic definition is predicated on the outcome of ground-based testing. Therefore, the analysis here will be limited to an outline of the factors that should be considered in the final definition of these programs.

Aircraft Testing

The test planning for the aircraft experiments will consider a number of complex tasks that range from the pre-flight preparation through the analysis of the flight test data. These tasks can be briefly delineated as follows:

1. Perform flight test planning to establish the procedures for conducting the experiments. This effort shall include:

    a. Development of an experimental design and preparation of an analysis plan on the basis of the experimental design, making a final determination of flight test routes, flight profiles (altitude, velocity, etc.), direction with respect to sun, time of day, ground target locations and link conditions (i. e. up- or down-link, or both), number and length of time per encounter, and test schedules

    b. Establishment of pre-flight checkout and alignment procedures required

    c. Establishment of post-flight test procedures

    d. Establishment of measurement subsystems, data recording, reduction and analytical procedures

    e. Human factors support to experiment planning and treatment of data

2. Conducting of the flights in accordance with the test plans. This effort shall include:

   a. Scheduling of flights and obtaining clearance to operate the test aircraft over prescribed routes and altitudes

   b. Preparation of detailed flight cards for the flight crew

   c. Calibration and operation of data recording instrumentation

   d. Processing of all data such as film, oscillograph, and magnetic tape records

   e. Compilation of the flight test log

3. Performing of avionic equipment test engineering. This effort shall include:

   a. Avionic system ground test and calibration

   b. Compilation of the system log and preparation of system engineering data for inclusion in the flight reports

4. Reduction and analyzing of flight test data. This effort shall include:

   a. Reduction of flight data such as film, oscillograph, and magnetic tape records

   b. Compilation of reduced data

   c. Correlation of photographically derived parameters with recorded parameters

   d. Analysis of reduced data to establish functional and statistical relationships

5. Preparation of a final report presenting the results obtained from the experiments in accordance with the test objectives, experimental design, and analysis plan.

The experimental subsystem to assess the laser propagation effects will be established on the basis of the early ground tests. Some well-instrumented atmospheric research aircraft are available for this type of testing. A completely instrumented C-130 utilized by the Air Force Cambridge Research Center is typical of the test vehicles that could be

utilized. (See Appendix K for a listing of some of the instrumentation on this aircraft obtained during a LACE trip to the University of California Visibility Laboratory). In addition to the radiometric and meteorological equipment listed in the aforementioned reference, Table 8 gives a listing of some of the parameters that would be measured on board the aircraft during this type of experiment.

Table 8. Parameters to Record on Board a Laser Propagation Research Aircraft

Sub-System	Parameter	Instrument	Remarks
Meteorological parameters	Temperature	Vortex thermometer	No dynamic corrections required
	Temperature	Rosemount probe	High response rate
	Humidity	Infra-red hygrometer	
	Wind direction	Doppler radar system	
	Wind speed	Doppler radar system	
	Liquid water content	Paper-tape type	Electrical conduction principle
	Liquid water content	Hot-wire type	Electrical resistance principle
	Icing	Heated probe	On-off type instrument derives rate indirectly
	Absolute altitude	Radio altimeter	
	D-value	Hypsometer/ radio altimeter	
	Absolute pressure	Pressure transducer	
	Differential pressure	Pressure transducer	To derive accurate air speed for calibration computations
Flight condition	Pitch and roll	Gyro system	
	Indicated air speed	Pitot-static system	
	True air speed	Pitot-static system plus temp. sensor	

Table 8. Parameters to Record on Board a Laser Propagation Research Aircraft (Cont)

Sub-System	Parameter	Instrument	Remarks
	Pressure altitude	Pitot-static system	
	Drift angle	Doppler system	
	Heading	Compass system	
	Latitude & longitude	Doppler system	
Photographic system	Cloud photography	Time-lapse cameras	

The support and parameters to be measured at the ground sites would be similar to that specified for the ground-to-ground links, i. e. laser characteristics and complete micrometeorological, spatial and temporal statistical data.

Balloon Links

Balloon platforms have been considered because of the possibility of conducting experiments to high altitudes (near the outside extent of the atmosphere), which come close to simulating satellite conditions but for a much lower cost. Also, their potential payload flexibility and controllability is attractive for developmental experimentation. Both the free-lift and tethered balloon configurations appear to have application in the LACE program—the free-lift balloons for long range, high altitude, mobile platform application, and the tethered balloons for medium-range-and-altitude, semi-fixed platforms. The tethered balloon has been considered for use as both an experimental platform for measurement of optical effects and as a vertical extension of a meteorological tower (i. e. locating meteorological sensors and telemetry on the balloon and sampling the upper atmosphere at several different locations).

As in the case of aircraft links, the explicit utilization of balloons should only be defined subject to the results of ground experimentation. The planning tasks and equipment requirements for balloon platforms will be very nearly the same as those outlined for aircraft links; therefore planning and equipment requirements will be indicated only where there is a significant difference. To round out the present discussion of balloon applications as propagation links a review of current balloon technology follows (Appendix L).

SATELLITE LINKS

The principal analysis presented here considers the factors involved in the selection of a satellite orbit which best satisfied the requirements and constraints associated with optical experiments of the type proposed in this study. Both synchronous (high altitude) and intermediate orbits are examined from this viewpoint.

Analysis of other aspects concerning satellite links is limited to the specification of the tasks to be performed as part of a later experimental and payload definition phase and the preparation of some relevant study background information. This limited approach to the problem was taken for the same reasons given previously for airborne and balloon links.

These additional data are contained in three appendixes:

Appendix M. Study Outline for Space Vehicle Payload Final Definition

Appendix N. Satellite Vehicle Capability Summary Analysis

Appendix O. Summary of NASA Network Capability

The choice of a satellite orbit for implementing optical experiments can be approached in two ways. The first is to specify an orbit dictated entirely by the needs of the experiments; the second is to tailor the experiments to orbits capable of being achieved from existing launch facilities. Because of the variety of operational needs and equipment limitations neither of the choices approaches a fully controlled experiment in which the experimenter can select his operating parameters at will.

An orbit specified by the needs of the experiments would have the following properties. It would have low angular rates to alleviate the problems of fast tracking and the need to compensate for light aberration due to high orbital angular velocity. The orbit would be such that experiments could be carried out over a 24-hour period. The orbit would pass over geographic areas having weather patterns of interest, the areas themselves being selected for ease of access, knowledge of previous weather histories and ease of making meteorological measurements. Since refraction effects would complicate interpretation of data, the orbit should not introduce changes in the optical line of sight during the measurements. The methods used for initial satellite stabilization would utilize optical sensing of the satellite orientation—using either a laser beacon or a prominent terrain feature as a reference. Thus an orbit should be chosen which affords long periods for acquisition of the stabilization reference.

The effects of satellite stabilization and tracking error on the quality of the experimental data are also important. This can be calculated. In addition, the height and ellipticity of the orbit have a bearing on the laser power density on earth and at the satellite, on whether near or far field effects are being measured, and on the bandwidths needed for the measurements. Bandwidths are dependent on the relative velocity of the satellite with respect to the ground and to the turbulent air volumes in the atmosphers. The greater the relative velocities the greater the needed bandwidth in comparison with stationary (earth-based) experiments. Whether the measurements are being carried out in the near or far field of the scattered radiation cannot be judged at this time. More of the theory of narrow-beam transmission in a turbulent medium needs to be explored—both up-link and down-link—before this question can be answered. For all the experiments, an important parameter is the power density. Since c.w. laser transmitters are limited in power density (watts/sterad) and receiver apertures are limited in area, range will be an important factor in determining signal strength. According to this requirements, the range should be as small as practicable. Also, the orbit should be chosen to minimize background power at the receiver. Of course it may happen that the beamwidth of the transmitter is comparable to the tracking error of the receiver in which case the beamwidths will have to be widened to keep the signal at the receiver from fluctuating because of this effect.

All of these requirements cannot be met by a single choice of orbit. The best that can be done is to satisfy most of these conditions. There will be two types of orbits to consider. The first is a synchronous orbit and the second is an intermediate orbit. The exact placement of the intermediate orbit will require much more in investigation since there are so many trade-off considerations.

The synchronous orbit itself has many variations since synchronous, in its broadest usage, means a 24-hour orbit; the satellite need only appear directly over the earth station every 24 hours. From the standpoint of the experimental measurements, an equatorial synchronous orbit would be best since the associated relative velocities are small, thus minimizing the problems of tracking, bandwidth, and observation time. Disadvantages of this orbit are its greater range, the restricitions it imposes on the selection of suitable sites, and the lack of any launch facilities to easily achieve such orbits. The practical aspects of the problem dictate that existing launch facilities be used and that the orbit pass over areas with known weather patterns. When this is done, the time available for measurements per day is reduced. Initiating and maintaining a synchronous orbit requires a very sophisticated guidance and control system. Whether the added quality of the measurements obtained with a synchronous orbit is worth this added complexity can only be judged by a total mission analysis.

Somewhat the same situation exists for intermediate orbits. With present launch facilities, a variety of orbits are avialable which would pass over selected geographical areas. The intermediate orbit would lessen the range factor. However, in this case the other problems are accentuated. Bandwidth requirements go up, measurement time goes down, and angular rates and aberration effects become significant. Another important factor is that of path length changes and refractive effects.

APPENDIXES

APPENDIX A. LASER PERFORMANCE SUMMARY

This appendix covers those lasers which would be most applicable to the LACE experiments. The primary considerations for the choice of laser data are output power and linewidth. The laser data includes information on both CW and pulsed laser systems.

INTRODUCTION AND SUMMARY

The CW laser systems covered in this report are as follows:

Gas Lasers

a. He-Ne

b. Ar^+

c. N2: CO_2

Injection Lasers

a. Ga As Diode

Optically Pumped CW Lasers

a. Nd: YAG

b. Nd: Ca WO_4

c. Dy: Ca F_2

Information on these laser systems includes:

1. CW output power
2. Emission linewidth
3. Frequency stability and mode structure
4. Angular beamwidth
5. Conversion efficiencies

9. Repetition rates

10. Q-switching

11. Oscillator-Amplifier combination data

12. Size and weight

13. Input power

14. Cooling requirements

15. Environmental sensitivity

All of this data is given for commercially available lasers. In the case of experimental lasers, only part of this information is available because some of these parameters have not yet been determined.

CW LASERS

Gas Phase Lasers

Since 1961, when Javan, Bennett, and Herriot first observed CW laser oscillations (population inversions) from a Ne-Ne gas discharge, CW laser oscillation has been obtained with more than 300 optical transitions ranging from the ultraviolet (.3μ) to the far infrared (400μ) region, and from many different gas systems, employing at least four different excitation mechanisms. The four predominant excitation mechanisms in gas lasers are:

1. Inelastic electron-atom collisions followed by atom-atom collison.

2. Inelastic electron-atom collisions.

3. Inelastic electron-atom collision followed by disassociation in excited atom-molecule collision.

4. Direct optical pumping.

Since high output power and commercial availability are primary considerations for the applications treated in this study, the He-Ne and the Ar^+ ion gas laser system parameters will be discussed in detail, along with some additional comments on the experimental N_2 - CO_2 laser system.

The gas laser design most generally used in practice is composed of a linear quartz discharge tube with Brewster angle windows, an external mirror, and an optical resonator. The optical resonator can have any one

6. Amplitude stability
7. Size and weight
8. Input power
9. Cooling requirements
10. Environmental sensitivity

The pulsed laser systems covered in this discussion are as follows:

Optically Pumped Pulse Lasers

a. Ruby
b. Nd: glass
c. Nd: YAG

Pulsed Injection Lasers

a. Ga As Diode

Pulsed Gas Lasers

a. He-Ne

Information on these laser systems includes:

1. Peak output power
2. Energy/Pulse
3. Emission linewidth
4. Frequency stability and mode structure
5. Angular beamwidth
6. Conversion efficiencies
7. Amplitude stability
8. Pulse width

of several configurations. The configurations generally employed in practice because of their comparative insensitivity to angular misalignment are the confocal and the hemispherical configurations. In the latter configuration, one of the spherical mirrors is replaced with a flat mirror. This configuration is used for applications requiring an output beam with a single mode and uniform phase front (TEM_{00} mode). The confocal configuration is employed for applications requiring maximum output power (multimode). This external mirror technique not only allows greater ease of alignment of the resonator, but also permits the added flexibility of quick changes in the resonator configuration and the laser output wavelength. The laser wavelength shift is accomplished by interchanging the resonator mirror set with another whose peak reflectance corresponds to another laser transition in a given gas discharge system. The external resonator configuration lends itself very well to inter-cavity experiments within the laser.

The purpose of the Brewster windows on the discharge tube is to reduce the reflection losses for radiation polarized in the plane of incidence. This produces a laser output that is polarized, but also reduces resonator losses, thereby increasing the laser output power.

The discharge in the tube can be excited by either of two methods. The first method is to apply RF energy to the discharge tube by means of external electrodes. The second method is to excite a glow discharge by applying a DC voltage between two internal electrodes. The general design described above is employed for almost all gas lasers.

He-Ne Laser

Population inversion in this gas system is achieved by the first of the excitation mechanisms listed above. The excitation energy of the He atom is transferred by resonance transfer to the Ne atom, which is the lasing atom. More than thirty laser transitions have been observed for the He-Ne gas system. Out of these thirty laser transitions, three are predominant, and therefore produce the laser emission lines containing the greatest output power for this system. The wavelengths of these three laser lines are 0.6328 μ, 1.1523 μ, and 3.3913 μ, in order of their relative output power. Thus the 0.6328 μ line is the strongest of the three. The ratio of output powers for those three lines is approximately 5:2.4:1 for a gas mixture optimized for 0.6328 μ. This ratio holds for oscillations at a single frequency. The ratio for simultaneous oscillations at 0.6328 and 1.1523 μ, or 1.1523 and 3.3913 μ, would be somewhat different.

The current state-of-the-art power output lies in the range of 50 - 100 mw CW at 0.6328 μ, for the TEM_{00} mode of a hemispherical resonator. The TEM_{00} mode represents the lowest order transverse mode for this resonator configuration, and therefore has the simplest symmetry

which provides an output beam with the characteristics of a uniform phase front. By changing to a confocal resonator configuration, the power output would be approximately doubled; however, the output beam would contain oscillations from many transverse modes operating simultaneously. Therefore, the beam output phase front would be highly non-uniform.

The output power for a given wavelength depends upon the following parameters: (1) Resonator mirror characteristics - resonator mirrors with reflectance peaked to the desired operating wavelength, with minimum absorption losses, and with optimum transmittance value for maximum output power. This is achieved by using mirrors with dielectric coatings. (2) Discharge tube length - the output power at a given wavelength for a constant discharge tube and resonator parameter varies directly with the discharge tube length. A discharge tube with (a) given inside diameter, (b) optimum partial pressure ratio (5:1 He: Ne at 0.6328 μ), (c) optimum total pressure for the given inside diameter, (d) optimum discharge electron density, has an optimum power output per unit length; hence the direct variation of output power with length of the discharge tube. (3) Inside diameter of discharge tube - with a gas system like He-Ne, where wall collision of the excited Ne atoms is a necessary part of the excitation process to produce laser emission (population inversion), the output varies inversely with inside diameter, assuming all other parameters are kept constant.

In the normal multi-longitudinal-mode laser, the center frequency, linewidth, and frequency stability of the laser emission depend upon the characteristics and stability of the resonator configuration, the total laser output is composed of several narrow emission lines oscillating simultaneously. The total number of lines depends upon the number of cavity resonances lying within the Doppler linewidth of the excited atom and having sufficient gain to overcome all cavity losses, on the length of the resonator and on the wavelength of the emission and the degree of pumping. The higher the power within the Doppler linewidth of the excited atom, the greater the number of laser oscillations which will occur within the total emission linewidth, assuming a constant cavity length and emission wavelength. The longer the laser resonator, the smaller the frequency interval between cavity resonances, and therefore the larger the number of laser oscillations per Doppler linewidth. Therefore, the total emission linewidth depends upon output power, optimum pump power, resonator length, and the Doppler linewidth. The total emission linewidth will be approximately 1/2 - 1 Doppler linewidth, depending on the degree of pumping. A decrease in pump power will decrease the number of modes oscillating within the Doppler linewidth, and therefore within the total emission linewidth. However, at the same time, output power will be decreased. Shortening of the resonator length will reduce the total emission linewidth; however, this requires a shorter discharge tube, and therefore will reduce the output power at the optimum electron density. The Doppler linewidth at 0.6328 μ is approximately

1500 mc, at 1.1523 μ it is approximately 800 mc, and at 3.3913 μ, approximately 270 mc. In a multi-longitudinal mode laser (resonator), frequency stability for the total output line is not critical because of the large number of modes oscillating simultaneously, and for the same reason, amplitude fluctuation due to resonator mechanical and thermal random tuning is negligible. This, together with instability of the discharge, represents a fluctuation of usually less than 1 percent. In a single mode, single frequency laser (where the resonator length provides a mode frequency interval such that only one mode exists in the high gain region of the Doppler linewidth), resonator mechanical and thermal stability must be extremely good. The mean value of the combined thermal and mechanical tuning fluctuation determines the center frequency of the laser emission. The emission linewidth is determined by the maximum value of the fluctuations mentioned above. A detailed examination of the resonance conditions shows that small variations in resonator length provide rather large amplitude variations in laser emission. Therefore in single-frequency lasers, the resonator must be constructed of materials having low expansion coefficients, and operating temperature must also be controlled. The use of piezoelectric-controlled resonator mirrors in a servo-system is required to keep the laser tuned to its maximum output power.

The beam diameter of a gas laser with either a confocal or hemispherical resonator is determined primarily by the resonator length and radius of curvature of the mirrors, for a given wavelength and pump power. It is also a function of the degree of pumping. However, when the discharge tube is operated at its optimum electron density, the beam diameter is very nearly the calculated value. The beam divergence is a function of the beam diameter and the geometry and optical quality of the output mirrors. Most resonator optics configurations provide near-diffraction-limited performance. The beam divergence for most gas lasers with a hemispherical resonator is on the order of 3 minutes of arc or less; for the confocal configuration, it is of the order of 20 minutes of arc or less.

The conversion efficiency for most gas lasers is of the order of 0.001 to 0.1 percent. This is the ratio of the power converted to light output to the total electrical input power.

The current state of the art in commercial He-Ne gas laser design is illustrated by the Spectra-Physics Model 125 laser. The specifications are as follows:

Spectra-Physics Model 125 Laser

Active Medium: He-Ne

Output Power: (For the hemispherical resonator configuration)	0.6328 μ	50.0 mw (observed output power as high as 85 mw)
	0.6118 μ	5.0 mw
	1.08 μ	5.0 mw
	1.1523 μ	20.0 mw
	3.3913 μ	is suppressed to achieve maximum output power at 0.6328 μ
Resonator Length:	1.8 meters	
Beam Diameter: (Hemispherical)	1.8 mm	
Beam Divergence: (Hemispherical)	104.0 sec of arc	
Emission Linewidth:	Less than Doppler Width; $\Delta f\alpha \approx$ 1500 mc (0.6328 μ)	
Amplitude Fluctuation:	< 1%	
Frequency Stability:	Not known	

Resonator cavity is mechanically decoupled from case, and thermally decouples from heat generating elements.

Pumping Method:	DC discharge and RF pumping	
DC Pumping Power:	2500 V at 30 ma	75.0 watts
Conversion Efficiency:	0.6328 μ	0.066% min.

RF Pumping contribution is approximately 10% of total output power. The main purpose of RF pumping is to provide increased arc discharge stability.

Power Supply:

Input Power:	500 Watts, 110 V AC 60 V
Weight:	100 lbs (approx.)

Head Size:

Height:	11"
Width:	11"
Length:	5.5 feet
Weight:	100 lbs.

No cooling is required for He-Ne lasers.

For multi-longitudinal-mode lasers, the sensitivity to temperature, pressure or vibration insofar as output power is concerned is negligible for the reasons explained above. The main effect of these parameters would be observed in the longitudinal-mode properties. In a multi-longitudinal-mode laser, the optical center frequency, oscillation frequency interval, and frequency stability for the individual modes under the Doppler linewidth of the excited Ne atom are determined by the resonator parameters and the pump power and output power per mode. The effect of temperature, pressure and vibration would certainly be pronounced in a laser such as the Spectra-Physics Model 125, which does not have a frequency stabilization system such as found in the Spectra-Physics Model 119. If the longitudinal-mode frequency spacing stability were to become an important parameter in a particular application, then considerable work would have to be done on the stabilization of the Model 125 resonator. Normal stability as represented by the emitted mode linewidth is generally of the order of 50 Kc to 1 Mc. The center frequency and linewidth stability of the overall emitted line are determined by the properties of the He-Ne discharge and pump power. With constant input power to the discharge, the variation of these parameters with temperature, pressure and vibration is negligible. However, in the case of single longitudinal-mode lasers, these factors would drastically affect the output power, output frequency, frequency stability, amplitude stability, and output linewidth. With a temperature-controlled resonator structure and a piezoelectric modulator (resonator) mirror servo-system, it is possible to minimize these effects. The short cavity length necessary for single mode operation on the 0.6328 μ line of He-Ne severely limits the length of the discharge tube, and thereby output power as well. The state of the art in stable, single frequency lasers is represented by the specifications of the Spectra-Physics Model 119.

Ar^+ Ion Laser

This is a relatively new arrival on the laser scene, but it shows great promise for future development. It is capable of considerable output power for both CW- and pulsed-mode operation.

The principal method of discharge excitation employs a quartz discharge with internal electrodes, between which a DC or pulsed voltage is applied for respectively, CW or pulsed operation. The electrodes and the main body of the discharge are water-jacketed to provide the cooling necessary to protect the discharge tube from the high temperatures generated by the high input powers required for this laser operation.

The principal excitation mechanism for this laser is an inelastic electron-atom collision process. For the Ar^+ laser, sufficient energy must be imparted to the electroncs emitted from the cathode by the electric field between anode and cathode to singly ionize the Ar atoms upon collision. The power applied to the discharge tube must be sufficient to produce the singly ionized Ar atoms and the population inversion of the upper Ar^+ levels so generated. Several emission wavelengths for Ar^+ atoms in the visible region have been observed to have very large output powers. The wavelengths so observed are at 4765 Å, 4880 Å, 4965 Å, 5017 Å, and 5145 Å. In an experiment with the discharge tube operating in a long-pulse, or quasi-CW mode, and with an output pulsewidth of 1 - 2 milliseconds, the Ar^+ laser produced output power at the above wavelengths as follows:

λ(Å)	4765	4880	4965	5017	5145
CW Power (Watts)	0.2	1.0	0.2	0.1	10.0

These powers were achieved with a peak discharge current of 10^3 amps, and a gas pressure of approximately 0.03 Torr. The discharge tube with Brewster windows was approximately 3 meters long, with an inside diameter of 5.0 mm. The resonator was a confocal configuration. The measured conversion efficiencies are of the order of 10^{-5} to 10^{-4}. The 10.0 watt output at 5145 Å would require a peak input power of approximately 10^6 watts at worst.

In another experiment where the discharge tube was operated in a steady-state mode (CW), an output power of approximately 0.5 watts for one of the more efficient transitions of Ar^+ was observed. The measured conversion efficiency was about 10^{-3}. The increased conversion efficiency for the CW mode is accounted for by assuming a variation of the normal pulse-excitation process.

Since the Ar^+ laser is still in the experimental stages, data on the measured state-of-the-art values for the following parameters has not yet been determined: Doppler linewidth, frequency stability, mode structure, beamwidth, and amplitude fluctuation stability. An estimate of the Doppler linewidth for these visible transitions of Ar^+, from consideration of the higher gas discharge temperature, would be at least twice the width of the 0.6328 μ line of the He-Ne system. Since the mode frequency stability, mode structure, output beamwidth, and one component of the amplitude fluctuation stability are determined by the resonator parameters and the transition wavelength, it is reasonable to assume that these parameters for the visible transitions of Ar^+ would be close in value to the value of a He-Ne system of equal dimensions. The component of the amplitude fluctuation stability due to discharge parameters for Ar^+ would probably be considerably worse because of the more pronounced instability of this discharge due to the larger magnitude of the plasma oscillations and other effects in this gas system.

In the consideration of the parameters of gain/length and conversion efficiencies for the more efficient transition of Ar^+, it is conceivable that the laser head size and weight would be comparable to the Spectra-Physics Model 125. The relatively high electrical power requirement for this laser (orders of magnitude greater than for the He-Ne system) must be met, however, if the higher output potential of this system is to be realized. This input power requirement, as determined by the conversion efficiencies stated above, is approximately 10^3 - 10^6 watts. Because of these high input powers, the discharge tube requires water cooling at low temperatures and high flow rates. Sensitivity to temperature, pressure and vibration should be comparable to the Spectra-Physics Model 125.

N_2-CO_2 Gas Laser

This experimental gas laser system is a very promising one. In a recent informal report, the following parameters were announced. Output wavelength of 10.6 μ; output power 16.0 watts CW; conversion efficiency of 4.0%. Therefore, the input power is around 400.0 watts, which is a considerable improvement over the Ar^+ laser. No other parameters were given. The lasing molecule in this case is the CO_2 molecule. The initial experimental data and the theory of this gas laser system are given in a recent paper (Reference 23).

The output power observed at 10.5915 μ was greater than 1.0 mw for less than 100 watts of RF input power. The resonator configuration is confocal with the mirrors spaced 1.3 meters apart, and the mirrors are gold-vacuum deposited with an 0.5 mm aperture in the output mirror to couple out the output power. No information is available on the Doppler linewidth of the dominant transition. The angular beamwidth from this

laser, assuming diffraction-limited optics, is approximately 80 times the beamwidth of the Spectra-Physics Model 125 He-Ne laser at 0.6328 μ. No information was given on the amplitude stability, however, because of the use of RF excitation and the low pumping level. It seems reasonable to assume that it is quite small and comparable in value to the value given for the Spectra-Physics Model 125.

From information given in Reference 23 it appears that the size and weight of the laser head and power supply would be approximately equal to that given for the Spectra-Physics Model 125. However, additional equipment would be necessary for its operation; namely, one pump for the CO_2 and one for the N_2, plus flow metering for both gases. High flow-rate air cooling would be adequate for the high output power application. Sensitivity to environment should be approximately the same as for the Spectra-Physics Model 125, since the environmental parameters of temperature, pressure and vibration would have their greatest effect on the resonator structure, which in turn would have the greatest effect on the output mode structure, assuming multimode operation.

Injection Laser (CW)

Ga-As Diode Laser (CW)

The Ga-As injection laser is a very efficient lasing system. The active region (region of population inversion) is located in the plane of the junction of the diode. The excitation process for achieving population inversion is as follows: The diode is forward-biased with a voltage of the corrected polarity, and electrons from the valence band raise the junction to the high energy conduction band of the diode. If a sufficient number of electrons per unit time (current) are supplied to the conduction band, an inversion of the normal Boltzmann electron distribution between these levels will occur (this is the necessary condition for achieving stimulated emission). When the inverted electrons return to the valence band by the spontaneous emission (recombination) process, the energy of the emitted photon is approximately equal to the energy gap between the valence and the conduction bands of the diode. The emission wavelengths corresponding to the energy of Ga-As range from approximately 8350 Å to 8450 Å depending on the temperature and the diode material parameters. The resonator for this laser is a plane-parallel Fabry-Perot configuration. The resonator structure is built into the diode crystal by cleaving two faces perpendicular to the plane of the junction, parallel to each other and perpendicular to the long dimension of the crystal. The faces of the crystal parallel to its length are roughened to discourage the excitation of non-axial modes.

The output power is approximately 7-12 watts CW for a diode 1.7 cm long and operated at 4.0 K. This is currently limited by electrical lead resistance dissipation. The linewidth of individual cavity modes is

approximately 1/40 Å. The total linewidth represented by the modes in the high-gain region of the atomic linewidth ranges from less than 1 up to 30 Å, depending on the degree of pumping above threshold (Reference 24). The frequency stability with respect to temperature variations is approximately 2.5 Å/degree at room temperature and 1 Å/degree at 77° K. Because of the rectangular aperture of the emitting surface of the diode, the emitted beamwidth is in the shape of a fan with the narrow angular horizontal region in the plane of the junction and the wide angular vertical region perpendicular to the junction plane. Nominal beamwidth is approximately 5° horizontally and 15° in the vertical plane. The efficiency of these lasing systems is quite high (Reference 24), with conversion efficiencies ranging from 25 to 40 percent, depending on the operating temperature and heat sink design. The amplitude fluctuation should be of the order of 1 percent, assuming the use of a power supply with extremely low ripple and high regulation, and a heat sink design that provides a constant low temperature without direct immersion of the diode.

Information on size, weight and cooling requirements is available from Korad and Maser-Optics (Reference 25). For maximum output power, the diode must be operated at liquid helium (4° K) temperature (Reference). Operation at 77° K would provide an output power of less than half the value for 4° K operation. Typical dewar design is shown in the Korad specification sheets of Reference 26. The input power requirements for a 7-12 watt experiment (Reference 26) were 30.0 watts.

Optically Pumped, Solid State Lasers

YAG:Nd Laser

This is a very efficient laser system. Being an optically pumped system, the YAG:Nd can be pumped in any of several pump-cavity configurations. The Nd ion is the lasing ion in this material. The increased efficiency over other Nd-doped laser materials is due mainly to broadening of the laser pumping bands. The laser resonator may be one of the commonly used configurations, either built into the laser rod or formed by the use of external mirrors.

The dominant emission wavelength of the Nd: YAG laser is approximately 1.06 μ. The highest power observed for Nd: YAG is about 1.5 watts CW, near room temperature (Reference 27). The Nd: YAG rod in this experiment was probably pumped in an elliptical, gold coated cavity, with a Tungsten-Iodine pump lamp. The Tungsten-Iodine lamp spectral output matches more closely the spectral region of the Nd: YAG pump bands than most other pumping sources. The atomic linewidth for the 1.06 μ line at room temperature is 6.5 cm^{-1}, or 1.0-1.5 cm^{-1} at 77° K (Reference 28). This represents the upper limit of total laser linewidth for these

temperatures. The state-of-the-art level of development for the laser system is described by the Korad specifications for their portable YAG Laser Model KY-1 (Reference 29). The environmental sensitivity is probably comparable to that of a ruby laser of equivalent size and power input. The laser resonator is probably a plane parallel configuration built into the end of the Nd: YAG rod.

A more recently discovered laser system with higher conversion efficiency is the crossed-pumped Cr^{3+}=Nd^{+3} :YAG system (Reference 30). Experimentation with this system indicates an increase of conversion efficiency of 2-3 times over that of the Nd:YAG system. The reason for this is twofold: (1) the pump bands for the Cr^{3+} ion are much wider than that of the Nd^{3+} ion; (2) the upper level for the Cr^{3+} is in near energy coincidence with the upper laser level of the Nd^{3+} ion, thereby providing an efficient energy transfer system between the Cr^{3+} ion and the Nd^{3+} ion. The wider pump bands for this system provide much greater optical coupling with the wide-band pump sources, thereby achieving greater conversion efficiency with currently available pump sources. Details of the initial work on this system are given in Reference 30.

Other low-threshold CW, optically pumped laser materials are (1) Nd:$CaWO_4$, emission wavelength around 1.06 μ; CW output powers of approximately 1.0 watt have been observed at room temperature for this system. Poor optical quality is the main drawback of this laser system; only Nd:$CaWO_4$ rods of the highest quality will lase in the CW mode; (2) DY^{+2}:CaF_2, emission wavelength is about 2.36 μ. This material has a very low threshold energy. It has produced CW laser action with a 50 watt light bulb, with an output power in the milliwatt region. This low threshold is only achieved at temperatures below 25° K. This system will not operate above 77° K. When used with flash lamp pump sources, the DY^{2+} changes to DY^{3+} under the irradiation of ultraviolet emission.

HIGH-POWER, PULSED, SOLID-STATE LASERS

The laser materials which exhibit the highest peak pulse powers and pulse energy are ruby, Nd: glass, Nd: $CaWO_4$, and Nd: YAG. In these laser systems, the laser material is pumped by an electronic flash lamp (usually a xenon arc) in an appropriate pumping cavity configuration. The purpose of the pumping cavity is to achieve optimum optical coupling of the pump source to the laser rod, thereby optimizing the conversion efficiency of the entire system. In these laser systems, the resonator configuration is either constructed on the ends of the laser rod, or is formed by external mirrors in much the same manner as was mentioned above for gas lasers. The resonator configurations generally employed in these pulsed laser systems are the plane-parallel resonator and variations thereof, and the confocal resonator. The geometrical shape of the resonator mirrors is

determined by the geometry of the mirror substrate. The reflectance properties of the resonator are determined by the dielectric vacuum-deposited coatings on the surface of the mirror substrate. The reflectance coatings are so ordered as to produce a reflectance which is peaked to a wavelength corresponding to the lasing ion wavelength, which is 6943 Å for ruby, and 1.06 μ for Nd: $CaWO_4$, Nd: glass, and Nd: YAG. Low- and medium-output power, non-"Q"-spoiled lasers usually employ resonators constructed on the ends of the rod. The ends are ground to the desired geometrical configuration and the reflective coating is deposited thereon. High power lasers usually employ a plane-parallel (or variation) resonator configuration with external mirrors. This allows the insertion of active or passive "Q"-spoiling devices or other devices for various intercavity experiments.

Kerr cells and Pockel cells are active "Q" spoilers. "Q" spoiling is a method for producing single or multiple small-pulsewidth, high-peak-power pulses. Kerr cell and Pockel cell "Q" spoilers can accurately control pulse time intervals of the laser output. The passive "Q" spoilers are generally in the form of a solution of bleachable organic dye in an optical cell placed in the optical path. The dynamics and operating parameters for these passive "Q" spoilers are given in Reference 31. These dyes are available for "Q" spoiling at the ruby wavelength 6943 Å, and at the Nd^3 wavelength of 1.06 μ. Control of the pulsewidth, repetition rate, and amplitude is difficult to achieve with passive "Q" spoilers. However, they produce a more narrow linewidth than the Kerr cell or Pockel cell "Q" spoilers.

Ruby Pulsed, Optically Pumped Laser

The ruby laser emission is at 6943 Å. The highest reported pulse energy for a single-pulse, non-"Q"-spoiled ruby laser oscillator is 1500 joules. For details and specifications of a ruby laser that claims this output pulse energy, see the specifications for Maser Optics Model 4500 High Power Laser (Reference 32). The 1500 joules was obtained by pumping a pulse energy of 120,000 joules into four flash tubes in an elliptical pumping cavity having four sub-cavities. The 6943 Å linewidth at 77° K is of the order of 0.3 cm^{-1}. Beamwidth is of the order of 2-10 milliradians. The current state of the art for "Q"-switched giant pulse, ruby laser oscillators yields peak output powers of 500-750 megawatts with Kerr cell "Q" switching. A good example for this class of ruby laser is the Korad K-2Q giant pulse ruby laser (Reference 33). The greatest peak pulse power is obtained with the oscillator-amplifier laser configuration, which is a laser oscillator followed by laser amplifier which amplifies the oscillator peak pulse output power by a factor of 2-10 times, under "Q" switching conditions. A good

commercial example is the Korad K-2000 Giant pulse ruby laser. The specifications for this laser are as follows:

Korad Model K-2000

Ruby: Oscillator and amplifier ruby rods are each 8" long by 3/4" in diameter

Emission Wavelength: 6943 Å

Linewidth: 0.4 Å (Kerr cell "Q" switch)

0.02 Å (Passive "Q" switch)

Peak Pulse Output Power: 1.5 Gigawatts

Output Pulse Energy: 20.0 joules/pulse

Pulse Rates: 1 pulse/30 sec or 2 pulses/min.

Pulsewidth (50%): 10.0 nanoseconds

Pulsewidth (50%): 1.5 - 7 milliradians

Input Power: 110V AC, 60 ~, 40 amps.

(Single Pulse) Peak Output Power: 3-6 Gigawatts

Maser optics, Model 6400 is roughly equivalent to the K-2000.

A representative example of the state-of-the-art development in high energy, high repetition rate ruby lasers is given in the Maser Optics Series 6-860 lasers (Reference 34). The total linewidth and beamwidth should be approximately the same as for the Korad K-2000 and K-2Q Models.

Because of the poor optical quality of ruby and the lack of an efficient pump source, present conversion efficiencies are limited to approximately 1.0%. Improvement of ruby optical quality and coupling methods will, in the future, allow conversion efficiencies to increase to approximately 10.0%. Future improvement in ruby optical quality would result also in a reduction of beamwidths to less than 1.0 milliradian. In ruby rods of good optical quality the spectral width of individual longitudinal modes will be of the order of 10^{-4} Å. Mode linewidth will be dependent upon the resonator length and "Q", and the degree of pumping. The center wavelength of the ruby laser emission has a temperature dependence which follows the temperature dependence of the ruby fluorescence emission. Temperature dependence for laser emission is 0.065 Å/degree for the 25° to 80°C range, and has an average value of 0.045 Å/degree for the -180° to 0°C range.

The general method for excitation of the flash lamp pump source is to discharge a charged capacitor bank through the flash tube upon ionization of the gas with an external high voltage pulse applied to the flash tube.

Nd: Glass, Pulsed, Optically Pumped Laser

The excitation of this laser material system can easily be accomplished with any of the ruby excitation systems described above. It would be just a matter of substituting the Nd: glass rod for the ruby rod and changing the resonator mirrors to a set with the reflectance peaked 1.06 μ.

The emission wavelength for this material is 1.06 μ. Total laser emission linewidth is of the order of 50-150 Å depending on the optical quality of the glass. Pulse energy of approximately 2000 joules for a single pulse has been reported for Nd: glass in a non-"Q"-spoiled laser at room temperature. Because of the excellent optical quality of the Nd: glass laser material, beam divergence is usually less than 2.0 milliradians for a plane-parallel resonator or a collimated spherical type. Conversion efficiencies as high as 5.0% have been observed for this material in a pumping cavity with a good coupling coefficient. The primary reason for the increased conversion efficiency is that the Nd^{3+} lasing ion is a four-level atomic excitation system which has a very much lower threshold energy than ruby. Because of the lower fracture threshold for Nd: glass as compared to ruby, larger rods of Nd: glass are required for operation in the high-output-pulse-energy (2000 joules) region. Therefore, if Nd: glass rods of optimum doping density and equal size were substituted for the ruby oscillator-amplifier rods in the Korad K-2000, the peak output power at near-fracture threshold would be considerably smaller than for the ruby. Amplitude variations for both ruby and Nd: glass lasers at high repetition rates would be approximately 10.0%.

Nd: YAG Pulsed, Optically Pumped Laser

This laser material system has proven to be rather efficient for both pulse and CW operation. CW operation was discussed previously.

This laser system is still in the experimental stages at this time. However, these early experimental results should be of interest. The lasing ion is the $Nd:^{3+}$ ion. The emission wavelength is 1.06 μ. For a pulse-pumped, "Q"-switched Nd: YAG laser with an input energy of 10 joules to the pump flash lamp, a peak output power of greater than 2×10^5 watts with a pulse duration of 10 nanoseconds was observed. In another experiment where the Nd: YAG was continuously pumped, a repetitive "Q"-switched peak output power of 250 watts was observed. This peak output power was observed for a pump-lamp input power of 1000 watts and a "Q" switch rotational speed of greater than 100 rps. The "Q" switch

device in these experiments is a rotating flat resonator mirror. Since the rotational speed of the "Q" switcher determines the repetition rate of the laser output pulse, the repetition rate observed was 100 cps with a pulse width of approximately 200 nanoseconds. Further data and construction details are given in Reference 34.

Pulsed Injection Lasers

Ga-As Diodes

Excitation mechanisms and geometry for these laser systems are given in Section IIB. Peak output power in excess of 100 watts has been reported, with an average power of 1 watt. These numbers imply that for a 1.0 μ sec pulse width, a repetition frequency of 10 KC is possible. The specification and operating parameters for commercially available pulsed Ga As injection lasers and their associated equipment such as Dewar and pulse generators is given in Reference 26.

Pulsed Gas Lasers

He-Ne Pulsed Gas Lasers

High peak powers have been observed for a pulsed He-Ne discharge laser operating at 1.1523 Å with an internal-electrode discharge tube filled with the normal CW operating total gas pressure and with a high voltage pulse applied to the tube to achieve electric fields of several hundred volts/cm in the gas. The output peak power was more than 50 times the normal CW power. In another experiment with an internal electrode discharge tube filled with a high pressure mixture of helium (240 mm Hg) and neon (5 mm Hg), and pulsed with a 35 KV in 35 amp pulses, a peak power of 84 watts was observed. This 84 watts of peak power was obtained with a pulse repetition frequency of 250 sec^{-1}. The mean average output power was 27.3 mw.

A representative example of an available commercial laser employing the above mentioned gas system is the Energy System Inc. Model 3351 (Reference 35).

APPENDIX B. LASER TRANSMITTER OPTICS

The transmitter optical system regulates the cross-sectional area of the laser beam. A small beam permits reduction of the background by reducing the receiver field of view, and it also concentrates the beam upon reflectors or targets. Considerations of beam size indicate that different systems are appropriate for different ranges. For most experiments an inverted telescope is recommended.

OPTICAL PARAMETERS

A laser beam is highly parallel as it emerges from the exit surface, and the slight angular divergence present is produced primarily by diffraction. The sketch of Figure 7 depicts the initial beam diameter D_o and the divergence angle θ_o.

In general, the diameter D and divergence angle θ are functions of the distance x along the beam axis. Lens and mirrors are used to modify D and θ. The optical components are described in terms of focal points, principal planes, and aperture size.

PARAMETER RELATIONSHIPS

Because diffraction produces the initial angular divergence, the divergence angle is directly proportional to the wavelength and inversely proportional to the diameter of the beam.

The proportionality factor depends upon the electric field distribution within the exit pupil of the laser and also upon the definition of beamwidth. For example, a plane wave falling upon a circular aperture yields the well-known Airy disk, for which the proportionality factor is 2.44. However, the electric field of a helium-neon laser has a Gaussian distribution, and the width of the beam is defined arbitrarily as a standard deviation. If the aperture is much less than this width, the diffraction pattern is given by the Airy formula (Reference 8). If the aperture is much greater than this width, the diffraction pattern has a Gaussian distribution so that the resulting width is again given by a standard deviation. Consequently, for the present discussion, a round number of 2 is sufficiently accurate, and the relationship can be stated in the form

$$\theta_o = 2\lambda/D_o \qquad \text{(B.1)}$$

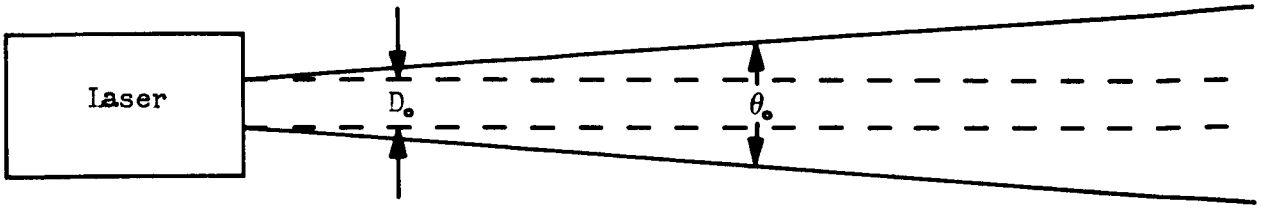

Figure 7. Initial Beam Diameter and Divergency Angle for a Laser Beam

This relationship is plotted in Figure 8 for the wavelength 0.633μ corresponding to the red line from a helium-neon laser. The graph shows that typical laser diameters of a fraction of a centimeter produce divergence angles of a few minutes of arc. Consequently, the diameter as a function of distance x measured from the laser can be expressed as

$$D(x) = D_o + x\theta_o = D_o + 2\lambda x/D_o \qquad (B.2)$$

Figures 9 and 10 show how beam diameter varies with the range. Except very close to the laser, the initially larger beam gives a smaller spot.

Consider the use of a convergent lens to focus the laser beam to a smaller spot, as indicated in Figure 11. The lens is indicated by its principal planes PP' and back focal plane F'. The plane P' lies at a distance x_1 from the laser. The distance f between P' and F' is by definition the focal length. Because the beam is almost parallel, the lens focuses it almost to a point at the focal point B. Assuming that x_1 is small enough so that $D(x_1)$ is practically D_o and that the diameter of the lens is greater than D_o, the diameter of the beam at the focus approximates to

$$D_f = 2\lambda f/D_o. \qquad (B.3)$$

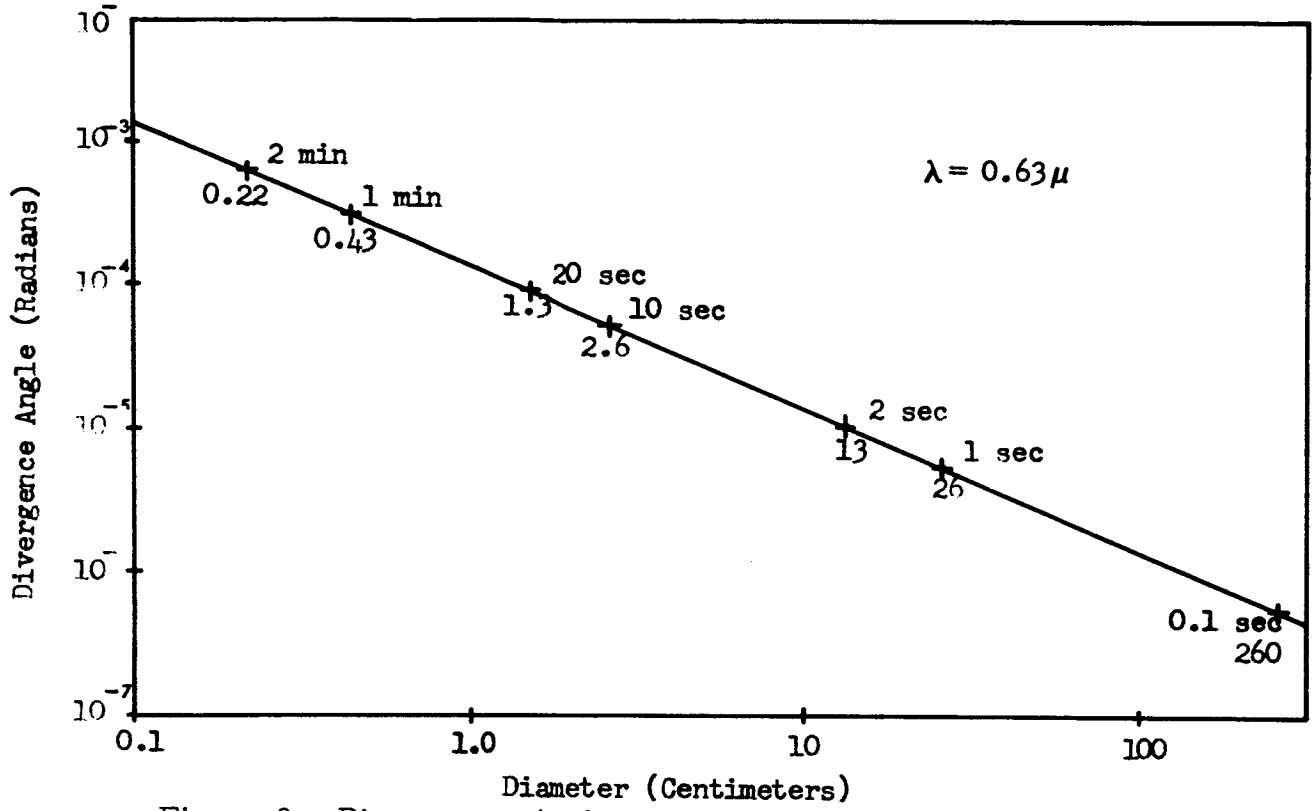

Figure 8. Divergency Angle vs. Initial Laser Beam Diameter

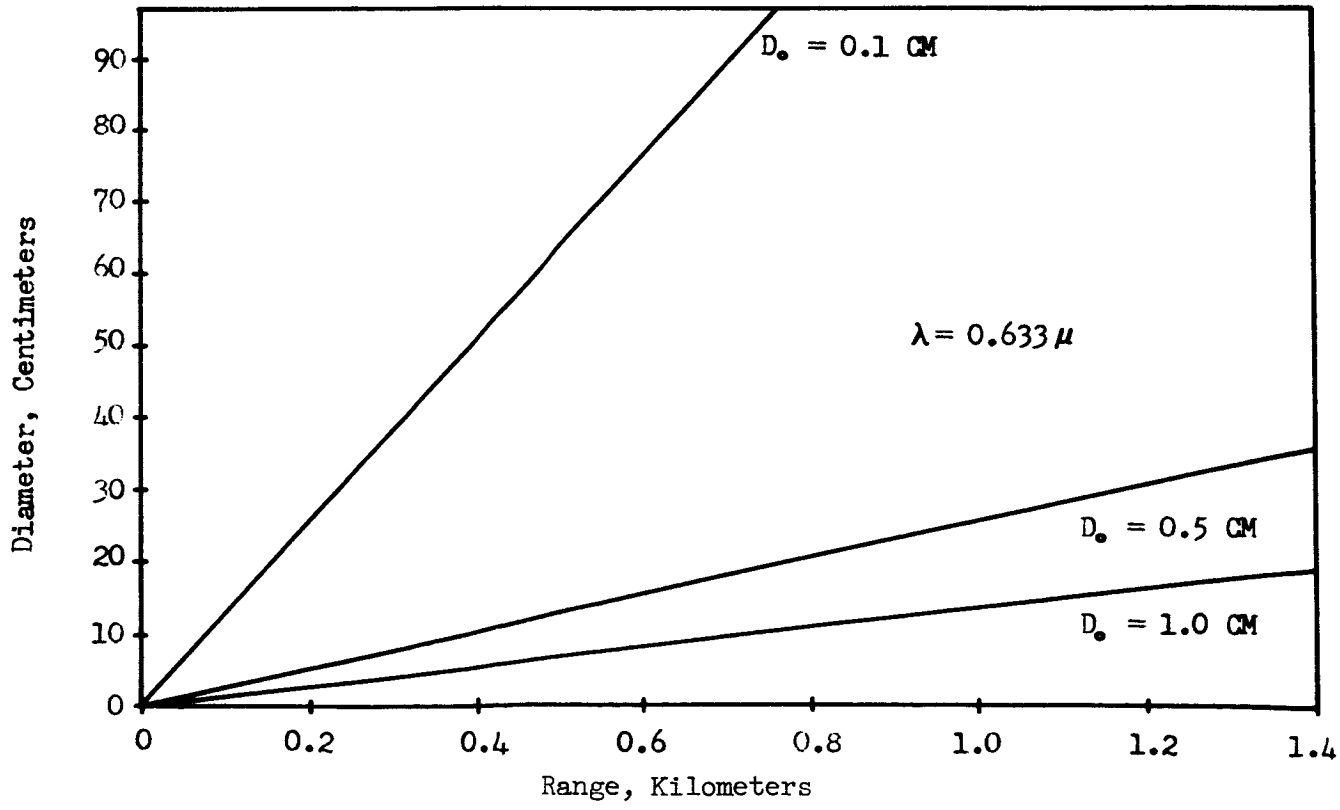

Figure 9. Beam Diameter vs. Short Range

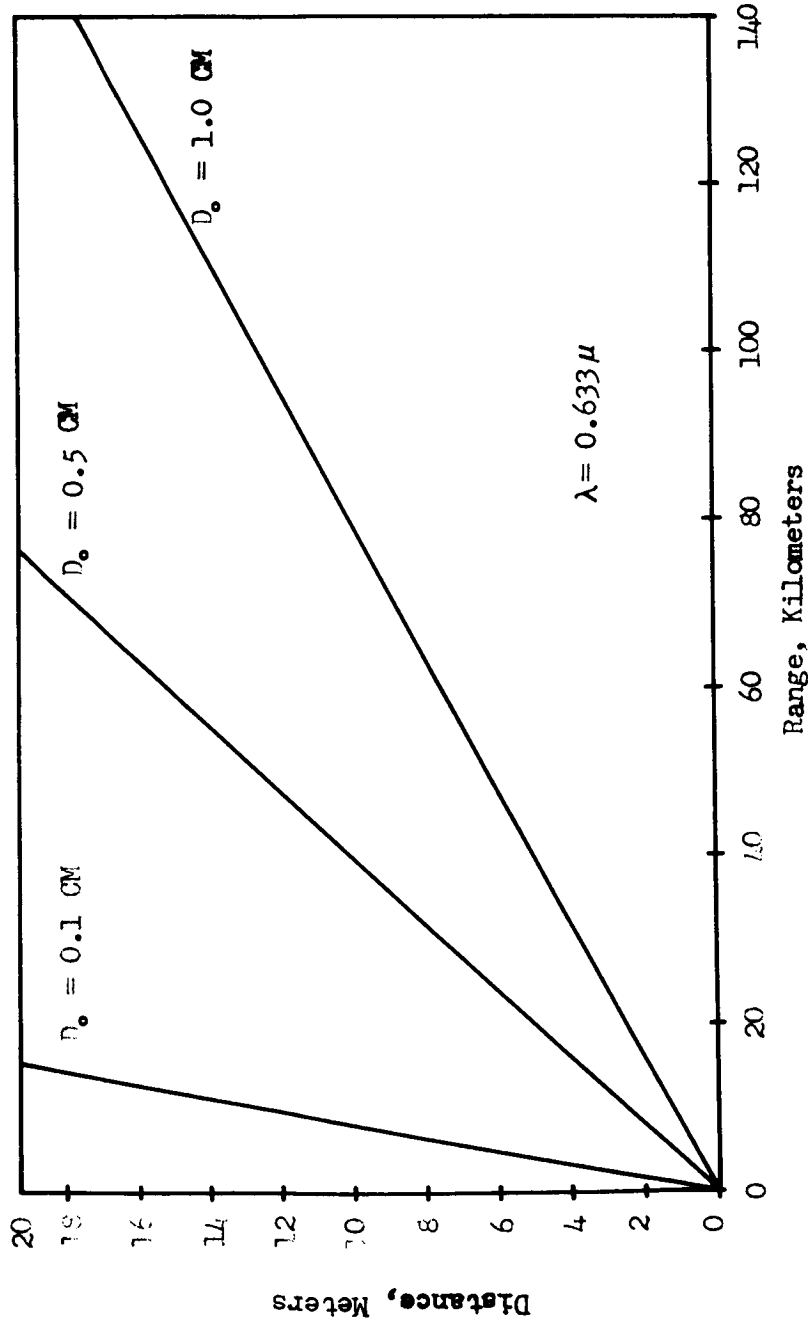

Figure 10. Beam Diameter vs. Long Range

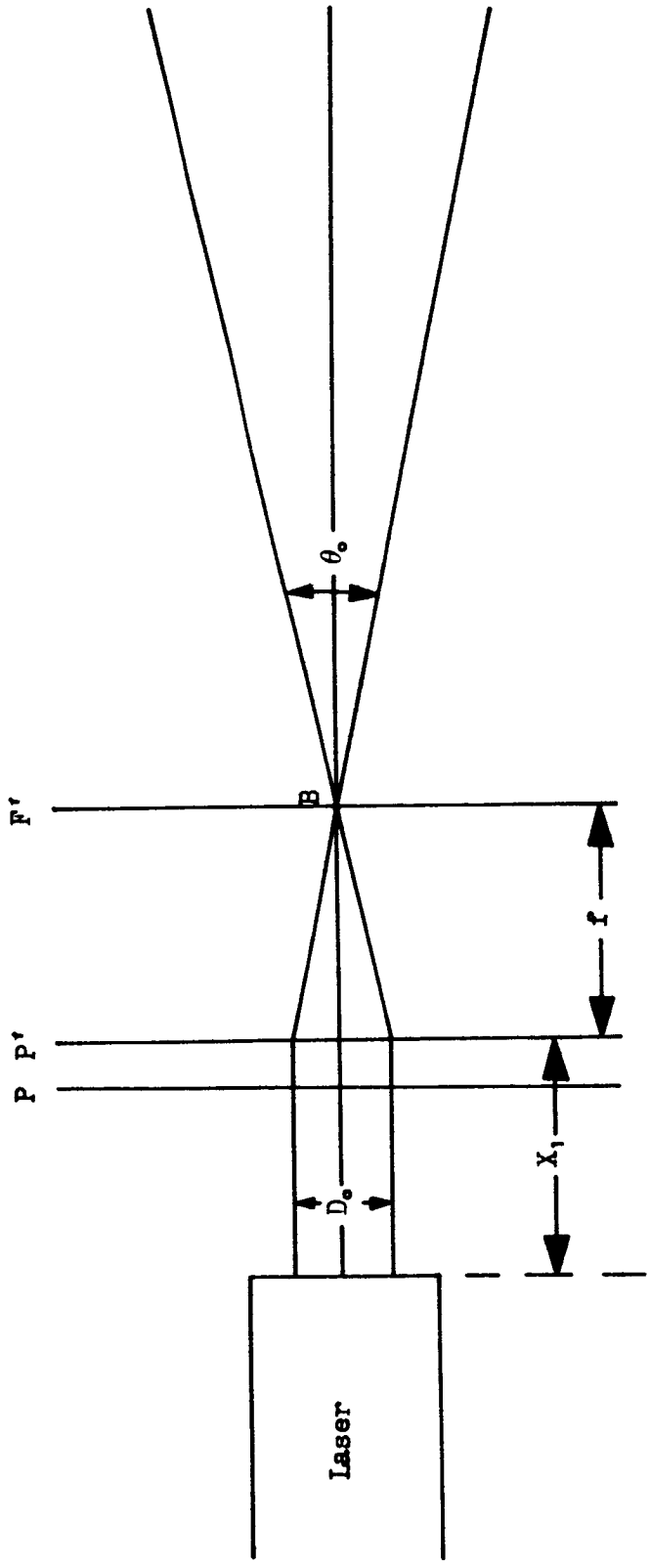

Figure 11. Laser System with Convergent Lens

Then if f lies in the range of 10 to 20 cm, the focused diameter is of the order of 20 λ to 400 λ for D_o in the range of 1 to 0.1 cm.

The use of a single lens has several disadvantages. The small spot is restricted to a single range, which moreover is very close to the laser. Furthermore, the beam divergence beyond the focal point is increased tremendously. The new angle of divergence θ_1 is given by

$$\theta_1 = D_o/f \tag{B.4}$$

which is of the order of 10^{-2} to 10^{-1} radians.

Now improve the system by adding a second lens of larger diameter and focal length as shown in Figure 12. The separation of F_1' and F_2 is a, and consequently the beam spot at F_1' is focused again at a point B lying a distance f^2/a beyond F_2'; therefore, the distance of B is given by

$$x_B = x_2 + f_2 + f_2^2/a, \tag{B.5}$$

where f_2 is the focal length of the second lens. Also, from Figure 12,

$$x_2 = x_1 + f_1 + a + f_2 + d_2 \tag{B.6}$$

To see how x_B varies with a, suppose that f_1 is 0.1 m, that f_2 is 1 m, and that $x_1 + d_2$ is about 0.1 m. Then from Equations B.5 and B.6

$$x_B = 1/a + a + 2.2 \tag{B.7}$$

where x_B and a are in meters. The course of the spot range x_B is illustrated in Figure 13. It has a minimum of 4.2 m for a = 1 m. As a increases further, x_B increases because the telescope formed of the lenses is being extended. The case of interest here is the increase of x_B as a decreases, approaching infinity as a approaches zero.

The geometric angle of convergence θ_t is small enough so that it is given by

$$\theta_t = \frac{D_1}{f_1 + f_2^2/a} \tag{B.8}$$

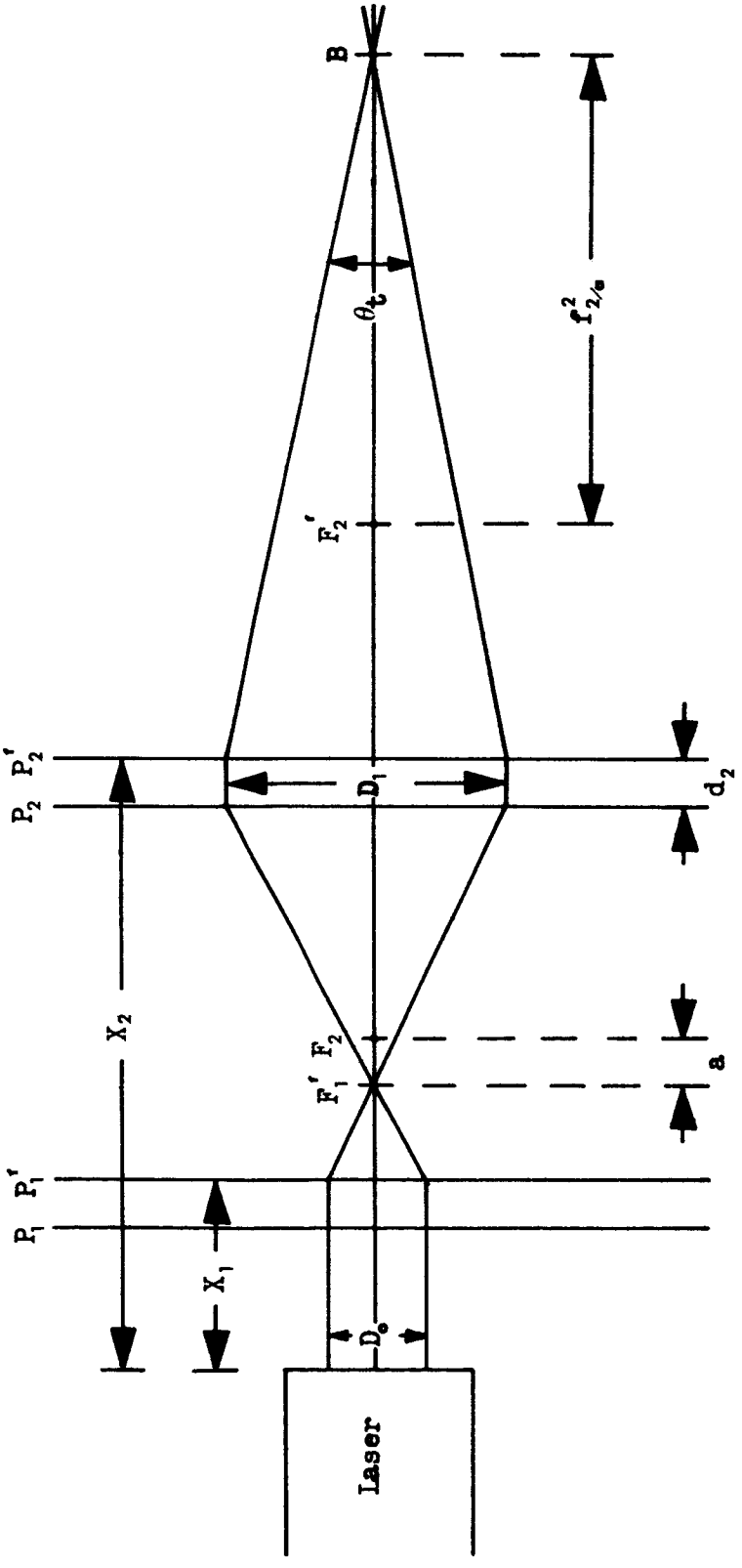

Figure 12. Laser System Using Collimating Optics

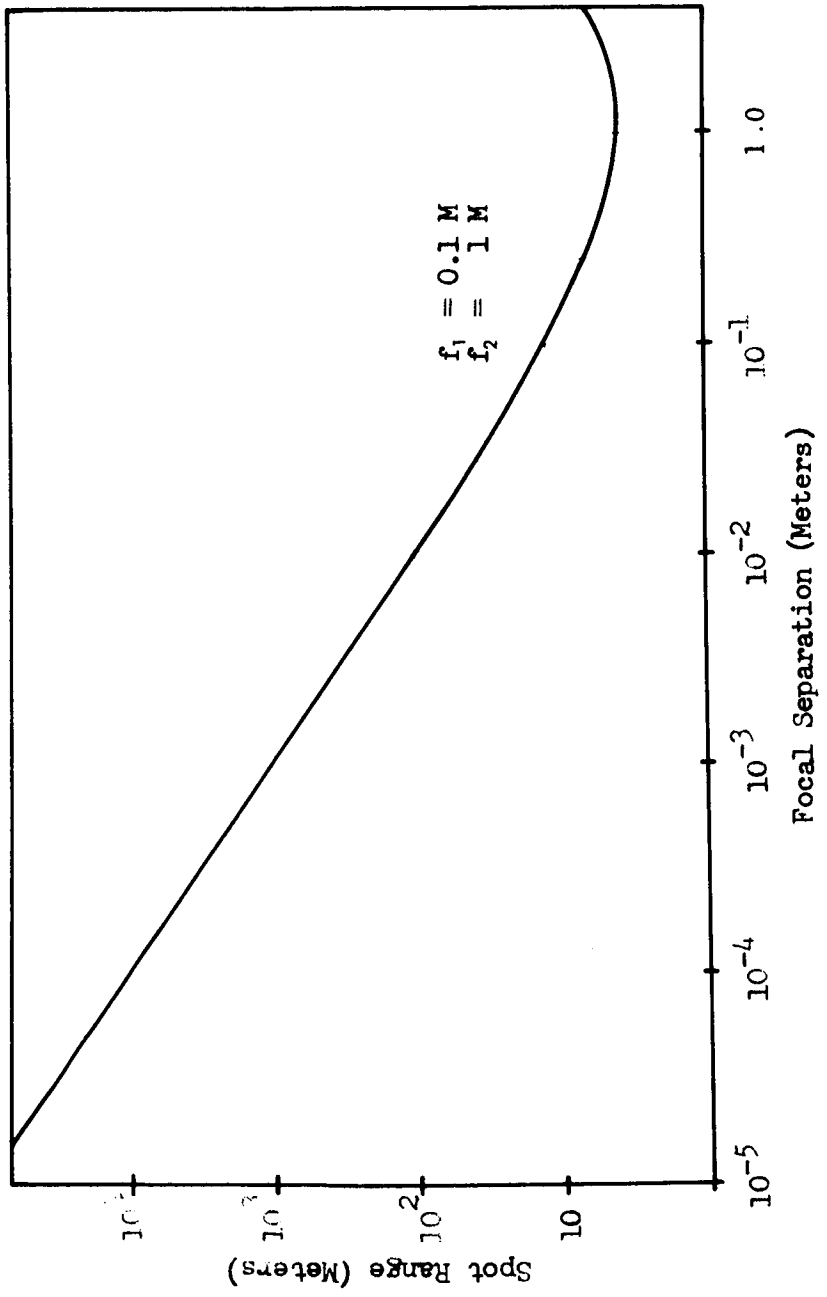

Figure 13. Focal Distance vs. Focal Separation

where D_1 is the diameter of the laser beam as it emerges from the telescope. For x between x_2 and x_B, the diameter of the beam can be expressed in the form

$$D(x) = (x_B - x)\,\theta_t + 2\,\frac{\lambda}{D_1}\,(x - x_2). \qquad \text{(B. 9)}$$

The first term on the right represents geometric focusing, and the second represents diffraction. Rearranging Equation B. 9 in the form

$$D(x) = (x_B - x)\,\theta_t + \frac{2}{D_1}(x - x_B) + \frac{2\lambda}{D_1}\,(x_B - x_2) \qquad \text{(B. 10)}$$

It is seen that when x takes the value x_B, the spot size is given by

$$D(x_B) = \frac{2\lambda}{D_1}\,f_2\,\frac{(f_2 + a)}{a} \qquad \text{(B. 11)}$$

which is analogous to Equation B. 3. In fact, Figure 12 shows that

$$D_1 = D_o\,(f_2 + a)/f_1 \qquad \text{(B. 12)}$$

so that Equation B. 11 can be expressed in the alternative form

$$D(x_B) = \frac{2\,\lambda\,f_1}{D_o}\,\frac{(f_2)}{a} \qquad \text{(B. 13)}$$

In other words, $D(x_B)$ equals the spot size formed by the first lens, increased by the ratio f_2/a.

Rearranging Equation B. 9 in the form

$$D(x) = (x_B - x_2)\,\theta_t - (x - x_2)\,\theta_t + \frac{2\lambda}{D_1}\,(x - x_2) \qquad \text{(B. 14)}$$

shows that it can be expressed as

$$D(x) = D_1 \left[1 - \frac{(x - x_2)}{f_2(f_2 + a)} \right] + \frac{2\lambda}{D_1} (x - x_2) \qquad \text{(B. 15)}$$

In the limit as a approaches zero, that is, as F_1' and F_2 are made to coincide, the emergent beam becomes almost parallel, and D(x) assumes the form

$$D_t(x) = D_1 + \frac{2\lambda}{D_1} (x - x_2) \qquad \text{(B. 16)}$$

as it should for a parallel beam emerging from the plane $x = x_2$ with the diameter D_1, where D_1 is given by

$$D_1 = D_o f_2/f_1 \qquad \text{(B. 17)}$$

Comparison of Equations B. 11 and B. 14 to Equations B. 15 and B. 16 that for a less than f_2, the spot size is practically that of the telescope system focused at infinity.

In Figure 14 $D_t(x)$ for $D_1 = 10$ cm is compared to D(x) for $D_o = 1$ cm. The reduction in spot size obtained by employing an inverted telescope to transmit recommended as the transmitter optical system.

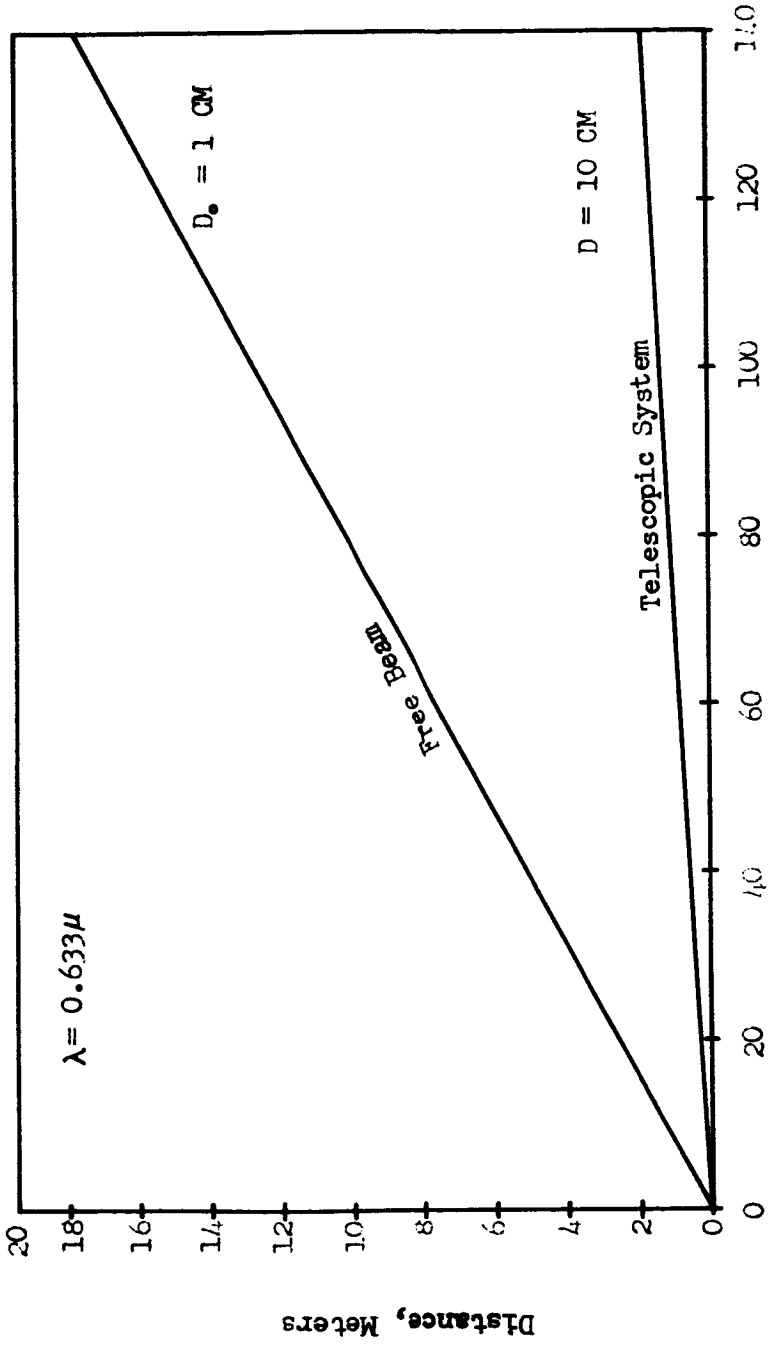

Figure 14. Comparison at Laser Beam Diameter for Free Beam and Collimated Beam

APPENDIX C. PHOTODETECTOR PERFORMANCE SUMMARY

SUMMARY

The photodetector data presented here is oriented towards detectors with high sensitivity, high modulation bandwidth, and having a peak spectral responsivity coincident with laser emission wavelengths for He-Ne and ruby laser systems. The types of photodetectors covered in this report are as follows:

1. Photomultipliers
2. Microwave phototubes
3. Microwave traveling-wave phototubes
4. High frequency photodiodes.

Information on these photodetectors includes:

1. Spectral response
2. Noise
3. Sensitivity
4. Modulation bandwidth
5. Power requirements
6. Cooling requirements
7. Sensitivity to environment.

INTRODUCTION

There are two basic types of photodetectors, photo-emission tubes and photo-semiconductors. Each of these types may be subdivided into further categories. Although a variety of detectors are available covering a wide range of spectral response, the devices discussed here are those which are most suitable for applications involving visible and near-infrared radiation, corresponding to the laser sources envisioned for the LACE experiments.

Because of its pre-eminent position among the photodetectors, the photomultiplier is discussed first and at somewhat greater length than the other detectors. The latter include the vacuum phototube, the photo-mixer traveling-wave tube, the photodiode, and the vidicon and image orthicon image tubes.

PHOTOMULTIPLIER

This detector, because of its spectral response, good sensitivity, high output current, and short response time, is particularly suited to the requirements of the experiments proposed in this study.

The operating mechanism for this device is photoemission of electrons from a photocathode, resulting from energy transfer from the incident photons, followed by a multistage electron-multiplier to amplify the low-level photocurrent to usable output levels. The photomultiplier, by virtue of its electron multiplication ability, has the highest sensitivity, responsitivity, and dynamic range of any photodetector. These detectors have very low noise values at room temperature, which can be reduced further by cooling. The primary noise mechanisms in a photomultiplier are shot noise in the photocurrent due to the randomness of photoelectron emission when irradiated by target and background photons, and thermionic (dark current) emission of the cathode.

The spectral responsitivity of these detectors is determined by the spectral responsitivity of the photocathode material. The long wavelength cutoff is determined by the band-gap energy levels of the photocathode material. The energy band gap for all known photoemissive, low-work-function cathode materials corresponds to photon wavelengths in the region from the near IR to the UV region of the spectrum. The spectral region of greatest sensitivity for these photocathodes is the visible-to-UV region.

In application where He-Ne laser wavelength of 6328 Å is used, an S-20 surface will provide maximum sensitivity. It is desirable to optimize detector sensitivity to provide for those cases in which extremely low light flux densities may be received.

At least two multiplier phototubes having S-20 surfaces are suitable for photometry and flying spot scanning. These are the RCA[1] types 7265

[1] RCA is not the only supplier of S-20 photosurface multiplier tubes. Similar types by some other manufacturers are: Ampex XP1002; Dumont K1927; EMI 9558B, 9607B.

and 7326. Since the tubes are rated at 1 milliampere maximum average anode current, the output may be expected to be non-linear for light intensities greater than that corresponding to this output level.

The multiplier phototube has a linear range which extends over several orders of magnitude. At the lower end of the range, the sensitivity is limited by noise in the tube, in the external circuitry, and in the light beam itself. The upper limit is set by physical changes in the phototube material, including permanent damage, and/or by the creation of an electron cloud which produces the so-called space charge effect in the last two dynode stages. Space charge effects can be minimized by proper choice of dynode voltages but they cannot be removed entirely. RCA is careful to point out that linearity is achieved only by uniform illumination and proper orientation of the photocathode surface - one which has not been subjected to agin effects such as extreme light levels. Thus, if the illumination is non-uniform (and perhaps even wanders) the linearity of the tube output will be affected.

Design factors such as the number of dynode stages also influence the linear range of the PM tubes, High gain tubes are more sensitive to light but saturate (because of space charge) at a lower light level than do the tubes having lower gain. The saturation limit, referred to incident illuminance, varies dramatically with the gain of the tube, while the noise limit tends to remain constant. According to Reference 36, thermionic emission noise will usually dominate the output noise power and will tend to be a constant quantity for fixed temperature, anode voltage, photocathode surface area and overall current gain.

The bandwidth of the multiplier phototube is more than adequate for most communications problems. The modulation frequency response of the photomultiplier can be from 0-500 MC with good external circuit design, and can extend to 2000 MC with extreme care. The upper frequency cutoff is controlled by electron transit time effects and external circuit parameters. The noise spectral density of the photomultiplier tube output actually contains a 1/f noise which becomes significant at very low frequencies (Reference 37). The importance of this additive noise term is that it causes difficulty in predicting the d-c level of the noise over an extended period of time. Because of this effect, long term measurement of a steady light flux will contain an undesirable degree of noise uncertainty. To remove this noise when a PM is used in a laser atmospheric experiment it may be necessary to employ one of the following techniques:

1. Calibrate the output current reading frequently with a standard light source of known intensity.

2. Chop either the outgoing laser beam or the received laser beam at a frequency that is large relative to the expected rate of variation in beam intensity (e.g., at a rate of 1,000 or 10,000 cps). Two subcarriers will then be created which differ from the received optical frequency by twice the chopping frequency. These subcarriers will contain sidebands whose amplitudes are proportional to the variations of the laser beam amplitude resulting from atmosphere disturbances. The subcarriers must be filtered and detected by a conventional amplitude detector. The output of the amplitude detector contains a voltage proportional to these amplitude fluctuations and a stationary dc level which does not contain the 1/f detector noise.

The photomultiplier tube usually requires a high voltage, low current power supply. The required power supply voltage is usually in the 500-1500 V range. The power supply must deliver current up to 10-20 milliamps at these voltages for some applications.

VACUUM PHOTOTUBE

The vacuum phototube detector is a photoemissive detector like the photomultiplier. The sensitivity of the phototube is, however, many orders of magnitude less than the photomultiplier because the phototube does not have an electron multiplier. The vacuum phototube is composed of a photoemissive cathode, together with an anode structure inside of an evacuated glass envelope. The spectral response of these detectors covers the same spectral range as the photomultipliers because the same photocathode materials are used in both cases. The noise at room temperature is low for these devices. The noise mechanism for these detectors is the same as for photomultipliers. Considerable improvement in noise value can be achieved by cooling the device to minimize cathode thermionic emission. The modulation bandwidth for these devices is rather large. For example, a 1P42 phototube optimally matched to a coaxial transmission line was used in an optical mixing experiment to measure the difference frequency between several intervals of longitudinal cavity modes from a ruby laser. Difference frequencies up to 10 KMC were detected. Since a coaxial transmission line does not have a low frequency cutoff, this detection scheme should have a modulation bandwidth of from 0 to at least 10 KMC. The phototube required a bias of 500 volts for these experiments. The sensitivity of these devices

is comparable to the sensitivity of photo-microwave traveling-wave tubes when directly detecting the laser beam. For further details of these experiments, see Reference 38. The optical, electrical, and mechanical specifications and properties of a number of different commercially available phototubes are also given in Reference .

PHOTO-MIXER TRAVELING-WAVE TUBE

This photodetector is a high frequency detector that was especially designed for laser optical mixing and laser mode structure studies. It is a traveling-wave tube amplifier with a photocathode. Microwave difference frequencies in the photocurrent emitted from the cathode are amplified in the traveling-wave structure. The microwave signal is detected with a normal microwave receiver. The spectral response for these devices is the same as for the photomultiplier tubes because the same photoemissive cathode materials are used in both devices. The noise values at room temperature for these devices is low and S/N ratios are high, but the sensitivity is much lower than for a photomultiplier. The output signal is at a very low level and microwave receivers with low noise figures must be used to detect the output with a good S/N ratio. The modulation bandwidth is determined by the bandwidth of the TWT structure. The usual bandwidth of such a structure is approximately an octave. No cooling of the tube is required for its normal operation. However, cooling of the cathode would result in some reduction of noise in the output. The power supply requirements for this device are moderate. The optical, electrical, and mechanical specifications for some commercially available units are given in Reference 39. This data includes information on output power, spectral sensitivity, noise power output, and S/N ratio as a function of receiver bandwidth, detector bandwidth, and operating voltages and currents. These commercially available tubes are only available with S1, S4, and S20 photocathodes, with detector bandwidths of 1.0 to 2.0 Gc, 2.0 to 4.0 Gc, and 8.0 to 11.0 Gc. A paper describing a group of ruby laser mode-structure experiments and another giving detailed information on the commercial and experimental units are given in Reference 40. These devices are excellent as optical video detection systems for wideband microwave modulated light transmitters and as mixers for optical heterodyne detection systems.

PHOTODIODE

The high-speed junction and point-contact photodiodes considered here were developed for laser optical heterodyning and mixing for application to laser mode studies and optical communication and radar systems. Information for both Ge and Si diodes is included.

The spectral response for Si diodes is approximately .35 to 1.3μ, for Ge diodes, .5 - 1.7μ. Diode detectors can have noise levels which are

fairly low, but still high compared to the noise figure for a photomultiplier. The sensitivity of these devices is on a par with the microwave T. W. phototube but is low compared to the sensitivity of a photomultiplier. The relative sensitivities of the Ge and Si diodes depend upon the type of construction. Bandwidth for junction diodes is approximately 0 - 20 Gc. Point contact can be extended to a higher frequency cutoff. Power requirements for diode detectors are modest, of the order of 1 to 100 volts with currents up to 1 milliamp. Under normal operation, these devices do not require cooling. However, cooling would improve sensitivity, decrease noise, and improve the S/N ratio. These detectors are sensitive to overexposure to high energy radiation fields. Details of recent research in junction and point contact Ge and Si high frequency detectors and in diodes of other material systems are given in Reference 41. Optical, electrical, and mechanical data for several commercially available detector diodes is given in References 42, 43, and 44. These devices are excellent optical mixers and high frequency video light detectors, provided sufficient signal strength is available. The Ge and Si diodes, by virtue of their spectral response, would be excellent for use with either ruby or Nd:^{3} lasers.

All of the photoemissive type detectors discussed in this section are sensitive to photocathode damage from high light fluxes. Caution must be exercised in the use of these devices so as not to overexpose the photocathode, since this will create irreversible deterioration in the sensitivity. The maximum light flux for any given photodetector is usually given in the specification data for that detector.

IMAGE TUBES

The basic principle of operation for both the vidicon and image orthicon is as follows. A photocathode surface is illuminated by an image formed by the lens system. The photoelectric effect produces an electron conductivity or voltage field which is measured by a scanning electron beam. The resulting tube output thus contains peaks and valleys which correspond to variations of light intensity over the raster scanned by the beam.

As with the photomultiplier, care must be taken not to damage the photoemissive surface. Beam-spreading lenses and attenuators can be used for this purpose. It should be noted that the resolution of light levels within the incident beam increases as the percentage of the photosurface illuminated is increased. However, since resolution should not be a great problem in most cases, the photosurface can be used for recording wander of a laser beam over several beam diameters. This is possible because of a line resolution which ranges as high as 600 to 1000 lines per frame. It is also advisable to employ standard light levels for calibration. These light beams would illuminate the photosurface at a position near to that of the beam being measured. The light levels serve to standardize the raster voltage levels,

compensate for gross raster non-uniformities, and provide a simple real time intensity reference. It will be remembered that a similar light intensity standard is required for the film recording technique.

There are a number of different devices that can be used to simply record light intensity at a position within the beam. As mentioned before, they fall into the categories of phototube and solid state photodetection. Table 9 illustrates the relative performance of these detectors for a specific application (Reference 44). The information presented in Table 9 is of interest to the LACE experiments, regardless of the choice of subcarrier frequency. The irradiance levels at the photodetector surface depend on the experimental configuration and the available laser power. The configuration must always be such that a light level of roughly 10^{-10} watts/cm^2 per cps of output bandwidth or greater is received at the photosurface; otherwise, the output of the photodetector is likely to be too noisy to adequately measure the light fluctuation of interest.

Table 9. Relative Photodetector Performance

Device	Quantum Efficiency η	Gain G	Response at 5GC $\lvert f(\omega T) \rvert$	Equivalent Load Imped. R_{eg} ohms	Optical Power Watts for S/N = 20 db	Comments
Perfect Quantumcounter	1				$3. \times 10^{-7}$	
Silicon Avalanche Photodiode	0.5	36	0.3	30	7.8×10^{-6}	R_{eq} for C = 1 pf series resistance = 25 ohms
Crossed field photomultiplier	10^{-2}	5×10^{-5}	-1	50	3×10^{-5}	Base bandwidth >4 Gc
Traveling-wave phototube	10^{-2}	1	1	5×10^{5}	3.5×10^{-5}	Bandwidth of one octave or more possible
Germanium p-i-n diode	0.3	1	-1	250	3.7×10^{-5}	R_{eq} for C = 1 pf series resistance = 2.5 ohms
CdSe photo conductor	0.6	1	5×10^{-3}	5000 ohms for 5 Mc bandwidth	8.3×10^{-4}	Measured R_{eq} for a plate 1 mm square
InSb photoconductor at 3.39 μ	0.5	0.04	0.5	75	3.6×10^{-3}	Very broadband since shunt capacitance is negligible
Note: λ = 6328A f_{sc} = 5 Gc B = 150 Mcps						

APPENDIX D. RECORDING MATERIALS

An analysis of photographic film characteristics that relate to implementation requirements for data recording on several of the experiments is presented in this appendix. Essentially, the analysis compares the properties of free radical film, direct thermal recording and Kalvar.

This analysis, although directly related to LACE, was prepared under NAA/S&ID research and development.

FREE RADICAL FILM

The name, Free Radical Photography, was coined at Horizons Incorporated to identify a new light-activated color-forming chemical reaction invented by Dr. Eugene Wainer in 1958. Since that time, it has been developed in Horizons' Chemistry Department with financial support from the Air Force. The name originated from the theory (experimentally confirmed) that the color forming reaction was initiated by the splitting of carbon tetrabromide (CBr_4) under the influence of light into two free radicals, followed by chain-propagated condensation or oxidation reactions which yield several molecules of dye for each photon absorbed. This new photosystem has the advantage that both initiation and propagation steps take place during the light exposure. The visible image is formed without further development, creating an "instant-picture" capability.

A system code-named "2S," has the great advantage over previous free radical systems of being fixable by heat with no solvent-extraction being necessary. The "2S" system is sensitive to red and green light, with very little sensitivity to blue - a distinct advantage for aerial photography where the longer wavelengths are less scattered by atmospheric haze. Use of different activators gives this system a broad range of contrast. If bromacetic acid is used as the activator, the film has a spectral response from 5500A° to 6800A°. The image is fixed by heating to 150° C in a convection oven. The film has an exposure speed of 1 miscrosecond with a resolution of 250 lines per mm.

The free radical film should withstand the 12 month 85° C internal probe environment with very little exposure, if any. The sterilization temperature of 145° C will evaporate the emulsion and render it insensitive to light. It is highly probably that further study of the free-radical system, with particular emphasis on the high temperature application, would result

in a suitable free-radical storage material. The resolution of the free-radical system is better than the resolution of the optical recording system.

DIRECT THERMAL RECORDING

In the case of the General Electric TPR process, an electron beam lays down a charge pattern which corresponds to the image to be recorded. Upon subsequent heating of the film the coulomb forces distort the plastic film surface. The surface deformations scatter incident collimated light, and with Schlieren optics the scattered radiation can form an image. Certain limitations are inherent to the method. They can be overcome by one or several of the thermoplastic recording techniques developed by North American Aviation.

One technique uses a uniformly deposited charge layer. The charges are deposited by any convenient technique such as by exposure to a beta-emitting radioactive isotope, by corone discharge, dielectric polarization, flood exposure to an electron gun, etc. The charges act only as a motor and by themselves do not contain any information.

A laser beam, which is made to lase at an infrared wavelength for which the thermoplastic material employed has an absorption maximum, is modulated and focused onto the recording material. There it causes local heating and melting of the thermoplastic where the degree of viscosity depends on the energy dissipated. The lower the viscosity of the plastic, the more readily will the coulomb forces distort the film surface. The degree of distortion now depends on the modulation of the laser beam and not the desity of the charges.

The film is preheated to near the melting point prior to the entry of information. The laser, therefore, only provides the energy required to raise the plastic to the melting point, which corresponds to a dc bias or a constant energy increment and beyond that the energy to "temperature" modulate the focal spot. For example, at 80% depth of modulation, 20% can be used to help bring the film temperature from ambient to the melting point, and from 0 to 80% of the energy is now available for the recording of analog information or digital information, if desired.

Additional simplicity of the recording system is obtainable by using a storage medium which contains latent energy. For example, certain plastics can be made to shrink by the application of heat. These plastics shrink by as much as 50%. A film can be made of this plastic and the laser beam will cause shrinking in the focal spot where the degree of shrinking depends on the temperature or the amount of energy delivered in a certain time element.

This film cannot be updated in contrast to the earlier method; however, the need for charge deposition techniques is eliminated, resulting in simplification of the system and a corresponding increase in reliability.

Advantages of both systems over any other recording technique using light are that the image is created by the light and, once exposed, needs no other treatment. Exposure, development and fixing are events that occur simultaneously in these thermoplastic recording techniques.

There are two distinct differences in the appearance of the bits. In the first case where coulomb forces distort the film surface, the material is redistributed but the volumes remain unchanged. In a typical bit of this type, material removed from the central crater is piled up to form a wall at the periphery of the crater. Surface tension causes the wall material to assume smooth curved surfaces.

In the case of the heat shrinkable plastic, the total volume changes so that there is little mass material left. The stresses in the film are of higher magnitude than the surface tension so that a more sharply defined bit remains.

Resolution - Bit Density

The unique properties of CW lasers are their ability to emit light which is of equal phase across the diameter of the beam, their degree of spectral purity and coherence in the time domain. Such light makes it possible to reach practical results in applied optics extremely close to the theoretical limitations imposed by physical optics. This advantage of laser light results in the ability to obtain diffraction-limited focal spots, i. e., focal spots of a size reaching the theoretical lower limit.

The cross-section of the diffraction-limited focal spot depends directly on the wavelength of the light, aside from lens consideration, so that smaller focal spots can be produced with shorter wavelengths.

The energy distribution within the focal spot assumes the shape shown in Figure 15.

The resolution of an image, which depends on the ability to differentiate two adjacent points, would then depend on the degree of superposition of the diffraction image shown in Figure 15. For example, assuming a 40% differentiation of two spots, Figure 15 would be redrawn to Figure 16.

If a recording material would be able to "see" the whole curve of Figure 16 the resultant response would be the product of the response curve of the material and the curve of Figure 16.

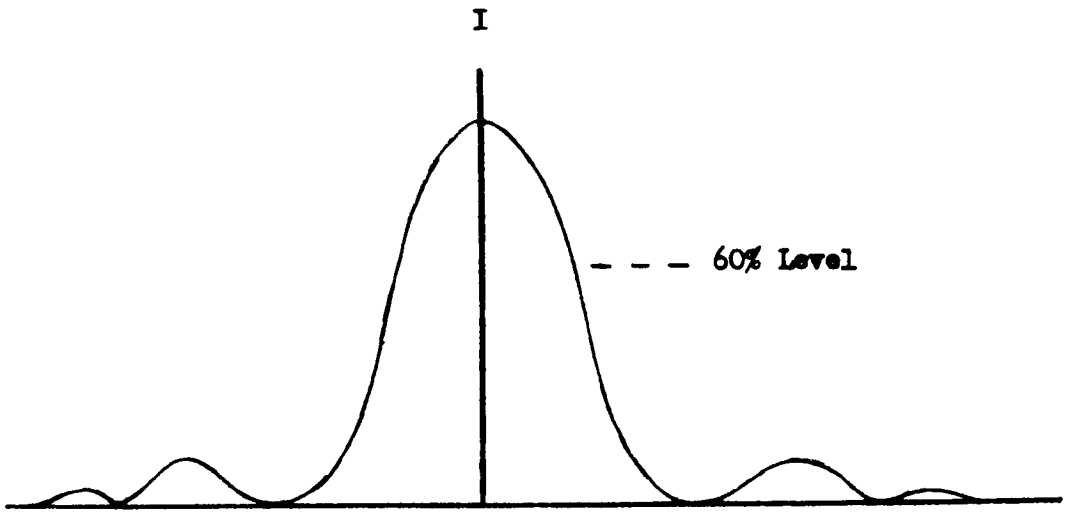

Figure 15. Energy Distribution in Focused Spot

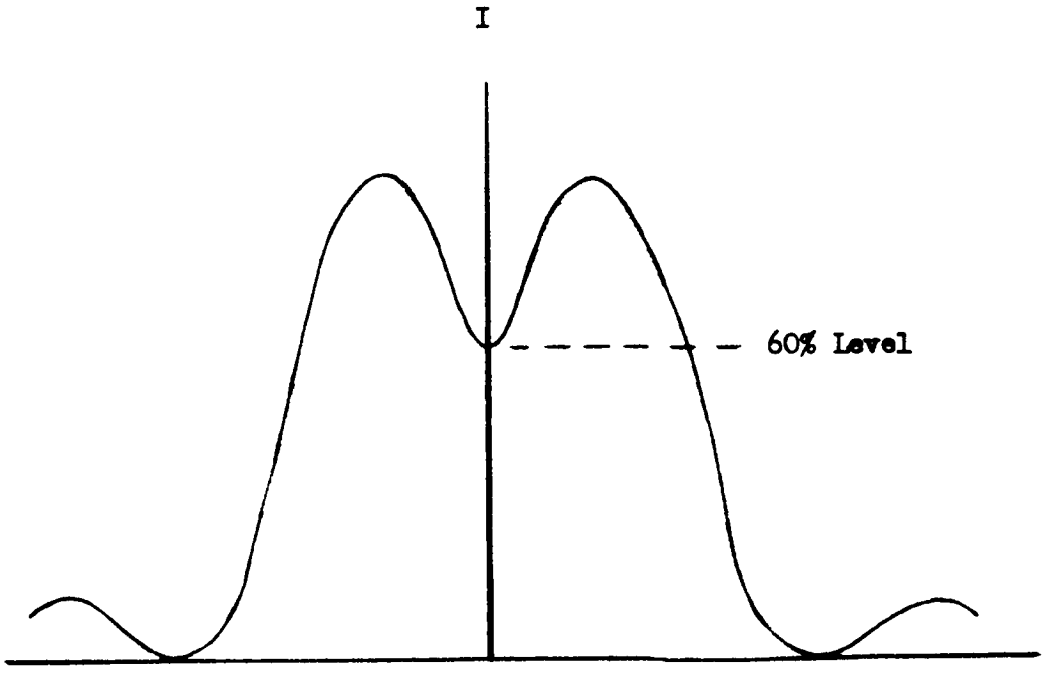

Figure 16. Forty-Percent Differentiation of Two Focused Spots

In the case of a thermoplastic material the incident light causes heating of the plastic to a certain temperature. It is obvious that the energy incident on the film according to Figure 15 would result in an isothermic line of about the shape shown in Figure 17.

The size of the film surface above the isothermic line is smaller than the base of the diffraction pattern. The rest of the base of the energy curve does not contribute to the recording but merely heats the area without causing surface deformation. It follows that the size of the recorded spot is smaller than the size of the focal spot and that an inadequate resolution on the basis of the energy curve can provide adequate resolution of the recorded spot.

For practical considerations the base of the energy curve can be expected to have a 3λ diameter. This is to say that all the available energy must be delivered through a cross sectional area given by $(3\lambda)^2 \pi/4$. However, the resultant recorded spot, or bit, may only have a diameter of 2λ so that the actual bit size is only 2/3 of the focal spot area.

The resolution of the incident elements can be lower than the resolution requirement that will result. The resolution of the record, however, is determined by the recorded resolution and must be read out with a focal spot equalling the resolution of the recorded information. For a closed system where the recording light will read out also, the resolution of the record must be matched to the resolution of the readout system.

With a spot 3λ wide, the separation of spots by 1.5λ will give excellent resolving capability (Figure 18).

Assuming a space requirement of $3\lambda \times 4.5\lambda$ per bit and a wavelength of 1.15×10^{-4} cm, 1×10^5 bits would require $3.45 \times 10^{-4} \times 5.13 \times 10^{-4} \times 1 \times 10^{-5} = 17.9 \times 10^{-3}$/cm. This corresponds to 3.5×10^7 bits per square inch.

Typically, if one could work at $\lambda = 3000$ Å $= 3 \times 10^{-5}$ cm the above space requirement would turn out to be 1.2×10^{-3} cm^2 corresponding to a bit density of 5.2×10^8 bits per square inch.

Lasers which emit at this approximate wavelength, 3000 Å, are currently available, but must be pulsed. CW lasers at 3000 Å at the present rate of laser development can be expected shortly. It should be pointed out that the storage density can be increased by decreasing the size of the resolution element diameter to 2λ or 1.5λ and using shorter wavelengths. Typically for a spot diameter of 2λ with $\lambda = 2 \times 10^{-5}$ cm and a spot separation of one the storage density would be $3\lambda \times 2\lambda \times 1 \times 10^5 = 24 \times 10^{-5}$ bits

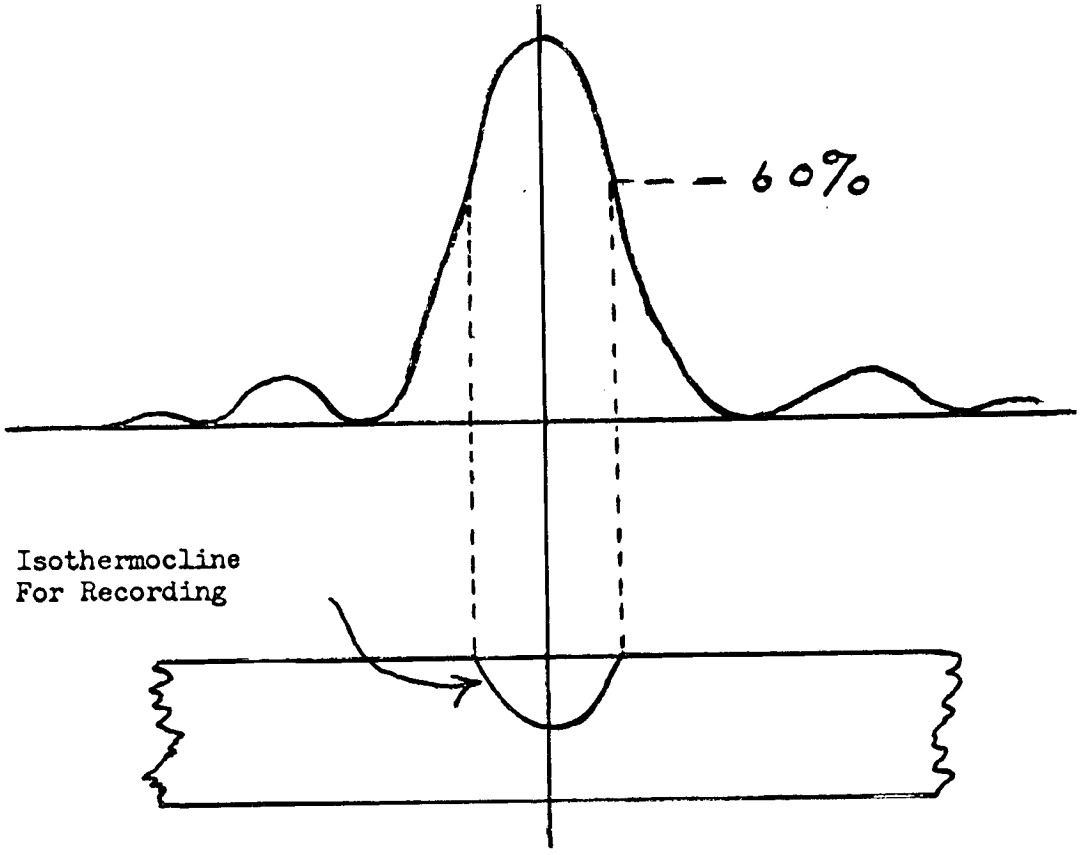

Figure 17. Comparison of Focused Light Spot Size to Recorded Spot Size

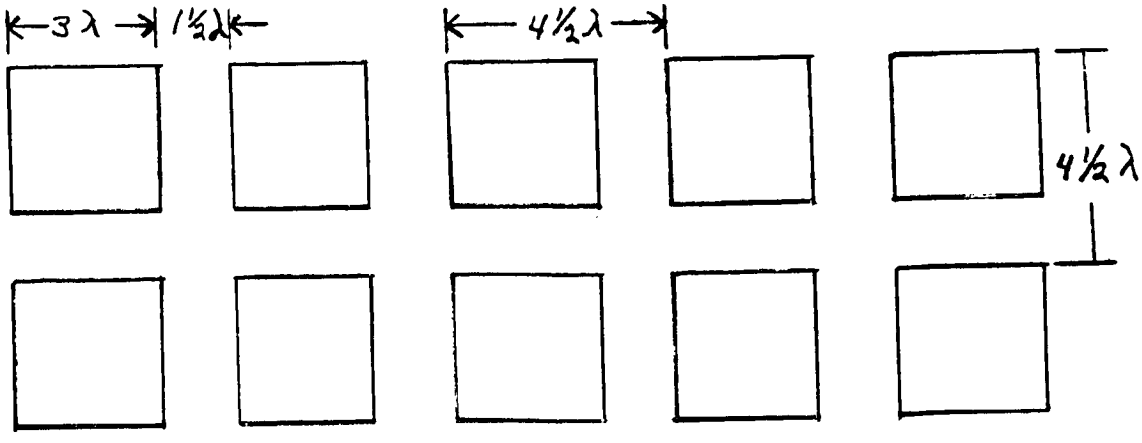

Figure 18. Recorded Spots on Format

per square centimeter or 2.6×10^9 bits per square inch. The possibility of obtaining such density is presently considered realistic for the case of an available CW ultraviolet laser.

However, with the size of a resolution element decreasing and the width of the record not decreasing also, the cost of a lens capable of performing such fine focusing becomes very high.

Power Considerations

With the feasible bit density of 5×10^8 bits per square inch, one of the questions to be considered regards the availability of adequate laser power. In the following equations these symbols are being used:

T = Temperature differential from ambient to recording temperature

C = Specific heat of the plastic

ρ = Specific density of the plastic

λ = Wavelength of the laser

d = Depth of liquefied plastic pool in one resolution element or bit

k = Absorption coefficient of the plastic

N = Number of bits per second

P_r = Power requirement of the recorded bits

P_i = Power requirement of the laser to dissipate P_r in the plastic film

These variables are given the following values:

ΔT	20	°C
C	0.5	cal gr^{-1}
ρ	1.0	gr cm^{-3}
λ	1.15×10^{-4}	cm
N	1×10^5	sec^{-1}

$d =$	2.3×10^{-4}	cm
$A = \frac{(3\lambda)^2 \pi}{4}$		= Surface area of one resolution element
$m =$	Apd	= mass of plastic to be heated per second
$M =$	mN	= mass of total plastic to be heated per second
$P =$ MATC		= energy required per second

The laser power required to be dissipated within the plastic is 2.14×10^{-5} cal sec^{-1}. The energy density E_A required to record on such film is:

$$E_A = \frac{P}{NA} = \frac{2.14 \times 10^{-5}}{1 \times 10^5 . 9 \times 10^{-8}} = 2.38 \times 10^7 \text{ cal - cm}^2$$

$$= 1 \times 10^8 \text{ joule - cm}^{-2}$$

$$= 10 \text{ erg - cm}^{-2}$$

The value of 2.14×10^{-5} sec^{-1} is the fraction of the incident power which actually has to be dissipated within the plastic to raise the temperature.

With the aid of suitable dyes and the optimization of plastic film parameters it is possible to obtain an absorption coefficient of 50% per mm typically, with higher values being possible. For a 50% absorption per mm and an absorption layer of 2.5×10^{-3} mm, the incident laser power would have to be 80 mw. Such lasers are commonplace today, and much higher powers are available. In fact, a one watt CW laser has recently been marketed, so that even for future information rate requirements power will not be a limiting factor.

Film Handling

Thermoplastic film using charge-induced deformations can tolerate more severe temperature extremes prior to recording than the temperatures needed for recording. One must keep in mind the possibility of the film surfaces sticking together when exposed to high temperatures while rolled up. During recording where the laser power has been selected for a certain

temperature rise, typically 20° C, the ambient temperature prior to recording must be brought to 130° C.

Once the image is recorded, the plastic of the charge-deformation type film must not reach the melting point because surface tension will tend to erase the information.

For temperature below the melting point, typically 85° C, the storage time without image degradation can be indefinitely long. For heat-shrinkable film, essentially the same precautions are valid. The erasure of information takes place by uniform shrinking of the film at storage or peak temperatures beyond the working temperature. Also, this film cannot be exposed to temperatures beyond or at working temperatures either prior to or after recording.

KALVAR

Kalvar photographic materials are based upon light scattering rather than light absorption, as are conventional silver halide materials. Kalvar material consists of a thermoplastic resin coated upon either a transparent backing material or an opaque black paper. Within the thermoplastic resin, there is uniformly dispersed an ultraviolet-sensitive compound. Upon the application of heat, the un-decomposed products react to form microscopic crystals. These crystals, since they are of a different index or refraction than the surrounding medium, scatter light incident upon them and thus form the image.

The maximum photosensitivity of Kalvar film is at 3850Å. The amount of radiation required to produce maximum density is about 200 milliwatt seconds/cm^2. The amount of energy to satisfactorily expose Kalvar for binary use is approximately 10 milliwatt sec/cm^2, or 10^5 erg/cm^2. Kalvar is thus much slower than the silver halide films.

The time required to expose Kalvar film depends upon the intensity of the light source. Exposure times are determined only by the time required to get 200 milliwatt-seconds/cm^2 of energy on this film. In practices exposure times below 0.01 seconds have been used.

The temperature of the film during exposure should not be above 110° F. Otherwise, premature development and degradation of the density and resolution of the image will result.

Development of Kalvar film by infrared radiation is possible but not recommended except in applications where a combination of convection and

radiation, detrimental to the formation of the image, does not occur. The calculated energy required to develop the Kalvar film is approximately 0.5 cal/cm^2 of film.

It should be emphasized that the latent image in Kalvar film is unstable and will decay at a finite rate. Noticeable image deterioration may occur if more than 1 minute elapses between exposure and development. In applications where the exposed and developed material is subject to light and heat, a fixing technique is necessary. The fixing technique consists of exposing the film to ultraviolet light, applying about four times the amount required for a maximum exposure, to completely decompose the residual sensitizer. The film must then be protected from a temperature above 110° F for several hours so that the gas may completely diffuse from the film.

The resolution of Kalvar microfilm is greater than 144 lines/mm when contact copies of a resolution chart are made. Kalvar emulsions are available which can render more than 500 lines/mm.

Tabulated Characteristics of Kalvar Film

1. Kalvar Films in both unexposed and exposed state are resistant to nuclear radiation.
2. Shelf life 5 years.
3. Kalvar films are dimensionally stable
4. Image stability - excellent
5. Emulsion thickness 0.0004 ± 0.000015
6. Light scattering element size 0.5-2.0 microns
7. Exposure energy for max. density 200 milliwatt sec at 3850Å
8. Temperature of exposure 110° F maximum
9. Maximum time of exposure 3 minutes.
10. Development energy 0.5 cal/cm^2
11. Development time and temperature 1 second at 235° F.

The Kalvar film technology has been developed to a very high degree and it is possible to obtain a wide range of sensitivities, densities and resolution capabilities.

Sensitivities are adjusted by means of selecting the proper reagent. Apparently an adequate spectrum of reagents is available for this purpose. Densities can be adjusted b the addition of small amounts of a blueish dye. A small addition of dye causes large attenuation for the scattered radiation. The resolution of Kalvar film is influenced by the number of scattering centers and the thickness of the sensitized layer, since the scattering is in all directions. Diffraction effects increase inversely with the size of the scattering centers and directly with the number of scattering centers. A comparison of the various recording techniques is given in Table 10.

Table 10. Comparative Properties of Recording Materials

Characteristics	Silver Halide Film	Free Radicals	Photo-chromics	Thermal Plastics	Kalvar
Spectral Range	UV to 1	5500 to 6800	UV to 4500A°	Far UV to Far IR	3350 4300
Minimum Exposure (ERGS/cm^2)	10	L. E. S. 10^{-6} sec		10	10^5 (3850A°)
Practical Resolution (Line Pair/mm)	700	250	700	156	500
Maximum Storage Bits/$inch^2$	10^9	109	109	5×10^8	10^9
Effect of 145° C Temperature Soak	Probably could take it.	Ruined	None For properly prepared samples	None For proper materials	Exposed
Operate at 85° C 12 Months Storage	Probably ruined	No	Yes	Yes	No

APPENDIX E. ANALYSIS OF ANGULAR ALIGNMENT OF TWO BEAMS

In Experiments 1 and 2, the degree of alignment of the incoming waves at the photodetector will affect the unperturbed average power. For very poor alignment, losses up to 10-20 db can be expected. Here the degree of alignment of the beams for a circular aperture is discussed. The aperture may be considered to be the field stop (taken as the aperture of the lens which focuses the beam on the photocathode), or in the case where no lenses are used, the illuminated circular portion of the photocathode. In evaluating the effects of the degree of alignment when lenses are used, it makes no difference whether the analysis is done in the plane of the lens or in the plane of the phototube, as long as the first maximum of the diffraction pattern of either wave still lies on the phototube surface and if both beams are focused. Here the alignment problem is analyzed at the lens aperture.

Let the aperture be in the x - y plane and the direction of propagation (normals to be wavefronts of the beams) vectors be near the z axis. The propagation vectors are given by

$$\hat{n}_1 = \sin\theta_1 \cos\phi_1 \hat{x} + \sin\theta_1 \sin\phi_1 \hat{y} + \cos\theta_1 \hat{Z}$$

$$\hat{n}_2 = \sin\theta_2 \cos\phi_2 \hat{x} + \sin\theta_2 \sin\phi_2 \hat{y} + \cos\theta_2 \hat{Z}. \qquad \text{(E. 1)}$$

The fields in the plane of the aperture are simply

$$\bar{E}_1 = E_1 \cos\left(\omega_o t - k\,\hat{n}_1 \bullet \bar{\rho} + \alpha_1\right)\hat{r}_1 \qquad \text{(E. 2)}$$

$$\bar{E}_2 = E_2 \cos\left(\omega_o t - k\,\hat{n}_2 \bullet \bar{\rho} + \alpha_2\right)\hat{r}_2$$

where

$\bar{\rho}$ is the radius vector in the x-y plane,

k is the wave number = $2\pi/\lambda$

α_1 and α_2 are arbitrary phases

E_1 and E_2 are the amplitudes of the incident fields,

$\hat{r}_1$ and $\hat{r}_2$ are polarization vectors ($\hat{n}_1 \cdot \hat{r}_1 = 0$).

The signal current, i(t) is proportional to

$$i(t) \propto \int_A E_1 E_2 \cos\left(\omega_o t - k\,\hat{n}_1 \cdot \bar{\rho} + \alpha_1\right) \quad x$$

$$\cos\left(\omega_o t - k\,\hat{n}_2 \cdot \bar{\rho} + \alpha_2\right) \cos\left(\hat{r}_1 \cdot \hat{r}_2\right) dA \qquad \text{(E. 3)}$$

where

$\cos\left(\hat{r}_1 \bullet \hat{r}_2\right)$ is the cosine of the angle between the electric field vectors.

It is assumed that the beams are aligned well enough so that approximations $\sin x \approx x$ and $\cos x \approx 1$ can be used. Since the polarizations are practically the same, $\phi_1 \approx \phi_2$ and $\cos(\hat{r}_1 \bullet \hat{r}_2) \approx 1$. As far as the analysis of the effects of misalignment is concerned, the x - y axis may be rotated so that $\phi_1 = \phi_2 = 0$.

Then

$$i(t) \propto \frac{E_1 E_2}{2} \int_o^{\alpha} \int_o^{2\pi} \rho \cos\left| k\,\bar{\rho} \cdot (\hat{n}_2 - \hat{n}_1) + \alpha_1 - \alpha_2 \right| d\rho\, d\phi \qquad \text{(E. 4)}$$

where the term involving the sum of the frequencies is not important.

Expanding this,

$$i(t) \propto \frac{E_1 E_2}{2} \int_o^{\alpha} \int_o^{2\pi} \rho \cos\left| k\rho\,(\theta_2 - \theta_1) \cos\phi \right| d\rho\, d\phi \qquad \text{(E. 5)}$$

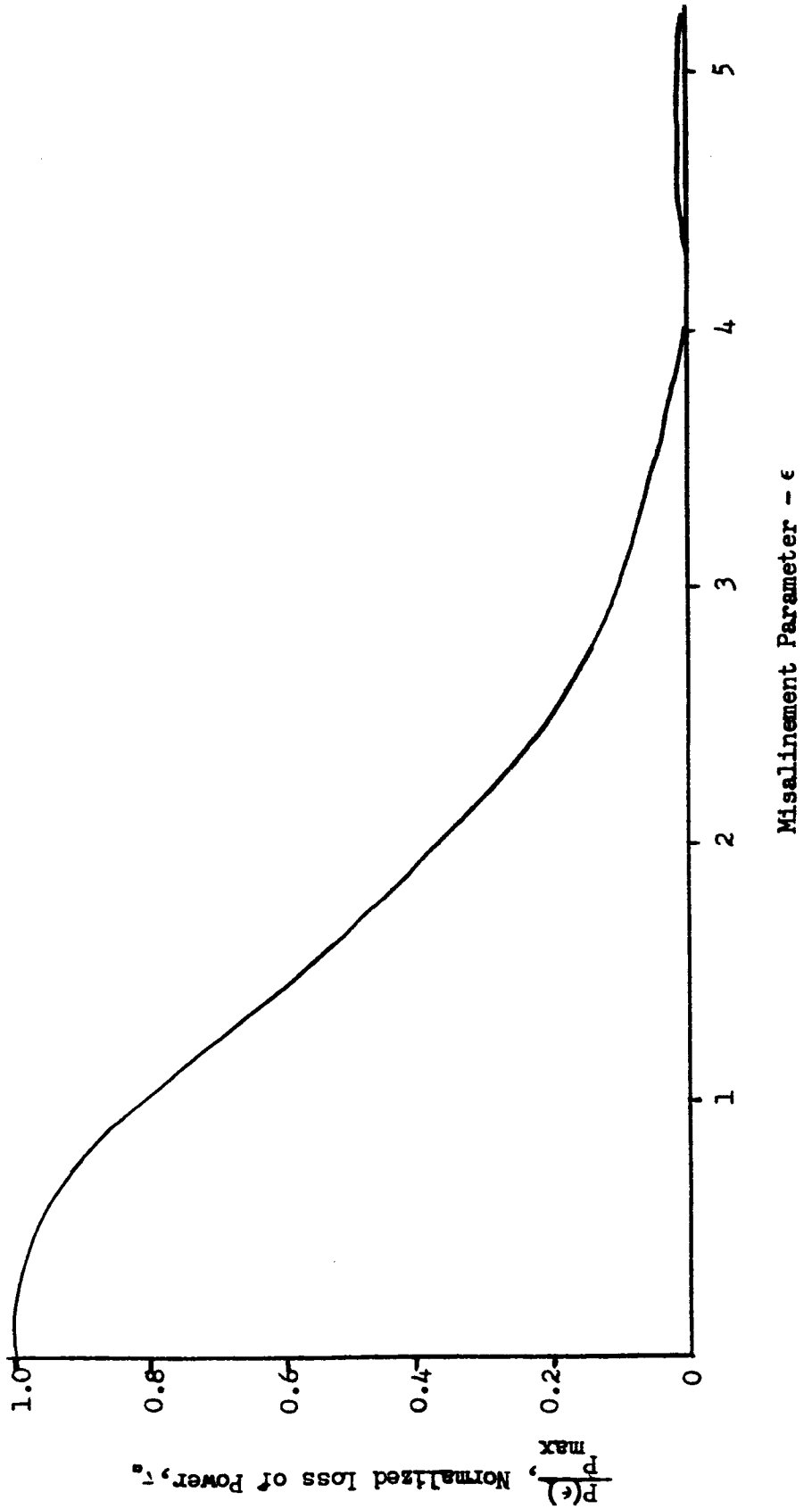

Figure 19. Loss of Power Due to Angular Misalignment

where $\alpha_1 - \alpha_2$ has been set equal to zero, is the aperture radius and $\sin \theta_2 - \sin \theta_1 \approx \theta_2 - \theta_1 = \theta$, θ being the angular misalignment of the beam. Integration gives

$$i(t) \alpha \pi E_1 E_2 a^2 k^2 \frac{J_1 (2\pi \theta a/\lambda)}{(2\pi \theta a/\lambda)} \qquad \text{(E. 6)}$$

$J_1 (x)$ is the 1st order Bessel Function.

The normalized loss of power due to angular misalignment is then

$$\tau_\alpha = \frac{P(\epsilon)}{Pmax} = \frac{2 J_1^2 (\epsilon)}{\epsilon^2} , \qquad \text{(E. 7)}$$

where

$$\epsilon = 2\pi \theta a/\lambda. \qquad \text{(E. 8)}$$

This is plotted in Figure 19.

APPENDIX F. BACKGROUND RADIATION

The problem of calculating the noise background power is many-faceted. An overall analysis would have to give weight to the following factors: (1) the possibility of scattered-in radiation from geographic features—rough terrain, lakes, oceans, etc. —in the case of earth-based systems; (2) the relationship between the optical system's line-of-site, the local zenith and the earth-sun line; (3) weather conditions; and (4) in the case of a satellite system, the earth's albedo. The type of molecular and other particle scatterers present and the wavelength of the radiation would also be factors. The impracticability of such calculations to cover all possible operating conditions is apparent.

In order to estimate the magnitude of the background radiation which would be encountered in a well-designed experiment—one in which large scatterers and radiant objects were excluded from the field-of-view—it is assumed that the sun's irradiance at the earth (Reference 45) is scattered isotropically to give the spectral sky background radiance which an optical system will encounter. Table 11 lists daytime spectral radiances centered at the wavelengths indicated.

Table 11. Daytime Spectral Radiances

Wavelength (Angstroms, Å)	Spectral Radiance (watts/cm^2-ster. -Å) x 10^{-8}
3,000	5.5
4,000	53.0
5,000	35.0
6,000	19.0
7,000	12.0
8,000	6.5
9,000	3.2
10,000	2.3

Using these figures, the background noise power caused by the daytime sky can be calculated.

APPENDIX G. EVALUATION OF WIENER SPECTRUM OF PHASE-LOCKED LOOP OUTPUT

The starting point of the analysis is the equation of the output of the p. l. l:

$$\dot{\psi}(t) = K \int_{-\infty}^{\infty} h(t - \lambda) \sin \left(\phi_{12}(\lambda) - \psi(\lambda)\right) d\lambda \qquad \text{(G. 1)}$$

where

$\psi(t)$ is the output phase, [rad.]

$\phi_{12}(t)$ is the input phase, [rad.]

$h(t)$ is the loop filter impulse response

K is the loop gain, [rad/sec/volt]

Using the piecewise-linear approximation $\sin x = \frac{2}{\pi} x$ by assuming $\phi_{12} - \psi \leq \pm \frac{\pi}{2}$, the output can be written

$$\dot{\psi}(t) = \frac{2K}{\pi} \int_{-\infty}^{\infty} h(t - \lambda) \left(\phi_{12}(\lambda) - \psi(\lambda)\right) d\lambda \qquad \text{(G. 2)}$$

The correlation function $\langle \dot{\psi}(t)\, \dot{\psi}(t + \tau) \rangle_T$ may be found from Equation G. 2 and from this the spectral relation,

$$S_{\dot{\psi}}(\omega) = \left(\frac{2K}{\pi}\right)^2 |H^2(\omega)| \left\{ \left(S_{\phi_{12}}(\omega) + S_{\psi}(\omega)\right) - \left(S_{\phi_{12}\psi}(\omega) + S_{\psi\phi_{12}}(\omega)\right) \right\} \qquad \text{(G. 3)}$$

The correlation function to which the spectra correspond is evident from the subscripts.

Digressing a moment from the analysis to state some useful relations, if $x_1(t)$ and $x_2(t)$ are differentiable functions of time, several correlation functions can be defined as follows.

$$C_{x_1}(\tau) = \left\langle x_1(t)\, x_1(t+\tau) \right\rangle_T \; ; \; C_{\dot{x}_1}(\tau) = \left\langle \dot{x}_1(t)\, \dot{x}_1(t+\tau) \right\rangle_T$$

$$C_{x_1 x_2}(\tau) = \left\langle x_1(t)\, x_2(t+\tau) \right\rangle_T \; ; \; C_{x_2 x_1}(\tau) = \left\langle x_2(\tau)\, x_1(t+\tau) \right\rangle_T .$$

The following relationships among the spectra of these correlation functions can be derived (Reference 46):

1. $S_{\dot{x}_1}(\omega) = \omega^2 S_{x_1}(\omega)$

2. $S_{\dot{x}_1 x_1}(\omega) = j\omega S_{x_1}(\omega)$

3. $S_{x_1 x_2}(\omega) = S_{x_2 x_1}(-\omega)$

Equation G.2 can be used to derive $S_{\dot{\psi}\phi_{12}}(\omega)$ by post-multiplying by $\phi_{12}(t+\tau)$, finding the correlation function, and taking the Wiener transform. The result is

$$S_{\dot{\psi}\phi_{12}}(\omega) = \frac{2K}{\pi} H(\omega) \left[S_{\phi_{12}}(\omega) - S_{\psi\phi_{12}}(\omega) \right] \qquad \text{(G.4)}$$

From the stated relations,

$$S_{\psi\phi_{12}}(\omega) = j\omega\, S_{\psi\phi_{12}}(\omega)$$

and

$$S_{\phi_{12}\psi}(\omega) = S_{\psi\phi_{12}}(-\omega) .$$

Then from Equation G.4,

$$S_{\psi\phi_{12}}(\omega) = \frac{S_{\phi_{12}}(\omega)}{1 + j\,\frac{\omega\pi}{2KH(\omega)}}$$

and

$$S_{\phi_{12}\psi}(\omega) = \frac{S_{\phi_{12}}(-\omega)}{1 - j\frac{\omega\pi}{2KH(-\omega)}} = \frac{S_{\phi_{12}}(\omega)}{1 - j\frac{\omega\pi}{2KH^*(\omega)}},$$

the last equation resulting from the fact that $C_{\phi_{12}}(\tau)$ is an even function and that $H(-\omega) = H^*(\omega)$ (Reference 46).

Equation G. 3 may now be solved for $S_{\psi\mu}(\omega)$. After some lengthy algebra, the result is

$$S(\omega) = \frac{\left(\frac{2K}{\pi\omega}\right)^2}{\left(\frac{2K}{\pi\omega}\right)^2 - 1}\left[\frac{8K^2|H^2(\omega)| + 4K\omega\pi I_m\{H(\omega)\}}{4K^2|H^2(\omega)| + (\omega\pi)^2} - 1\right]. \qquad \text{(G. 5)}$$

Here $I_m\{H(\omega)\}$ is the imaginary part of the system function $H(\omega)$. Note that $S_x(\omega)$ is a real quantity. As $K \longrightarrow \infty$,

$$S_\psi(\omega) = \lim_{K\to\infty} S_{\phi_{12}}(\omega)\left[\frac{1}{1 - \frac{1}{\left(\frac{2K}{\pi\omega}\right)}}\right]\left[\frac{2 + \frac{\omega\pi I_m\{H(\omega)\}}{K|H^2(\omega)|}}{1 + \frac{(\omega\pi)^2}{4K^2|H^2(\omega)|}} - 1\right]$$

$$= [1]\,[2 - 1]\; S_{\phi_{12}}(\omega)$$

$$= S_{\phi_{12}}(\omega),$$

which shows that the output spectrum approaches the input spectrum as the loop gain becomes infinite.

The last result (Equation G. 5) is the expression used in evaluating ϕ_ϵ defined in Experiment No. 2.

APPENDIX H. NAA S&ID OPTICAL LINK

The optical link that has been established by the Electro-Optical Laboratory of North American Aviation S&ID, has a five-mile atmospheric path that extends from one termination point at the laboratory facility (receiver station) to another termination point in the Palos Verdes Hills (transmitter station).

Figure 20 is a topographical profile over which the beam is transmitted. The optical link has been located such that the transmitted beam is greater than 50 feet above the ground along its path except at the termination points. In this manner, air turbulence from ground effects is minimized except at the transmitter and receiver station. At the transmitter station, the laser is mounted on a 6-inch steel pipe that has been sunk down to rock (approximately 3 feet below the surface) and secured with approximately one ton of concrete. For pointing the laser at the receiver station, an "AZ-EL" pointing head is used. With the pointing head and the aid of two-way radio communication, the laser beam can be pointed to within approximately 2 arc seconds. After proper beam pointing is achieved, the head has provisions for being locked in place. Power at the transmitter station is provided by a gasoline powered 3 KW alternator. The receiver station is used for both data collection and data reduction. For data collection, a concrete pad 8 x 8 feet, 2 feet high has been constructed. This not only provides a stable pad for the optical receiver systems, but also puts the centerline of most optical collector systems at least 7 feet above ground level, thus helping somewhat to reduce the problems of ground effects. The data collected from the different experiments are recorded on tape with a magnetic data recorder. Utilization of the data recorder has minimized the number of experimental runs since repetitive observations of each data run can be made until all useful information has been extracted. For data reduction, the receiver station has been provided with a variety of equipment. The primary instrument, however, is a small analog computer.

At the optical link receiver station, to reference the atmospheric turbulence at the time data is being collected, equipment has been provided to make two weather measurements. One measurement is the speed and direction of the wind with a vane/anemometer mounted 10 meters above the ground and the other is the temperature gradient from ground level to an elevation of 9 meters. The temperature-gradient measurement is made using 10 copper-constantan thermocouples starting at ground level and mounted at 1-meter intervals up to the 9-meter level. Each thermocouple is mounted in the center of a cross-drilled hole in the wood mounting bracket and is capped with a fiberglass shield to protect it from direct sunlight. The

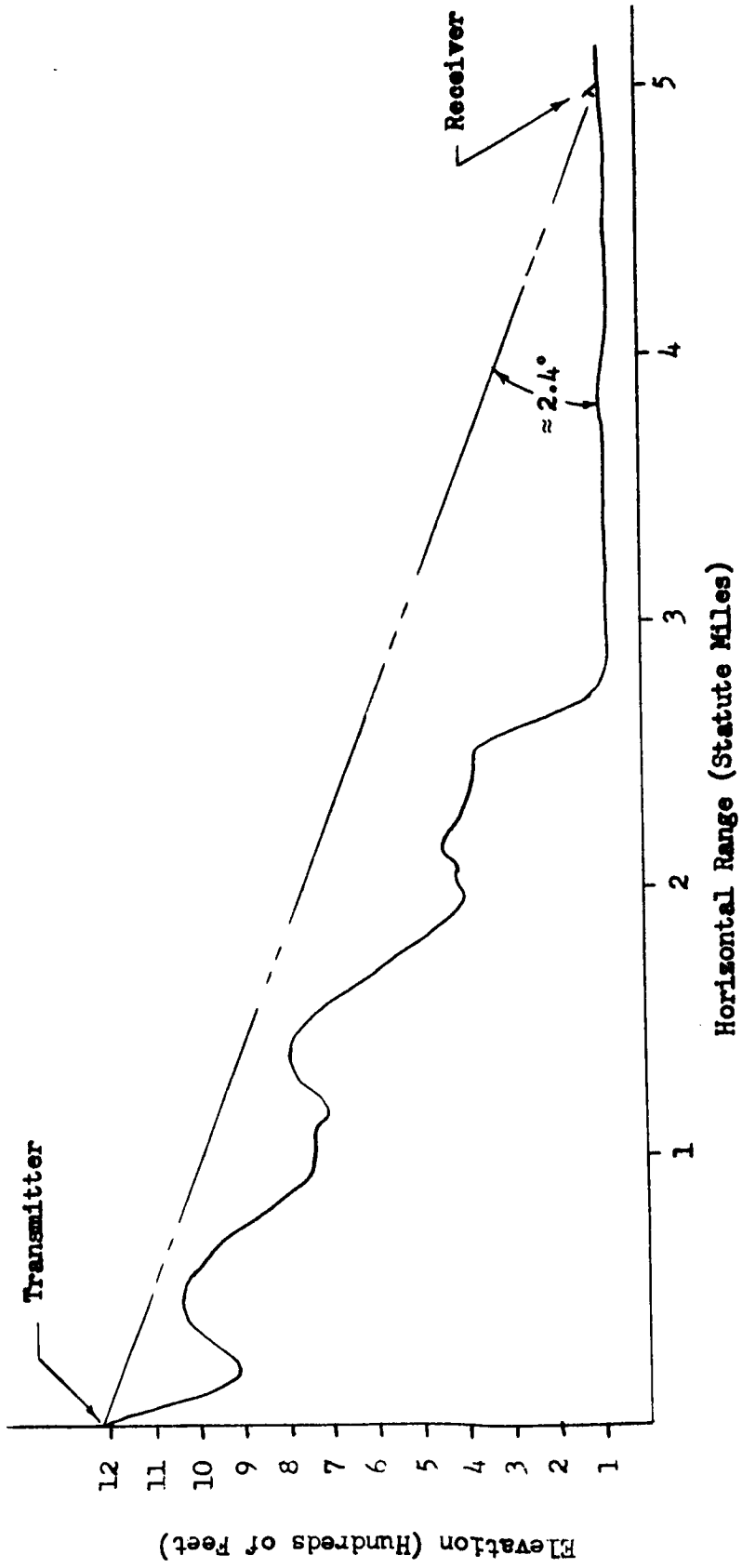

Figure 20. Topographical Profile of Optical Path - S&ID, NAA Laser Link

weather data instrumentation is provided with remote reading equipment so that the temperature gradient may be measured immediately before and/or after a data collection run is made and the wind speed can be monitored continuously during the run. In the near future, similar weather data instrumentation will be located at the transmitter station.

APPENDIX I. METEOROLOGICAL INSTRUMENTATION

This appendix contains a brief description of some of the meteorological instrumentation that is available at a number of the sites contemplated for use during the LACE implementation phase.

RAWINSONDE SYSTEM

The rawinsonde system (either AN/GMD-1A or AN/GMD-2) is a radio direction finder used to automatically track a balloon-borne radiosonde to altitudes beyond 100,000 ft. and over horizontal distances up to 125 miles. The set measures and records the azimuth and elevation angles of the radiosonde. As part of a rawinsonde system, it also receives, amplifies, demodulates, and passes to a recorder the radiosonde signals from which temperature, relative humidity, and atmospheric pressure are computed. Wind speed and direction are computed from temperature and pressure data, using azimuth and elevation angles with altitude.

WIRESONDE SET

The wiresonde is a portable, low-altitude (0 to 2000 ft.) atmospheric wind, temperature and humidity measuring service. A captive kite balloon carries the measuring elements aloft. A powered winch controls balloon altitude. A clinometer, or measuring line, determines the exact balloon height.

The data collected is transmitted to a summation bridge on the ground through the transmission cable. The bridge then transforms the data into dry- and wet-bulb temperatures.

AN/GMQ-13A CLOUD HEIGHT SET

The AN/GMQ-13A is a rotating beam-type ceilometer which provides frequent and accurate observations of the height of the lowest cloud layer. This equipment is capable of observing cloud heights during the day as well as at night.

AN/GMQ-2 CEILOMETER

The AN/GMQ-2 is a complete electronic-electromechanical device used to obtain a continuous day-and-night record of cloud ceiling data.

ML-121 CEILING LIGHT PROJECTOR

The ML-121 is used to determine cloud heights up to 10,000 ft. at night. It is a fixed installation consisting of a powerful incandescent lamp housed in a weatherproof metal case having a reflector and focusing system. A vertically concentrated light beam is focused on the cloud base, and an observer with a clinometer stationed a measured distance (750 to 1,000 ft.) from the projector can find the cloud height from the inclination angle.

AN/GMQ-11 WIND MEASURING SET

An AN/GMQ-11 wind measuring set is a fixed unit which visually indicates wind speed and direction at complexes, pads, gantries, control tower, and weather stations. It uses a synchro system to indicate wind direction, and a tachometer-magnetovoltmeter system to measure wind speed. Wind directions are given in 5-deg increments through 360 deg and wind speed is measured from 0 to 120 kt in 2-kt increments.

AN/GMQ-1A WIND SET

This unit consists of a tower-mounted anemometer rotor, wind vane, and indicator panel. It measures wind speeds from about 2 to 150 mph. An ac generator driven by the anemometer rotor measures wind speed. An ac milliammeter, calibrated in mph, gives wind speed. The wind direction indicator is a selsyn-type rotor driven by the wind vane. A repeater gives wind direction in degrees.

THEODOLITE

A theodolite follows and measures the movement of pilot balloons. The speed and direction of the wind at various levels can be plotted from the balloon track. The theodolite is similar to the ordinary transit used by civil engineers, but is of the so-called "broken-axis" or "right-angle telescope" type, which makes it particularly adaptable to balloon observation work.

MERCURIAL BAROMETER

Barometer ML-2-H is a Fortin-type (adjustable cistern) mercury barometer and thermometer for use at fixed locations.

ANEROID BAROMETER

A portable, high-accuracy, aneroid barometer used in fixed or mobile stations. It can be hand-carried, and is used when a mercury barometer would be inconvenient or impractical.

BAROGRAPH

A precision instrument to measure and record atmospheric pressure. It makes a continuous, visible record for a 4-day period on a paper chart.

PSYCHROMETER

This is a dry- and wet-bulb thermometer (fixed or portable) for measuring temperature and dew point, from which temperature and relative humidity data may be derived.

HYGROTHERMOGRAPH

This automatic mechanical device records temperature and humidity on a chart.

ARCAS METEOROLOGICAL ROCKET SYSTEM

This system consists of a high-performance rocket motor which carries payloads of 5 to 20 lb. to altitudes of 40 miles, and a closed breach launcher for firing the rocket.

AN/GMQ-14 (AND OTHERS) - AUTOMATIC WEATHER STATION

The semi-automatic meteorological station (AN/GMQ-14) and other similar automatic remote indicating and recording systems measure surface temperature, pressure, dew point temperature, wind speed and direction, and precipitation. Depending upon the design, the equipment records or transmits the data on command or on a specific sequence.

AN/UMQ-5 WIND SET

This equipment provides both a visual and permanent record of wind direction and velocity to an accuracy of 2 knots and 5 degrees.

AN/GMQ-10 TRANSMISSOMETER

Automatically measures and records the visibility.

AN/AMQ-8 AEROGRAPH SET

Mounted on aircraft for measurement and recording of temperature, pressure, and relative humidity during flight.

LOKI II METEOROLOGICAL ROCKET SYSTEM

The solid propellant Loki II rocket lifts a 2-lb. payload about 220,000 ft. The payload is S-band chaff inside a dart. When the chaff is released, it is tracked by radars to furnish wind direction and velocity to a computer. The launcher consists of a rifled barrel on an adjustable A-frame.

APPENDIX J. DESCRIPTION OF LASER APPLICATIONS LABORATORY (LAR)

The Laser Applications Research Mobile Laboratory has been constructed to support S&ID's Information Systems Division in electro-optical research and development programs specifically pointing to (1) satellite detection and tracking, (2) space communications, (3) coherent detection, (4) beam steering, (5) laser link measurement, and (6) atmospheric turbulence.

The laboratory consists of a 21-foot-long air-conditioned trailer with a portable power generator. The trailer houses a six-bay, open-rack cabinet giving sufficient capacity for not only basic hardware but also any special equipment necessary for a particular task. For simple field maintenance, the trailer has a work area with a bench and the necessary general hand tools. There is also a storage compartment at the rear of the trailer with a hoist to handle the equipment within the trailer.

The electronic support equipment presently installed consists of a radio transceiver and an 8-channel strip-chart recorder, a 14-channel magnetic tape recorder with FM as well as direct-record capability, and general purpose test equipment. The optical support equipment consists of (1) Power-Tronics Optical Tracking Mount, Mode 321, which has a pointing accuracy of better than 30 arc seconds and a tracking accuracy of better than two arc seconds, (2) an optical receiver consisting of a large-diameter collector, and (4) 0.1 watt HeNe Laser and a 1 watt Argon Laser.

A list of the major equipment presently included and planned is given as Tables 12 and 13 and photographs of the interior and exterior as Figures 21 and 22.

Table 12. Equipment on Hand

Item	Model
VTVM	Hewlett Packard 400H
Oscilloscope	Tektronix RM 585A
Magnetic Tape System	Sanborn (Hewlett Packard) 3924A
Magnetic Tape Amplifiers (2)	Sanborn (Part of 3924A)
Frequency Standard	American Time Products 2111CP
Time Code Generator	Electronic Engineering 811
Strip Chart Recorder	Sanborn 4500
Take-up Reel (Strip Chart)	Sanborn 650-900
Amplifiers (Strip Chart)	Sanborn 658-3400-3
5,000V Power Supply (2)	NJE S-327
600V Power Supply	Sorensen 600B
300V Power Supply	Dressen-Barnes 62-113
60V Power Supply (4)	Hewlett Packard 6271A
Laser (Argon)	Raytheon LG12

Table 13. Additional Equipment to be Available or Installed
(Projected Within six Months)

Counter & DVM	Loran-C Receiver & Precision Time Delay
Test Oscillator	Bases (2)
Pulse Generator	Optical Receiver
Noise Generator	400 cps Converter
5,000 V. Power Supply	Magnetic Tape Amplifiers
Precision Rotary Table	Logarithmic Amplifier
Test Light Source	D. C. Amplifiers (4 Gen. Purpose)
Theodolite & Tripod	Patch Panel & Cabling
Paper Tape Reader	Spectrum Analyzer
Paper Tape Drive Logic	Amplitude Distribution Analyzer
Paper Tape Spooler	Wave Analyzer
Time Code Generator	True RMS Meter
Receiver Pedestal	Analog Computer
Pedestal Angle Readouts	Water Cooling System for Argon Laser
Servo Electronics for Receiver Pedestal	Intercom System
Servo Electronics for Transmitter Pedestal	Shelters
Resolvers	Short Range Walkie-Talkie
WWV Receiver	Regulated Power Transformers

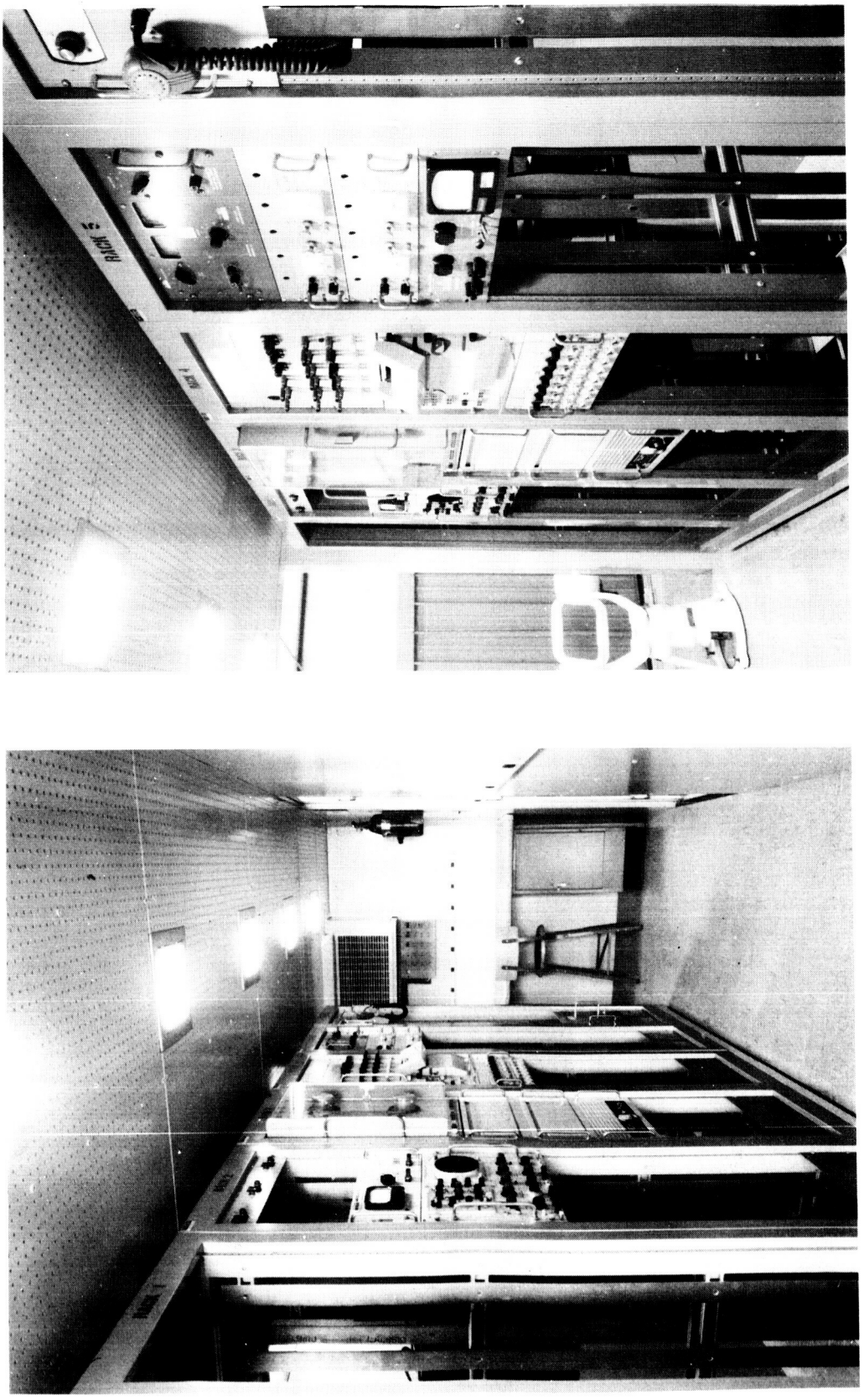

Figure 21. Interior View of Laboratory Showing Electronic Equipment Racks, Workbench, and Two-Axis Optical Mount

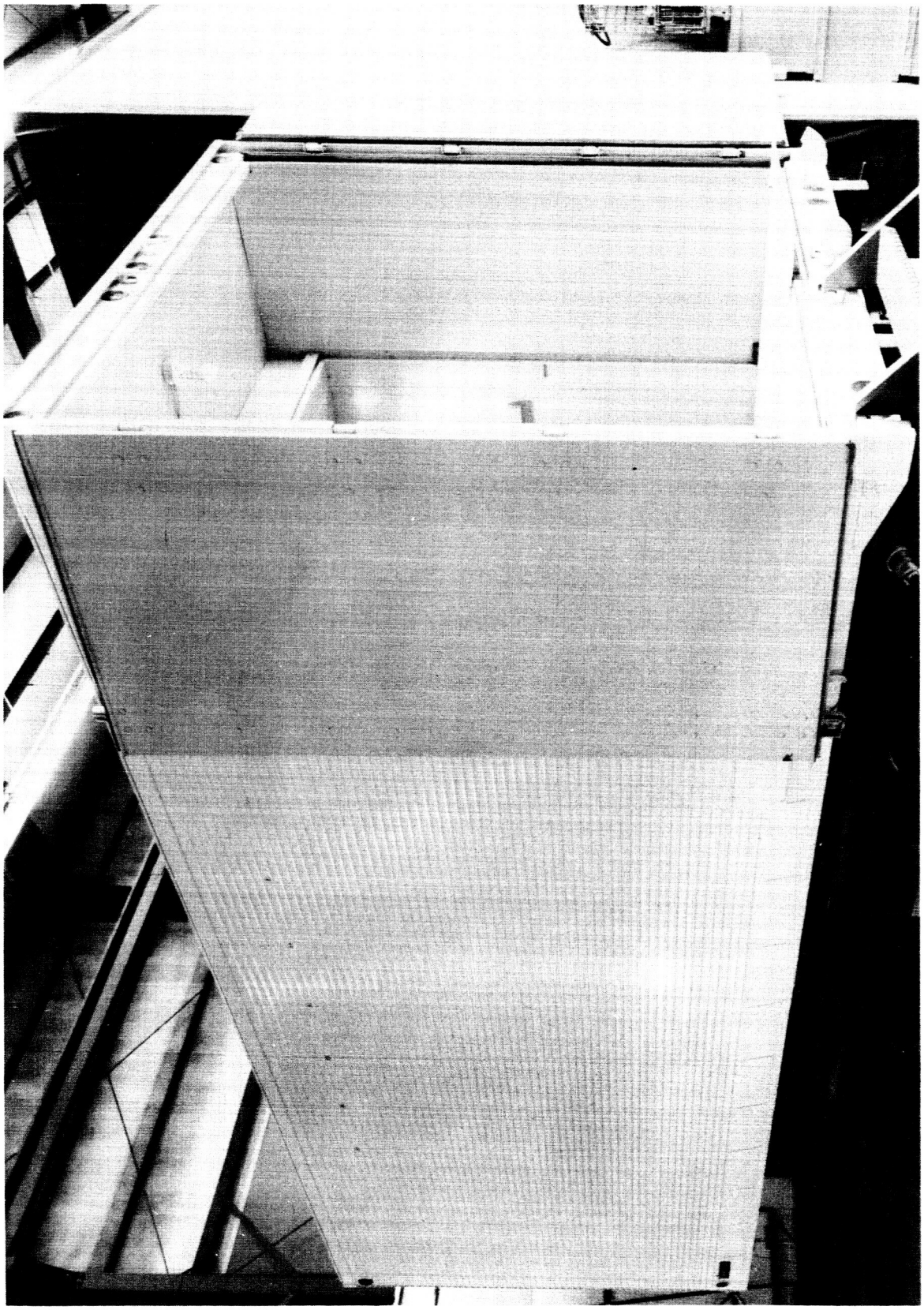

Figure 22. Exterior View of LAR Facility

APPENDIX K. C-130 AIRCRAFT INSTRUMENTED FOR SCIENTIFIC RESEARCH

The Air Force Cambridge Research Laboratory has an instrumented C-130 for use in atmospheric optics measurement work, and it would have a possible application in the LACE airborne link experiments. It is presently being used by the University of California Visibility Laboratory at San Diego, California, and seems to be generally available for government sponsored research programs. The atmospheric measurement equipment on the aircraft is as follows:

Radiometric

1. Irradiometers (flat plates with blanking devices) to measure upward and downward flux
2. Path Function Meter (horizontal only) mounted on top of fuselage
3. Equilibrium Radiance Telephotometer
4. Upper and Lower Sky Radiometers
5. Zenith and Nadir Telephotometers
6. Scaler Irradiance Meter (one on each wing tip)

The photometric equipment is 2-5% accurate.

Meteorological Equipment

1. Microwave Refractometer used to measure the partial pressure of water vapor
2. AMQ-8 Vortex Thermometer
3. Pressure Transducer
4. Ion Counter (large ions)
5. Conductivity Meter (small ions)
6. Aerosol Spectrometer
7. AMQ-17 Aerograph which measures and records temperature, pressure and humidity.

APPENDIX L. ANALYSIS OF BALLOON CAPABILITIES

A review of the literature has been performed to examine the balloon test-bed capability. The subject matter covered consists of such topics as typical missions, platform considerations, design stability, control, launch, and costs. Most of the discussion is concerned with free lift balloons; however, with some appropriate modification most of it applies equally well to tethered balloons.

BALLOON MISSIONS

Plastic balloons and balloons made from reinforced or laminated material can carry loads ranging from a few pounds to several thousand pounds. Using relatively small balloons, significant payloads can be carried to 100,000 ft. With present-day material limitations, the current altitude record of 150,000 ft. with a payload of 100 lbs. cannot be greatly exceeded, even using extremely large balloons, although with heavy payloads, reduced altitudes are attainable.

Flight tests concerned primarily with lifting a payload include:

1. Vertical Profile Samplers—Measured data on visibility, conductivity, atmospheric constituents and pollutants may be recorded and recovered, or telemetered to receivers in escort vans on the ground, or in planes.

2. Equipment Drop Tests—After being carried to high altitudes, equipment is dropped to study deployment subsystems, recovery techniques, tracking systems, or to simulate high velocity re-entry characteristics.

3. Low Density Firing Platforms—As demonstrated in projects "Rockoon" and "Farside," a balloon serves as a first stage booster from which rockets are fired after reaching a low density environment.

There are four advantages of balloons compared to other systems for lifting scientific equipment:

1. Low cost

2. Low shock on launching and recovery, reducing instrument design problems.

3. Slow rate of rise - under 1,000 feet per minute - to facilitate sampling.

4. Operations are not restricted to a rocket range.

Most plastic and modern fabric balloons are used for more than simple load lifters. Their natural buoyancy provides a stable platform for tests from a high altitude. These tests may include manned or unmanned observations of the environment of the balloon itself.

From such a near-space platform, observations may be made of objects above the balloon; i.e., astronomical objects, meteors or satellites. Likewise, a balloon platform will permit observations of objects below. This use is exemplified by flights made to calibrate components of the Tiros weather satellite system.

One of the most serious weaknesses of balloon systems is that they drift with the air streams through which they move. In temperate latitudes, there is generally a west-to-east flow from near the surface to some 60,000 ft. This same pattern continues into higher altitudes in winter months. In the summer, however, a reverse flow is encountered, above the westerly current.

For some experiments, this drift of the balloon is detrimental. On winter projects which must be recovered, balloons cannot be kept aloft for more than 48 hours without passing outside the United States or similar areas suitable for recovery.

BALLOON DESIGN

Today's balloons fall into three categories: tethered aerodynamic balloons, free zero-pressure balloons, and free superpressure balloons, which are presented in Table 14. The tethered balloons are, in general, aerodynamically shaped, are made of a coated fabric, and are reusable. Present altitude capabilities are 20,000 - 30,000 ft., but this will be increased soon with the advent of new lightweight fiberglass cables. The largest captive balloon lifted a payload of 7,000 pounds to 5,000 ft.

Zero-pressure balloons are the most frequently used. These balloons are open to the atmosphere and are therefore sensitive to the diurnal gas temperature changes which affect the gas volume, and consequently the balloon altitude. Present capabilities range from 10,000 pound payloads to 80,000 ft. to about 100 pound payloads to 150,000 ft. Most zero-pressure balloons are made of polyethylene, but generally those carrying over 4000 pound payloads use a Mylar-Dacron scrim laminate. Considerable ballast is carried on zero-pressure balloons if they are to maintain altitude longer than 12 hours.

Table 14. Types of Balloons

Category	Shapes	Basic Materials	Characteristics and Uses
High Altitude, Free-Floating Balloons	Natural-shaped (variations of tear-drop)	Polyethylene and other plastic films	Scientific exploration to 150, 000 feet.
		Scrim-reinforced plastic films	Heavy payload operations - several tons presently feasible.
	Sphere	Mylar, scrim-reinforced plastic films	Superpressure balloons and space inflatables used as reflectors and radar targets; solar collectors, antennas, etc.
Tethered Balloons	Aerodynamically shaped with stabilizing fins, single- and twin-bodied	Coated fabrics (nylon, dacron, hypalon, etc.)	A refined aerodynamic shape is designated Aerocap, used for prolonged tethered missions in relatively high winds.
		Plastic films	A smaller and less refined aerodynamic shape is designated Aerokite, and is used for relatively brief tethered missions, light payloads, and moderate winds.
	Sphere, natural-shaped, tetrahedron, cylinder	Coated fabrics and plastic films	Special lifting missions, usually brief, in light winds.

Superpressure balloons are closed so they maintain an internal pressure. This allows these balloons to maintain float altitude regardless of lifting gas temperature changes because the internal volume does not change. Some superpressure balloons have flown at altitude for over a month. Present maximum capability of these balloons is 300 pounds to 100,000 feet altitude.

ALTITUDE CONSIDERATIONS

Three factors must be balanced in determining the altitude to which a balloon can go: balloon volume, balloon weight, and other weight (payload). For example, a balloon with a volume of 4 million cu. ft. made from the coated fabric material used in Explorer II will weigh some 7300 lbs; it will carry itself to 85,000 ft., and will carry a gross load of 9500 lbs. at 80,000 ft. This gross load includes the balloon weight, and permits a payload of 2200 lbs. to be carried at that height.

If a million cu. ft. balloon is built from 2 mil polyethylene, without reinforcement, it will weigh 900 lbs., and can carry itself to 115,000 ft. With a payload of 600 lbs., the ceiling altitude is reduced to 103,000 ft.

As the volume of the balloon increases, so does the weight. For any given skin material there comes a point when the balloon cannot safely lift itself. For larger balloons it is necessary to add strength, either by increasing film thickness, by the use of load distribution tapes, or by special construction techniques. All of these add weight, with the result that increasing balloon size becomes less and less efficient. Thus, it was possible to build a 6 million cu. ft. balloon from 1/2 mil polyethylene. Such a balloon weighs 425 lbs. and has carried 140 lbs. to 150,000 ft. For an 8 million cu. ft. balloon carrying the same load, however, it is necessary to add load tapes or use 1 mil material to have the same safety factor. Such a balloon weighs 1100 lbs. and can carry 140 lbs. to 140,000 feet. For heavier payloads, either of these balloons would require reinforcing tapes which would add significantly to the system weight and reduce the altitude attainable. For most astronomical considerations a heavier (1 mil or thicker), taped polyethylene balloon seems to be indicated.

Limitations on size will be determined by this matter of diminishing efficiency and, of course, by balloon design competence. At the present time balloons of 6 million cu. ft. volume have been flown with repeated success, and two different designs of 10 million cu. ft. balloons have been flown successfully.

The strength-to-weight ratio of polyethylene and other materials used for balloon films now presents a practical limitation to increased size, and increased altitude. To improve the limits (150, 000 ft. altitude; 20,000,000 cu. ft. volume) significantly, it will be necessary to make use of materials not yet developed.

FLIGHT DURATION

When a balloon system is floating at its maximum altitude, it is in a condition of equilibrium. Loss of buoyancy will result from loss of lifting gas through diffusion, skin porosity, etc., or from an increase in gas density (cooling) relative to the ambient atmosphere.

In either case, continued floating can be maintained by decreasing the gross load of the system, as by dropping disposable ballast. It is necessary to provide for such ballast action if flight durations of more than a few hours are desired, or if the balloon will encounter a sunset after it has reached equilibrium.

Both radio command and servo controls have been developed for ballasting and present no technical problems. The major consideration is that of weight. The disposable ballast required must be part of the initial gross load carried by the balloon and for a given altitude, a larger balloon must be used to stay aloft for a longer period of time. A figure of 10 percent per day may be applied to the gross lift of a system when computing expected ballast needs for polyethylene balloons.

Not only does the cost of the balloon system increase with the size of the balloon, but operational problems such as those related to tracking over extended trajectories, inflation and launching and flawless fabrication are increased. When a manned observer is involved, problems related to comfort and even survival militate against longer flights. A careful evaluation of specific flight objectives will suggest whether one, two, or more sunsets should be encountered by a single balloon, or whether a larger number of shorter flights can be more effective.

STABILITY

When a balloon system is rising, air-screw action tends to induce axial rotation which may amount to several revolutions per minute. A single point suspension attaches the gondola to the balloon (for example, a nylon line); a torsion winding and unwinding may persist for hours after the balloon has otherwise reached equilibrium. During this relatively quiet condition, slow rotations of perhaps 2-4 r.p.h. are likely to be encountered.

Thus, it is necessary to control the orientation of any balloon-borne observatory. Equipment has been developed for use on a number of programs, including:

University of Colorado and Ball Brothers, Inc.	Sunseeker for Stratoscope
Librascope Co.	Star tracker for Stratolab IV
Hi-Altitude Instrument Co.	Sunseeker for I-R Spectroscopy
Smithsonian Astrophysical Observatory - MIT	Star tracker for Scintillation Studies

FLIGHT CONTROL INSTRUMENTATION

Because balloon altitude is related to ambient pressure, a pressure measuring device is an important part of the instrumentation. The pressure range being measured determines the type of instrumentation needed (i.e., at altitudes greater than 100,000 feet, the standard aneroid capsule is not sensitive enough to register the slight pressure changes experienced). Pressure at those levels is measured by Pirani gauges and by hypsometers. For balloon work conducted below 100,000 feet, the aneroid capsule is used.

LAUNCH CONSIDERATIONS

Launchers may be (1) Ships, (2) Windbreaks, (3) Mechanical.

Ships which can maneuver to reduce the relative wind to near zero have been used. This is generally highly successful technically, but correspondingly difficult to arrange logistically. A large ship, such as an aircraft carrier is not required, but the vessel's speed must be reasonable when compared with prevailing winds in the area of operation.

A serious drawback of such natural windbreak pits as the Stratobowl of South Dakota, or the Iron Mines of Minnesota, is that many of these pits lack very light prevailing winds over the entire area. Winds across the lip can drive the gondola into a side wall or produce intolerable shear stresses.

The best use of the natural wind-screen technique is at Holloman Air Force Base. B. D. Gildenberg has recently carried out microclimatological surveys on a number of accessible box-canyons in the mountains adjacent to the Air Force Missile Development Center. With a variety of sites to choose from, and a good history of micrometeorology for the entire area as well as the individual sites, it appears probable that launchings from such a base can be done with more regularity than is now possible from any of the land stations now used.

From time to time, rather haphazard attempts have been made to develop techniques for launching on land in winds of 5 to 15 or 20 knots. Mechanical devices, trucks, cranes, shrouds, and wooden and canvas shelters have been built and tried. Among current practices is the use of a truck to carry the payload under the balloon after inflation has been completed.

In at least one respect, launching a balloon flight resembles a rocket firing; without a successful take-off there is no flight. Like a rocket launch, the procedure is governed by a long and meticulous checklist. Every step of the operation is carefully planned and executed, from assembling the men and equipment to the final countdown and launch.

COSTS

Exact costs cannot be presented because of the variable factors, such as: size of balloon (load, altitude, duration of observation), launching site (remote, mobile or fixed, shipboard), frequency of flights, and method of tracking and recovery.

Clearly, major cost items are those of ship support and aircraft recovery. For an uncomplicated balloon flight from land, the cost of control gear, pre-flight preparation, launching, tracking, and recovery by land vehicles is a few thousand dollars depending on the system complexity, launching site, waiting time, etc. To this must be added the costs of the observational equipment, stability systems, and the balloon costs.

Typical balloon prices are shown below:

Balloon Volume (cu. ft.)	Total Load to be Carried Below Balloon (lb)	Altitude (ft)	Approximate Cost
2,000,000	150	127,000	$ 2,500.00
2,000,000	1500	95,000	3,000.00
2,000,000	3500	82,000	3,500.00
4,000,000	1000	115,000	4,500.00
6,000,000	100	153,000	6,000.00
6,000,000	1500	119,000	6,500.00
6,000,000	3000	106,000	7,000.00
9,000,000	1500	126,000	9,000.00
9,000,000	4500	107,000	10,000.00

Raven's prices for various balloons and equipment are as follows:

Balloon Diameter (ft)	Volume (cu ft)	Price (each)
18	2,500	$ 50
30	10,000	110
41	28,800	156
53	58,000	285
58	80,000	320
69	135,000	390
79	180,000	500

Instruments	Price
FAA switch and timer	$ 725
Photobarograph	950
Beacon and altitude telemeter	625
Low frequency radio command receiver (airborne)	650
6 channel output section	425
6 channel modulator	800
3 channel output section	250
3 channel modulator	500
Radio command transceiver (ground)	1250
Ballast-control system	750

APPENDIX M. STUDY OUTLINE FOR SPACE VEHICLE PAYLOAD FINAL DEFINITION

This appendix contains a comprehensive approach to the problems of arriving at a system for performing future satellite experiments concerning atmospheric effects on optical propagation. Included are the basic tasks to be performed, as well as a detailed outline of the inputs and outputs of the study program. It is believed that a study of this nature should be conducted in the later phases of a pilot experimental program.

SPACE VEHICLE PAYLOAD DESIGN TASK OUTLINE

Study Program Tasks

Design, develop and package optical experiment hardware, including adjustment, alignment, and on-board test of equipment and signal generating devices, for installation and operation in the space vehicle; design on-board auxiliary equipment as required to support or assist in preparation or execution of the optical experiments.

Design the guidance and control system to accomplish space vehicle station keeping and attitude measurement, command, and stabilization.

Design space vehicle systems for radio command, telemetry, signal conditioning, beacons, data storage and processing, on-board programming, and on-board test equipment for these.

Inputs to Study Program Tasks (As derived from pilot tests and other related studies and space programs)

General for all tasks

Mission Analysis

Launch profile

Time line

Orbital elements

Ground test environment

Launch environment

Space environment

Experimental System and Component Specifications

Physical description—weight, volume, shape, mounting arrangements, connections

Power requirements and duty cycle

Operating principles and procedures

Calibration, adjustment, and alignment procedures

Prelaunch

Orbital

Auto/Manual

Environmental requirements (capabilities)

Test procedures

Experiment Information System

Command inputs

Housekeeping (condition) measurements

Experiment signal outputs

Transducer descriptions

Signal formats, levels, rates, processing requirements, conditioning

Operational requirements

Angular positions and derivatives—inertial, wrt the earth, wrt vehicle and other equipment

Translational requirements wrt other equipment

Stabilization requirements

Temperature gradient limitations

Auxiliary equipment required for calibration, adjustment and alignment

Role of a human operator in calibration, adjustment, alignment, and experimental procedure

Prelaunch

In parking orbit (if applicable)

At experiment orbit

Vehicle Information System

Signal sources and destinations

Format, levels, rates

On-board storage, processing, and conditioning requirements

Transmission means

Vehicle Dynamics

Attitude vs time

Structural deflections

Vibration

Temperature gradient effects

On-board torque disturbances

External torque disturbances

Operational Procedure

All steps to support or assist in preparation and execution of the optical experiments

Interface with other systems.

Outputs of Study Program Tasks

- Review of Existing Conceptual Designs
- Conceptual System Definition
- Design Criteria
- Design Drawings
  - Assembly drawings
  - Envelope drawings
  - Block diagrams
  - Schematics
  - Charts, diagrams, graphs
- Design Analysis
  - Dynamic
  - Kinematic
  - Stability
  - Error
  - Thermal
  - Stress
  - Reliability
- Narrative Descriptions
  - Physical description
  - Principles of operation
  - Operating procedure
  - Interface definition
  - Packaging techniques

Performance parameters

Weight, volume, and power tables

Functional, system, and subsystem specifications

Operational Analysis

- Prelaunch checkout
- In-flight checkout and adjustment
- Conduct of experiments
- Operational sequencing
- Failure modes and detection
- Data management

Quality Assurance documentation

Resources Plan

- Design plan
- Test plan
- Manufacturing plan
- Schedule and manpower requirements plan
- Cost plan
- Facilities plan

Indicated additional research and development

Engineering reports.

APPENDIX N.
SATELLITE VEHICLE CAPABILITY SUMMARY ANALYSIS

During the later phases of a LACE experimental program it has been indicated that satellite propagation link experiments will be planned and executed. As a basis for the mission and configuration definition of this phase, a brief preliminary analysis has been conducted to collect and summarize some of the more important satellite characteristics that will be applicable to these future studies.

The data collected has been tabulated as follows:

1. Typical Orbit Inclination Achievable. Table 15.
2. Typical Satellite Which Can Just See the Poles. Table 16.
3. Satellite Launch Vehicle Capabilities. Table 17.
4. Payload Diameters. Table 18.

Table 15. Typical Orbit Inclinations Achievable

Launch Sites			
	Lat.	Long.	Allowable Launch Azimuths
AMR	28.5° N.	80.8° W.	44° to 110°
PMR	35.0° N.	120.5° W.	170° to 301°
Wallops	37.8° N.	75.5° W.	~67° to 143°

Realizable Orbit Inclinations *			
	i	Satellite Moving	
AMR	28.5° to 52.4°	Eastward	
PMR	34.7° to 90.0°	Westward	Southward for 90°
	81.8° to 90.0°	Eastward	
Wallops	~38° to 60°	Eastward	

*Without post-boost maneuver

Table 16. Typical Satellites Which Can Just See the Poles

Altitude (n. mi.)	Orbit Period (min.)	Satellite Velocity (ft/sec.)	Minimum Inclination (deg.)
200	91.717	25,228	70.8
500	103.300	24,248	60.8
2000	167.684	20,636	39.3

Table 17. Satellite Launch Vehicle Capabilities

Vehicle	Payload (lb)	Altitude		Period (min.)	Satellite Examples	Launch Site	Incli-nation	Restart Capability*
		Perigee (n mi)	Apogee (n mi)					
Scout (NASA) (in '63)	240	260	260			PMR or Wallops		
Scout	165	151	815		Ariel 2 (NASA/uk)	PMR		
Scout (Blue Scout (USAF)	135	375	395	99.2	Transit 5A	PMR	89.3 °	
Scout	80	343	1395	118.3	Explorer IX	Wallops	38.63°	
Scout	187	152	526	97.3	Explorer XII	Wallops	36.4 °	
Scout	222	407	631	104.3	Explorer XVI	Wallops	51.99°	
Improved Scout (NASA) (Has uprated Castor 2nd stage) operational in Mid '65	340	260	260			PMR or Wallops		
Delta (NASA) Thor Delta (If launch facility for PMR is authorized in 1965, would be operational in 1966)	480	300	300		100# to escape velocity	AMR		
Delta	132	556	1032	114.4	Echo I	AMR		
Delta (Delta is same booster as Thor-Able II except for new Guidance)	132	210	654	100.9	Ariel-1	AMR	53.87°	
Delta	100	150	900		Explorer 5-3C			
Delta	142	100	19,300		Syncom I	AMR	33.5 °	

*Of final stage

Table 17. Satellite Launch Vehicle Capabilities (Cont)

Vehicle	Payload (lb)	Altitude		Period (min.)	Satellite Examples	Launch Site	Inclination	Restart Capability*
		Perigee (n mi)	Apogee (n mi)					
Delta	110	500	740		S-66	AMR		
Delta	172	1128	4000		Relay 2	AMR	46.3 °	
Delta	170	518	5820	225	Telstar 2	AMR	42.76°	
Delta	490	280	300		OSO	AMR	33°	
Delta	290	341.5	344	97.4	Tiros 7	AMR	58.23°	
Delta	290	374	428	99.3	Tiros 8	AMR	58.47°	
Delta	83	156.2	41,500 3	26.5 hr	Explorer XII	AMR	33.3 °	(Has est. 1 yr. lifetime in orbit)
Improved Delta (will launch 360 lb. GEOS)	800 250	300 6000	300 6000		120# to escape 145# to synchronous orbit			
Delta	101	190	15,800	7.7 hrs	Explorer 26	AMR	21°	EPE-D
Thor-Able-Star (USAF	355	584	733	107.8	Anna	AMR	50°	-
Thor-Able-Star	501	435	580		Currier I-B	AMR	28.3°	-
Thor-Able-Star	900	100 Circular						
Thor-Able II	270	373	406	99.2	Tiros I	AMR	48.2 °	-
Thor-Able-Star	400	505	608	105.6	TRAAC/Transit 4B	AMR	32.2 °	-
Thor-Able-Star	275	533	563	103.8	Transit 4A Greb Injun	PMR	66.82°	

*Of final stage.

Table 17. Satellite Launch Vehicle Capabilities (Cont)

Vehicle	Payload (lb)	Altitude		Period (min.)	Satellite Examples	Launch Site	Incli-nation	Restart Capability*
		Perigee (n mi)	Apogee (n mi)					
TAD (NASA) Thrust Augmented Delta	1000	260 Circular	150 lb to escape			AMR		-
TAD (TAD is Delta + 3 strap-on solids 55KT ea.)	140	60M	Interplan-etary		Pioneers	AMR		-
Improved TAD (NASA) (Has larger 2nd stage tanks)	1200	260 Circular	220# to escape					
Improved TAD Dia. x 2 (Thrust Augmented Delta)	1175	230	Circular		Bio-Satellite	AMR	28.5°	
TAT-Agena (NASA/USAF)	500	6000	Circular Polar		Possible booster for Comsat	PMR	90°	Yes
TAT-Agena (NASA/USAF) (Thrust Augmented Thor-Agena) + 3 Stap-Ons	2500	100	Circular					Yes
Thor-Agena B (USAF/NASA)	650	600	Circular-Polar			PMR		Yes
Thor-Agena B (USAF/NASA)	650	575			Nimbus	PMR	90°	Yes
Thor-Agena B (USAF/NASA)	547	556	710	108.7	Echo 2	PMR	81.49°	Yes
Thor-Agena B (USAF/NASA)	320	538	555	105.5	Alonette Also for POGO	PMR	80.46	Yes

*Of final stage

Table 17. Satellite Launch Vehicle Capabilities (Cont)

Vehicle	Payload (lb)	Altitude		Period (min.)	Satellite Examples	Launch Site	Inclination	Restart Capability*
		Perigee (n mi)	Apogee (n mi)					
Thor-Agena D	1600	260	Circular-Polar	100# to escape				
Thor-Agena D Payload loss per deg. inclination less than 90° = 8#/deg. westward launched)	946	300	300		AOSO	PMR	90°	
Atlas D	3000	104	140+		Mercury	AMR		-
Atlas SLV-3	~4000	100	Circular			AMR & PMR		-
Floxed Atlas SLV-3 (USAF) Atlas D 1st stage thrust = 360 k lbs. Atlas SLV-3 1st stage thrust = 389 k lbs.	7000	100	Circular			AMR & PMR		-
Titan II	~1000	6000			Like MACS	AMR		Yes
Titan II	7000-8000	161	260		Gemini	AMR		Yes
Titan 3X (USAF)	7250	100	Circular			AMR		-
Titan 3A (USAF)	4000	260	Circular			AMR		Yes
Titan 3C (USAF)	25,000	100	Circular			AMR	28°	Yes
Titan 3C (USAF)	2140	19,300	Circular			AMR	28°	Yes
Titan 3C (USAF)	1045	19,300	Circular			AMR	0°	Yes
Titan 3C (USAF)	13,000	2,000	Circular			AMR		Yes

*Of final stage

Table 17. Satellite Launch Vehicle Capabilities (Cont)

Vehicle	Payload (lb)	Altitude		Period (min.)	Satellite Examples	Launch Site	Inclination	Restart Capability*
		Perigee (n mi)	Apogee (n mi)					
Titan 3C (USAF)	5100	To Escape	Circular			AMR		Yes
Atlas-Agena	~1000+	6000	6000		Like MACS	PMR/AMR		Yes
Atlas-Agena	1500	100	6000		ATS	AMR	29°	Yes
Atlas D - Agena B	800	Lunar	Impact		Rangers 6 to 9 & Nimbus 2	AMR		Yes
Atlas D - Agena B	447				Mariner R or II			Yes
Atlas D - Agena B	550	100	19,300		Syncom II	AMR	0°	Yes
Atlas D - Agena B	1000	100	60,000		NDS I & II			
Atlas D - Agena B	3600	500	Circular		OAO	AMR	31°	Yes
Atlas D - Agena D	5000	300	300	750# to escape and 400 # for planetary		AMR/PMR		Yes
Atlas D - Agena D (USAF)	820	In lunar orbit or to Sync. eq. orbit altitude					0°	Yes
Atlas D - Agena D	575	To Mars, V escape = 25,600 fps			Mariner 4	AMR		Yes
Atlas D - Agena D	1000	100	50,000		OGO			Yes
Atlas-Centaur (NASA)	8500	300	300	2300# to escape and 1300# for planetary		AMR		Yes
Atlas-Centaur (NASA)	1800	To moon			Lunar Orbiter	AMR		Yes
Atlas-Centaur (NASA)	2104	Single burn Centaur version			Surveyor without Earth Parking			1 Restart
Atlas-Centaur (NASA)	2400	To Moon			Surveyor with Earth Parking Orbit			Yes
Improved Atlas-Centaur by 1967	2500# for Lunar Orbiters							Yes

*Of final stage

Table 17. Satellite Launch Vehicle Capabilities (Cont)

Vehicle	Payload (lb)	Altitude		Period (min.)	Satellite Examples	Launch Site	Incli-nation	Restart Capability*
		Perigee (n mi)	Apogee (n mi)					
Titan 3A - Centaur	9500+	300	300	3300# to Escape		AMR		Yes
Titan 3A - Centaur	1800	19,300	19,300					Yes
Titan 3A - Centaur	1800	To Lunar Orbit						
Saturn 1 (NASA)	24,000	100	100			AMR		Yes
Saturn 1 (NASA)	15,000	300	300					
Saturn 1 (NASA)	4,000	550	550					
Saturn 1B (NASA)	35,000	100	100			AMR		Yes
Saturn 1B (NASA)	28,500	300	300			AMR		Yes
Saturn 1B/Centaur					For Voyager and 7,000# planetary missions in 1968			
Saturn 5 (NASA)	240,000	100	100			AMR		Yes
Saturn 5 (NASA)	220,000	300	300					
Saturn 5 (NASA)	90,000	To Escape						
Saturn 5 (NASA)	70,000	For Planetary Missions						

*Of final stage

Table 18. Payload Diameters

Vehicle	Diameter
Scout	2' ± ~ 2
Agena	5' to 10'
Centaur	10'
Saturn	22'
Titan	10'
Ablestar	4.5'
Atlas	10'
Delta	~2' ± 2'

APPENDIX O. SUMMARY OF NASA NETWORK CAPABILITY

The three NASA networks used for tracking, Data Acquisition, Command, and Communications are summarized in this appendix for application to future siting planning studies in connection with LACE; and to illustrate the scope of possible future siting potential. The networks are classified as follows: Satellite Network; Deep Space Network; Manned Space Flight Network.

SATELLITE NETWORK

General

i 14 Fixed Stations (and Baker-Nunn Optical Stations)

ii Some Mobile (Ship) Stations

iii For smaller scientific and applications satellites

iv Tracking and data acquisition

v Present data collection rate (7 million words/day) 16 satellites.

Parabolic antenna CDA stations for data acquisition support for observatory satellites (OAO, POGO, EGO):

Fairbanks, Alaska Rosman, North Carolina Canberra, Australia	85' diameter dishes
Quito, Ecuador Santiago, Chile Johannesburg, South Africa	40' diameter dishes

(85' stations for highly eccentric satellites and very wide band transmissions from satellites such as NIMBUS).

Minitrack angular tracking system is also part of the Satellite Network:

Woomera, Australia	Fort Meyers, Florida
Fairbanks, Alaska*	Quito, Ecuador
East Grand Forks, Minn.*	Lima, Peru
Mohave, California	Santiago, Chile
St. Johns, Canada*	Winkfield, England*
Blossom Point, Md.	Johannesburg, South Africa

Improved tracking systems for determining range and velocity are being implemented at Rosman, Woomera, Johannesburg, Fairbanks and Santiago—for highly elliptic and synchronous satellites.

Present TIROS read-out stations: PMR and Wallops

NIMBUS will use Fairbanks and Rosman

Future TIROS will also use Fairbanks and Wallops (Orbital tracking will be by Minitrack)

Tracking and data acquisition support (status of spacecraft and commands) by Satellite Network to Echo, Relay, Telstar, and Syncom.

DEEP SPACE NETWORK (DSF)

For tracking and data acquisition support for lunar (ORBITER, RANGER) and interplanetary missions (MARINER AND PIONEER). Includes:

85' dishes at

Woomera

Johannesburg

Goldstone, California - 2 dishes here

Canberra, Australia
Madrid, Spain
} Presently under construction

*Stations for Polar or Near Polar Satellites

210' dishes at

Goldstone (is under construction)

Canberra } Future plans

Madrid }

MANNED SPACE FLIGHT NETWORK (MSFN)

Gemini

Kano, Nigeria

Zanzibar

Canton, Is.

PMR

White Sands

Eglin, Florida

Grand Canary Island } With modifications over Mercury equipments

Cape Kennedy

Bermuda

Hawaii

Guaymas, Mexico

Corpus Christi, Texas

2 ships

Carpervon, Australia

Apollo - 30' dishes. S-band for tracking, command, and telemetry.

AMR
Bermuda
Hawaii
Guaymas
Corpus Christi

} With modifications of Gemini equipment

5 ships
Antigua
Ascension Islands
N. W. Pacific - Guam
Goldstone
Spain
Canberra
Instrumented A/C
Carnarvon, Australia

i Special 85' antenna for Apollo only
ii DSF's at these locations will be backups

REFERENCES

1. Specification of Atmospheric Laser Propagation Experiments: Task II, Vol. 2. NAA S&ID, SID 65-1275 (15 Sept. 1965), p. 23.

2. Definition of Optical Atmospheric Effects on Laser Propagation: Vol. 3. NAA S&ID, SID 65-1084 (4 Aug. 1965).

3. Experimental Laser Space Communications Program: Task I, Problem Definition, Vol. 2. NAA S&ID, SID 64-1894-2 (9 Oct. 1964).

4. Sherman, J.W., III. "Properties of Focused Apertures in the Fresnel Region," IRE Trans. on Antennas and Propagation, Vol. AP-10 (July 1962).

5. Stratton, J.A. Electromagnetic Theory, Ch. 9. New York: McGraw-Hill Book Company, Inc. (1941).

6. Experimental Laser Space Communications Program: Task I, Problem Definition, Vol. 2. NAA S&ID, SID 64-1894-2, TM 118 (9 Oct. 1964).

7. Laser Modulation Development. NAA S&ID, SID 63-753 (1 July 1963).

8. Born and Wolf. Principles of Optics. New York: McGraw-Hill Book Company, Inc., Ch. 12 (1964).

9. Kleinhaus, W., and D. L. Fried. Efficient Diffraction of Light from Acoustic Waves, SID-IS-TM65-88 (May 1965).

10. Victor and Blockman. "The Application of Linear Servo Theory to the Design of AGC Loops," Proc. of the IRE, Vol. 48 (Feb. 1960).

11. Specification of Atmospheric Laser Propagation Experiments: Task II, Vol. I. NAA S&ID, SID 64-2085 (16 Nov. 1964).

12. Viterbi, A.J. "Phase-Locked Loop Dynamics in the Presence of Noise by Fokker-Planck Techniques," Proc. IEEE, Vol. 51 (Dec. 1963).

13. Munick, R.J. Turbulence-Produced Irradiance Fluctuations in Ground-to-Satellite Light Beams, presented at Spring 1965 meeting of O.S.A.

14. Schilling, D. L. "The Response of an Automatic Phase Control System to FM Signals and Noise," Proc. IEEE, Vol. 51 (Oct. 1963).

15. Soroka, W. W. Analog Methods in Computation and Simulation. New York: McGraw-Hill Book Company, Inc. (1954).

16. Tartarski, V. I. Wave Propagation in a Turbulent Medium. New York: McGraw-Hill Book Company, Inc. (1961).

17. RCA Phototubes and Photocells. Technical Manual PT-60, Radio Corporation of America, Lancaster, Pa. (1963).

18. Subramanian, M., and J. A. Collison. "Modulation of Laser Beams by Atmospheric Turbulence," Bell System Tech. J., 44 (Mar. 1965).

19. Davenport, W. B., Jr. "Signal-to-Noise Ratios in Bandpass Limiters," J. Appl. Phys., Vol. 24, No. 6 (June 1963).

20. Heterodyne Detection in Optical Communications. TRG, Inc., AD 603-622 (July 1964).

21. Anon. Technical Information for the Engineer, Kearfott Company, Inc., Little Falls, N. J. (1958-61).

22. Smith, O. E., L. E. Truppi, and H. L. Crutcher. Interparameter Statistical Analysis of Surface Wind Speed, Total Opaque Cloud Cover, and Maximum Wind Speed Aloft at Cape Kennedy, Florida. NASA TM X-53037, George C. Marshall Space Flight Center, Huntsville, Alabama (22 Apr. 1964).

23. Patel, C. K. N. "Selective Excitation Through Vibrational Energy Transfer and Optical Maser Action in N_2-CO_2," Physical Review Letters, Vol. 13, No. 21 (23 Nov. 1964).

24. Ciftan, M., and P. O. Debye. "On the Parameters Which Affect the C. W. Output of GaAs Lasers," Applied Physics Letters, Vol. 6, No. 6 (15 Mar. 1965).

25. Laser Diodes Specification Sheet; and Diode Laser Pulse Generators, Series DLP (DLP-1, DLP-2, DLP-3), Maser Optics, Inc.

26. GaAs Semiconductor Laser Diodes and Incoherent Emitters (Models K-S1, K-S2, K-S3, K-H1, K-H2, K-H3, K-R1, K-R2, KB-1), K-C1 Laser Diode Cooling System, Semiconductor Laser Pulser - Model K-P1; KORAD - Laser Demonstration Kit - K-S1, Korad Technical Bulletin.

27. Geusic, J.E., M.L. Hensel, and R.G. Smith. "A Repetitively Q-Switched, Continuously Pumped Yag; Nd Laser," Applied Physics Letters, Vol. 6, No. 9 (1 May 1965).

28. Geusic, J.E., H.M. Marcos, and L.G. Van Uitert. "Laser Oscillations in Nd-Doped Yttrium Aluminum, Yttrium Gallium and Gadolinium Garnets," Applied Physics Letters, Vol. 4, No. 10 (15 May 1964).

29. Specification Sheet Portable Yag Laser - Model KY-1, Korad Technical Bulletin; Specification Sheet Solid State CW Laser - Model CW-1, Maser Optics, Inc.

30. Kiss, Z.J., and R.C. Duncan. "Cross-Pumped Cr^{3+}-Nd^{3+}: Yag Laser System," Applied Physics Letters, Vol. 5, No. 10 (15 Nov. 1964).

31. Soffer, B.H. "Giant Pulse Laser Operation by a Passive, Reversibly Bleachable Absorber," Korad, reprinted from Journal of Applied Physics, Vol. 35, No. 8, 2551 (Aug. 1964).

32. Specification Sheet on High Power Laser, Model 4500. Maser Optics, Inc.

33. Specification Sheet, K-2Q 500-Megawatt Giant Pulse Laser. Korad.

34. Specification Sheet on High Repetition Lasers, Series 6-860. Maser Optics, Inc.

35. Specification Sheet on Universal Gas Laser - Series 3000. Energy Systems, Inc.

36. Spicer, W.E., and F. Wooten. "Photoemission and Photomultipliers," Proc. of IEEE (1963).

37. Specification Sheets on Latest Developments in Multiplier Phototubes. Dumont Laboratories, Inc.

38. "Optical Mixing in Phototubes," Proc. of the IRE (Nov. 1962).

39. Targ, R., D.E. Caddes, and B.J. McMurtry. The Traveling Wave Phototube - Part II, Experimental Analysis. Sylvania Electric Products, Inc., Microwave Device Division, Mountain View Components Laboratory.

40. McMurtry, B.J. "Investigation of Ruby Optical Maser Characteristics Using Microwave Phototubes," Applied Optics, Vol. 2, No. 8 (Aug. 1963).

41. DiDomenico, M., Jr., W.M. Sharpless, and J.J. McNicol. "High Speed Photodetection in Germanium and Silicon Cartridge-Type Point-Contact Photodiodes," Applied Optics, Vol. 4, No. 6 (June 1965).

42. Philco Special Products Data Sheet - L4500 Series Photomixer/ Photodetector Diodes (L4501, L4502, L4503, L4530).

43. CP Series Laser Detectors (Types CP-1, CP-1A, CP-2, CP-2A). CBS Laboratories Technical Bulletin (Jan. 1964).

44. Fast Response Light Detector Operating in the Visible and Near Infrared Regions. Edgerton, Germeshausen & Grier, Inc. - Data Sheet #012 SD-100.

45. Allen, C.W. Astrophysical Quantities. The Athlone Press, University of London (1963).

46. Papoulis, A. The Fourier Integral and Its Applications. New York: McGraw-Hill Book Company, Inc. (1962).

47. Subramanian, M., and J.A. Collinson. Modulation of Laser Beams by Atmospheric Turbulence. B.S.T.J., 44 (Mar. 1965).

48. Hinchman, W.R., and A.L. Burk. "Fluctuations in a Laser Beam Over 9- and 90-Mile Paths," Proc. of IEEE, 52 (Mar. 1964).

49. Mevers, G.E., D.L. Fried, and M.P. Keister, Jr. Experimental Measurements of the Character of Intensity Fluctuations of a Laser Beam Propagating in the Atmosphere. NAA, TM 252 (Sept. 1965).

50. Goldstein, I., P.A. Miles, and A. Cabot. "Heterodyne Measurements of Light Propagation Through Atmospheric Turbulence," Proc. of IEEE, Vol. 53, No. 9.